frontiers | Research Topics

Advancing precision therapies in glioblastoma

Edited by
Konstantinos Gousias, Theophilos Tzaridis and Marike Broekman

Published in
Frontiers in Oncology
Frontiers in Neurology

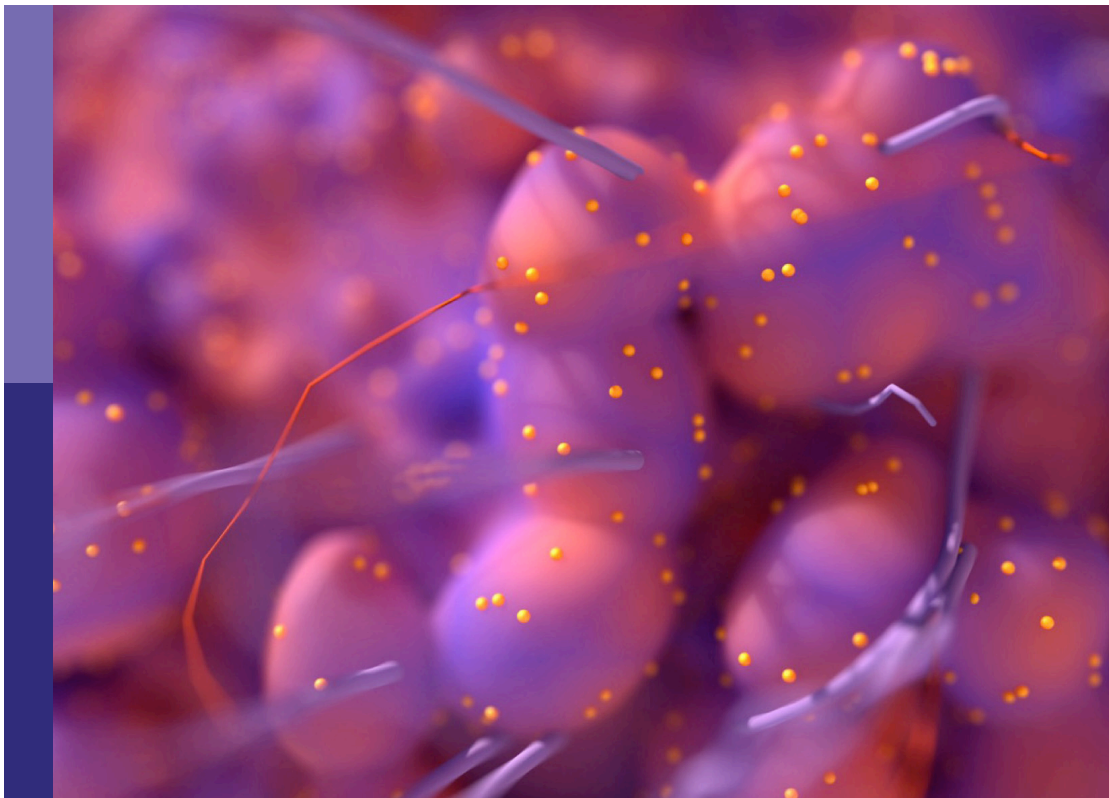

ISSN 1664-8714
ISBN 978-2-8325-6446-2
DOI 10.3389/978-2-8325-6446-2

About Frontiers

Frontiers is more than just an open access publisher of scholarly articles: it is a pioneering approach to the world of academia, radically improving the way scholarly research is managed. The grand vision of Frontiers is a world where all people have an equal opportunity to seek, share and generate knowledge. Frontiers provides immediate and permanent online open access to all its publications, but this alone is not enough to realize our grand goals.

Frontiers journal series

The Frontiers journal series is a multi-tier and interdisciplinary set of open-access, online journals, promising a paradigm shift from the current review, selection and dissemination processes in academic publishing. All Frontiers journals are driven by researchers for researchers; therefore, they constitute a service to the scholarly community. At the same time, the *Frontiers journal series* operates on a revolutionary invention, the tiered publishing system, initially addressing specific communities of scholars, and gradually climbing up to broader public understanding, thus serving the interests of the lay society, too.

Dedication to quality

Each Frontiers article is a landmark of the highest quality, thanks to genuinely collaborative interactions between authors and review editors, who include some of the world's best academicians. Research must be certified by peers before entering a stream of knowledge that may eventually reach the public - and shape society; therefore, Frontiers only applies the most rigorous and unbiased reviews. Frontiers revolutionizes research publishing by freely delivering the most outstanding research, evaluated with no bias from both the academic and social point of view. By applying the most advanced information technologies, Frontiers is catapulting scholarly publishing into a new generation.

What are Frontiers Research Topics?

Frontiers Research Topics are very popular trademarks of the *Frontiers journals series*: they are collections of at least ten articles, all centered on a particular subject. With their unique mix of varied contributions from Original Research to Review Articles, Frontiers Research Topics unify the most influential researchers, the latest key findings and historical advances in a hot research area.

Find out more on how to host your own Frontiers Research Topic or contribute to one as an author by contacting the Frontiers editorial office: frontiersin.org/about/contact

Advancing precision therapies in glioblastoma

Topic editors

Konstantinos Gousias — University of Münster, Germany

Theophilos Tzaridis — Sanford Burnham Prebys Medical Discovery Institute, United States

Marike Broekman — Department of Neurosurgery, Haaglanden Medical Center, Netherlands

Citation

Gousias, K., Tzaridis, T., Broekman, M., eds. (2025). *Advancing precision therapies in glioblastoma*. Lausanne: Frontiers Media SA. doi: 10.3389/978-2-8325-6446-2

Table of contents

04 A systematic review on intra-arterial cerebral infusions of chemotherapeutics in the treatment of glioblastoma multiforme: The state-of-the-art
Mateusz Pinkiewicz, Milosz Pinkiewicz, Jerzy Walecki and Michał Zawadzki

25 Case report: ATIC-ALK fusion in infant-type hemispheric glioma and response to lorlatinib
Shubin W. Shahab, Matthew Schniederjan, Jose Velazquez Vega, Stephen Little, Andrew Reisner, Tobey MacDonald and Dolly Aguilera

31 High-frequency irreversible electroporation improves survival and immune cell infiltration in rodents with malignant gliomas
Sabrina N. Campelo, Melvin F. Lorenzo, Brittanie Partridge, Nastaran Alinezhadbalalami, Yukitaka Kani, Josefa Garcia, Sofie Saunier, Sean C. Thomas, Jonathan Hinckley, Scott S. Verbridge, Rafael V. Davalos and John H. Rossmeisl Jr.

49 CAR-NK cell therapy for glioblastoma: what to do next?
Qi Xiong, Jiao Zhu, Yong Zhang and Hongxin Deng

64 Glioblastoma-on-a-chip construction and therapeutic applications
Zuorun Xie, Maosong Chen, Jiangfang Lian, Hongcai Wang and Jingyun Ma

79 Feasibility of intraoperative neuromonitoring and cortical/subcortical mapping in patients with cerebral lesions of highly functional localizations—pathway to case adapted monitoring and mapping procedures
Franziska Staub-Bartelt, Marion Rapp and Michael Sabel

93 Generating *Shigella* that internalize into glioblastoma cells
Austin Shipley, Gabriel Frampton, Bryan W. Davies and Benjamin J. Umlauf

106 Roles of extracellular vesicles in glioblastoma: foes, friends and informers
Taral R. Lunavat, Lisa Nieland, Anne B. Vrijmoet, Ayrton Zargani-Piccardi, Youssef Samaha, Koen Breyne and Xandra O. Breakefield

118 Preoperative validation of edema-corrected tractography in neurosurgical practice: translating surgeon insights into novel software implementation
Sebastian F. Koga, Wesley B. Hodges, Hayk Adamyan, Tim Hayes, Peter E. Fecci, Vadim Tsvankin, Gustavo Pradilla, Kimberly B. Hoang, Ian Y. Lee, Eric W. Sankey, Patrick J. Codd, David Huie, Brad E. Zacharia, Ragini Verma and Vatche G. Baboyan

130 Deciphering glycosylation-driven prognostic insights and therapeutic prospects in glioblastoma through a comprehensive regulatory model
Xingyi Jin, Zhuo Chen and Hang Zhao

frontiers | Frontiers in Oncology

TYPE Systematic Review
PUBLISHED 23 September 2022
DOI 10.3389/fonc.2022.950167

OPEN ACCESS

EDITED BY
David Fortin,
Université de Sherbrooke, Canada

REVIEWED BY
Michael Schulder,
Donald and Barbara Zucker School of Medicine at Hofstra-Northwell, United States
Arshak Alexanian,
Medical College of Wisconsin, United States
Beatrice Detti,
Careggi University Hospital, Italy

*CORRESPONDENCE
Michał Zawadzki
mzawpl@gmail.com

This article was submitted to Neuro-Oncology and Neurosurgical Oncology, a section of the journal Frontiers in Oncology

SPECIALTY SECTION
RECEIVED 22 May 2022
ACCEPTED 02 September 2022
PUBLISHED 23 September 2022

CITATION
Pinkiewicz M, Pinkiewicz M, Walecki J and Zawadzki M (2022) A systematic review on intra-arterial cerebral infusions of chemotherapeutics in the treatment of glioblastoma multiforme: The state-of-the-art.
Front. Oncol. 12:950167.
doi: 10.3389/fonc.2022.950167

A systematic review on intra-arterial cerebral infusions of chemotherapeutics in the treatment of glioblastoma multiforme: The state-of-the-art

Mateusz Pinkiewicz[1], Milosz Pinkiewicz[2], Jerzy Walecki[3] and Michał Zawadzki[3]*

[1]Department of Diagnostic Imaging, Mazowiecki Regional Hospital in Siedlce, Siedlce, Poland, [2]English Division, Faculty of Medicine, Wroclaw Medical University, Wroclaw, Poland, [3]Division of Interventional Neuroradiology of the Central Clinical Hospital of the Ministry of Interior and Administration, Department of Radiology, Centre of Postgraduate Medical Education, Warsaw, Poland

Objective: To provide a comprehensive review of intra-arterial cerebral infusions of chemotherapeutics in glioblastoma multiforme treatment and discuss potential research aims. We describe technical aspects of the intra-arterial delivery, methods of blood-brain barrier disruption, the role of intraoperative imaging and clinical trials involving intra-arterial cerebral infusions of chemotherapeutics in the treatment of glioblastoma multiforme.

Method: 159 articles in English were reviewed and used as the foundation for this paper. The Medline/Pubmed, Cochrane databases, Google Scholar, Scielo and PEDro databases have been used to select the most relevant and influential papers on the intra-arterial cerebral infusions of chemotherapeutics in the treatment of glioblastoma multiforme. Additionally, we have included some relevant clinical trials involving intra-arterial delivery of chemotherapeutics to other than GBM brain tumours.

Conclusion: Considering that conventional treatments for glioblastoma multiforme fall short of providing a significant therapeutic benefit, with a majority of patients relapsing, the neuro-oncological community has considered intra-arterial administration of chemotherapeutics as an alternative to oral or intravenous administration. Numerous studies have proven the safety of IA delivery of chemotherapy and its ability to ensure higher drug concentrations in targeted areas, simultaneously limiting systemic toxicity. *Nonetheless*, the scarcity of phase III trials prevents any declaration of a therapeutic benefit. Given that the likelihood of a single therapeutic agent which will be effective for the treatment of glioblastoma multiforme is extremely low, it is paramount to establish an adequate multimodal therapy

which will have a synergistic effect on the diverse pathogenesis of GBM. Precise quantitative and spatial monitoring is necessary to guarantee the accurate delivery of the therapeutic to the tumour. New and comprehensive pharmacokinetic models, a more elaborate understanding of glioblastoma biology and effective methods of diminishing treatment-related neurotoxicity are paramount for intra-arterial cerebral infusion of chemotherapeutics to become a mainstay treatment for glioblastoma multiforme. Additional use of other imaging methods like MRI guidance during the procedure could have an edge over X-ray alone and aid in selecting proper arteries as well as infusion parameters of chemotherapeutics making the procedure safer and more effective.

KEYWORDS

glioblastoma, IA chemotherapy, SIACI, glioblastoma chemotherapy, IA delivery, bevacizumab in glioblastoma, cetuximab in glioblastoma

Introduction

Glioblastoma (GBM) multiforme is the most common type of brain cancer, accounting for approximately 40% of all primary malignant brain tumours (1–3).

This distinct pathological entity is known for its aggressive progression and poor prognosis, with a median patient survival duration of 14-17 months in the case of contemporary clinical trials and ~12 months in population-based studies (1–3). Only 5% of patients manage to achieve a 5-year survival. Standard therapy has consisted of surgical resection, external beam radiation or both (4).

Since its publication in 2005, the Stupp protocol, consisting of radiotherapy (2 Gy per/day x 30 days, 60 Gy total) and oral temozolomide (75 mg/m2), has been the gold standard for the treatment of glioblastoma multiforme (GBM) (5, 6). Nonetheless, the majority of patients relapse after six months (7). Consequently, despite the concerted efforts of the medical community, available methods of treatment fall short of providing any significant improvements, causing GBM to be incurable. The failure of conventional chemotherapy to increase overall survival is attributable to low penetration of the blood-brain barrier and systemic toxicity (5–8). Consequently, aside from intra-arterial delivery, researchers have been driven to explore other drug delivery methods, such as intrathecal, intracavitary and convection-enhanced delivery. However, although preclinical studies demonstrated promising results, these novel approaches to drug delivery require further clinical investigation before they become the mainstay of treatment (8).

Intra-arterial chemotherapy of GBM is not a new concept, in fact, it is one of the oldest treatments attempted for this deadly disease, introduced in the 50s coincidently with the introduction of radiotherapy for brain tumours (9). The underlying hypothesis behind intra-arterial drug administration was that achieving a higher concentration of the pharmaceutic in the specified area of the tumour would lead to an increased likelihood of tumour cell death. Furthermore, the possibility of reducing the toxicity, so pronounced in the case of the systematic approach, could also provide the opportunity of using higher doses of chemotherapeutics (10). These potential advantages resulted in a considerable body of literature reporting the use of IA delivery in the 50s, 70s and 90s. Nonetheless, the significant neurotoxicity of chemotherapeutics available at the time eventually discouraged further research (10, 11).

As of now, approximately 3000 IA dd procedures have been reported all over the world (12). This is attributable to the growth of personalised oncology, improvement of imaging techniques, and new endovascular tools. Developments like dual lumen balloons, large-bore distal access catheters, and soft microcatheters allow for modification of blood flow in the brain vessels to an unprecedented degree. Intra-arterial infusions do not require craniotomy, are easy to repeat, and in experienced hands are safe and reproducible. Nonetheless, although the intra-arterial route seems to be the most physiological way to administer any drug to the brain, there is a substantial obstacle in overcoming the blood-brain barrier, responsible for blocking the majority of drugs from entering the brain tissue (13). Although mannitol remains the widely-used method for transient BBB disruption, there are numerous promising techniques being developed. Almost all published intra-arterial infusions were performed under X-ray guidance in cath labs designed to treat pathologies of relatively big vessels in the brain. X-ray angiography has a high spatial resolution, accurately depicts the intracranial vessels, and allows for safe microcatheter navigation into distal intracranial arteries. However, the possibility to visualise parenchymal flow in brain

tumours and surrounding tissue is limited. Real-time monitoring of infusion has recently become possible in MRI during the procedure. First such procedures were already performed in humans. Moreover, combining interventional MR with PET can even further expand the ability to monitor chemical processes and labelled-drug accumulation in the brain in a real-time manner.

A wide range of new therapeutics administered intra-arterially may not only include chemotherapeutics but also antibodies, cells (e.g. carTcells), modified viruses or radiotherapeutics. Before we start composing new trials, we should thoroughly know why our predecessors failed. Some anecdotal, spectacular successes will also be analysed and gathered in this review.

Methodological approach

Search strategy and selection criteria

A systematic literature review was carried out to review all available relevant data. During the article selection process, the authors followed the recommendations made by the Preferred Reporting Items for Systematic Reviews and Meta-Analyses (PRISMA). All authors independently have searched the Medline/Pubmed, Cochrane databases, Google Scholar, Scielo and PEDro databases by using the following keywords "Glioblastoma", "IA chemotherapy", "SIACI", "SSIACI", "glioblastoma treatment", "glioblastoma chemotherapy", "IA delivery", "bevacizumab in glioblastoma", "cetuximab in glioblastoma".

Additional search has included the Scielo and PEDro databases. The last search was conducted in May 2022. The references of the publications of interest were also screened for relevant papers.

Study selection and data extraction

All of the selected articles were read in full text. Only papers written in English have been considered. Non-peer-reviewed papers and records not available in the full text have not been included. Also, studies were excluded if there was incomplete or missing data. We have excluded conference abstracts. The eligibility and quality of publications have been independently evaluated by three reviewers. We have chosen articles for inclusion on the grounds of study quality and design. The primary selection had no limitations regarding the publication date. We have included studies focusing on technical aspects of IA delivery, established and new methods of blood-brain barrier disruption, drugs used for intra-arterial cerebral infusions for the treatment of glioblastoma multiforme and intraoperative imaging. Additionally, we have described novel studies concerning gene and cell therapy. We have reviewed and included selected preclinical and clinical studies concerning IA therapy for glioblastoma multiforme. Some papers describing emerging therapies for glioblastoma multiforme have also been reviewed and added. The judgments concerning the risk of bias were formed by a single reviewer and subsequently double-checked by another reviewer

Results

A total of 3,294 papers were retrieved from The Medline/Pubmed, Cochrane databases, Google Scholar, Scielo and PEDro databases. Screening for duplicates and their removal resulted in a total of 1846 articles. Subsequently, we have excluded 890 articles due to language and study design. Titles or abstracts of 1068 articles were screened, obtaining 207 papers not meeting any exclusion criterion. After full-text evaluation, we have excluded 48 papers. This has led to the inclusion of 159 articles. The flow diagram represents our process of article selection (Figure 1).

Historical aspect

Intra-arterial delivery of chemotherapeutics has been pioneered by Bierman et al. (14) and Klopp et al. (15) who have designed techniques for the delivery of high-doses of nitrogen mustard directly to the liver tumours *via* its arterial blood supply (10). Multiple administrations of nitrogen mustard responsible for tumour regression in rabbits with extracranial xenografts have prompted Klopp et al., as well as inspired French et al., to use IA delivery of chemotherapeutics in humans for malignant progressive gliomas (15, 16). However, despite the enthusiasm, nitrogen mustard delivery was associated with poor therapeutic benefits and significant damage to the hematopoietic system (15). In the 1970s, Eckmann had lent credence to previous assumptions made by Wilson et al. and successfully proved that IA delivery of chemotherapeutics allowed obtaining higher drug concentrations in targeted tumours than that in non-targeted tissues (17–19). Stanley Rapaport's findings concerning the fundamental role of tight junctions in BBB permeability, as well as the demonstration that hyperosmolar BBB disruption causes dehydration of endothelial cells and subsequent disruption of tight junctions in a reversible fashion, have laid the groundwork for Neuwelt research which proved that hyperosmolar BBB disruption increased concentrations of chemotherapies in targeted sites for central nervous system lymphomas (20–25). In 1978, Levin et al. reported that IA infusion offered a 2.5–5-fold increase in drug delivery drug over IV infusion after comparing intravenous to intracarotid artery (ICA) administration of 14C-labelled carmustine in squirrel monkeys (26). Multiple studies following have broadened the substantive scaffolding, further

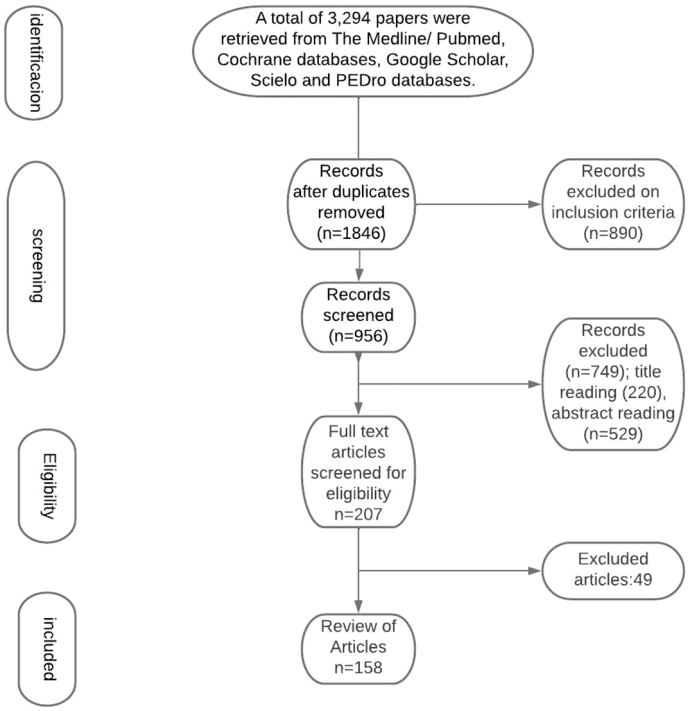

FIGURE 1
Flow Diagram represents our process of article selection.

highlighting the efficacy of the intra-arterial delivery of chemotherapeutics into the vessels supplying the brain (10, 21–25). Given that the chemotherapeutics available at the time were associated with significant neurotoxicity, the interest in IA delivery slowly began to fade (10, 11, 25–27). This, paradoxically, has started to take place at the height of technological advances in endovascular methods (10, 11). Although numerous preclinical and clinical studies have proven the validity of that is intra-arterial delivery of chemotherapeutics, not until the development of new drugs and availability of new selective microcatheters and other endovascular devices did the interest of the IA once again awaken.

Blood-brain barrier disruption

The blood-brain barrier, responsible for the cellular and molecular exchange between the blood vessels and brain parenchyma, is highly selective, blocking the passage of ionised molecules whose molecular weights are larger than 180 Da (11, 21, 28, 29). Given that most chemotherapeutics' size is in the range of 200-1200 Da, the blood-brain barrier is a significant impediment in the treatment of brain tumours (28). Even if some drugs manage to penetrate the BBB, they usually fail to reach effective local concentrations (11). The poor prognosis of GBM is in large part due to the lack of successful drug delivery through the blood-brain tumour barrier (BBTB). The BBTB consists of already existing and newly formed blood vessels, which are responsible for the delivery of nutrients and oxygen to the tumour, as well as the glioma cell migration to other parts of the brain (29). High expression of VEGF and subsequent angiogenesis result in the formation of abnormal vessels and a flawed BBTB (29). Although the BBTB of high-grade gliomas is considered to be "leaky", lower-grade gliomas have an almost fully functional BBB, prompting the passage of chemotherapeutics to be ineffective (29). Glioblastomas are known to have different regions of BBTB integrity. Bulky tumours are characterised by completely dysfunctional BBTB, less invasive circumferential regions have a leaking BBTB, whereas areas far from the tumour bulk can display a fully functional BBTB (29). Overexpression of receptors that mediate ligand-dependent drug delivery has been observed in brain tumour capillaries. This could be exploited to selectively enhance drug delivery to tumour tissues (29, 30). Extensive research over the last decades has resulted in various methods of brain-barrier disruption. This section will focus on describing available methods as well as discuss the nearest future.

Osmotic blood-brain barrier disruption

Rapoport et al. were the first to demonstrate that an intra-arterial infusion of a hyperosmotic solution of mannitol will result in a temporary shrinkage of endothelial cells due to the creation of an osmotic gradient and, consequently lead to the opening of the tight junctions (20, 22). Reportedly, osmotic disruption can increase the levels of successfully infused chemotherapeutics by up to 90-fold (11). Non-selective opening of the BBB results in an increase of brain fluid, as well as in an influx of molecular compounds, which can lead to neurological toxicity, aphasia and hemiparesis (29, 31). Thus, using hypertonic solutions demands caution. Nonetheless, studies have shown that osmotic disruption can be safe and of therapeutic value in capable hands (31–37). Due to individual factors, there is no exact dose and infusion time. Numerous research has described osmotic BBB disruption by intra-arterial infusion of 1.37 mmol/L mannitol (25%) (38–40). Boockvar et al. report relying on the mannitol infusion rate of 0.083 mL/s for 120 seconds, whereas Siegal et al. infused at a rate of 3 to 11 ml/second over 30 seconds (10, 31). Despite the staggering amount of more than 4200 osmotic BBB disruption procedures having been performed at multiple centres in more than 400 patients, there is no consensus in regard to the maximum permeability effect of osmotic BBB disruption (31). According to Siegal et al., the maximum effect in humans lasts up to 40 minutes which is preceded by a rapid decline in permeability, with the normal threshold restored between 6 and 8 hours after the osmotic disruption (31). These findings differ from those of Zünkeler et al. who used rubidium-82 to measure blood-to-tissue influx and estimated that the mean half time for the return of permeability to almost baseline values was only 8 minutes in the normal brain (31, 36).

Bradykinin receptor-mediated BBTB opening

Bradykinin is a potent vasodilator, capable of increasing capillary permeability (41). In 1986, Raymond et al. demonstrated that high doses of bradykinin will result in the breakdown of the normal blood-brain barrier (41). Inamura et al. have successfully proved that low doses of bradykinin led to the selective increase of the permeability of abnormal brain tissue capillaries to low and high molecular weight neuropharmaceuticals (42). This has brought about the clinical development of bradykinin analogs such as Cereport or labramidil (29). Research has demonstrated that using synthetic bradykinin analogs to improve the delivery of IA carboplatin is a safe method, allowing for a two-fold increase in drug delivery. Nonetheless, there was no clear clinical benefit demonstrated in the randomised, double-blind, placebo-controlled phase II study of RMP-7 in combination with carboplatin or in the Phase II trial of intravenous lobradimil and carboplatin used in the treatment of childhood brain tumours (29, 43, 44). This may be due to an inadequate dose level of RMP-7 of 300 ng/kg. However, there were no subsequent studies with different doses, leaving this matter unsettled (29, 43, 44)

Magnetic-resonance- guided focused ultrasound

Magnetic-resonance- guided focused ultrasound (MRgFUS) is a promising technology used for the treatment of a variety of neurological disorders. Most importantly, MRgFUS is also used for the opening of the blood-brain barrier (BBB) in combination with intravenously administered microbubbles (45–50). Regional contrast extravasation on the MR images correlates with the amount of delivered drug, thus allowing for precise targeting of BBB disruption (47). According to research, pulsed ultrasound is capable of safely opening the BBB and providing spatial and temporal specificity (45–50). Ultrasound parameters like intensity and sonication time, as well as the size and concentration of intravenously administered microbubbles, decide on the exact extent of BBB opening (45–50). Reportedly, the possible BBB opening is temporary and lasts for almost 4-6 hours after the treatment (47, 50). Consequently, the transport of various chemotherapeutics used for the treatment of brain tumours can be significantly improved (10, 11).

Inhibition of drug efflux transporters

Studies have shown that some drugs have an improved brain penetration once drug efflux transporters are absent (51). Therefore, inhibition of such multidrug resistance efflux transporters by specific inhibitors could be an effective method of boosting drug penetration into the brain without altering the integrity of the endothelial layer and tight junctions, which could avoid the potential toxicity observed with BBBD. Pharmaceutical companies aimed to reverse the multidrug resistance phenotype of tumours by developing elacridar and tariquidar, which inhibit ABCB1 and ABCG2. However, given that clinical trials in solid tumours demonstrated failure, the interest in developing inhibitors has waned (52). Nonetheless, the idea of incorporating these reversal agents to enhance BBB drug penetration is wholly different from using these agents to block multidrug resistance in genomically unstable cancer cells. The goal here would be to increase the accessibility of a sanctuary site by targeting ABC transporters in genomically stable endothelial cells. The ability to block drug efflux transporters will strongly depend on finding a potent inhibitor with proper systemic bioavailability and a 'commuter' agent with moderate affinity for these efflux transporters.

Pardridge et al. have reported various receptor-mediated uptake systems for improving the brain uptake of drugs and radiopharmaceuticals (53). GRN1005 (formerly ANG1005) is a conjugate of paclitaxel and the angiopep-2 peptide that targets the lipoprotein receptor-related protein 1 (LRP1) and crosses the BBB

by transcytosis (54). A Phase I study has demonstrated promising results, which should be further evaluated by ongoing 3 phase II clinical trials for glioma (Clintrials.gov: NCT01967810) and breast cancer brain metastasis (NCT02048059 and NCT01480583). A clinical trial has also shown similarly encouraging outcomes with the use of 2B3-101 (Clintrial.gov ID: NCT01386580, NCT01818713), which is a PEGylated liposome that is conjugated with glutathione (GSH) (55).

One study has demonstrated that the docosahexaenoic transporter Mfsd2a acts by suppressing transcytosis in CNS endothelial cells (56). According to van Tellingen et al., by interfering with its function or expression it could be possible to enhance transcytosis and consequently enhance drug delivery *via* this route (29).

Novel methods with potential

Laser interstitial thermal therapy (LITT) is an emerging method of delivering targeted thermal therapy and has been used in brain tumour ablations. Research suggests that hyperthermia induced by LITT may result in the disruption of BBB (57). Research on mice has shown that laser ablation is capable of increasing BBB/BTB permeability, with peak permeability occurring within 1 week and lasting up to 30 days after ablation. Furthermore, molecules as large as human IgG (approximately 150 kDa) were able to pass the BBB after LITT (57). Leuthardt et al. have reported increased serum levels of brain-specific enolase, which is limited to the CNS, after laser ablation in patients suffering from recurrent glioblastoma (58). Authors have suggested that increased permeability in the peritumoral region is attributable to LITT and reaches its peak 1-2 weeks from ablation and returns to the normal threshold by 4-6 weeks (58). The obtained time window provides the potential for the enhancement of IA drug delivery (58). Besides the therapeutic benefit, LITT could also be associated with crucial immunological consequences, given that immunoproteins are being continuously released outside the CNS compartment and could trigger an immune response (58). All of these factors prompt LITT to be a highly interesting phenomenon, albeit requiring much more research.

The advancements in nanotechnology could result in using nanoparticles in intra-arterial administration. Nanoparticles (NP) could be modified to cross the BBB through different transport mechanisms and stay at the targeted area for a longer time, allowing for a gradual release of loaded chemotherapy (59–61). Studies have demonstrated the ability of NP to enhance the half-life of the drug in circulation (59–61). According to Zhao et al., the half-life of TMZ was increased to 13.4 h in comparison to 1.8 h of the free drug by encapsulation in a chitosan-based nanoparticle (61). Ongoing clinical trials involving nanoparticle-based cancer treatment in GBM should evaluate their efficacy, thus allowing for further development in NP-treatment.

Convection enhanced delivery relies on the direct and continuous injection of a chemotherapeutic agent under positive pressure by using stereotactically placed intraparenchymal microcatheters, which allow the passage of molecules of different charges and sizes to any part of the brain (62–65). Although showing potential, neuro-oncological clinical trials with CED have demonstrated poor drug distribution to more peripheral areas of diffuse gliomas and drug reflux, leading to complications and subtherapeutic drug concentrations within the tumour target cells (66, 67). Also, CED has more disadvantages, such as the lack of visualisation of the distribution of the infused drug and unacceptable device-related adverse events (68). Ongoing clinical and preclinical imaging studies may optimise drug distribution *via* CED.

Lately, research has shown that by establishing a local positive pressure gradient convection-enhanced delivery (CED) using catheters stereotactically inserted into brain tumours is capable of improving drug delivery into these tumours and surrounding brain tissue (69, 70). Although a Phase I clinical trial evaluating CED of carboplatin has offered a therapeutic benefit for glioblastomas patients, there are numerous side effects resulting from the use of CED, involving headache, seizure, fever, nausea, vomiting, fatigue, erythema, and in some cases liver enzyme perturbations and haematological changes, which are associated with the time and location of the treatment (71–73). More research is required to provide unequivocal evidence for a benefit of CED in glioblastoma patients.

A study has found that TTFields improve membrane permeability by increasing both the number and the size of pores in the membrane of glioma cells (74, 75). Moreover, the authors reported a substantial increase in the uptake of membrane-associating reagents with a size of 20 kDa and no larger than 50 kDa into glioma cells with TTFields that was reversible, returning to normal within 24 of ceasing TTFields treatment (74, 75). Another suggested that by transiently disrupting the localisation of tight-junction proteins such as claudin 5 and ZO-1, the TTFields therapy can interfere with the integrity of the blood-brain barrier (76).

Mannitol continues to be the most effective method for transient BBB disruption. Studies have demonstrated its safety and good tolerance in combination with intra-arterial chemotherapy. Nonetheless, mannitol mediated BBB disruption may cause an unexpected increase in transcapillary transport of anticancer drugs into healthy brain tissues (77). High-frequency and high-amplitude electroencephalography (EEG) signals suggest that an intra-arterial injection of mannitol through the anterior circulation could have a direct effect on the motor cortex, regardless of the chemotherapy regimen or the size and location of the tumour (78). There are numerous complications that could result from mannitol

mediated BBB disruption, such as transient aphasia, hemiparesis, or even oedema-induced intracranial herniation (79). However, studies most often report tachycardia, increased intracranial pressure, vomiting, nausea and headache (79).

Technical aspects of contemporary intra-arterial drug delivery

The central concept behind intra-arterial drug administrations was to achieve a higher concentration of the pharmaceutic in the specified area of the tumour and, at the same time, reduce systemic side effects. A Randomised Phase III study comparing intravenous and intra-arterial administrations in newly diagnosed primary glioblastomas patients has shown that intra-arterial delivery of chemotherapeutics has the advantages of smaller toxicity, longer total drug exposure and a higher peak concentration (80). IA injection allows increasing local concentrations of chemotherapeutics to brain tumours up to over 300 times more than the intravenous approach (81). Another study relying on positron emission tomography (PET) measurements has shown that IA delivery had a 50-fold increase in brain tumour tissue concentrations in comparison to IV injections (82). Thanks to the osmotic opening of the blood-brain barrier, IA delivery provided a 300 times higher local concentration of chemotherapeutics to brain tumours than the intravenous approach (81). Technological progress has led to the emergence of selective intra-arterial cerebral infusion (SIACI). This is a technique relying on state-of-the-art microcatheters, which are inserted into the femoral artery and subsequently navigated directly to the tumour supplying vessels (10). This method has an edge over unselective IA infusions like vertebral or carotid infusion as the volume of distribution (Vd) is limited to the targeted area and adjacent tissue sharing the vascular supply (11). Consequently, high selectiveness and reduced neurotoxicity are provided. Microcatheter is navigated with the use of guidewire assistance and road-mapping control in the angiographic suite (10). As much as SIACI is a highly advantageous technique, it is not ideal. To reduce neurotoxicity and assure high drug levels in the corresponding brain region, it is paramount to address the problem of inadequate dosing and "streaming". Gobin et al. have proposed using a spatial dose fractionation algorithm that selects the proper dose on the basis of cerebral vascular territories rather than weight or body surface area (83). This algorithm relies on the vascular perfusion of the vessel and thus may optimise IA drug delivery (83–85). Various studies blame streaming for high neurotoxicity and unsuccessful treatment (11, 83, 84). Streaming occurs when drugs delivered by the IA method are distributed unequally to different areas of the brain and is caused by the layering of blood flow in the arteries. Some layers stream drugs favourably to one or two arterial branches causing accumulation in supplied areas, while other branches of the same artery do not receive drugs at all. This faulty distribution is attributable to the infusion rate being smaller than 20% of the background blood flow (11, 83). Recognition of this phenomenon has resulted in numerous techniques diminishing this effect. Among them, we can distinguish the incorporation of catheters with side ports, pulsatile injections at rates higher than 20% of the background flow rate and injections during the diastole (11, 86). Furthermore, the notion that tumours with low blood flow respond better to chemotherapy resulted in the use of single or double-balloon catheters to isolate proximal and distal arterial flow, thus successfully maximising local delivery and reducing local and regional complications (10, 11). Research done on computational models and in preclinical settings has vividly shown that cerebral hypoperfusion improves local drug delivery by lowering hydrodynamic stress on the injected molecules and increasing drug transit time through cerebral circulation. Consequently, the pure drug is delivered to the vascular endothelium and opsonization by serum proteins and blood cells is significantly decreased (10, 11, 87–90). As with any operative technique, there are associated risks. These include complications resulting from vascular access and subsequent catheter positioning, systemic toxicities associated with chemotherapy, and, most importantly, the possibility of seizures (33, 39). Reportedly, abnormally small carotid arteries or the presence of two branches rather than three or more increases the possibility of neurologic complications (84, 89, 91). Potential complications associated with intra-arterial drug delivery of chemotherapeutics in the treatment of glioblastoma are shown in Figure 2.

Clinical IA drug deliveries in glioblastoma patients

The more profound understanding of glioblastomas multiforme, the technological improvements and promising outcomes associated with IA chemotherapy in the treatment of retinoblastoma (92), breast cancer (93), head and neck tumours (94) and advanced liver cancers (95, 96) have propelled researches to attest the efficacy of IA chemotherapy in the treatment of glioblastoma multiforme. Table 1 summarises completed clinical studies focusing on treating glioblastoma multiforme and other brain entities with selective or nonselective IA chemotherapeutic delivery (32, 80, 81, 83, 97–115)

Mannitol continues to be the prevalent BBBD agent, although some recent studies relied on the bradykinin B2 receptor agonist Cereport. As of now (https://clinicaltrials.gov last accessed on 1st of May), there are four clinical trials that have been recently completed (NCT01180816, NCT01238237, NCT00968240, NCT00870181), six are still recruiting (NCT01269853, NCT05271240, NCT02285959, NCT02861898, NCT01884740, NCT02800486), one is active but not recruiting (NCT01811498), one has been suspended (NCT01386710), and

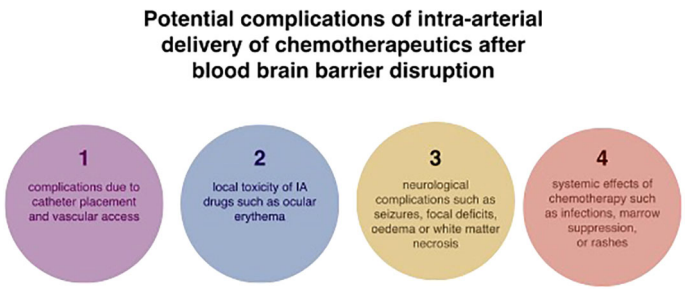

FIGURE 2
Potential complications associated with intra-arterial drug delivery of chemotherapeutics in the treatment of glioblastoma.

one is of an unknown status (NCT03672721). Results available from these trials have been described in detail in the following parts of the review. Table 2 presents detailed information on ongoing clinical trials relying on IA delivery for the treatment of glioblastoma multiforme and other brain tumours.

Clinical IA trials of the last couple of decades tested the efficacy and safety of IA delivery of platinum analogues (cisplatin and carboplatin), methotrexate, vincristine, nitrosourea derivatives, including carmustine (BCNU), nimustine (ACNU) or 1-(2-hydroxyethyl) chloroethyl nitrosourea (HeCNU), diaziquone, etoposide, and idarubicin. The most recent clinical trials have focused on evaluating the role of new antibodies like bevacizumab and cetuximab. Enrolled patients had surgery and were in favourable clinical condition (10). Although certain studies included patients who had a Karnofsky performance scale score (KPS) of 20, the prevailing majority of clinical trials required a KPS of a minimum of 60 (10).

Nitrosourea derivatives

First clinical studies of IA nitrosourea derivatives showed encouraging results, but the resulting neurotoxicity quickly diminished the enthusiasm (10, 116–118). In 1986, Feun and colleagues demonstrated in a follow-up phase II trial that IA BCNU may lead to severe leukoencephalopathy and blindness (119). These suggestions were proven valid by Tonn et al. and Kleinschmidt-DeMasters et al., who demonstrated in treated patients a significant risk of local cerebral necrosis as well as leukoencephalopathy (116, 120, 121). Follow-ups of patients have shown that IA BNCU may result in leukoencephalopathy, blindness and increased risk of cerebral necrosis (10, 116, 118–121). The interest in IA nitrosourea derivatives began to wane after a randomised phase III trial comparing IA with IV BCNU showed that IA BCNU is unsafe and lacks effectiveness in regard to increasing patient survival (121). More recently, Fauchon et al. evaluated the role of intracarotid HeCNU (120 mg/m2) in 40 patients before the start of irradiation (122). The authors reported a median TTP of 32 weeks, with an overall median survival of 48 weeks. Neurological toxicity involved visual loss (15%) and leukoencephalopathy (10%) (122).

Platinum analogs

Ever since Follézou et al. demonstrated that IA of 400 mg/m2 carboplatin led to a partial response in malignant glioma patients, numerous studies evaluating the role of IA of platinum analogs followed (10, 123). Gobin et al. reported the IA delivery of up to 1400 mg/hemisphere of carboplatin in their dose-escalation study based on cerebral blood flow, reporting median survival of 39 weeks and a response rate of 70% (50% SD and 20% PR) of 19 patients (124). In a more recent study, Cloughesy et al. reported a median survival of 11 months (from the time of beginning IA treatment) (111). The regimen involved IA delivery of carboplatin conducted every four weeks for up to 12 cycles (111). Reported toxicity was manageable, with 8% of patients demonstrating grade II neutropenia, 12% of grade II thrombocytopenia and 7% of grade III thrombocytopenia. In summary, the potential for visual loss seems to be greater for patients undergoing IA carmustine and other nitrosoureas than for patients receiving cisplatin or carboplatin.

Diaziquone, etoposide and idarubicin

Other drugs tested for single-agent IA chemotherapy of recurrent gliomas are diaziquone, etoposide and idarubicin. Greenberg et al. have studied IA diaziquone (10–30mg/m2) in 20 patients with recurrent astrocytomas (125). Two of 20 patients demonstrated partial responses of 5 and 8+ months, respectively. Four patients showed disease stabilisation of 3, 4, 5, and 8 months duration, respectively, and one of these patients achieved tumour shrinkage (125). The reported toxicity was similar to carmustine and cisplatin (125). According to the authors, IA diaziquone was no more effective when using the intravenous approach (125). Intracarotid etoposide (100–650

TABLE 1 Summary of studies using intra-arterial delivery of chemotherapeutics for the treatment of GBM.

Study (year)	Number of patients	Study type and phase	Brain tumors	Chemotherapeutic agent Dose	Method of delivery	BBBD Agent	Outcome	Neurotoxicity
Doolittle et al. (2000) (97)	221	MC,II	GBM, BSG, AO, O, MET, GCT, PCNSL, PNET	Carboplatin (200 mg/m2)	nS	Mannitol	(79%) achieved SD or better	Stroke (0.93%) and Herniation (1,2%)
Chow et al. (2000) (98)	46	SC,II	RGBM, AO, AAS	Carboplatin (600 mg/ hemisphere)	S	Cereport 300 ng/kg	32% SD or better, PFS 2.9 months average, median OS 6.8 months (23/41) and 10.8 months (18/41)	US
Kochi et al. (2001) (99)	42	MC,II†	NGBM	Nimustine (80 mg/m2)	nS	–	Median survival time 17 months/16 months† and PFS 6 months/11 months†	Reversible vision loss (2.4%)
Madajewicz et al. (2000) (100)	83	SC, II†	GBM,AAS	Etoposide (40) mg/m2 and Cisplatin (60 mg/m2)	nS	–	48% PR or better, Median survival time 18 months	Blurred vision (4.8%), Focal seizures (6%)
Ashby and Shapiro (2001) (101)	25	SC, II	RGBM, AAS, AO, AOA	Cisplatin (60 mg/m2)	nS	–	40% SD or better and PFS 4.5 months	Headache, Increased Seizure frequency, and Encephalopathy (45%)
Gobin et al. (2001) (83)	113	SC, not stated	GBM, AAS, MET, other	Carboplatin 100–1400 mg/ hemisphere	S	Cereport 300 ng/kg	–	Seizures (7%), Major Neurologic deterioration (<0.6%)
Qureshi et al. (2001) (102)	24	SC, not stated	RGBM, AAS, MET, mixed glioma	Carboplatin 34–277 mg/m2	S	Cereport 147–366 mg/m2	Decreased tumor size in 30%, Median OS > 12 months survival in 12 patients	Transient neurologic deficits (20%), Stroke (4%)
Newton et al. (2002) (103)	25	SC, II	AAS, AOA, AO, O, BSG, ME	Carboplatin (200 mg/m2/d)	nS	–	80% SD or better, PFS 6 months	Transient ischemic attack (8%)
Silvani et al. (2002) (104)	15	SC, II†	NGBM	Carboplatin 200 mg/m2 and ACNU 100 mg/m20	nS	–	78.6%/66% SD, PFS 5.2 months/5.8 months†	Seizures (6.6%), Intracerebral hemorrhage (6.6%)
Fortin et al. (2005) (32)	72	SC, II	GBM, AAS,AO, MET, other	Carboplatin protocol Carboplatin, 400 mg/m2 with Cyclophosphamide, 330–660 mg/m2 IV Etoposide 400mg/ m2 IV Methotrexate protocol Methotrexate 5000 mg with cyclophosphamide 500 mg/m2 IV andEtoposide 150 mg/m2 IV	nS	Mannitol	Median survival time 9.1 months, median PFS 4.1 months	Thrombocytopenia; Neutropenia; seizures; orbital myositis
Hall et al. (2006) (105)	8	MC, Retrospective analysis	Recurrent DIPG	Carboplatin, 400 mg/m2 Cyclophosphamide, 660 mg/ m2 IV Etoposide 400 mg/m^2 IV Methotresxate, 5000 mg Cyclophosphamide 1000 mg/ m2 IV Etoposide 400 mg/m^2 IV	nS	Mannitol 25% 4–10 cc/s for 30s	Median PFS 15 months, Median OS 27 months	Thrombocytopenia, Neutropenia, infections, neurological disorientation; hearing loss

(Continued)

TABLE 1 Continued

Study (year)	Number of patients	Study type and phase	Brain tumors	Chemotherapeutic agent Dose	Method of delivery	BBBD Agent	Outcome	Neurotoxicity
Imbesi et al. (2006) (80)	17	SC, III†	NGBM	Nimustin (ACNU) 80–100 mg/m2	nS	Mannitol 18% 250 ml	Median OS 17 months, Time to progression was 6 months in case of i.a. ACNU and 4 months for i.v. ACNU	Stroke (5.6%)
Angelov et al. (2009) (106)	149	MC, analysis	PCNSL	Methotrexate not stated, etoposide (150 mg/m2 IV) or cyclophosphamide (15 mg/kg IV and procarbazine (100 mg orally d. Between 1994 and 2005, etoposide or etoposide phosphate (150 mg/m2 IV days) and cyclophosphamide (500 mg/m2 IV) were used.	nS	Mannitol 25%	Median overall survival was 3.1 years (25% estimated survival at 8.5 years). Median progression-free survival (PFS) was 1.8 years, with 5-year PFS of 31% and 7-year PFS of 25%	focal seizures (9.2%)
Guillaume et al. (2010) (107)	13	SC, 1	AO,AOA	Carboplatin (IA, 200 mg/m2), etoposide phosphate (IV, 200 mg/m2), and melphalan (IA, dose escalation) every 4 weeks, for up to 1 year	nS	Mannitol	77% SD or better, PFS 11 months	Speech impairment (7.7%), Retinopathy (7.7%)
Boockvar et al. (2011) (108)	30	SC, 1	RGBM, AAS, AO	Bevacizumab 2–15 mg/kg	S	Mannitol 25% 1.4M	Naiüve group: 34.7% median tumor volume reduction Exposed group: 15.7% median tumor volume reduction	Seizures (6.6%)
Shin et al. (2012) (109)	3	SC, I/II	RGBM	Bevacizumab 13 mg/kg Temozolomide 83mL (199mg) + 22mL (53mg) Cetuximab 100mg/m2	S	Mannitol 25% 10 mL	Decreased tumor size a 1 month	Good tolerance
Jeon et al. (2012) (110)	18	I,II	RGBM	Bevacizumab 2-15 mg/kg	S	Mannitol 10 mL 25% 1.4 mol/L	SD at 10 months in 11 patients, PR in 5 patients, progression in 1 patient and mixed response in 1 patient	Good tolerance
Fortin et al. (2014) (111)	51	II	RGBM	Carboplatin 400 mg/m2 Melphalan 10mg/m2	nS	–	Median PFS 23 months, Median OS 11 months, CR in 3 patients, PR in 22 patients, SD in 14 patients, progression of tumor in 12 patients	Hematological complication
Chakraborty et al. (2016) (81)	15	I	RGBM	Cetuximab 100, 200, 250 mg/m2	S	Mannitol 20% 12,5 ml/120s	–	Good tolerance
Galla et al. (2017) (112)	65	I,II	RGBM	Bevacizumab 2-15 mg/kg	S	Mannitol 25% 1.4 M	41 patients survived less than 1 year 24 patients survived more than 1 year	–
Faltings et al. (2019) (113)	1	Case report	RGBM	Bevacizumab (15 mg/kg	S	Mannitol 20% 12.5 mL	OS was 24.1 months. Patient with recurrent GBM who had received treatment from 3 clinical trials, including a	Tolerable side effects

(Continued)

TABLE 1 Continued

Study (year)	Number of patients	Study type and phase	Brain tumors	Chemotherapeutic agent Dose	Method of delivery	BBBD Agent	Outcome	Neurotoxicity
							rechallenge with SIACI of bevacizumab. After the third trial, the MRI scan demonstrated improvement based on Response Assessment In Neuro-Oncology criteria.	
Patel et al. (2021) (114)	23	I,II	NGBM	Bevacizumab (15 mg/kg)	S	Mannitol 20% (12.5 ml over 120 s)	Median PFS was 11.5 months Median overall survival was 23.1 months	Tolerable side effects
McCrea et al. (2021) (115)	13	I	GBM, DIPG	Bevacizumab (15 mg/kg) with cetuximab (200 mg/m2)	S	12.5 ml of 20% mannitol	The mean overall survival for the 10 DIPG patients treated was 519 days. The ranges for overall survival for the 3 non-DIPG patients were 311–914 days.	epistaxis (2 patients) and grade I rash (2 patients)

GBM, glioblastoma multiforme; NGBM, newly diagnosed glioblastoma multiforme; RGBM, recurrent glioblastoma multiforme;BSG, brain stem glioma; AO, anaplastic oligodendroglioma; O, oligodendroglioma;AAS, anaplastic astrocytoma; AS, astrocytoma; OA, oligoastrocytoma; AOA, anaplastic oligoastrocytoma;MET, metastasis; PCNSL, primary CNS lymphoma; PNET, primitive neuroepithelial tumor; GCT, germ cell tumor; ME, malignant ependymoma; US, unspecified; S, selective;nS, not selective; SD, stable diseases; PR, partial response; PFS, progression free survival; † comparison of intra-arterial/intravenous delivery; SC, single center; MC, multi-center; IA, intra-arterial; IV,intravenous; CR, complete response; DIPG, diffuse intrinsic pontine glioma.

mg/m2) in 15 patients suffering from recurrent high-grade primary brain tumours demonstrated ambiguous results as some patients had a low objective response rate (7%), while another 33% showed stabilisation of disease over 8–40 weeks (126). More recently, Chehimi et al. have evaluated the efficacy of IA idarubicin (12mg/m2) in two recurrent and progressive GBM patients that had failed after temozolomide and bevacizumab treatment (127). Prior to starting the treatment, the authors tested idarubicin against four human GBM cell lines and observed sensitivity to concentrations in the range of 3 μg/mL of idarubicin (127). On the 3rd day after IA administration, the first patient experienced a neurological event that involved worsening left hemiparesis and severe cognitive impairment, making additional treatment impossible. In contrast, the second patient tolerated IA idarubicin, showing adverse events and a stable follow-up on an MRI scan after 4 weeks (127).

Although the Stupp protocol remains a gold standard for the treatment of GBM since its publication, the idea of IA delivery of temozolomide (TMZ) has been abandoned once studies have reported toxicities and decided that TMZ in its current formulation is unsafe for IA infusion (11, 128). The low efficacy of IA delivery of temozolomide is attributable to the fact that glioblastoma stem cells (GSCs) were proven to be resistant to it (129). In comparison, IA delivery of platinum analogs was associated with a smaller amount of cerebral side effects, especially after the incorporation of selective IA infusion (10, 11, 98, 102). In summary, side effects were shown to be reversible or manageable, proving the safety of IA delivery of platinum analogs. More importantly, according to numerous authors, IA delivery of platinum analogs may lead to a modest response rate and increased time to progression (10, 11, 98, 102, 103). Nonetheless, it is difficult to precisely evaluate the efficacy of platinum analogs as they were used in combination with other drugs (10, 11, 98, 102, 103). Consequently, the efficacy of IA delivery of platinum analogs necessitates further examination (10, 11, 103).

Intra-arterial delivery of carboplatin, methotrexate, cyclophosphamide and etoposide resulted in a high degree of tumour response in chemotherapy-sensitive tumours, such as primary central nervous system lymphoma (PCNSL), primitive neuroectodermal tumour (PNET), germ cell tumour and cancer metastasis to the brain (11, 97). According to a large, multi-institutional study of 149 patients with newly diagnosed primary CNS lymphoma, intracarotid or intra-vertebral IA delivery of methotrexate with osmotic BBB disruption led to a 5-year PFS of 31%, 7-year PFS of 25%, and median OS of 14 years in low-risk patients (11, 106). Nonetheless, results of IA delivery of the aforementioned drugs fall short of providing a relevant benefit in glioblastomas patients (11, 97). IA therapy of these drugs is not superior to IV chemotherapy in the treatment of glioblastomas (9). What could explain this phenomenon is glioblastomas' significant resistance to various anticancer drugs or the fact that some of these drugs have rapid transit through the CNS and, thus, a limited dwell time (9, 11). Last but not least, the inadequate mixing or streaming of the drug solution within the artery may result in variable drug distribution within the brain or the tumour after the intracarotid delivery (9, 11). Besides ensuring a large patient group and adequate follow-up, future clinical trials should approach these factors to allow for precise evaluation of the efficacy of the given agent.

TABLE 2 Current clinical trials concerning the use of IA for the treatment of GBM.

Study title	Location	Status	Brain tumour	Estimated enrollment	Method of delivery	Chemotherapeutic, dose	Mannitol dose	Phase
Repeated Super-selective Intraarterial Cerebral Infusion Of Bevacizumab Plus Carboplatin For Treatment Of Relapsed/Refractory GBM And Anaplastic Astrocytoma	Lenox Hill Brain Tumor Center	Suspended	Glioblastoma Multiforme Anaplastic Astrocytoma	54	SSIACI	Bevacizumab Up to 15 mg/kg Carboplatin 150 mg/m^2	NS	1 2
Super-Selective Intraarterial Cerebral Infusion Of Temozolomide (Temodar) For Treatment Of Newly Diagnosed GBM And AA	Lenox Hill Brain Tumor Center	Completed	Glioblastoma Multiforme Anaplastic Astrocytoma	21	SSIACI	Temozolomide 75–250 mg/m^2	NS	1
Repeated Super-selective Intraarterial Cerebral Infusion of Bevacizumab (Avastin) for Treatment of Relapsed GBM and AA	Lenox Hill Brain Tumor Center	Recruiting	Glioblastoma Multiforme Anaplastic Astrocytoma	54	SSIACI	Bevacizumab 15 mg/kg	20% 12.5 mL/s	1 2
Super-Selective Intraarterial Intracranial Infusion of Avastin (Bevacizumab)	Lenox Hill Brain Tumor Center	Completed	Glioblastoma Multiforme Anaplastic Astrocytoma	30	SSIACI	Bevacizumab 2–10 mg/kg	NS	1
Super-Selective Intraarterial Cerebral Infusion of Cetuximab (Erbitux) for Treatment of Relapsed/Refractory GBM and AA	Lenox Hill Brain Tumor Center	Completed	Glioblastoma Multiforme Anaplastic Astrocytoma	15	SSIACI	Cetuximab 100–500 mg/m^2	25% 3–10 mL	1
Super Selective Intra-arterial Repeated Infusion of Cetuximab (Erbitux) With Reirradiation for Treatment of Relapsed/Refractory GBM, AA, and AOA	Lenox Hill Brain Tumor Center	Recruiting	Glioblastoma Multiforme Anaplastic Astrocytoma Anaplastic Oligoastrocytoma	37	SSIACI	Cetuximab 250 mg/m^2	20% 12,5 mL	2
Super-Selective Intraarterial Intracranial Infusion of Bevacizumab (Avastin) for Glioblastoma Multiforme	Global Neurosciences Institute	Recruiting	Glioblastoma Multiforme	30	SSIACI	Bevacizumab 15 mg/kg	NS	1
Repeated Super-Selective Intraarterial Cerebral Infusion of Bevacizumab (Avastin) for Treatment of Newly Diagnosed GBM	Lenox Hill Brain Tumor Center	Active, not recruiting	Glioblastoma Multiforme Anaplastic Astrocytoma	25	SSIACI	Temozolomide 75–250 mg/m^2	NS	1 2
IA Carboplatin + Radiotherapy in Relapsing GBM	Université de Sherbrooke	Unknown	Glioblastoma Multiforme	35	IA	Carboplatin 400 mg/m^2	NA	1 2
Super-selective Intra-arterial Repeated Infusion of Cetuximab for the Treatment of Newly Diagnosed Glioblastoma	Lenox Hill Brain Tumor Center	Recruiting	Glioblastoma Multiforme	33	SSIACI	Cetuximab 250 mg/m^2	20% 12.5 mL	1 2
ADV-TK Improves Outcome of Recurrent High-Grade Glioma (HGG-01)	Huazhong University of Science and Technology	Completed	Glioblastoma Multiforme	47	IA	Replication-deficient adenovirus mutant ADV-TK, a total of 1×10^{12} viral administered in the clinical trial	25% 1.4 M mannitol	2
Oncolytic Adenovirus DNX-2401 in Treating Patients With Recurrent High-Grade Glioma	M.D. Anderson Cancer Center	Recruiting	Anaplastic Astrocytoma Glioblastoma Multiforme Recurrent Gliosarcoma Recurrent Malignant Glioma	36	IA	Oncolytic Adenovirus Ad5-DNX-2401, dose not stated	NS	1

(Continued)

TABLE 2 Continued

Study title	Location	Status	Brain tumour	Estimated enrollment	Method of delivery	Chemotherapeutic, dose	Mannitol dose	Phase
Intraarterial Infusion Of Erbitux and Bevacizumab For Relapsed/ Refractory Intracranial Glioma In Patients Under 22	Weill Medical College of Cornell University	Recruiting	Glioblastoma Multiforme Anaplastic Astrocytoma Diffuse Intrinsic Pontine Glioma	30	SSIACI	Erbitux 200 m/m^2 Bevacizumab 15 mg/kg	Mannitol 25% 10 mL	1 2

NS, not specified; SIACI, super-selective intra arterial cerebral infusion.

Monoclonal antibodies in IA for the treatment of GBM

Bevacizumab

Vascular endothelial growth factor A (VEGF-A) is the most overexpressed mediator of angiogenesis in glioblastomas multiforme, leading to poorer prognosis (11, 129). This provided rationale for the use of bevacizumab, a monoclonal antibody that blocks the binding of VEGF-A to its receptors in the perivascular niche, which is rich in GSCs and located externally to the luminal side of the vessel (11, 112). The pharmacological mechanism of catheter delivered bevacizumab in the treatment of glioblastoma has been illustrated in Figure 3. Results coming from studies, as well as clinical series, have shown that bevacizumab effectively inhibits the formation of new blood vessels and affects the existing brain vasculature leading to vascular normalisation, reduced permeability, and an increase in blood flow velocity (2, 130). This may aid in restoring the normal structure and function of blood vessels as well as decrease tumour-related oedema (130). Although bevacizumab has demonstrated highly encouraging results in patients with newly diagnosed and recurrent GBM by improving 6-month progression-free survival, there are no improvements in terms of overall survival (11, 37, 131, 132). According to Baumgarten, bevacizumab produces different dose-dependent effects on glioma blood vessels and tumour cells (2). Low doses result in a substantial reduction of the total vascular volume without affecting tumour cell viability or the overall tumour growth rates, whereas medium and high doses, besides providing a similar vascular regression, also significantly decrease tumour growth by inhibiting the ability of GSCs to self-renew (2, 10). Furthermore, bevacizumab inhibits the transformation of GSCs into endothelial cell progenitors, which subsequently grow into mature endothelial cells (10, 132). Nonetheless, despite the reasonable response rate during the first few months after bevacizumab treatment, patient survival does not improve as patients still progress and require salvage therapy (10, 108, 133). This may be attributable to the insufficient delivery of bevacizumab through the BBB. Considering that the pore size of BBB is approximately 12nm, bevacizumab, with its size of 15nm, is too big to efficiently penetrate through the BBB (10, 134). Boockvar et al. hypothesised that increasing the concentration of bevacizumab in the perivascular niche could increase the efficacy of inhibiting GCSs, consequently providing better therapeutic results (10). Research focusing on SSIACI of bevacizumab after hyperosmolar BBB disruption for recurrent GBM has evaluated that 15 mg/kg is the maximum tolerated dose (MTD) (10, 11, 108). IA treatment of bevacizumab has an edge over IV treatment, given that studies reported a median PFS of 3.9 months in case of IA bevacizumab and median PFS from

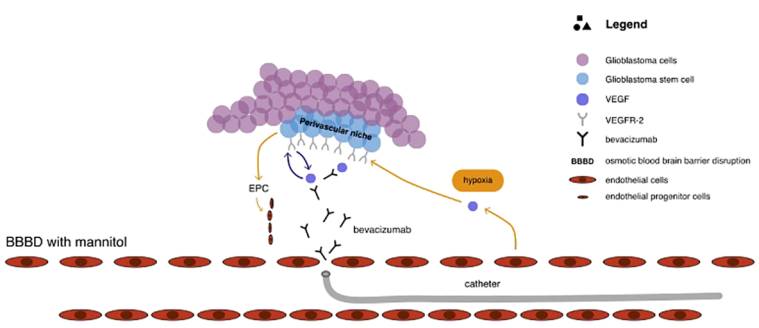

FIGURE 3
The pharmacological mechanism of catheter delivered bevacizumab in the treatment of glioblastoma.

3.3 to 3.7 months in case of IV treatment (11, 135, 136). Chakraborty et al. have evaluated that a single SIACI of BV at 15mg/kg after BBD with mannitol allowed obtaining similar or better PFS in comparison to a biweekly IV infusion of bevacizumab at 10mg/kg (137). Zawadzki et al. have performed three intra-arterial deliveries of bevacizumab under real-time MRI guidance in a patient with butterfly-shaped recurrent glioblastoma as a sole treatment (138). The patient managed to survive 6 months after MRI detection of aggressive regrowth (138). All administrations were safe and uneventful. According to the authors, the therapeutic effects of intra-arterial bevacizumab offered reproducible symptomatic relief which lasted 7-8weeks (138).

It remains unclear if repeated SIACI of bevacizumab after BBBD with mannitol have a long term therapeutic effect, but ongoing clinical trials (Table 2) should provide answers (11).

Cetuximab

Epidermal growth factor receptor (EGFR) is a potent oncogene, frequently amplified and mutated in high-grade gliomas, prompting diagnosis to be unfavourable (11, 139). Cetuximab is a chimeric human monoclonal antibody that binds and competitively inhibits EGFR, thus reducing signal transduction. Tumour growth is inhibited, and the ultimate result is cell death (81, 139). Given that cetuximab diminishes angiogenesis, combined therapy of cetuximab with bevacizumab could have a synergistic effect on angiogenesis (140). Studies have demonstrated that cetuximab increases activity with radiotherapy and chemotherapy and is capable of mediating antibody-dependent cell-mediated cytotoxicity (81, 140). Phase I study of SIACI of cetuximab after BBBD with mannitol in patients with malignant glioma has estimated that MTD of 250 mg/m is safe and well-tolerated (64). Reported complications included tolerable rash (2 patients), anaphylaxis (1 patient), isolated seizure (1 patient) and seizure with cerebral edema (1 patient) (81). There is an ongoing phase II study aiming at estimating the efficacy of repeated infusion of cetuximab with reirradiation in patients with relapsed/refractory glioblastoma (NCT02800486).

Recently, a phase I trial of 13 paediatric patients with refractory diffuse intrinsic pontine glioma (DIPG) and glioblastoma has shown that super-selective intra-arterial cerebral infusion (SIACI) of bevacizumab (15 mg/kg) and cetuximab (200 mg/m2) is well-tolerated (115). The mean overall survival for the 10 DIPG patients treated was 519 days, whereas the ranges for overall survival for the 3 non-DIPG patients were 311–914 days (115).

Emerging potential therapeutic approaches

Researchers have been actively evaluating and looking for potential therapeutic agents that could increase the survival of glioblastoma patients. Greenberg et al. have shown that catheter injection of anaerobic radiosensitizer such as bromodeoxyuridine into the external carotid artery led not only to an increased susceptibility of glioma cells to radiotherapy but also to increased survival time of GBM patients (141). Subsequently, research on animal models demonstrated that intra-carotid injection of recombinant human TNF and lymphotoxin allows producing significant anti-tumour effects in C6 and T9 gliomas (142). Yoshida et al. reported a 20% response rate after a non-selective administration of recombinant human tumour necrosis factor-a in malignant glioma patients (143).

Tumour-treating fields (TTFields) have been hypothesised as yet another potential treatment for recurrent as well as newly diagnosed glioblastoma. By delivering low-intensity (1-3 V/cm), intermediate-frequency (100-300 kHz) alternating electric fields *via* transducer arrays applied to the scalp, TTFields lead to mitotic arrest and apoptosis of quickly dividing cells. A randomised Phase III clinical trial involving 237 patients with recurrent glioblastoma, in whom prior therapy had failed, compared the TTFields as a monotherapy to chemotherapy (144). Even though there was no statistically significant difference in regard to survival, TTFields demonstrated efficacy and activity similar to the chemotherapy regimens, with lesser toxicity and overall improvement in quality of life (144). A 2009 Phase 3 clinical trial involving patients with newly diagnosed glioblastoma found that adding TTFields to maintenance temozolomide chemotherapy resulted in statistically significant improvement in survival (6.7 months vs 4.0 months) (145)

Gene therapy

Animal studies have shown the potential therapeutic benefits associated with gene therapy. The growth of Gli36 glioblastoma tissue carrying a missense-mutated p53 gene can be impeded by intra-arterial delivery of a p53-containing adenoviral vector, whereas intra-arterial administration of a plasmid encoding anti-angiogenic endostatin resulted in decreasing tumour vascular density, perfusion, and permeability, consequently allowing to prolong survival time in the rat 9L gliosarcoma model (69, 146, 147). A Phase II clinical trial evaluated an intra-arterial delivery of ganciclovir combined with replication-deficient adenovirus mutant thymidine kinase. Results demonstrated a significant improvement in 6-month progression-free survival, overall progression-free survival, and overall survival in patients suffering from recurrent high-grade gliomas (69, 148).

Cell therapy

A concerted effort in the development of new glioblastoma treatments has led to animal studies evaluating the role of cell therapy (69). Goerger and colleagues have shown that early-stage intracarotid delivery of a human cytotoxic T-cell line (TALL-104) in the 9L glioblastoma model significantly increased survival rates (149). A study on animal models has

shown that injection of a murine colon cancer cell line (CT-26) overexpressing interleukin-4 (IL- 4) or hemagglutinin antigen resulted in systemic immunity against liver and lung metastases but not against brain metastases (150).

Recently, the interest has shifted towards genetic engineering of T cells to express chimeric antigen receptors (CARs) directed against specific antigens (151). Once the tumour-associated antigen is identified, CAR T cells specific to that antigen can induce antitumor responses in a human leukocyte antigen (HLA)-independent manner (151). Early results of systemic delivery have shown safety and optimistic results in regard to efficacy (151). However, intra-arterial delivery has been only evaluated in studies with liver metastases due to colorectal cancer, demonstrating safety and encouraging results (152, 153). Nonetheless, the possibility of any therapeutic applications is strongly limited by the scarcity of research and lack of clinical trials.

What lays ahead

As much as the renewed interest brought new advancements and progress with IA therapies to neuro-oncology, there is still massive room for improvement. Glioblastomas multiforme constitute a highly heterogeneous entity, both functional and morphologic (129, 154). Although *in vitro* all clones demonstrate neuronal precursor phenotype, individual clone-derived populations overexpress various different GBM markers (such as EGFR, EGFRvIII, and PTEN) and characterise by a dissimilar response to a variety of drugs (129). Considering this, the likelihood of a single therapeutic agent which will be effective for the treatment of glioblastoma multiforme is extremely low. Thus, it is paramount to establish an adequate multimodal therapy, which will have a synergistic effect on the diverse pathogenesis of GBM (11, 129). Other approaches include a personalised choice of intra-arterial therapy based on tumour genetic phenotype and *in-vitro* testing. There are multiple mechanisms underlying the drug resistance of glioblastomas, depending on both tumour-intrinsic factors and tumour microenvironment-dependent factors. Effective treatment for glioblastoma demands obtaining detailed pathological, genomic, transcriptomic, and epigenetic data to precisely determine the source of drug resistance (7). Considering that there are numerous mechanisms of resistance and the high intra-tumour heterogeneity of glioblastoma, precision medicine will undoubtedly have to rely on multiple drugs leading to a synergistic effect (7).

As much as hyperosmolar disruption of the BBB is an effective and popular technique, a more profound understanding of the pharmacological kinetics of BBB will allow estimating the most effective dose for a specific agent (11, 29). In order to obtain the best results possible with SIACI, technical aspects such as the selection of cerebral vessels, incorporation of catheters with balloons, flow arrest, or pulsatile injections have to be adequately incorporated (11). Recent preclinical and clinical studies have demonstrated that adding MRI to guide IA infusion rather than relying solely on X-ray is highly advantageous (155, 156). Considering the low sensitivity of contrast agents, angiography demands a rapid bolus infusion of contrast, which significantly limits the visualisation of the smallest intracranial vessels (156). However, MRI contrast agents have a high sensitivity that allows detection of the smallest concentrations of contrast, particularly at the microcirculation level (156). MRI guidance provides the unique possibility of showing the territory of the brain parenchyma supplied by the catheter, which tends to be extremely dynamic and variable. Furthermore, MRI guidance permits modification of the infusion rate and catheter tip so that the infusion can be limited to the targeted.

Zawadzki et al. have reported the first-in-man targeted intra-arterial cerebral infusion under real-time MRI guidance to be technically feasible and safe (156). Real-time MRI guidance during microcatheter infusions offered essential quantification of the degree of overlap between the transcatheter perfusion territory and the enhancing mass, greatly helping in the selection of the faster infusion rate (156). The difference between fast and slow infusion rates and their influence on drug delivery has been illustrated in Figure 4. Given the variable vascularity of glioblastoma, angiography may fall short of localising the exact vascular supply of GBM (156, 157). According to Chen et al., who reported the first use of perfusion guidance during the infusion of mesenchymal stem cells loaded with Delta-24 (MSC-24) in the treatment of glioblastoma, the combination of preoperative anatomic MR images with real-time perfusion images from super-selective injection during angiography allows for accurate identification the vascular supply, consequently facilitating more effective intra-arterial delivery of chemotherapeutics (157). Cone-beam computed tomography (CBCT), being an inherent part of planning IA injection and determining the area of infusion, allows for generating perfusion maps, which greatly optimise the accuracy of IA delivery, limiting exposition of healthy brain parenchyma to delivered chemotherapeutics (157). Furthermore, uncomplicated determination of the perfusion volume facilitates the calculation of the adequate dose. However, what is still a limitation of this technique is the high dose of radiation during each cone-beam CT acquisition and the lack of real-time visualisation of administered drug distribution (157).

Impressive advancements in artificial intelligence throughout the last decade have resulted in the use of deep learning approaches, known as convolutional neural networks (CNNs), in glioma patients (158). Besides using MR data to grade gliomas and predict overall survival, different CNNs are used to predict the genetics of glioma on pre-operative MR images. According to a recent review, CNNs are effective in tumour grading and prediction of IDH mutation, 1p19q codeletion, MGMT promoter status, and OS, with accuracies of prediction reaching 80% to 90% (158).

10.3389/fonc.2022.950167

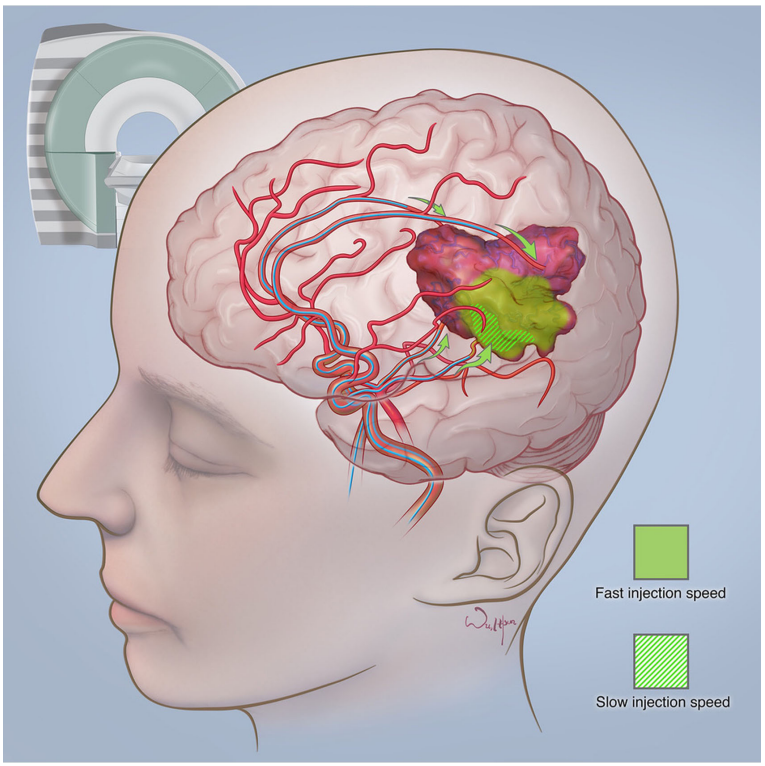

FIGURE 4
The difference between fast and slow infusion rates and their influence on drug delivery. Courtesy of the Society of Image guided Neurointerventions (SIGN).

There is a need for new robust pharmacokinetic models which will take into consideration hydrodynamic factors. It has been established that hydrodynamic factors such as the background blood flow, injection characteristics and vascular geometry have a significant role in determining tissue concentrations after IA drug injections (86). The advent of nanotechnology should also be taken into consideration, as smaller particles are subjected to substantially smaller hydrodynamic forces (86). Real-time tracking of tissue drug distribution and concentrations such as PET could significantly help in establishing reliable models (11, 86) Likewise, real-time monitoring of BBB disruption is essential for the improvement of IA cerebral infusions of chemotherapeutics in the treatment of glioblastoma multiforme. According to Kiviniemi et al., direct-current electroencephalography (DC-EEG) can be used to monitor the induced transient BBBD in anaesthetized human patients undergoing chemotherapy for PCNSL (13). DC-EEG allows for characterization of the spatiotemporal behaviour of scalp-recorded slow electrical signals during blood-brain barrier opening (13). The authors also monitored the patients with near-infrared spectroscopy (NIRS) in order to obtain information on cerebral hemodynamics that has a role in DC-EEG signal generation (13). Future clinical trials using IA delivery of chemotherapeutics in glioblastoma patients should try evaluating the use of DC-EEG for real-time monitoring of BBBD.

Conclusions

It is widely recognized that the intra-arterial route of administration ensures higher drug concentrations in targeted areas, limits systemic toxicity and is safe in experienced hands. However, although the results coming from various phase I studies are promising, due to the lack of phase III clinical trials, with only single-phase 1/phase 2 study reporting outcomes so far, it is impossible to declare the efficacy of IA delivery of chemotherapeutics in the treatment of glioblastoma multiforme. There are numerous areas of improvement necessary for the optimization of this technique and the treatment of GMB. These include: establishing an adequate multimodal therapy, which will have a synergistic effect on the diverse pathogenesis of GBM; relying on the combination of preoperative anatomic MR images with real-time perfusion images from super-selective injection during angiography to accurately identify the vascular supply; conducting precise quantitative and spatial monitoring necessary to guarantee the accurate delivery of the therapeutic to the tumour

andestimating the most effective dose of a specific agent for hyperosmolar BBB disruption. Considering the significant heterogeneity of GBM, treatment should be individualised to each patient after obtaining detailed pathological, genomic, transcriptomic, and epigenetic data. Quantum leaps in intrathecal, intracavitary and convection-enhanced delivery, or pharmacological advancements leading to the development of nanoparticles capable of effectively passing BBB, all could potentially challenge the whole premise of intra-arterial delivery. Nonetheless, we believe that the idea of IA infusion for the treatment of malignant brain tumours guided by the fusion of pre-procedural brain MRI to intra-procedural CBCT will not be abandoned for the sake of other methods of drug delivery. It is because controlled and highly precise catheter infusions are not only extremely effective at ensuring high local concentrations of the chemotherapeutic but are safe in experienced hands. With the development of effective agents against glioblastoma, intra-arterial cerebral infusions have the potential to become the mainstay of glioblastoma treatment and offer patients a chance at longer survival.

Data availability statement

The original contributions presented in the study are included in the article/supplementary material. Further inquiries can be directed to the corresponding author.

Author contributions

MaP analysed data and drafted the initial form of the manuscript. MiP analysed data, drafted the manuscript and created tables. JW edited the manuscript and analysed data. MZ analysed data, edited the manuscript and approved its final form. All authors contributed to the article and approved the submitted version.

Conflict of interest

The authors declare that the research was conducted in the absence of any commercial or financial relationships that could be construed as a potential conflict of interest.

Publisher's note

All claims expressed in this article are solely those of the authors and do not necessarily represent those of their affiliated organizations, or those of the publisher, the editors and the reviewers. Any product that may be evaluated in this article, or claim that may be made by its manufacturer, is not guaranteed or endorsed by the publisher.

References

1. Lesniak WG, Chu C, Jablonska A, Du Y, Pomper MG, Walczak P, et al. A distinct advantage to intraarterial delivery of 89Zr-bevacizumab in PET imaging of mice with and without osmotic opening of the blood-brain barrier. *J Nucl Med* (2019) 60(5):617–22. doi: 10.2967/jnumed.118.218792

2. von Baumgarten L, Brucker D, Tirniceru A, Kienast Y, Grau S, Burgold S, et al. Bevacizumab has differential and dose-dependent effects on glioma blood vessels and tumor cells. *Clin Cancer Res* (2011) 17(19):6192–205. doi: 10.1158/1078-0432.CCR-10-1868

3. Reifenberger G, Wirsching HG, Knobbe-Thomsen CB, Weller M. Advances in the molecular genetics of gliomas - implications for classification and therapy. *Nat Rev Clin Oncol* (2017) 14(7):434–52. doi: 10.1038/nrclinonc.2016.204

4. Bray F, Ferlay J, Soerjomataram I, Siegel RL, Torre LA , Jemal A. Global cancer statistics 2018: GLOBOCAN estimates of incidence and mortality worldwide for 36 cancers in 185 countries [published correction appears in CA cancer J clin. *CA Cancer J Clin* (2020) 68(6):394–424. doi: 10.3322/caac.21492

5. Jacques TS, Swales A, Brzozowski MJ, Henriquez NV, Linehan JM, Mirzadeh Z, et al. Combinations of genetic mutations in the adult neural stem cell compartment determine brain tumour phenotypes. *EMBO J* (2010) 29:222–35. doi: 10.1038/emboj.2009.327

6. Stupp R, Mason WP, van den Bent MJ, Weller M, Fisher B, Taphoorn MJ, et al. Radiotherapy plus concomitant and adjuvant temozolomide for glioblastoma. *N Engl J Med* (2005) 352(10):987–96. doi: 10.1056/NEJMoa043330

7. Kopecka J, Riganti C. Overcoming drug resistance in glioblastoma: new options in sight? *Cancer Drug Resist* (2021) 4:512–6. doi: 10.20517/cdr.2021.03

8. Fakhoury M. Drug delivery approaches for the treatment of glioblastoma multiforme. *Artif Cells Nanomed Biotechnol* (2016) 44(6):1365–73. doi: 10.3109/21691401.2015.1052467

9. Chen W, Wu Q, Mo L, Nassi M. Intra-arterial chemotherapy is not superior to intravenous chemotherapy for malignant gliomas: a systematic review and meta-analysis. *Eur Neurol* (2013) 70(1-2):124–32. doi: 10.1159/000346580

10. Burkhardt JK, Riina HA, Shin BJ, Moliterno JA, Hofstetter CP, Boockvar JA. Intra-arterial chemotherapy for malignant gliomas: a critical analysis [published correction appears in interv neuroradiol. *Interv Neuroradiol* (2011) 17(3):286–95:506. doi: 10.1177/159101991101700302

11. D'Amico RS, Khatri D, Reichman N, Patel NV, Wong T, Fraling SH, et al. Super selective intra-arterial cerebral infusion of modern chemotherapeutics after blood-brain barrier disruption: where are we now, and where we are going [published correction appears in J neurooncol. *J Neurooncol* (2020) 147(2):261–78. doi: 10.1007/s11060-020-03435-6

12. Basso U, Lonardi S, Brandes AA. Is intra-arterial chemotherapy useful in high-grade gliomas? *Expert Rev Anticancer Ther* (2002) 2(5):507–19. doi: 10.1586/14737140.2.5.507

13. Bierman HR, Byron RLJr., Miller ER, Shimkin MB. Effects of intra-arterial administration of nitrogen mustard. *Amer. J Med* (1950) 8:535. doi: 10.1016/0002-9343(50)90263-4

14. Bierman HR, Byron RLJr., Kelly KH. Therapy of inoperable visceral and regional metastases by intra-arterial catheterization in man. *Cancer Res* (1951) 11:236.

15. Klopp CT, Alford TC, Bateman J, Berry GN, Winship T. Fractionated intra-arterial cancer. Chemotherapy with methyl bis amine hydrochloride; A preliminary report. *Ann Surg* (1950) 132:811–32. doi: 10.1097/00000658-195010000-00018

16. French JD, West PM, Von Amerongen FK, Magoun HW. Effects of intracarotid administration of nitrogen mustard on normal brain and brain tumors. *J Neurosurg* (1952) 9:378–89. doi: 10.3171/jns.1952.9.4.0378

17. Wilson CB. Chemotherapy of brain tumors by continuous arterial infusion. *Surgery* (1964) 55:640–65321.

18. Owens G, Javid R, Belmusto L, Bender M, Blau M. Intra-arterial vincristine therapy of primary gliomas. (1965) 18:756–60. doi: 10.1002/1097-0142(196506)18:6<756::AID-CNCR2820180613>3.0.CO;2-#

19. Eckman WW, Patlak CS, Fenstermacher JD. A critical evaluation of the principles governing the advantages of intra-arterial infusions. *J Pharmacokinet Biopharm* (1974) 2:257–85. doi: 10.1007/BF01059765

20. Rapoport SI, Hori M, Klatzo I. Testing of a hypothesis for osmotic opening of the blood-brain barrier. *Am J Physiol* (1972) 223:323–31. doi: 10.1152/ajplegacy.1972.223.2.323

21. Neuwelt EA, Maravilla KR, Frenkel EP, Rapaport SI, Hill SA, Barnett PA. Osmotic blood-brain barrier disruption Computerized tomographic monitoring of chemotherapeutic agent delivery. *J Clin Invest* (1979) 64(2):684–8. doi: 10.1172/JCI109509

22. Neuwelt EA, Frenkel EP, Diehl JT, Maravilla KR, Vu LH, Clark WK, et al. Osmotic blood-brain barrier disruption: A new means of increasing chemotherapeutic agent delivery. *Trans Am Neurol Assoc* (1979) 104:256–60.

23. Neuwelt EA, Glasberg M, Diehl J, Frenkel EP, Barnett P. Osmotic blood-brain barrier disruption in the posterior fossa of the dog. *J Neurosurg* (1981) 55:742–8. doi: 10.3171/jns.1981.55.5.0742

24. Neuwelt EA, Frenkel EP, D'Agostino AN, Carney DN, Minna JD, Barnett PA, et al. Growth of human lung tumor in the brain of the nude rat as a model to evaluate antitumor agent delivery across the blood-brain barrier. *Cancer Res* (1985) 45:2827–33.

25. Neuwelt EA, Barnett PA, McCormick CI, Remsen LG, Kroll RA, Sexton G. Differential permeability of a human brain tumor xenograft in the nude rat: impact of tumor size and method of administration on optimizing delivery of biologically diverse agents. *Clin Cancer Res* (1998) 4:1549–55.

26. Levin VA, Kabra PM, Freeman-Dove MA. Pharmacokinetics of intracarotid artery 14C-BCNU in the squirrel monkey. *J Neurosurg* (1978) 48(4):587–93. doi: 10.3171/jns.1978.48.4.0587

27. Greenberg HS, Ensminger WD, Chandler WF, Layton PB, Junck L, Knake J, et al. Intra-arterial BCNU chemo- therapy for treatment of malignant gliomas of the central nerv- ous system. *J Neurosurg* (1984) 61:423–9. doi: 10.3171/jns.1984.61.3.0423

28. Fenstermacher JD, Johnson JA. Filtration and reflec- tion coefficients of the rabbit blood-brain barrier. *Am J Physiol* (1966) 211:341–6. doi: 10.1152/ajplegacy.1966.211.2.341

29. van Tellingen O, Yetkin-Arik B, de Gooijer MC, Wesseling P, Wurdinger T, de Vries HE. Overcoming the blood-brain tumor barrier for effective glioblastoma treatment. *Drug Resist Updat* (2015) 19:1–12. doi: 10.1016/j.drup.2015.02.002

30. Ningaraj NS, Rao M, Hashizume K, Asotra K, Black KL. Regulation of blood-brain tumor barrier permeability by calcium-activated potassium channels. *J Pharmacol Exp Ther* (2002) 301(3):838–51. doi: 10.1124/jpet.301.3.838

31. Siegal T, Rubinstein R, Bokstein F, Schwartz A, Lossos A, Shalom E, et al. *In vivo* assessment of the window of barrier opening after osmotic blood-brain barrier disruption in humans. *J Neurosurg* (2000) 92(4):599–605. doi: 10.3171/jns.2000.92.4.0599

32. Fortin D, Desjardins A, Benko A, Niyonsega T, Boudrias M. Enhanced chemotherapy delivery by intraarterial infusion and blood-brain barrier disruption in malignant brain tumors: the sherbrooke experience. *Cancer* (2005) 103:2606–2. doi: 10.1002/cncr.21112

33. Nakagawa H, Groothuis D, Blasberg RG. The effect of graded hypertonic intracarotid infusions on drug delivery to experimental RG-2 gliomas. *Neurology* (1984) 34:1571–81. doi: 10.1212/wnl.34.12.1571

34. Groothuis DR, Warkne PC, Molnar P, Lapin GD, Mikhael MA. Effect of hyperosmotic blood-brain barrier disruption on transcapillary transport in canine brain tumors. *J Neurosurg* (1990) 72:441–9. doi: 10.3171/jns.1990.72.3.0441

35. Neuwelt EA, Goldman DL, Dahlborg SA, Crossen J, Ram- sey F, Roman-Goldstein S, et al. Primary CNS lymphoma treated with osmotic blood-brain barrier disruption: prolonged survival and preservation of cognitive function. *J Clin Oncol* (1991) 9:1580–90. doi: 10.1200/JCO.1991.9.9.1580

36. Zünkeler B, RE C, Olson J, Blasberg RG, DeVroom H, Lutz RJ, et al. Quantification and pharmacokinetics of blood-brain barrier disruption in humans. *J Neurosurg* (1996) 85:1056–65. doi: 10.3171/jns.1996.85.6.1056

37. Burkhardt JK, Riina H, Shin BJ, Christos P, Kesavabhotla K, Hofstetter CP, et al. Intra-arterial delivery of bevacizumab after blood-brain barrier disruption for the treatment of recurrent glioblastoma: progression-free survival and overall survival. *World Neurosurg* (2012) 77:130–4. doi: 10.1016/j.wneu.2011.05.056

38. Bartus RT. The blood-brain barrier as a target for pharmacological modulation. *Curr Opin Drug Discov Dev* (1999) 2:152–67.

39. Gumerlock MK, Neuwelt EA. The effect of anesthesia on osmotic blood-brain barrier disruption. *Neurosurgery* (1990) 26:268–77. doi: 10.1227/00006123-199002000-00014

40. Kroll RA, Neuwelt EA. Outwitting the blood-brain barrier for therapeutic purposes: osmotic opening and other means. *Neurosurgery* (1998) 42:1083–100. doi: 10.1097/00006123-199805000-00082

41. Raymond. JJ, Robertson DM, Dinsdale HB. Pharmacological modification of bradykinin induced breakdown of the blood-brain barrier. *Neurol Sci* (1986) 13:214–22. doi: 10.1017/S0317167100036301

42. Inamura T, Black KL. Bradykinin selectively opens blood-tumor barrier in experimental brain tumors, J. *Cerebr. Blood Flow Metabol* (1994) 14:862–70. doi: 10.1038/jcbfm.1994.108

43. Prados MD, S. Clifford Schold Jr., Howard AF, Kurt J, Fred H, et al, et al. A randomized, double-blind, placebo-controlled, phase 2 study of RMP-7 in combination with carboplatin administered intravenously for the treatment of recurrent malignant glioma. *Neuro-Oncology* (2003) 52:96–103. doi: 10.1093/neuonc/5.2.96

44. Warren K, Jakacki R, Widemann B, Aikin A, Libucha M, Packer R, et al. Phase II trial of intravenous lobradimil and carboplatin in childhood brain tumors: a report from the children's oncology group. *Cancer Chemother Pharmacol* (2006) 58:343. doi: 10.1007/s00280-005-0172-7

45. Lee EJ, Fomenko A, Lozano AM. Magnetic resonance-guided focused ultrasound : Current status and future perspectives in thermal ablation and blood-brain barrier opening. *J Korean Neurosurg Soc* (2019) 62(1):10–26. doi: 10.3340/jkns.2018.0180

46. Hynynen K, McDannold N, Vykhodtseva N, Jolesz FA. Noninvasive MR imaging-guided focal opening of the blood-brain barrier in rabbits. *Radiology* (2001) 220:640–6. doi: 10.1148/radiol.2202001804

47. Hynynen K, McDannold N, Vykhodtseva N, Raymond S, Weissleder R, Jolesz FA, et al. Focal disruption of the blood-brain barrier due to 260-kHz ultrasound bursts: a method for molecular imaging and targeted drug delivery. *J Neurosurg* (2006) 105:445–54. doi: 10.3171/jns.2006.105.3.445

48. McDannold N, Arvanitis CD, Vykhodtseva N, Livingstone MS. Temporary disruption of the blood-brain barrier by use of ultrasound and microbubbles: safety and efficacy evaluation in rhesus macaques. *Cancer Res* (2012) 72:3652–63. doi: 10.1158/0008-5472.CAN-12-0128

49. McDannold N, Vykhodtseva N, Raymond S, Jolesz FA, Hynynen K. MRIguided targeted blood-brain barrier disruption with focused ultrasound: histological findings in rabbits. *Ultrasound Med Biol* (2005) 31:1527–37. doi: 10.1016/j.ultrasmedbio.2005.07.010

50. Sheikov N, McDannold N, Sharma S, Hynynen K. Effect of focused ultrasound applied with an ultrasound contrast agent on the tight junctional integrity of the brain microvascular endothelium. *Ultrasound Med Biol* (2008) 34:1093–104. doi: 10.1016/j.ultrasmedbio.2007.12.015

51. Lin F, de Gooijer MC, Hanekamp D, Brandsma D, Beijnen JH, van Tellingen O. Targeting core (mutated) pathways of high-grade gliomas: challenges of intrinsic resistance and drug efflux. *CNS Oncol* (2013) 2(3):271–88. doi: 10.2217/cns.13.15

52. de Bruin M, Miyake K, Litman T, Robey R, Bates SE. Reversal of resistance by GF120918 in cell lines expressing the ABC half-transporter, MXR. *Cancer Lett* (1999) 146(2):117–26. doi: 10.1016/s0304-3835(99)00182-2

53. Pardridge WM. Drug transport across the blood-brain barrier. *J Cereb Blood Flow Metab Off J Int Soc Cereb Blood Flow Metab* (2012) 32:1959–72:11. doi: 10.1038/jcbfm.2012.126

54. Drappatz J, Brenner A, Wong ET, Eichler A, Schiff D, Groves MD, et al. Phase I study of GRN1005 in recurrent malignant glioma. *Clin Cancer Res* (2013) 19(6):1567–76. doi: 10.1158/1078-0432.CCR-12-2481

55. Hu Y, Gaillard PJ, Rip J, de Lange EC, Hammarlund-Udenaes M. *In vivo* quantitative understanding of PEGylated liposome's influence on brain delivery of diphenhydramine. *Mol Pharmaceutics* 15(12):5493–500. doi: 10.1021/Acs.Molpharmaceut.8B00611

56. Ben-Zvi A, Lacoste B, Kur E, Andreone BJ, Mayshar Y, Yan H, et al. Mfsd2a is critical for the formation and function of the blood-brain barrier. *Nature* (2014) 509(7501):507–11. doi: 10.1038/nature13324

57. Patel B, Yang PH, Kim AH. The effect of thermal therapy on the blood-brain barrier and blood-tumor barrier. *Int J Hyperthermia* (2020) 37(2):35–43. doi: 10.1080/02656736.2020.1783461

58. Leuthardt EC, Duan C, Kim MJ, Campian JL, Kim AH, Miller-Thomas MM, et al. Hyperthermic laser ablation of recurrent glioblastoma leads to temporary disruption of the peritumoral blood brain barrier. *PloS One* (2016) 11(2):e0148613. doi: 10.1371/journal.pone.0148613

59. Rechberger JS, Thiele F, Daniels DJ. Status quo and trends of intra-arterial therapy for brain tumors: A bibliometric and clinical trials analysis. *Pharmaceutics* (2021) 13(11):1885. doi: 10.3390/pharmaceutics13111885

60. Zhao M, van Straten D, Broekman MLD, Préat V, Schiffelers RM. Nanocarrier-based drug combination therapy for glioblastoma. *Theranostics* (2020) 10(3):1355–72. doi: 10.7150/thno.38147

61. Fang C, Wang K, Stephen ZR, Mu Q, Kievit FM, Chiu DT, et al. Temozolomide nanoparticles for targeted glioblastoma therapy. *ACS Appl Mater Interfaces* (2015) 7(12):6674–82. doi: 10.1021/am5092165

62. Allhenn D, Boushehri MA, Lamprecht A. Drug delivery strategies for the treatment of malignant gliomas. *Int J Pharm* (2012) 436(1-2):299–310. doi: 10.1016/j.ijpharm.2012.06.025

63. Barua NU, Gill SS, Love S. Convection-enhanced drug delivery to the brain: therapeutic potential and neuropathological considerations. *Brain Pathol* (2014) 24 (2):117–27. doi: 10.1111/bpa.12082

64. Bidros DS, Liu JK, Vogelbaum MA. Future of convection-enhanced delivery in the treatment of brain tumors. *Future Oncol* (2010) 6(1):117–25. doi: 10.2217/fon.09.135

65. Westphal M, Lamszus K. The neurobiology of gliomas: from cell biology to the development of therapeutic approaches. *Nat Rev Neurosci* (2011) 12(9):495–508. doi: 10.1038/nrn3060

66. Mueller S, Polley MY, Lee B, Kunwar S, Pedain C, Wembacher-Schröder E, et al. Effect of imaging and catheter characteristics on clinical outcome for patients in the PRECISE study. *J Neurooncol* (2011) 101(2):267–77. doi: 10.1007/s11060-010-0255-0

67. Sampson JH, Archer G, Pedain C, Wembacher-Schröder E, Westphal M, Kunwar S, et al. Poor drug distribution as a possible explanation for the results of the PRECISE trial. *J Neurosurg* (2010) 113(2):301–9. doi: 10.3171/2009.11.JNS091052

68. Chittiboina P, Heiss JD, Warren KE, Lonser RR. Magnetic resonance imaging properties of convective delivery in diffuse intrinsic pontine gliomas. *J Neurosurg Pediatr* (2014) 13(3):276–82. doi: 10.3171/2013.11.PEDS136

69. Huang R, Boltze J, Li S. Strategies for improved intra-arterial treatments targeting brain tumors: a systematic review. *Front Oncol* (2020) 10:1443. doi: 10.3389/fonc.2020.01443

70. Jahangiri A, Chin AT, Flanigan PM, Chen R, Bankiewicz K, Aghi MK. Convection-enhanced delivery in glioblastoma: a review of preclinical and clinical studies. *J Neurosurg* (2017) 126:191–200. doi: 10.3171/2016.1.JNS151591

71. White E, Bienemann A, Taylor H, Hopkins K, Cameron A, Gill S. A phase I trial of carboplatin administered by convection-enhanced delivery to patients with recurrent/progressive glioblastoma multiforme. *Contemp Clin Trials* (2012) 33:320–31. doi: 10.1016/j.cct.2011.10.010

72. Carpentier A, Laigle-Donadey F, Zohar S, Capelle L, Behin A, Tibi A, et al. Phase 1 trial of a CpG oligodeoxynucleotide for patients with recurrent glioblastoma. *Neuro Oncol* (2006) 8:60–6. doi: 10.1215/S1522851705000475

73. Kunwar S, Chang SM, Prados MD, Berger MS, Sampson JH, Croteau D, et al. Safety of intraparenchymal convection-enhanced delivery of cintredekin besudotox in early-phase studies. *Neurosurg Focus* (2006) 20:E15. doi: 10.1155/2019/9342796

74. Chang E, Patel CB, Pohling C, Young C, Song J, Flores TA, et al. Tumor treating fields increases membrane permeability in glioblastoma cells. *Cell Death Discov* (2018) 4:113. doi: 10.1038/s41420-018-0130-x

75. Rominiyi O, Vanderlinden A, Clenton SJ, Bridgewater C, Al-Tamimi Y, Collis SJ. Tumour treating fields therapy for glioblastoma: current advances and future directions [published correction appears in br J cancer. *Br J Cancer* (2021) 124(4):697–709. doi: 10.1038/s41416-020-01136-5

76. Kessler AF, Salvador E, Domröse D, Burek M, Schaeffer C, Brami T,C, et al. Blood brain barrier (BBB) integrity is affected by tumor treating fields (TTFields) *in vitro* and *in vivo*. *Int J Radiat Oncol* (2019) 105:S162–3. doi: 10.1016/j.ijrobp.2019.06.182

77. Groothuis DR, Warkne PC, Molnar P, Lapin GD, Mikhael MA. Effect of hyperosmotic blood-brain barrier disruption on transcapillary transport in canine brain tumors. *J Neurosurg* (1990) 72(3):441–9. doi: 10.3171/jns.1990.72.3.0441

78. Marchi N, Angelov L, Masaryk T, Fazio V, Granata T, Hernandez N, et al. Seizure-promoting effect of blood-brain barrier disruption. *Epilepsia* (2007) 48:732–42. doi: 10.1111/j.1528-1167.2007.00988

79. Huang R, Boltze J, Li S. Strategies for improved intra-arterial treatments targeting brain tumors: A systematic review. *Front Oncol* (2020) 10:1443. doi: 10.3389/fonc.2020.01443

80. Imbesi F, Marchioni E, Benericetti E, Zappoli F, Galli A, Corato M, et al. A randomized phase III study: comparison between intravenous and intraarterial ACNU administration in newly diagnosed primary glioblastomas. *Anticancer Res* (2006) 26(1B):553–8.

81. Chakraborty S, Filippi CG, Wong T, Ray A, Fralin S, Tsiouris AJ, et al. Superselective intraarterial cerebral infusion of cetuximab after osmotic blood/brain barrier disruption for recurrent malignant glioma: phase I study. *J Neurooncol* (2016) 128(3):405–15. doi: 10.1007/s11060-016-2099-8

82. YL Y, Diksic M, Theron J, JG V, Worthington C, AC E, et al. Pharmacokinet- ics of superselective intra-arterial and intravenous [11C]BCNU evaluated by PET. *J Nucl Med* (1986) 27:775–80.

83. Gobin YP, Cloughesy TF, Chow KL, Duckwiler GR, Sayre JW, Milanese K, et al. Intraarterial chemotherapy for brain tumors by using a spatial dose fractionation algorithm and pulsatile delivery. *Radiology* (2001) 218(3):724–32. doi: 10.1148/radiology.218.3.r01mr41724

84. Singh-Moon RP, Roblyer DM, Bigio IJ, Joshi S. Spatial mapping of drug delivery to brain tissue using hyperspectral spatial frequency-domain imaging. *J Biomed Optics* (2014) 19(9):96003. doi: 10.1117/1.jbo.19.9.096003.096003

85. Saris SC, Bigner SH, Bigner DD. Intracerebral transplantation of a human glioma line in immunosuppressed rats. *J Neu- Rosurg* (1984) 60:582–8. doi: 10.3171/jns.1984.60.3.0582

86. Ellis JA, Banu M, Hossain SS, Singh-Moon R, Lavine SD, Bruce JN, et al. Reassessing the role of intra-arterial drug delivery for glioblastoma multiforme treatment. *J Drug Deliv* (2015) 2015):405735. doi: 10.1155/2015/405735

87. Joshi S, Singh-Moon RP, Ellis JA, Chaudhuri DB, Wang M, Reif R, et al. Cerebral hypoperfusion-assisted intra-arterial deposition of liposomes in normal and glioma-bearing rats. *Neurosurgery* (2015) 76(1):92–100. doi: 10.1227/NEU.0000000000000552

88. Joshi S, Singh-Moon RP, Wang M, Chaudhuri DB, Holcomb M, Straubinger NL, et al. Transient cerebral hypoperfusion assisted intraarterial cationic liposome delivery to brain tissue. *J Neuro-Oncolo* (2014) 118(1):73–82. doi: 10.1007/s11060-014-1421-6

89. Stewart DJ, Belanger JME, Grahovac Z, Curuvija S, Gionet LR, Aitken SE, et al. Phase I study of intracarotid administration of carboplatin. *Neurosurgery* (1992) 30:512–7. doi: 10.1227/00006123-199204000-00007

90. Joshi S, Wang M, Etu JJ, Suckow RF, Cooper TB, Feinmark SJ, et al. Transient cerebral hypoperfusion enhances intraarterial carmustine deposition into brain tissue. *J Neuro-Oncolo* (2008) 86(2):123–32. doi: 10.1007/s11060-007-9450-z

91. Bobo H, Kapp JP, Vance R. Effect of intraarterial cisplatin and 1,3-bis (2chloroethyl)- 1-nitrosourea (BCNU) dosage on radiographic response and regional toxicity in malignant glioma patients: proposal of a new method of intra-arterial dosage calculation. *J Neurooncol* (1992) 13:291–9. doi: 10.1007/BF00172483

92. Francis JH, Gobin YP, Brodie SE, Marr BP, Dunkel IJ, Abramson DH. Experience of intra-arterial chemosurgery with single agent carboplatin for retinoblastoma. *Br J Ophthalmol* (2012) 96:1270–1. doi: 10.1136/bjophthalmol-2012-301686

93. Wang X, Gan C, Li H, Wei Y, Zhu D, Yang G, et al. Main complications and results of treatment with intra-arterial infusion chemotherapy through the subclavian and thoracic arteries for locally advanced breast cancer. *Mol Clin Oncol* (2013) 1:745–8. doi: 10.3892/mco.2013.129

94. Nakasato T, Katoh K, Sone M, Ehara S, Tamakawa Y, Hoshi H, et al. Superselective continuous arterial infusion chemotherapy through the superficial temporal artery for oral cavity tumors. *AJNR Am J Neuroradiol* (2000) 21:1917–22.

95. Cristina V, Pracht M, Lachenal Y, Adib S, Boubaker A, Prior J, et al. Interventional radiology procedures for malignancies of the liver treatment: intraarterial procedures. *Rev Med Suisse* (2014) 10(1130–1132):1134–5.

96. Rashid OM, Sloot S, Zager JS. Regional therapy in met- astatic melanoma: an update on minimally invasive intraarte- rial isolated limb infusion and percutaneous hepatic perfusion. *Expert Opin Drug Metab Toxicol* (2014) 10:1355–64. doi: 10.1517/17425255.2014.951330

97. Doolittle ND, Miner ME, Hall WA, Siegal T, Jerome E, Osztie E, et al. Safety and efficacy of a multicenter study using intraarterial chemotherapy in conjunction with osmotic opening of the blood-brain barrier for the treatment of patients with malignant brain tumors. *Cancer* (2000) 88(3):637–47. doi: 10.1002/(SICI)1097-0142(20000201)88:3<637::AID-CNCR22>3.0.CO;2-Y

98. Chow KL, Gobin YP, Cloughesy T, Sayre JW, Villablanca JP, Vinuela F. Prognostic factors in recurrent glioblastoma multiforme and anaplastic astrocytoma treated with selec- tive intra-arterial chemotherapy. *AJNR Am J Neuroradiol* (2000) 21:471–8.

99. Kochi M, Kitamura I, Goto T, Nishi T, Takeshima H, Saito Y, et al. Randomised comparison of intra- arterial versus intravenous infusion of ACNU for newly diagnosed patients with glioblastoma. *J Neurooncol* (2000) 49(1):63–70. doi: 10.1023/a:1006457502972

100. Madajewicz S, Chowhan N, Tfayli A, Roque C, Meek A, Davis R, et al. Therapy for patients with high grade astrocytoma using intraarterial chemotherapy and radiation therapy. *Cancer* (2000) 88(10):2350–6. doi: 10.1002/(SICI)1097-0142(20000515)88:10<2350::AID-CNCR20>3.0.CO;2-R

101. Ashby LS, Shapiro WR. Intra-arterial cisplatin plus oral etoposide for the treatment of recurrent malignant glioma : a phase II study. *J Neurooncol* (2001) 51 (1):67–86. doi: 10.1023/A:1006441104260

102. Qureshi AI, Suri MF, Khan J, Sharma M, Olson K, Guterman LR, et al. Superselective intra-arterial carboplatin for treatment of intracranial neoplasms: experience in 100 pro- cedures. *J Neurooncol* (2001) 51:151–1. doi: 10.1023/A:1010683128853

103. Newton HB, Slivka MA, Stevens CL, Bourekas EC, Christoforidis GA, Baujan MA, et al. Intra-arterial carboplatin and intravenous etoposide for the

treatment of recurrent and progressive non-GBM gliomas. *J Neurooncol* (2002) 56 (1):79–86. doi: 10.1023/a:1014498225405

104. Silvani A, Eoli M, Salmaggi A, Erbetta A, Fariselli L, Boiardi A. Intra-arterial ACNU and carboplatin versus intravenous chemotherapy with cisplatin and BCNU in newly diagnosed patients with glioblastoma. *Neurol Sci* (2002) 23 (5):219–24. doi: 10.1007/s100720200044

105. Hall WA, Doolittle ND, Daman M, Bruns PK, Muldoon L, Fortin D, et al. Osmotic blood-brain barrier disruption chemotherapy for diffuse pontine gliomas. *J Neurooncol* (2006) 77(3):279–84. doi: 10.1007/s11060-005-9038-4

106. Angelov L, Doolittle ND, Kraemer DF, Siegal T, Barnett GH, Peereboom DM, et al. Blood-brain barrier dis- ruption and intra-arterial methotrexate-based therapy for newly diagnosed primary CNS lymphoma: a multi-institutional experience. *J Clin Oncol* (2009) 27:3503–9. doi: 10.1200/JCO.2008.19.3789

107. Guillaume DJ, Doolittle ND, Gahramanov S, Hedrick NA, Delashaw JB, Neuwelt EA. Intra-arterial chemotherapy with osmotic blood-brain barrier disruption for aggressive oligodendroglial tumors: results of a phase I study. *Neurosurgery* (2010) 66(1):48–58. doi: 10.1227/01

108. Boockvar JA, Tsiouris AJ, Hofstetter CP, Kovanlikaya I, Fra- lin S, Kesavabhotla K, et al. Safety and maximum tol- erated dose of superselective intraarterial cerebral infusion of bevacizumab after osmotic blood-brain barrier disruption for recurrent malignant glioma. *J Neurosurg* (2011) 114:624–32. doi: 10.3171/2010.9.JNS101223

109. Shin BJ, Burkhardt JK, Riina HA, Boockvar JA. Superse- lective intra-arterial cerebral infusion of novel agents after blood- brain disruption for the treatment of recurrent glioblastoma multiforme: A technical case series. *Neurosurg Clin* (2012) 23(323– 329):ix–x. doi: 10.1016/j.nec.2012.01.008

110. Jeon JY, Kovanlikaya I, Boockvar JA, Mao X, Shin B, Burkhardt JK, et al. Metabolic response of glioblastoma to superselec- tive intra-arterial cerebral infusion of bevacizumab: a proton MR spectroscopic imaging study. *AJNR Am J Neuroradiol* (2012) 33(11):2095–102. doi: 10.3174/ajnr.A3091

111. Fortin D, Morin PA, Belzile F, Mathieu D, Pare FM. Intra- arterial carboplatin as a salvage strategy in the treatment of recur- rent glioblastoma multiforme. *J Neurooncol* (2014) 119:397–403. doi: 10.1007/s11060-014-1504-4

112. Galla N, Chiang G, Chakraborty S, Singh R, John Tsiouris A, Boockvar J, et al. Apparent diffusion coefficient changes predict survival after intra-arterial bevacizumab treat- ment in recurrent glioblastoma. *Neuroradiology* (2017) 59:499–505. doi: 10.1007/s00234-017-1820-4

113. Faltings L, Kulason KO, Patel NV, Wong T, Fralin S, Li M, et al. Rechallenging recurrent glioblastoma with intra-arterial bevacizumab with blood brain-barrier disruption results in radiographic response. *World Neurosurg* (2019) 131:234–41. doi: 10.1016/j.wneu.2019.07.137

114. Patel NV, Wong T, Fralin SR, Li M, McKeown A, Gruber D, et al. Repeated superselective intraarterial bevacizumab after blood brain barrier disruption for newly diagnosed glioblastoma: A phase I/II clinical trial. *J Neurooncol* (2021) 155 (2):117–24. doi: 10.1007/s11060-021-03851-2.

115. McCrea HJ, Ivanidze J, O'Connor A, Hersh EH, Boockvar JA, Gobin YP, et al. Intraarterial delivery of bevacizumab and cetuximab utilizing blood-brain barrier disruption in children with high-grade glioma and diffuse intrinsic pontine glioma: results of a phase I trial. *J Neurosurg Pediatr* (2021) 28(4):371–9. doi: 10.3171/2021.3.PEDS20738

116. Feun LG, Wallace S, Yung WK, Lee YY, Leavens ME, Moser R, et al. Phase-I trial of intracarotid BCNU and cisplatin in patients with malignant intracerebral tumors. *Cancer Drug Deliv* (1984) 1:239–45. doi: 10.1089/cdd.1984.1.239

117. Safdari H, Mompeon B, Dubois JB, Gros C. Intraarterial 1,3-bis(2-chloroethyl)-1-nitrosourea chemotherapy for the treatment of malignant gliomas of the brain: a preliminary report. *Surg Neurol* (1985) 24:490–7. doi: 10.1016/0090-3019(85)90262-9

118. Feun LG, Lee YY, Yung WK, Charnsangavej C, Savaraj N, Tang RA, et al. Phase II trial of intracarotid BCNU and cisplatin in primary malignant brain tumors. *Cancer Drug Deliv* (1986) 3:147–56. doi: 10.1089/cdd.1986.3.147

119. Kleinschmidt-DeMasters BK, Geier JM. Pathology of high-dose intraarterial BCNU. *Surg Neurol* (1989) 31:435–43. doi: 10.1016/0090-3019(89)90088-8

120. Tonn JC, Roosen K, Schachenmayr W. Brain necroses after intraarterial chemotherapy and irradiation of malignant gliomas–a complication of both ACNU and BCNU. *J Neurooncol* (1991) 11:241–2. doi: 10.1007/BF00165532

121. Shapiro WR, Green SB, Burger PC, Selker RG, VanGilder JC, Robertson JT, et al. A randomized comparison of intra-arterial versus intravenous BCNU, with or without intravenous 5-fluorouracil, for newly diagnosed patients with malignant glioma. *J Neurosurg* (1992) 76:772–81. doi: 10.3171/jns.1992.76.5.0772

122. Fauchon F, Davila L, Chatellier G, Fohanno D, Philippon J, Rey A, et al. Treatment of malignant gliomas with surgery, intraarterial infusions of 1-(2-hydroxyethyl) chloroethylnitrosourea and radiation therapy. *A phase II study. Neu- rosurgery* (1990) 27:231–4. doi: 10.1227/00006123-199008000-00010

123. Follézou JY, Fauchon F, Chiras J. Intraarterial infusion of carboplatin in the treatment of malignant gliomas: a phase II study. *Neoplasma* (1989) 36(3):349–52.

124. Cloughesy TF, Gobin YP, Black KL, Viñuela F, Taft F, Kadkhoda B, et al. Intra-arterial carboplatin chemotherapy for brain tumors: a dose escalation study based on cerebral blood flow. *J Neurooncol* (1997) 35:121–31. doi: 10.1023/A:1005856002264

125. Greenberg HS, Ensminger WD, Layton PB, Gebarski S, Meyer M, Chaffee B, et al. Phase I-II evalu- ation of intra-arterial diaziquone for recurrent malignant astrocy- tomas. *Cancer Treat Rep* (1986) 70:353–7.

126. Feun LG, Lee YY, Yung WKA, Savaraj N, Wallace S. Intracarotid VP-16 in malignant brain tumors. *J Neuro-Oncol* (1987) 4:397–401. doi: 10.1007/BF00195611

127. Chehimi M, Boone M, Chivot C, Deramond H, Constants JM, Ly MC, et al. Intra-arterial delivery of idar- ubicin in two patients with glioblastoma. *Case Rep Oncol* (2016) 9:499–505. doi: 10.1159/000448654

128. Muldoon LL, Pagel MA, Netto JP, Neuwelt EA. Intra-arterial administration improves temozolomide delivery and efficacy in a model of intracerebral metastasis, but has unexpected brain toxicity. *J Neurooncol* (2016) 126(3):447–54. doi: 10.1007/s11060-015-2000-1

129. Codrici E, Enciu AM, Popescu ID, Mihai S, Tanase C. Glioma stem cells and their microenvironments: Providers of challenging therapeutic targets. *Stem Cells Int* (2016) 2016:5728438. doi: 10.1155/2016/5728438

130. Riina HA, Knopman J, Greenfield JP, Fralin S, Gobin YP, Tsiouris AJ, et al. Balloon- assisted superselective intra-arterial cerebral infusion of bevaci- zumab for malignant brainstem glioma: a technical note. *Interv Neuroradiol* (2010) 16(1):71–6. doi: 10.1177/159101991001600109

131. Kaka N, Hafazalla K, Samawi H, Simpkin A, Perry J, Sahgal A, et al. Progression-free but no overall survival benefit for adult patients with bevacizumab therapy for the treatment of newly diagnosed glioblastoma: A systematic review and meta- analysis. *Cancers* (2019) 11(11):1723. doi: 10.3390/cancers11111723

132. Wang R, Chadalavada K, Wilshire J, Kowalik U, Hovinga KE, Geber A, et al. Glioblastoma stem-like cells give rise to tumour endothelium. *Nature* (2010) 468(7325):829–33. doi: 10.1038/nature09624

133. Zuniga RM, Torcuator R, Jain R, Anderson J, Doyle T, Ellika S, et al. Efficacy, safety and patterns of response and recurrence in patients with recurrent high-grade gliomas treated with bevacizumab plus irinotecan. *J Neurooncol* (2009) 91:329–36. doi: 10.1007/s11060-008-9718-y

134. Sarin H, Kanevsky AS, Wu H, Sousa AA, Wilson CM, Aronova MA, et al. Physiologic upper limit of pore size in the blood-tumor barrier of malignant solid tumors. *J Transl Med* (2009) 7:51. doi: 10.1186/1479-5876-7-51

135. Friedman HS, Prados MD, Wen PY, Mikkelsen T, Schiff D, Abrey LE, et al. Bev- acizumab alone and in combination with irinotecan in recur- rent glioblastoma. *J Clin Oncol* (2009) 27:4733–40. doi: 10.1200/JCO.2008.19.8721

136. Kreisl TN, Kim L, Moore K, Duic P, Royce C, Stroud I, et al. Phase II trial of single-agent bevacizumab fol- lowed by bevacizumab plus irinotecan at tumor progression in recurrent glioblastoma. *J Clin Oncol* (2009) 27:740–5. doi: 10.1200/JCO.2008.16.3055

137. Chakraborty S, Filippi CG, Burkhardt JK, Fralin S, Ray A, Wong T, et al. Durability of single dose intra-arterial bevacizumab after blood/brain barrier disruption for recurrent glioblastoma. *J Exp Ther Oncol* (2016) 11(4):261–7.

138. Zawadzki M, Walecki J, Kostkiewicz B, Kostyra K, Walczak P, Janowski M, et al. Follow-up of intra-arterial delivery of bevacizumab for treatment of butterfly glioblastoma in patient with first-in-human, real-time MRI-guided intra-arterial neurointervention. *J Neurointerv Surg* (2021) 13(11):1037–9. doi: 10.1136/neurintsurg-2021-017900

139. Saadeh FS, Mahfouz R, Assi HI. EGFR as a clinical marker in glioblastomas and other gliomas. *Int J Biol Markers* (2018) 33(1):22–32. doi: 10.5301/ijbm.5000301

140. Hasselbalch B, Lassen U, Hansen S, Holmberg M, Sørensen M, Kosteljanetz M, et al. Cetuximab, bevacizumab, and irinotecan for patients with primary glioblastoma and progression after radiation therapy and temozolomide: a phase II trial. *Neuro Oncol* (2010) 12:508–16. doi: 10.1093/neuonc/nop063

141. Greenberg HS, Chandler WF, Diaz RF, Ensminger WD, Junck L, Page MA, et al. Intra-arterial bromodeoxyuridine radiosensitization and radiation in treatment of malignant astrocytomas. *J Neurosurg* (1988) 69:500–5. doi: 10.3171/jns.1988.69.4.0500

142. Liu SK, Jakowatz JG, Pollack RB, Ceraldi C, Yamamoto R, Dett C, et al. Effects of intracarotid and intravenous infusion of human TNF and LT on established intracerebral rat gliomas. *Lymphokine Cytokine Res* (1991) 10:189–94.

143. Yoshida J, Wakabayashi T, Mizuno M, Sugita K, Yoshida T, Hori S, et al. Clinical effect of intra-arterial tumor necrosis factor-alpha for malignant glioma. *J Neurosurg* (1992) 771:78–83. doi: 10.3171/jns.1992.77.1.0078

144. Stupp R, Wong ET, Kanner AA, Steinberg D, Engelhard H, Heidecke V, et al. NovoTTF-100A versus physician's choice chemotherapy in recurrent

glioblastoma: a randomised phase III trial of a novel treatment modality. *Eur J Cancer (Oxford Engl 1990)* (2012) 4814:2192–202. doi: 10.1016/j.ejca.2012.04.011

145. Stupp R, Taillibert S, Kanner A, Read W, Steinberg D, Lhermitte B, et al. Effect of tumor-treating fields plus maintenance temozolomide vs maintenance temozolomide alone on survival in patients with glioblastoma: A randomized clinical trial. *JAMA* (2017) 318(23):2306–16. doi: 10.1001/jama.2017.18718

146. Abe T, Wakimoto H, Bookstein R, Maneval DC, Chiocca EA, Basilion JP. Intra-arterial delivery of p53-containing adenoviral vector into experimental brain tumors. *Cancer Gene Ther* (2002) 9:228–35. doi: 10.1038/sj.cgt.7700437

147. Barnett FH, Scharer-Schuksz M, Wood M, Yu X, Wagner TE, Friedlander M. Intra-arterial delivery of endostatin gene to brain tumors prolongs survival and alters tumor vessel ultrastructure. *Gene Ther* (2004) 11(16):1283–9. doi: 10.1038/sj.gt.3302287

148. Ji N, Weng D, Liu C, Gu Z, Chen S, Guo Y, et al. Adenovirus-mediated delivery of herpes simplex virus thymidine kinase administration improves outcome of recurrent high-grade glioma. *Oncotarget* (2016) 7(40):4369–78. doi: 10.18632/oncotarget.6737

149. Geoerger B, Tang CB, Cesano A, Visonneau S, Marwaha S, Judy KD, et al. Antitumor activity of a human cytotoxic T-cell line (TALL-104) in brain tumor xenografts. *Neuro-oncology* (2000) 2(2):103–13. doi: 10.1093/neuonc/2.2.103

150. Weilemann F, Steinmetz A, Kirsch M, Buttler A, Kunze S, Kuhlisch E, et al. Prevention of brain metastasis formation by local expression of interleukin-4 or hemagglutinin antigen. *Zentralblatt fur Neurochirurgie* (2003) 64(2):65–70. doi: 10.1055/s-2003-40374

151. Bagley SJ, Desai AS, Linette GP, June CH, O'Rourke DM, et al. CAR T-cell therapy for glioblastoma: Recent clinical advances and future challenges. *Neuro-Oncology* (2018) 20(11):1429–38. doi: 10.1093/neuonc/noy032

152. Katz SC, Burga RA, McCormack E, Wang LJ, Mooring W, Point GR, et al. Phase I hepatic immunotherapy for metastases study of intra-arterial chimeric antigen receptor-modified T-cell therapy for CEA+ liver metastases. *Clin Cancer Res an Off J Am Assoc Cancer Res* (2015) 21(14):3149–59. doi: 10.1158/1078-0432.CCR-14-1421

153. Saied A, Licata L, Burga RA, Thorn M, McCormack E, Stainken BF, et al. Neutrophil:lymphocyte ratios and serum cytokine changes after hepatic artery chimeric antigen receptor-modified T-cell infusions for liver metastases. *Cancer Gene Ther* (2014) 21(11):457–62. doi: 10.1038/cgt.2014.50

154. Schiffer D, Annovazzi L, Casalone C, Corona C, Mellai M. Glioblastoma: Microenvironment and niche concept. *Cancers (Basel)* (2018) 11(1):5. doi: 10.3390/cancers11010005

155. Janowski M, Walczak P, Pearl MS. Predicting and optimizing the territory of blood-brain barrier opening by superselective intra-arterial cerebral infusion under dynamic susceptibility contrast MRI guidance. *J Cereb Blood Flow Metab* (2016) 36(3):569–75. doi: 10.1177/0271678X15615875

156. Zawadzki M, Walecki J, Kostkiewicz B, Kostyra K, Pearl MS, Solaiyappan M, et al. Real-time MRI guidance for intra-arterial drug delivery in a patient with a brain tumor: technical note. *BMJ Case Rep* (2019) 12(1):e014469. doi: 10.1136/bcr-2018-01446

157. Chen SR, Chen MM, Ene C, Lang FF, Kan P. Perfusion-guided endovascular super-selective intra-arterial infusion for treatment of malignant brain tumors. *J Neurointerv Surg* (2021). doi: 10.1136/neurintsurg-2021-018190

158. Zlochower A, Chow DS, Chang P, Khatri D, Boockvar JA, Filippi CG, et al. Deep learning AI applications in the imaging of glioma. *Topics Magnetic Resonance Imaging TMRI* (2020) 29,2:115–0. doi: 10.1097/RMR.0000000000000237

frontiers | Frontiers in Oncology

TYPE Case Report
PUBLISHED 24 February 2023
DOI 10.3389/fonc.2023.1123378

OPEN ACCESS

EDITED BY
Theophilos Tzaridis,
Sanford Burnham Prebys Medical Discovery Institute, United States

REVIEWED BY
Angela Mastronuzzi,
Bambino Gesù Children's Hospital (IRCCS), Italy
Megan Paul,
University of California, San Diego, United States

*CORRESPONDENCE
Shubin W. Shahab
sshahab@emory.edu

SPECIALTY SECTION
This article was submitted to Neuro-Oncology and Neurosurgical Oncology, a section of the journal Frontiers in Oncology

RECEIVED 14 December 2022
ACCEPTED 09 February 2023
PUBLISHED 24 February 2023

CITATION
Shahab SW, Schniederjan M, Vega JV, Little S, Reisner A, MacDonald T and Aguilera D (2023) Case report: ATIC-ALK fusion in infant-type hemispheric glioma and response to lorlatinib.
Front. Oncol. 13:1123378.
doi: 10.3389/fonc.2023.1123378

Case report: ATIC-ALK fusion in infant-type hemispheric glioma and response to lorlatinib

Shubin W. Shahab [1,2]*, Matthew Schniederjan [3,4], Jose Velazquez Vega [3,4], Stephen Little [5], Andrew Reisner [2,4,6], Tobey MacDonald [1,2,7] and Dolly Aguilera [1,2]

[1]Aflac Cancer and Blood Disorders Center, Children's Healthcare of Atlanta, Atlanta, GA, United States, [2]Department of Pediatrics, Emory University School of Medicine, Atlanta, GA, United States, [3]Department of Pathology, Emory University School of Medicine, Atlanta, GA, United States, [4]Children's Healthcare of Atlanta, Atlanta, GA, United States, [5]Department of Radiology, Emory University School of Medicine, Atlanta, GA, United States, [6]Department of Neurosurgery, Emory University School of Medicine, Atlanta, GA, United States, [7]Winship Cancer Institute, Atlanta, GA, United States

Introduction: Infant type hemispheric gliomas are a rare tumor with unique molecular characteristics. In many cases these harbor mutations in receptor tyrosine kinase pathways and respond to targeted therapy. Here we describe the case of an infant with this type of tumor with a novel ATIC-ALK fusion that has responded dramatically to the ALK inhibitor lorlatinib, despite being refractory to standard chemotherapy.

Case description: The infant was initially treated with standard chemotherapy and found to have an ATIC-ALK fusion. When surveillance imaging revealed progressive disease, the patient was switched to the ALK-inhibitor lorlatinib at 47 mg/m^2/day. The patient demonstrated a significant clinical and radiographic response to the ALK inhibitor lorlatinib after just 3 months of treatment and a near complete response by 6 months of therapy.

Conclusion: The ALK inhibitor lorlatinib is an effective targeted therapy in infant type hemispheric glioma patients harboring ATIC-ALK fusion.

KEYWORDS

infant-type hemispheric glioma, high grade glioma, ALK fusion, lorlatinib, case report

Introduction

Infantile high-grade gliomas (HGG) are rare entities with unique molecular biology. These tumors are now codified in the World Health Organization (WHO) classification of Central Nervous System Tumors as infant-type hemispheric gliomas (herein referred to as ITHG) without a specific corresponding grade (1). In contrast to their adult counterpart, ITHGs exhibit better outcomes. Prior studies have demonstrated that patients under 4

years with HGG can have distinct molecular rearrangements and fusions and tend to have a more favorable prognosis compared to older patients (2, 3). One of the genes commonly altered in ITHGs is anaplastic lymphoma kinase (*ALK*), which encodes a receptor tyrosine kinase (RTK) that is also often rearranged, amplified or mutated in pediatric neoplasms, including anaplastic large cell lymphoma (ALCL), inflammatory myofibroblastic tumor (IMT), rhabdomyosarcoma, glioma and neuroblastoma (2). In a case series of infants with HGGs, a large number of cases demonstrated gene fusions that can be targeted with novel therapies. Among these, MET fusions were present in 4 samples, NTRK1/2/3 in 21 samples, ROS fusions in 9 samples and ALK fusions in 31 samples, the most common among which was the PPP1CB-ALK fusion (3). While the 5-aminoimidazole-4-carboxamide ribonucleotide formyltransferase *(ATIC)-ALK* fusion has been described in literature, it is a rare fusion event and has never been described in an ITHG. Here, we describe the case of a patient with an ITHG diagnosed at 3 months of age and exhibiting an *ATIC-ALK* fusion, who despite progression on standard chemotherapy, has had an extremely good radiographic and clinical response to the ALK inhibitor lorlatinib.

Case presentation

A 3-month-old patient presented with poor head control, increased fatigue, right hemiparesis, feeding difficulties, decreased peripheral vision on the right side and progressively increasing head circumference. Emergency department evaluation showed bulging fontanelle, increased irritability and macrocephaly. A head CT revealed a large, left sided supratentorial mass with midline shift and hydrocephalus, requiring ventricular drain placement. MRI of the brain confirmed a large tumor centered in the posterior left cerebral hemisphere with associated severe mass effect, including subfalcine, uncal, and ascending transtentorial herniation. There was no evidence of metastatic disease in the brain or spine. The patient underwent a subtotal resection with significant blood loss intraoperatively requiring initiation of massive transfusion protocol. Pathology revealed a densely cellular HGG with focal pseudopalisading necrosis, gemistocytic morphology in a proportion of the tumor as well as elevated mitotic activity. A panel of immunohistochemistry supported the diagnosis of HGG (Figure 1). Furthermore, DNA methylation analysis classified the tumor as an ITHG. The sarcoma fusion panel (Archer FusionPlex) revealed fusion between *ATIC* (exon 7) and *ALK* (exon 20) (Figure 2). Additional (Ashion) testing through the precision medicine program at our center confirmed the *ATIC-ALK* fusion at both the DNA and RNA level. There was no evidence of germline mutations. Initial treatment with multiagent chemotherapy per the Baby POG protocol (5) induced a partial tumor response; however, after 7 cycles of this chemotherapy regimen, routine surveillance brain MRI demonstrated progressive disease. The patient underwent a second subtotal resection and resumed Baby POG chemotherapy for an additional 8 months. Due to further tumor progression in multiple areas of the resection cavity on brain MRI, and considering the result of tumor sequencing, the patient's treatment was then switched to the ALK inhibitor lorlatinib at a dose of 47 mg/m^2/day *via* gastrostomy tube. Subsequent brain MR imaging after 10 weeks of daily lorlatinib treatment revealed a partial response in the largest residual tumor lesion and complete response on the smaller tumor nodules (Figure 3) and 6 months after starting lorlatinib, near complete

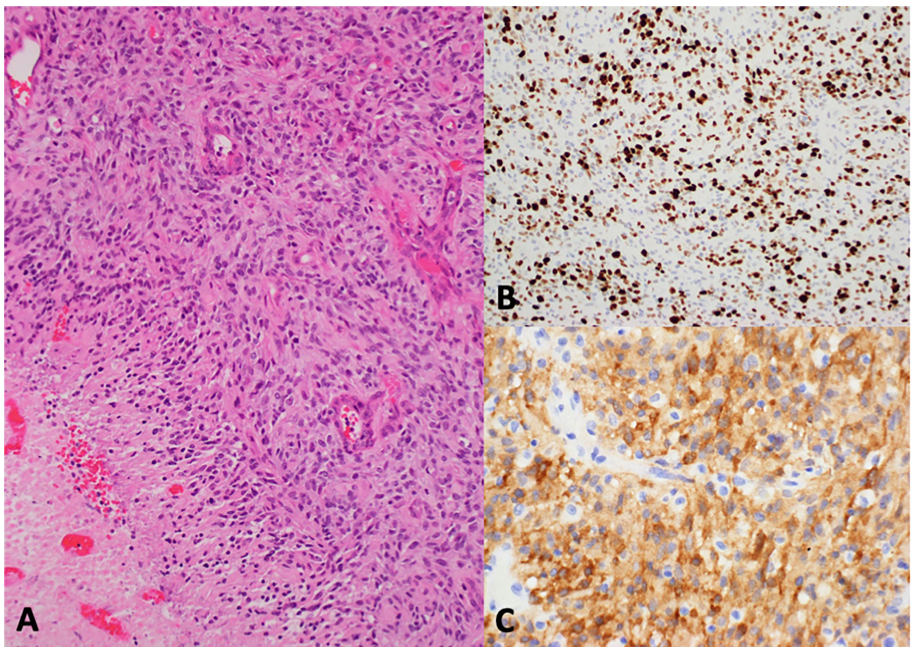

FIGURE 1
Histologic sections showed a highly cellular glial tumor with a solid growth pattern, brisk mitotic activity, microvascular proliferation, and palisading necrosis **(A)**. Immunohistochemistry revealed high Ki-67 expression **(B)** and strong cytoplasmic ALK expression **(C)**.

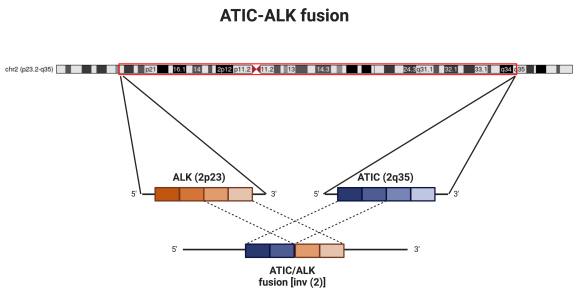

FIGURE 2
Schematic of ATIC-ALK fusion. Diagram showing chromosome 2 (courtesy of UCSC genome browser; http://genome.ucsc.edu (4); with approximate locations of ALK (2p23) and ATIC (2q35). The inversion and subsequent fusion between the 5′ end of ATIC to the 3′ end of ALK leads to activation of the ALK kinase. For our patient, the fusion is noted specifically between exon 7 of ATIC and exon 20 of ALK.

response on all the residual tumor nodules (Figure 3). At the time of this report, the patient continues on daily lorlatinib therapy (See timeline Figure 4). The only toxicities to date per common terminology criteria for adverse events (CTCAE, version 5.0) have been Grade 1 hypercholesterolemia, Grade 1 triglyceridemia and Grade 2 weight gain. No neurological toxicities have been observed. The clinical response has been remarkable with resolution of hemiparesis, improvement of gait, speech and language, and stabilization of visual deficits.

Caregiver perspective

The mother of the child shared the following with the primary oncologist: "Our quality of life has improved significantly since switching to lorlatinib. Our child has had no admissions for fever or neutropenia, no need for transfusion of blood products, and has experienced no nausea or vomiting or additional hearing loss. Her appetite is back to normal, she no longer needs g-tube feeds, and is now eating all meals by mouth. She has also achieved more developmental milestones since starting lorlatinib.

Also, we have had fewer clinic visits and lab draws as she has needed less monitoring, going from weekly visits during standard chemotherapy to once every 6 weeks after starting lorlatinib. The central line has been removed. Our child is back at day care. "

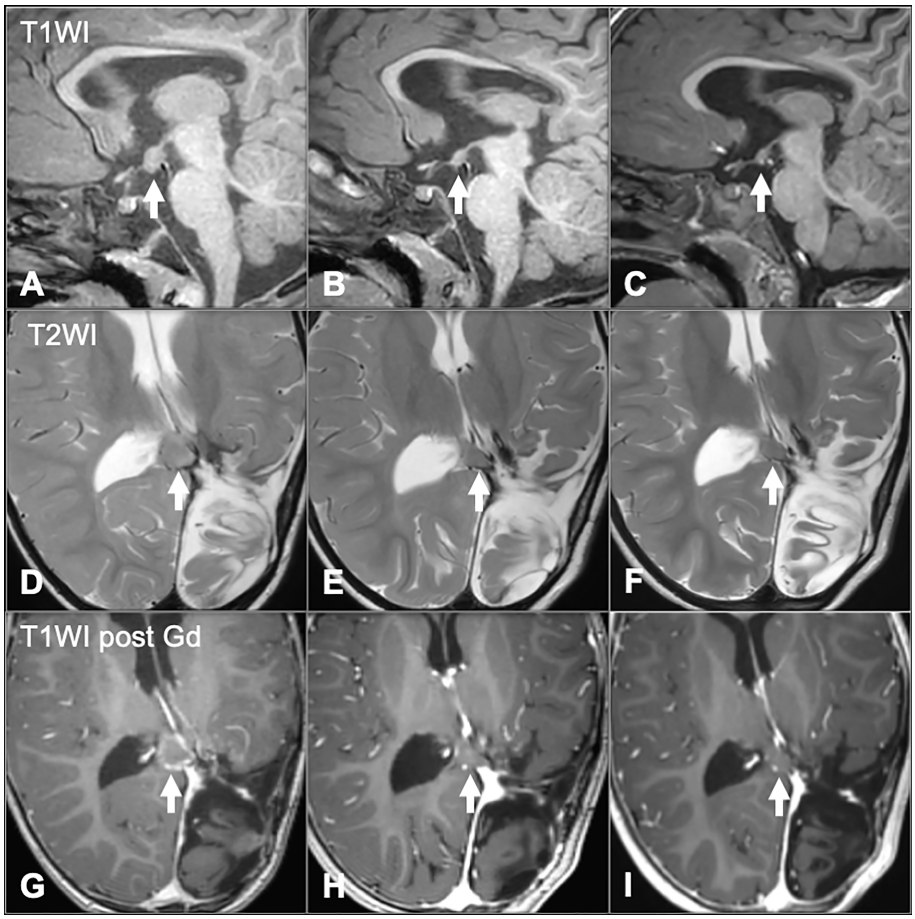

FIGURE 3
Pre **(A**, **D**, **G)**, Post 1 (10 weeks) **(B**, **E**, **H)** and Post 2 (6 months) **(C**, **F**, **I)** ALK inhibitor administration. Pre-treatment images demonstrate nodular lesions near the splenium of the corpus callosum (arrows in **D**, **G**) and along the floor of the third ventricle (arrow in **A**). Post-treatment images (Post 1) demonstrate substantial decrease in size of both lesions (arrows in **B**, **E**, **H**). Continued decrease in lesion size is seen on Post 2 images (arrows in **C**, **F**, **I**).

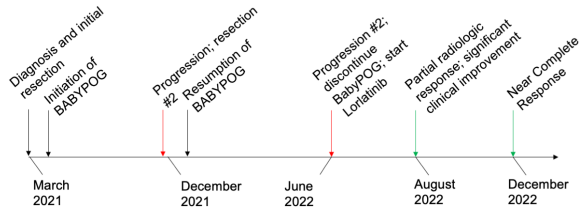

FIGURE 4
Timeline of major clinical events since diagnosis to present day.

Discussion

ALK is a tyrosine kinase that can often be aberrantly expressed in cancers due to rearrangements or mutations and amplification events. In ALCL, where ALK oncogenic fusions were first described, the most frequent fusion partner is nucleolar protein nucleophosmin (NPM) and accounts for 40-60% of cases. Overall, ALK fusions occur in up to 90% of ALCLs in children, and up to 50% of adult cases (6). Other common fusion partners for ALK include TPM3, TPM4, CLTC and EML4, which are found across different tumor histologies including ALCL, IMT, papillary thyroid cancer, and renal cell carcinoma (2). The *ATIC-ALK* fusion is a rarer occurrence; The *ATIC* gene encodes a bifunctional enzyme involved in purine biosynthesis. During the rearrangement the portion of *ATIC* gene encoding the amino terminus is fused with the portion of *ALK* gene encoding its carboxy terminus, the product of which leads to a constitutively active ALK tyrosine kinase (7) (Figure 2).

The *ATIC-ALK* fusion has been reported in a variety of cancers including in IMT, ALCL, and NSCLC (2, 6–14); overall, it still accounts for only 0.1% of reported AACR Genie cases of ALK fusions (15). Thus, to our knowledge, this is the first report of a patient with an ITHG with the *ATIC-ALK* fusion treated with targeted therapy using an ALK inhibitor, even though other groups have reported the use of lorlatinib for ITHG with other ALK fusions (16).

ITHGs are unique in that most of these tumors harbor alterations in RTK oncogenes (up to 80% in one study (17)). It is possible that the presence of these RTK alterations may drive the biology behind the favorable prognosis seen in infant HGG (17) and may display maturation/differentiation following treatment.

ALK fusions in infant brain tumors have been reported (3, 18–21). In a large multi-institutional international cohort study (17) of infant gliomas, the reported ALK fusions were CCDC88A-ALK, EML4-ALK, PPP1CB-ALK and KTN1-ALK. In this study infants with ALK fusion positive HGGs had a worse outcome compared to ALK fusion positive low grade glioma (LGG), with only 57.1% alive at 3 years of median follow up. In another large study CLIP2-ALK, HIP1-ALK, MAD1L1-ALK, MAP2-ALK, MSI2-ALK, PRKAR2A-ALK, SPECC1L-ALK, SYNDIG1L-ALK and ZC3H7A-ALK fusions were reported (3). In one study, an infant with HGG and PPP1CB-ALK fusion had a complete resection and has not had progression of the tumor 3 years since diagnosis without additional therapy (22). On the other hand, more aggressive courses have been reported with ALK fusion positive infant HGG, and in some cases, response to targeted therapy with ALK inhibitors has been documented (16). ALK inhibitors have also demonstrated efficacy in patients with metastatic NSCLC (non-small cell lung cancer) to the brain, as well as in neuroblastoma and there are several clinical trials that are currently looking into the efficacy of ALK inhibitors in both CNS and non-CNS tumors (NCT03236675, NCT04774718, NCT02201992, NCT02568267, NCT03052608, NCT04589845, NCT02693535, NCT04541407, NCT04094610, NCT02650401).

Lorlatinib is a 3rd generation ALK inhibitor with improved CNS penetration compared to earlier generations, and may have some neurological toxicities including peripheral neuropathy, mental status and mood changes (23). In a clinical trial for adult patients with advanced ALK-positive lung cancer the 12-month event-free survival was 78% in the lorlatinib arm vs. 39% in the crizotinib arm. Additionally, the responses were significantly better with lorlatinib for subjects with intracranial metastatic disease, a subset in which 71% in the lorlatinib group achieved complete response in the brain (as opposed to 8% for crizotinib) (24).

At this time, the optimal pediatric dose, duration of treatment, or anticipated long term toxicities of using lorlatinib in children, let alone in infants, are not known. Our patient has so far experienced the most common toxicities of hypercholesterolemia, hypertriglyceridemia and weight gain, although some neurocognitive effects may be difficult to assess at this age. In a previously published case report of lorlatinib use in a child with HGG, the patient was treated with 95 mg/m^2/day (twice the dose used in our patient) with similar toxicity profile (16). That patient received treatment for 8 months (with a 20% dose reduction due to weight gain) and then therapy was discontinued for a period before having to be resumed due to relapse. Another case of a young child with a recurrent infant-type hemispheric glioma with the *ZNF397-ALK* fusion has recently been published (25). In that study the patient received lorlatinib at 95 mg/m2/day as well. Significant complications were reported including weight gain greater than 130% from baseline. A dose reduction of 50% of lorlatinib was started, and while weight gain slowed, it did not stop. Eventually lorlatinib was discontinued after more than 1 year of treatment. Prior use of lorlatinib in children also included a phase I trial to evaluate doses on relapsed or recurrent neuroblastoma patients with ALK mutations/amplification who might have had prior exposure to other ALK inhibitors (26). In that study 5 dose levels (45, 60, 75, 95, 115 mg/m2/day) were evaluated in pediatric patients. Dose limiting toxicity (DLT) was the primary endpoint on the first 28 days and neurocognitive toxicity within 54 days of starting drug. Of note the youngest patient getting lorlatinib on this trial reported was 2 years old. No DLT was observed at the lowest 3 dose levels. At a dose of 95mg/m2/day 50% enrolled patients (5/10) had DLT's. At 115/mg/m2/day 33% of enrolled patients (1/3; with expansion ongoing at the time of abstract publication) had a DLT of grade 3 diarrhea. Overall weight gain, hyperlipidemia, concentration/memory impairment, peripheral neuropathy, and peripheral edema were the most common adverse events reported. Interestingly, responses were seen early (median of 2 courses) and across dose levels.

Given that responses were seen at the lowest dose level, we selected this dose to start the treatment of our patient. Our patient has only experienced Grade 1 hypercholesterolemia, Grade 1

triglyceridemia and Grade 2 weight gain to date and as highlighted in the caregiver perspective has had significant improvement in quality of life. While targeted therapy clearly has a role in the relapsed/refractory setting, it remains to be seen whether this approach will be widely adopted as 1st line. In patients with ALK-rearranged non-small cell lung cancer targeted therapy appears to be superior than chemotherapy only regimens (27). Recently a meta-analysis investigated whether ALK-inhibitor therapy should be used first line in ALK-positive lung cancer patients who were also given chemotherapy (28). The authors noted that while there was an improvement in progression free survival, there was no significant improvement in overall survival. We recognize that ALK-positive lung cancer is a very different disease in a significantly older age group compared to ALK-positive infantile high-grade glioma and therefore, the outcomes may be very different. Furthermore, as with any case report, our observations may have been influenced by our subjective biases and may not be generalizable to other cases of high-grade glioma or even infants with IHTG. Thus, more studies are clearly needed. However, given the rarity of these fusions and the age of many of these patients, accruing enough patients for clinical trials may be difficult, although some data may be extrapolated from non-CNS studies or pathology agnostic trials in older patients.

This case highlights the importance of molecular information directing therapy in the clinical setting. We initially chose to treat our patient with standard chemotherapy per Baby POG after discussion within our group and with the parents. Specifically, the age of the child and the lack of data published in children less than 2 years of age were driving factors behind our decision. Additionally, the potential for development of resistance with prolonged exposure to this agent is also a consideration. Molecular profiling at the time of progression may help in our understanding of the pathways to resistance development and help find an alternative treatment. While there are no established combination treatment regimens with ALK inhibitors, several clinical trials are investigating rational strategies of combining ALK inhibitors with other agents.

Data availability statement

The original contributions presented in the study are included in the article/supplementary material. Further inquiries can be directed to the corresponding author.

Ethics statement

Ethical review and approval were not required for the study on human participants in accordance with the local legislation and institutional requirements. Written informed consent to participate in this study was provided by the participants' legal guardian/next of kin. Written informed consent was obtained from the minor(s)' legal guardian/next of kin for the publication of any potentially identifiable images or data included in this article.

Author contributions

SS, TM and DA contributed to the study conception and design. Sample collection was performed by AR. Imaging analysis and interpretation were performed by SL. Histopathological slide preparation and interpretation were performed by MS and JV. The first draft of the manuscript was written by SS and all authors commented on previous versions of the manuscript. All authors contributed to the article and approved the submitted version.

Funding

Sequencing costs were covered by the Aflac Precision Medicine Program, which receives generous support from the CURE Childhood Cancer Foundation.

Acknowledgments

The authors would like to acknowledge the American Association for Cancer Research and its financial and material support in the development of the AACR Project GENIE registry, as well as members of the consortium for their commitment to data sharing. Interpretations are the responsibility of study authors. We would also like to thank CURE childhood cancer foundation for supporting Aflac Precision Medicine Program. We are also forever grateful to the parents of our patient who agreed to share their story for the benefit of other children/families.

Conflict of interest

The authors declare that the research was conducted in the absence of any commercial or financial relationships that could be construed as a potential conflict of interest.

Publisher's note

References

1. Louis DN, Perry A, Wesseling P, Brat DJ, Cree IA, Figarella-Branger D, et al. The 2021 WHO classification of tumors of the central nervous system: A summary. *Neuro Oncol* (2021) 23(8):1231–51. doi: 10.1093/neuonc/noab106

2. Takita J. The role of anaplastic lymphoma kinase in pediatric cancers. *Cancer Sci* (2017) 108(10):1913–20. doi: 10.1111/cas.13333

3. Clarke M, Mackay A, Ismer B, Pickles JC, Tatevossian RG, Newman S, et al. Infant high-grade gliomas comprise multiple subgroups characterized by novel targetable gene fusions and favorable outcomes. *Cancer Discov* (2020) 10(7):942–63. doi: 10.1158/2159-8290.CD-19-1030

4. Kent WJ, Sugnet CW, Furey TS, Roskin KM, Pringle TH, Zahler AM, et al. The human genome browser at UCSC. *Genome Res* (2002) 12(6):996–1006. doi: 10.1101/gr.229102

5. Duffner PK, Horowitz ME, Krischer JP, Burger PC, Cohen ME, Sanford RA, et al. The treatment of malignant brain tumors in infants and very young children: an update of the pediatric oncology group experience. *Neuro Oncol* (1999) 1(2):152–61. doi: 10.1093/neuonc/1.2.152

6. Cao Z, Gao Q, Fu M, Ni N, Pei Y, Ou WB. Anaplastic lymphoma kinase fusions: Roles in cancer and therapeutic perspectives. *Oncol Lett* (2019) 17(2):2020–30. doi: 10.3892/ol.2018.9856

7. Colleoni GW, Bridge JA, Garicochea B, Liu J, Filippa DA, Ladanyi M. ATIC-ALK: A novel variant ALK gene fusion in anaplastic large cell lymphoma resulting from the recurrent cryptic chromosomal inversion, inv(2)(p23q35). *Am J Pathol* (2000) 156 (3):781–9. doi: 10.1016/S0002-9440(10)64945-0

8. Trinei M, Lanfrancone L, Campo E, Pulford K, Mason DY, Pelicci PG, et al. A new variant anaplastic lymphoma kinase (ALK)-fusion protein (ATIC-ALK) in a case of ALK-positive anaplastic large cell lymphoma. *Cancer Res* (2000) 60(4):793–8. doi: 10.3892/or.2020.7767

9. Maes B, Vanhentenrijk V, Wlodarska I, Cools J, Peeters B, Marynen P, et al. The NPM-ALK and the ATIC-ALK fusion genes can be detected in non-neoplastic cells. *Am J Pathol* (2001) 158(6):2185–93. doi: 10.1016/S0002-9440(10)64690-1

10. Debiec-Rychter M, Marynen P, Hagemeijer A, Pauwels P. ALK-ATIC fusion in urinary bladder inflammatory myofibroblastic tumor. *Genes Chromosomes Cancer* (2003) 38(2):187–90. doi: 10.1002/gcc.10267

11. Matsubara K, Tanaka T, Taki T, Nakagawa A, Nigami H, Tamura A, et al. [ATIC-ALK-positive anaplastic large cell lymphoma: A case report and review of the literature]. *Rinsho Ketsueki* (2008) 49(5):325–30.

12. Damm-Welk C, Klapper W, Oschlies I, Gesk S, Rottgers S, Bradtke J, et al. Distribution of NPM1-ALK and X-ALK fusion transcripts in paediatric anaplastic large cell lymphoma: A molecular-histological correlation. *Br J Haematol* (2009) 146(3):306–9. doi: 10.1111/j.1365-2141.2009.07754.x

13. Tateishi Y, Okudela K, Kawai S, Suzuki T, Umeda S, Matsumura M, et al. Intraosseous inflammatory myofibroblastic tumor of the mandible with a novel ATIC-ALK fusion mutation: A case report. *Diagn Pathol* (2016) 11(1):132. doi: 10.1186/s13000-016-0586-z

14. Wu X, Zhou H, He Z, Zhang Z, Feng W, Zhao J, et al. Coexistence of a novel CCNY-ALK and ATIC-ALK double-fusion in one patient with ALK-positive NSCLC and response to crizotinib: a case report. *Transl Lung Cancer Res* (2020) 9(6):2494–9. doi: 10.21037/tlcr-20-1049

15. Consortium APG. AACR project GENIE: Powering precision medicine through an international consortium. *Cancer Discov* (2017) 7(8):818–31. doi: 10.1158/2159-8290.CD-17-0151

16. Bagchi A, Orr BA, Campagne O, Dhanda S, Nair S, Tran Q, et al. Lorlatinib in a child with ALK-Fusion-Positive high-grade glioma. *N Engl J Med* (2021) 385(8):761–3. doi: 10.1056/NEJMc2101264

17. Guerreiro Stucklin AS, Ryall S, Fukuoka K, Zapotocky M, Lassaletta A, Li C, et al. Alterations in ALK/ROS1/NTRK/MET drive a group of infantile hemispheric gliomas. *Nat Commun* (2019) 10(1):4343. doi: 10.1038/s41467-019-12187-5

18. Gilani A, Donson A, Davies KD, Whiteway SL, Lake J, Desisto J, et al. Targetable molecular alterations in congenital glioblastoma. *J Neurooncol* (2020) 146(2):247–52. doi: 10.1007/s11060-019-03377-8

19. Mrowczynski OD, Payne R, Pu C, Greiner R, Rizk E. A unique case of a high-grade neuroepithelial tumor with EML4-ALK fusion in a five-Month-Old. *Cureus* (2020) 12(6):e8654. doi: 10.7759/cureus.8654

20. Zhong Y, Lin F, Xu F, Schubert J, Wu J, Wainwright L, et al. Genomic characterization of a PPP1CB-ALK fusion with fusion gene amplification in a congenital glioblastoma. *Cancer Genet* (2021) 252-253:37–42. doi: 10.1016/j.cancergen.2020.12.005

21. Roosen M, Ode Z, Bunt J, Kool M. The oncogenic fusion landscape in pediatric CNS neoplasms. *Acta Neuropathol* (2022) 143(4):427–51. doi: 10.1007/s00401-022-02405-8

22. Aghajan Y, Levy ML, Malicki DM, Crawford JR. Novel PPP1CB-ALK fusion protein in a high-grade glioma of infancy. *BMJ Case Rep* (2016) 2016. doi: 10.1136/bcr-2016-217189

23. Nagasaka M, Ge Y, Sukari A, Kukreja G, Ou SI. A user's guide to lorlatinib. *Crit Rev Oncol Hematol* (2020) 151:102969. doi: 10.1016/j.critrevonc.2020.102969

24. Shaw AT, Bauer TM, De Marinis F, Felip E, Goto Y, Liu G, et al. First-line lorlatinib or crizotinib in advanced ALK-positive lung cancer. *N Engl J Med* (2020) 383 (21):2018–29. doi: 10.1056/NEJMoa2027187

25. Greenwell AM, Baughan S, Altinok D, Marupudi NI, Kupsky W, Kumar-Sinha C, et al. Lorlatinib for the treatment of ALK fusion-positive infant-type hemispheric glioma: A case report. *JCO Precis Oncol* (2022) 6:e2200255. doi: 10.1200/PO.22.00255

26. Goldsmith KC, Kayser K, Groshen SG, Chioda M, Thurm HC, Chen J, et al. Phase I trial of lorlatinib in patients with ALK-driven refractory or relapsed neuroblastoma: A new approaches to neuroblastoma consortium study. *J Clin Oncol* (2020) 38(15_suppl):10504–4. doi: 10.1200/JCO.2020.38.15_suppl.10504

27. Kron A, Alidousty C, Scheffler M, Merkelbach-Bruse S, Seidel D, Riedel R, et al. Impact of TP53 mutation status on systemic treatment outcome in ALK-rearranged non-small-cell lung cancer. *Ann Oncol* (2018) 29(10):2068–75. doi: 10.1093/annonc/mdy333

28. Lee YC, Hsieh CC, Lee YL, Li CY. Which should be used first for ALK-positive non-Small-Cell lung cancer: Chemotherapy or targeted therapy? A meta-analysis of five randomized trials. *Medicina (Kaunas)* (2019) 55(2):29. doi: 10.3390/medicina55020029

frontiers | Frontiers in Oncology

TYPE Original Research
PUBLISHED 05 May 2023
DOI 10.3389/fonc.2023.1171278

OPEN ACCESS

EDITED BY
Yonehiro Kanemura,
Osaka National Hospital (NHO), Japan

REVIEWED BY
Yoshihiro Otani,
Okayama University, Japan
Siqi Guo,
Old Dominion University, United States

*CORRESPONDENCE
John H. Rossmeisl Jr.
jrossmei@vt.edu

†These authors have contributed equally to this work

RECEIVED 23 February 2023
ACCEPTED 24 April 2023
PUBLISHED 05 May 2023

CITATION
Campelo SN, Lorenzo MF, Partridge B, Alinezhadbalalami N, Kani Y, Garcia J, Saunier S, Thomas SC, Hinckley J, Verbridge SS, Davalos RV and Rossmeisl JH Jr. (2023) High-frequency irreversible electroporation improves survival and immune cell infiltration in rodents with malignant gliomas. *Front. Oncol.* 13:1171278. doi: 10.3389/fonc.2023.1171278

High-frequency irreversible electroporation improves survival and immune cell infiltration in rodents with malignant gliomas

Sabrina N. Campelo[1,2†], Melvin F. Lorenzo[1,2†], Brittanie Partridge[3], Nastaran Alinezhadbalalami[1,2], Yukitaka Kani[3], Josefa Garcia[3], Sofie Saunier[1,2], Sean C. Thomas[2], Jonathan Hinckley[3], Scott S. Verbridge[2], Rafael V. Davalos[1,2] and John H. Rossmeisl Jr.[3*]

[1]Bioelectromechanical Systems Laboratory, Virginia Tech, Blacksburg, VA, United States, [2]School of Biomedical Engineering and Sciences, Virginia Tech-Wake Forest University, Blacksburg, VA, United States, [3]Department of Small Animal Clinical Sciences, Virginia Tech, Blacksburg, VA, United States

Background: Irreversible electroporation (IRE) has been previously investigated in preclinical trials as a treatment for intracranial malignancies. Here, we investigate next generation high-frequency irreversible electroporation (H-FIRE), as both a monotherapy and a combinatorial therapy, for the treatment of malignant gliomas.

Methods: Hydrogel tissue scaffolds and numerical modeling were used to inform *in-vivo* H-FIRE pulsing parameters for our orthotopic tumor-bearing glioma model. Fischer rats were separated into five treatment cohorts including high-dose H-FIRE (1750V/cm), low-dose H-FIRE (600V/cm), combinatorial high-dose H-FIRE + liposomal doxorubicin, low-dose H-FIRE + liposomal doxorubicin, and standalone liposomal doxorubicin groups. Cohorts were compared against a standalone tumor-bearing sham group which received no therapeutic intervention. To further enhance the translational value of our work, we characterize the local and systemic immune responses to intracranial H-FIRE at the study timepoint.

Results: The median survival for each cohort are as follows: 31 days (high-dose H-FIRE), 38 days (low-dose H-FIRE), 37.5 days (high-dose H-FIRE + liposomal doxorubicin), 27 days (low-dose H-FIRE + liposomal doxorubicin), 20 days (liposomal doxorubicin), and 26 days (sham). A statistically greater overall survival fraction was noted in the high-dose H-FIRE + liposomal doxorubicin (50%, $p = 0.044$), high-dose H-FIRE (28.6%, $p = 0.034$), and the low-dose H-FIRE (20%, $p = 0.0214$) compared to the sham control (0%). Compared to sham controls, brain sections of rats treated with H-FIRE demonstrated significant increases in IHC scores for CD3+ T-cells ($p = 0.0014$), CD79a+ B-cells ($p = 0.01$),

IBA-1+ dendritic cells/microglia (p = 0.04), CD8+ cytotoxic T-cells (p = 0.0004), and CD86+ M1 macrophages (p = 0.01).

Conclusions: H-FIRE may be used as both a monotherapy and a combinatorial therapy to improve survival in the treatment of malignant gliomas while also promoting the presence of infiltrative immune cells.

KEYWORDS

glioblastoma, intracranial, electroporation, blood-brain barrier disruption, immune response, numerical modeling, pulsed electric field (PEF)

1 Introduction

The most common and aggressive malignant brain tumor, glioblastoma (GBM), demonstrates a 5-year survival rate of only 6.8% (1). Notable difficulties arising from efficacious GBM treatment include: (i) an inability of current standard of care to target highly invasive GBM cells which have migrated beyond the visible tumor into healthy brain parenchyma; (ii) limitations in delivering therapeutic agents to diseased regions in the brain, due in part to the impeditive functions of the blood-brain barrier (BBB); and (iii) gross, microscopic, and genetic intratumor heterogeneity, complicating molecular targeting of the GBM tumor (2–6). A significant advancement in the management of GBM arose from the introduction of the chemotherapeutic agent temozolomide to the standard of care, extending median overall survival from ~12.1 months to ~15 months (7). Despite these promising results, GBM remains a highly dismal prognosis.

Standard of care for GBM consists of tumor debulking with surgical resection, followed by radiation therapy and concomitant and adjuvant temozolomide (8). Two proposed alternate therapies include tumor treating fields (TTFields) and laser interstitial thermal therapy (LITT). TTFields is a non-invasive therapy which uses scalp electrodes to induce a dielectrophoretic force on GBM cells and inhibits cell division (9). A randomized clinical trial in patients undergoing either maintenance temozolomide or TTFields with maintenance temozolomide showed the TTFields-treated group had an increased median overall survival (16 vs. 20.9 months, respectively) (10). TTFields has significantly impacted the management of GBM, though further investigation of this therapy is warranted as implementing TTFields currently requires high patient adherence to wearing scalp electrodes >18 hr per day, which can lead to secondary effects such as contact dermatitis (11). Secondly, LITT is a minimally invasive thermal therapy utilizing catheter-based, MRI-guided laser heating to ablate GBM tumor tissue. Laser heating (either 90 vs 1064 nm) is used to induce focal hyperthermia and intraoperative real-time feedback of treatment progression is acquired using either a thermocouple or MRI-thermometry (12). LITT is currently under clinical investigation and shows promise in treating tumors near sensitive structures where surgery is not amenable (13–15). It should be noted that the diffuse thermal energy deposited during LITT may inadvertently damage eloquent structures by causing charring and carbonization of tissues adjacent to the tip, and that MRI thermometry is currently not achievable adjacent to bone.

These drawbacks highlight the need for an alternative approach for tumor cytoreduction in conjunction with enhanced peritumoral drug delivery. To this end, electroporation-based therapies have previously been investigated for intracranial applications, including CNS tumor ablation and transient disruption of the BBB (16–18). Electroporation therapies use high amplitude pulsed electric fields to exogenously raise the transmembrane potential of a cell above a critical threshold, leading to formation of defects on the cell membrane (19). These defects facilitate an increase in cell membrane permeability and are suitable for applications in enhanced delivery of plasmid DNA (electrogene-transfer (EGT)), enhanced delivery of molecular adjuvants and chemotherapeutic reagents (electrochemotherapy (ECT)), induction of non-thermal cell death (irreversible electroporation (IRE)), and for tumor immunomodulation (20–22). IRE occurs when the applied electric field is beyond the cell death threshold. It has been suggested that the non-thermal cell death mechanism induced by IRE can improve upon the antigen presentation and consequently the immune response (23). The anti-tumor effects of IRE are improved by, but not dependent upon, its immunomodulatory outcomes.

Monophasic pulses of around 100 microseconds are commonly delivered in IRE treatments. Despite its promising outcomes, IRE treatments are associated with pain and muscle contractions. Thus, high-frequency irreversible electroporation (H-FIRE), a second-generation IRE treatment protocol, was developed to mitigate the limitations of IRE. H-FIRE is administered intracranially by inserting needle-electrodes through a burr hole craniectomy, where insulation along the electrode ensures only the target tissue is exposed to high-magnitude electric fields (24). Notable benefits of intracranial H-FIRE ablation include: (i) non-thermal cell death, where protein structures in the ablation region are spared; (ii) peri-ablative disruption of the BBB for a duration up to 72 hours post-treatment; (iii) sharp ablative boundary, with a sub-millimeter delineation between ablated and intact tissue; (iv) enhanced susceptibility of cancer cells to H-FIRE ablation *in vitro*; (v) cell death is in part pro-inflammatory (necrosis and pyroptosis), producing antigens that modulate and recruit the immune system; (vi) treatment is not significantly influenced by neighboring anatomical structures, enabling tumor ablation near

eloquent anatomies, such as the skull, ventricles, or vasculature in the brain (25–29). Unlike traditional IRE, H-FIRE utilizes bursts of biphasic pulsed electric fields to non-thermally ablate neoplastic and non-neoplastic tissue while mitigating excitation of skeletal muscle and nerves during tissue ablation. Additionally, the utilization of bipolar pulses results in a net charge delivery of zero contributing to a reduction of electrolysis which when present, produces unwanted electrochemical effects including pH changes which may affect the cellular response to treatment (25).

Several electroporation-based treatments have been utilized for treating preclinical models of GBM. The safety and technical feasibility of intracranial electroporation has been established, though few efficacy studies have been conducted (30). Sharabi et al. (31) recently investigated the preclinical efficacy of ECT, a non-ablative electroporation modality used to focally increase the cytotoxicity of molecular adjuvants, for treatment of rodent glioblastoma. It was demonstrated ECT (cisplatin + electroporation) extended median survival from 15 to 22 days, compared to the cisplatin only group (31). Rossmeisl et al. investigated first generation IRE therapy for in situ, non-thermal ablation of high-grade glioma in canine patients presenting with spontaneous brain tumors. The median 14-day post-IRE Karnofsky Performance Score of subjects surviving to discharge (n=6/7) was improved over pre-treatment values in all cases by an average 16 points (32). Agerholm-Larsen et al. investigated preclinical efficacy of ECT (electroporation + bleomycin) for treatment of N32 glioma in rodents. Similarly, there was a significant improvement in survival ($P<0.001$) between the ECT group and the comparison group (electroporation only, bleomycin only, or no treatment) (33). These studies support intracranial application of electroporation, with improved neurocognitive outcomes.

To build upon preclinical studies of first-generation electroporation-based therapies for brain malignancies, here, we investigate the efficacy of both monotherapy and combinatorial (liposomal doxorubicin) H-FIRE for the management of GBM. To further develop our understanding of tumor response to H-FIRE, we briefly investigate the recruitment of the immune system post H-FIRE treatment. This survival endpoint study utilizes an orthotopic F98 rodent glioma model and survival is conducted against a sham, no treatment group.

2 Material and methods

2.1 Bioluminescent F98 rodent glioma cell lines

Our orthotopic tumor model comprises the Fischer rat strain and the highly infiltrative Rattus norvegicus F98 undifferentiated malignant glioma cell line (certified pathogen free, ATCC, Manassas, VA). The F98 glioma model was selected as it shares many characteristics with human GBM gliomas including an infiltrative growth pattern. Prior to implantation, F98 cells were transfected to express a plasmid coding for red-shifted firefly luciferase (pLL-EF1a-Luciferase-T2A-Puro Lenti-Labeler Lentivector Virus, Systems Biosciences Incorporated) for bioluminescent imaging allowing for tumor growth progression. Cells were maintained using conventional cell culture technique and prepped for both *in vitro* and *in vivo* investigations. Briefly, F98 cells were maintained at 5% CO2 and 37°C in Dulbecco's Modified Eagle Medium (ATCC) supplemented with 1% penicillin/streptomycin (Life Technologies), and 10% fetal bovine serum (R&D systems). Cells were routinely passaged at 70-90% confluence.

2.2 Assurances and surgical procedures

The study was performed in accordance with the principles of Guide for the Care and Use of Laboratory Animals and was approved by the Institutional Animal Care and Use Committee (IACUC #19-217). Study animals were adult male Fischer rats, weighing between 200-225g at the time of treatment. Following a 2-week acclimation period, rodents were premedicated with a subcutaneous (1mg/kg) injection of buprenorphine (Ethiqa XR. Fidelis Pharmaceuticals, North Brunswick, NJ), anesthetized using isoflurane induction (3-4%: 95% isoflurane: oxygen mixture), and then maintained with isoflurane (2-3.5%: 95% isoflurane: oxygen mixture) delivered *via* nosecone. The dorsum of the head from the intercanthal area to the cranial cervical region was clipped and prepared for aseptic surgery. Anesthetized rats were instrumented in a small animal stereotactic headframe (Model 1350M; David Kopf Instruments, Tujunga, CA, USA). A unilateral rostrotentorial surgical approach to the skull was performed and a 4 mm x 2.5 mm rectangular, parietal craniectomy defect was created in the skull of each rodent using a high-speed electric drill (Dremel 3000 Series; Mount Prospect IL, USA) with a 2.4 mm diameter, round burr.

Using the newly formed craniectomy defect, F98 malignant glioma cells were implanted using sterile, stereotactic surgery. A total of 10,000 cells in 5 µL of phosphate-buffered saline (PBS) were injected into the brain using a 29-gauge needle during a period of 2 minutes to prevent efflux. After the injection, the needle was kept in place for 1 minute, and then slowly retracted to prevent the spread of tumor cells. The incision was closed, and therefore after reopened at the 7-day timepoint (as determined during the tumor growth study), in preparation for H-FIRE treatment. Following H-FIRE pulse delivery, the electrodes were retracted, the craniectomy defect covered with bone wax (Ethicon), and the skin incision closed with 4-0 Monocryl interrupted skin sutures (Ethicon, Somerville, NJ, USA). Rats were recovered from anesthesia and monitored until their predetermined survival endpoints.

2.3 Characterization of the bioluminescence kinetic curve and tumor growth study

Bioluminescent imaging with *In Vivo* Imaging System (IVIS) (Perkin Elmer), is understood to be a transient process. Therefore, a standard kinetic curve was developed to determine an optimal time window for characterization of the luminescent signal. Rodents were anesthetized and administered an intraperitoneal 30 µg/ml (150 mg/kg body weight) injection of D-luciferin (Perkin Elmer).

Secondly, a tumor growth study was conducted to determine the optimal timeframe post inoculation for delivering H-FIRE treatment to tumor bearing rodents. Tumor growth was characterized *via* IVIS bioluminescence. Additionally, rodents were sacrificed on days 7, 14, 21, and 28 to acquire T2W MRI (7.0 T), H&E-stained tumor dimensions, and end-point immune cell infiltration.

2.4 High-frequency irreversible electroporation

A custom pulse generator (VoltMed Inc., Blacksburg, Virginia) was used to deliver bursts of biphasic pulsed electric fields both *in vitro* and *in vivo*. This generator is capable of producing voltage waveforms with pulse rise times of 100 ns and a maximum voltage/current output of 5kV/100A. Voltage and current waveforms were recorded using a WaveSurfer 2034z oscilloscope (Teledyne LeCroy, Chestnut Ridge, NY) with a 1000X high voltage probe (Enhancer 3000, BTX, Holliston, MA) and 10X current probe (2877, Pearson Electronics, Palo Alto, CA). Schematics of the three H-FIRE waveforms investigated are shown in Figure 1 for the 1-5-1 µs, 5-5-5 µs, and 10-5-10 µs waveforms.

2.5 Fabrication of collagen hydrogel tissue mimics for *in vitro* H-FIRE studies

Type I collagen from rat tail (Corning) was neutralized using 1N NaOH solution (Sigma) (2% of initial collagen volume) followed by dilution to a final concentration of 5 mg/ml using 10X DMEM (Sigma) (10% of the final volume) and 1X DMEM (ATCC). Cells, either healthy rodent astrocytes (DI TNC1) or rodent glioma (F98), suspended in solution at a density of 2×10^6 cells per milliliter. PDMS (Polydimethylsiloxane) molds were used to form the collagen hydrogel scaffolds into the geometry shown in Figure 2. To enhance the attachment of collagen to PDMS, the molds were pretreated with 1% PEI solution (Acros organics) for 10 minutes followed by a 20-minute treatment with 0.1% glutaraldehyde (Fisher chemical) solution. Approximately 400 µl of collagen mixture was placed in each PDMS mold (100 µl in each chip × 4). PDMS molds were placed into a rectangular 8 well plate, followed by 25 minutes of incubation at 37°C. 2 µl of media was added on top of the scaffolds after solidification and hydrogels were incubated for 24 hours prior to pulsing.

Treatment for *in vitro* tumor constructs was accomplished using a mobile incubator maintained at 37°C. A sample size n > 8 was achieved for each H-FIRE waveform and each cell line. After treatment, media was replenished and cells were incubated for another 24 hours to allow for development of the lesion. For staining, media was aspirated from each well and replaced with aa staining solution consisting of PBS, 2 µM calcein AM (Invitrogen), and 23 µM PI (Invitrogen). Hydrogels were incubated at 37°C and 5% CO2 for 30 minutes, thereafter, were washed twice with PBS prior to imaging using an inverted microscope (DMI 6000B, Leica Microsystems) with a 5× objective. The appropriate filters were used to image calcein AM (Ex:460–500; DC:505; EM:570–640) and propidium iodide (EX:545/26, DC:565, EM:605/70).

Images were processed in Image J (National Institute of Health (NIH)). A rectangular (22.35 × 1.35 mm) region of interest (ROI) was defined which spans the length of the chip, the intensity of each channel was averaged across the width of the ROI. This analysis yielded a profile describing the average intensity of calcein/PI as a function of distance along individual chips. Numerical methods (described below) were then used to solve for the electric field distribution along this chip, and the relationship between the local electric field and the distance along the chip was extracted. Finally, the datasets were mapped to one another, and the average intensities were normalized to then obtain the normalized intensity vs. local electric field (Figure 2).

2.6 Numerical methods for determination of pulsing parameters

A numerical model was constructed in COMSOL Multiphysics v5.6 (COMSOL Inc., Stockholm, Sweden) to determine the electrode configuration and pulsing parameters for adequate tumor coverage in ablative electric fields. The tumor was approximated as a 12.6 mm^3 sphere, as determined by the tumor growth study, and a realistic rodent brain domain was defined using a 3D reconstruction from a T1W MRI scan (3D Slicer 4.11). The final domain, including the brain, tumor sphere, and two monopolar electrodes, consisted of 207,836 tetrahedral elements resulting from an "extra fine" mesh setting within COMSOL. After

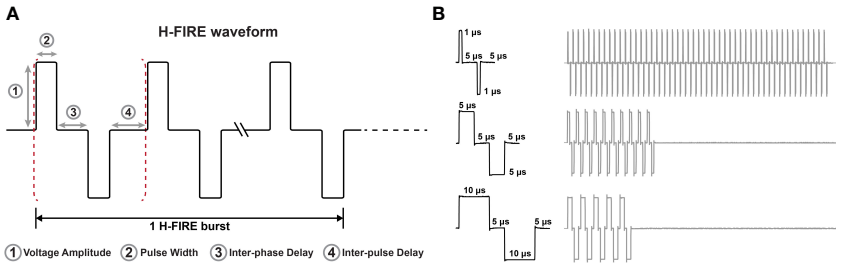

FIGURE 1
Representative H-FIRE waveforms. **(A)** Schematic that represents the nomenclature associated with the H-FIRE waveform and **(B)** recording of voltage waveforms during treatment depicting differences in pulse width and the burst period.

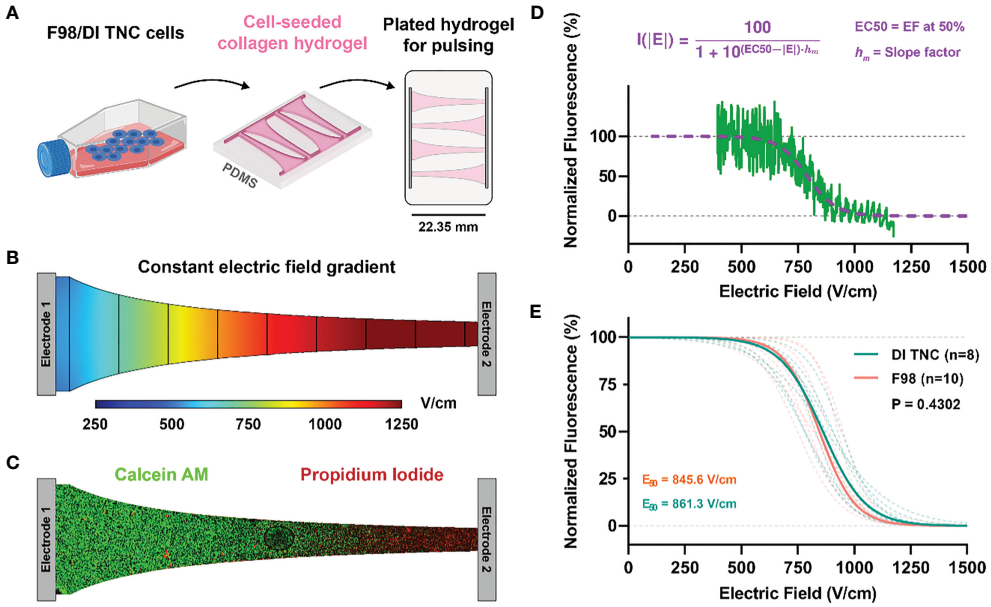

FIGURE 2
(A) Schematic of cell lines (either healthy DI TNC or malignant F98) were individually cultured and then seeded within a microfluidic device experiencing a **(B)** constant electric field gradient as demonstrated by a numerical simulation of the channel. **(C)** Live/dead fluorescent imaging of calcein/PI-stained cells demonstrated a **(D)** sigmoidal fall off of fluorescence along the narrow band of the channel that was then correlated with specific electric field values as determined by numerical methods. **(E)** Electric field thresholds for both DI TNC and F98 cell lines were determined by the EC50 correlating with the 50% survival point.

mesh generation, the electric potential distribution was modeled using Equation 1.

$$\nabla \cdot (\sigma \nabla \phi) = 0 \quad (1)$$

Here, σ is the electrical conductivity as a function of the electric field E and ϕ is the electric potential.

A pre-treatment voltage ramp was performed to characterize the baseline electrical conductivity reflecting the tissue properties of tumor tissue. Results from the *in vitro* study informed the use of the H-FIRE 5-5-5 µs burst scheme to be applied *in vivo* (Section 3.1). Thus, for treatment of glioma-bearing rodents, H-FIRE therapy was administered as 200 bursts (100 µs of energy per burst) delivered at a rate of 1 burst per second, and a delivery across two blunt-tipped stainless steel electrodes. Parameters including applied voltage, electrode exposure, and electrode spacing were parametrically swept through until desired field distributions were predicted. Two desired protocols were established based on the field distribution: the high-dose H-FIRE protocol, where strong ablation-strength fields predominantly encapsulated the tumor, and the low-dose H-FIRE protocol, where low-strength BBB disruption strength fields encapsulated the majority of the tumor while minimizing the extent of ablation strength fields. The latter was utilized to observe the effects of enhanced delivery of a combinatorial adjuvant from the expected BBB disruption while eliminating the therapeutic effects of ablative strength high-dose H-FIRE fields.

Volume coverage was based on field thresholds from *in-vitro* studies (861.3 V/cm for ablation coverage) and previous *in-vivo* work from our group (113.5 V/cm for BBB disruption volume coverage (17)). Numerical modeling informed use of a 2.5 mm electrode exposure, 3 mm electrode spacing, and an applied potential of 180 V or 525 V producing a voltage-to-distance ratio of either 600 V/cm (low dose BBB disruption protocol), or 1,750 V/cm (high-dose ablation protocol) respectively. On treatment day, the electrodes were advanced into the brain using the micromanipulator arm of the stereotactic frame according to stereotactic coordinates references to the location of the rostral electrode (bregma 4mm caudal, 3.5 mm lateral, at a depth of -4 mm relative the surface of the dura).

Three bursts of 25, 50, 100, 150, 180 (low-dose treatment voltage), and 525 V (high-dose treatment voltage) were applied. The low-dose and high-dose H-FIRE groups received voltage ramps only up to their respective treatment voltage. Corresponding voltage and current profiles were recorded on an oscilloscope (Teledyne LeCroy, Chestnut Ridge, NY, USA) with a 1000× high voltage probe (Enhancer 3000, BTX, Holliston, MA, USA) and 10× current probe (2877, Pearson Electronics, Palo Alto, CA, USA). The final 2 µs of the final pulse for each recorded voltage and current burst was averaged and plotted on a current vs voltage plot. Experimental conditions were replicated in COMSOL Multiphysics v5.6 (COMSOL Inc., Stockholm, Sweden) and initial electrical properties were derived from reported values for healthy rodent astrocyte tissue (17) and malignant canine glioma tissue (26). A comprehensive parametric study varying parameters σ_0, E_{del}, E_{range}, and A was performed to design two sigmoidal conductivity curves, fitting the experimental voltage and current data collected from the pre-treatment voltage ramps for healthy rodent brain, and malignant tumor tissue (Figure 3). Healthy brain tissue properties were determined in rodents with low or no IVIS signal. The conductivity sigmoid is comprised of an initial value σ_0 which

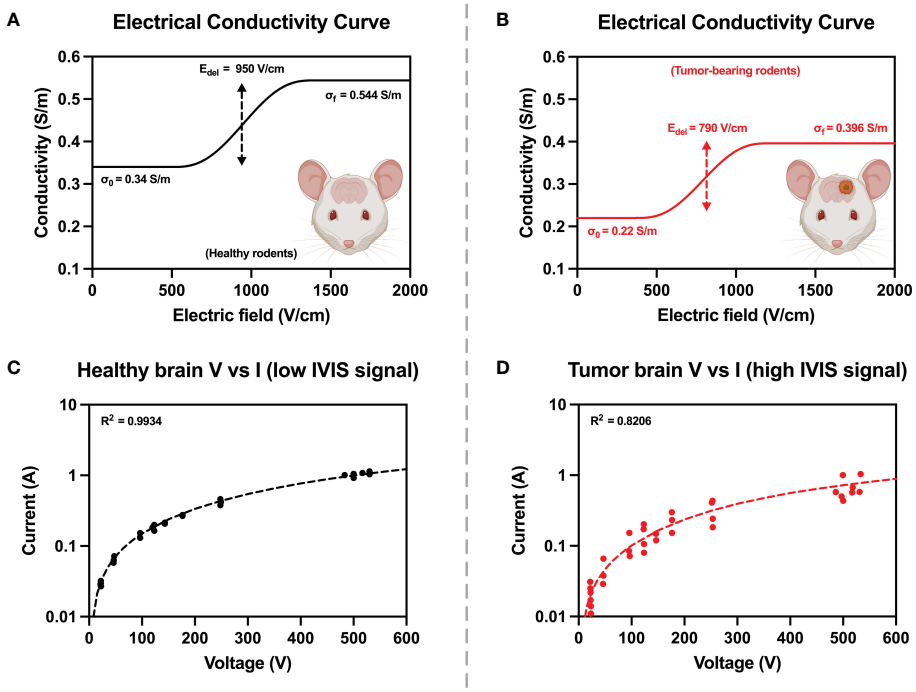

FIGURE 3
Electrical tissue conductivity curves for **(A)** healthy and **(B)** tumor-bearing rodents were reconstructed by ensuring agreement between experimental and numerical values from pre-treatment voltage and current ramps **(C, D)**. Numerical modelling was used to manipulate parameters of the conductivity curves until simulated current and voltage (dashed lines) were in good agreement with experimentally measured values (solid points).

represents the initial conductivity of the tissue prior to entering an electroporated state, and plateaus to a value of σ_f once the tissue has entered a state of complete electroporation. The transition of an un-electroporated to electroporated state occurs over a range $\pm 2 \cdot E_{range}$ centered about a point E_{delta}.

$$\sigma(E) = \sigma_0 \ (1 + A \cdot flc2hs(E - E_{del}, E_{range})) \quad (2)$$

Following the characterization of rat brain tissue conductivity, an electric potential boundary condition (ϕ = 180V or 525V) and a grounding boundary condition was applied on either electrode. Thermal dissipation and Joule heating effects were calculated using a modified bioheat equation (Equation 3):

$$\rho c_p \frac{\partial T}{\partial t} = \nabla \cdot (k \nabla T) + \omega_b \rho_b c_b (T_b - T) + \frac{\sigma \cdot |E|^2 \cdot p}{\tau} \quad (3)$$

where ρ is the tissue density; c_p the specific heat; k is the thermal conductivity; and ω_b is the distributed blood perfusion coefficient. In this study, T_b, ρ_b, and c_b were 32.2°C, 1050 kg/m^3, and 3617 J/(kg·K), respectively. The terms p and τ represent the duty cycle normalization terms, which allow for high frequency electroporation thermal contributions to be represented as a continuous heat source rather than a periodic heat source, as the latter would require drastic changes in solver time-stepping. Here p is the burst on-time (100x10^{-6} s) and τ is the period of burst delivery (1 s). Additional parameter values used in this model are represented in Table 1.

2.7 Combinatorial doxorubicin + H-FIRE

To investigate the combinatorial effects of H-FIRE in conjunction with a molecular adjuvant, select rodents were enrolled to receive liposomal doxorubicin either as a monotherapy or as an adjuvant to H-FIRE. The selection of liposomal doxorubicin (Lipodox) as the drug for this model was based on the high expression levels of alkyltransferase in F98 cells. Alkyltransferase is an enzyme that inactivates alkylating agents, such as the standard of care therapeutic agent, temozolomide. This selection was based on a rationale that considers the specific characteristics of F98 cells and the pharmacological properties of Lipodox. These rodents received an IP injection of 5mg/kg Lipodox (2mg/mL, Cardinal Health). According to the manufacturer's instructions, Lipodox was prepared to a final concentration of 0.5mg/mL in D5W and supplied using a closed system transfer device (Equashield) coupled to a 22G retractable butterfly catheter. To ensure that the complete volume of chemotherapy was delivered, the system was flushed with 0.5 mL of sterile saline. For rodents in the combinatorial high-dose/low-dose H-FIRE + DOX group, Lipodox was administered 30-60 minutes before H-FIRE administration.

Parallel to the survival study, a separate investigation using tumor bearing rodents was used to quantify the concentrations of Lipodox in both tumor and healthy brain tissue. Concentrations were measured in 4 groups (n=3 each): 1) within the homologous contralateral striatum of tumor bearing rat brains of Lipodox treated animals; 2) within the homologous contralateral striatum

TABLE 1 Electrical and thermal values for the numerical model.

Material	Parameter	Value	Units
Brain tissue	Density, ρ	1046	kg/m^3
	Specific heat, c	3630	J/(kg·K)
	Thermal conductivity, k	0.51	W/(m·K)
	Blood perfusion coefficient, ω	$1.75x10^{-3}$	1/s
Insulation	Density, ρ	1190	kg/m^3
	Specific heat, c	1470	J/(kg·K)
	Thermal conductivity, k	0.18	W/(m·K)
	Electrical conductivity, σ	$2.5x10^{-14}$	S/m
Stainless steel	Density, ρ	7850	kg/m^3
	Specific heat, c	475	J/(kg·K)
	Thermal conductivity, k	44.5	W/(m·K)
	Electrical conductivity, σ	$4.03x10^6$	S/m

Material properties were attained from IT'IS database (https://itis.swiss).

of tumor bearing Lipodox + H-FIRE treated animals; 3) within the F98 tumor after Lipodox treatment only; and 4) within the F98 tumor after Lipodox and high-dose H-FIRE ablative treatment. One hour after IP liposomal doxorubicin (Lipodox) administration and H-FIRE treatment, rats were sacrificed, and their brains extracted and loaded into a 2 mm matrix slicer brain matrix (Zivic Instruments, Pittsburg, PA, USA). As Lipodox has a plasma half-life of 2–3 days, we presumed the entire representative dose was still present in the circulation at the one-hour time point (34). Transverse sections of the brain containing implanted tumor and a homologous section of unaffected contralateral brain were harvested. Tumor samples were obtained at the peripheral margin of the tumor at its interface with peritumoral brain tissue, as these are contrast-enhancing tumors regions on MRI examinations. Harvested brain sections were trimmed to 0.03 g, placed into 1.5 ml centrifuge tube containing 600 µL of acidified alcohol extraction solution (0.3 N HCl in 50% EtOH), homogenized (TissueRuptor II, Qiagen), and then refrigerated at 4°C for 24 hours. Samples were then centrifuged at 4,000 g for 20 min at 4°C. The supernatant was extracted and intensity measurements (excitation/emission wavelengths: 480/590 nm) performed using a fluorometer (VersaFluor; Bio-Red Laboratories, Hercules, CA). Lipodox concentrations were quantified by linear regression and a standard curve obtained from eight serial stock Lipodox concentrations. The concentration of doxorubicin in each sample was obtained by taking the average of three fluorometric readings. Fluorometric readings were normalized to measurements from normal control animals that only received vehicle (D5W) control treatments (n=3) to correct for autofluorescence.

2.8 Survival endpoint determination

Subjects were euthanized once they met the criteria for a humane endpoint as indicated by rodent neurologic severity score (RNSS), physical observation score (PO), body condition score (BC), and body weight (BW). The study was concluded at a timepoint 40 days post treatment. Specific scoring criteria may be found in the Supplemental Material (Data Sheet 1).

2.9 Characterizing immune response following H-FIRE treatment

2.9.1 Characterizing the innate and adaptive immune response following H-FIRE treatment

A secondary controlled study was designed to capture the innate and adaptive immune responses following high-dose H-FIRE treatment. In this parallel study, rats were sacrificed at a predetermined endpoint which was either 24 hours (n=4) or 10 days (n=4) post-H-FIRE treatment for innate and adaptive responses, respectively. The euthanasia process involved administering an IP injection of pentobarbital sodium (Fatal-Plus, Vortech Pharmaceuticals) after isoflurane anesthesia. The brains were transversely sectioned into 1mm-thick segments and divided, along with cervical lymph nodes, for preservation and subsequent analysis using either 10% Formalin or RNA later.

2.9.1.1 Serum cytokine analysis

Blood samples were collected through cardiac puncture immediately after euthanasia for serum cytokine analysis. Serum samples from rats with equal survival times were tested using the MAP Rat Cytokine Immunology Multiplex Assay (RECYMAG65K27PMX, Millipore Sigma), allowing for the simultaneous measurement of 14 chemokines and cytokines.

2.9.1.2 Gene expression and pathway analysis

After H-FIRE treatment, the Qiagen RNeasy Lipid Tissue Mini Kit was used to extract total RNA from brain sections. The RNA was quantified and utilized for cDNA synthesis, which was carried

out using an RT2 First Strand Kit (Qiagen). The RT2 Profiler PCR Array for Innate and Adaptive Immunity (Qiagen) was utilized for gene expression analysis, and triplicate PCR reactions were performed on each sample. The gene expression data were normalized to internal housekeeping genes and analyzed with online software from the manufacturer, Gene Globe (Qiagen) and iPathways (Advaita). The fold-change in gene expression was calculated using the mean Ct value of triplicate PCR reactions in comparison to the sham controls.

2.9.2 Immunohistochemical analysis

The local immune response to treatment was assessed by characterizing immune cell infiltrates within brain sections collected from high-dose H-FIRE ablation groups at the study endpoint. Tissue samples were sectioned and stained for presence of T cells (CD3, Dako), helper T cells (CD4, Origene), cytotoxic T cells (CD8, Invitrogene), regulatory T cells (FoxP3, Invitrigene), B cells (CD79a, Santa Cruz), microglia (IBA-1, FUJIFILM), M1 macrophages (CD86, Abcam), and M2 macrophages (CD163, Abcam). Methods were followed as presented by Koshkaki et al. (35). Samples were categorized as peritumoral region (healthy tissue), transition zone (submillimeter zone between the tumor mass and the peritumoral region), tumor mass, and the necrotic core. Tissue samples were imaged using a Nikon Eclipse Ni-U microscope using a Ds-Ri2 camera. The acquired images were analyzed using the NIS element BR software version 5.21.01.

Briefly, auto thresholding was done on all images followed by greyscale conversion. Mean gray values (*MGVi*) and gray area fractions (*AF*) were calculated using the software. The values were then used to find the final chromogen intensity (*f*) as follows:

$$f = 255 - MGVi \tag{4}$$

Mean *f* and *AF* values were next calculated using five high power fields from each slide. The immunohistochemistry (*IHC*) score was calculated using the mean values and the following equation:

$$IHC = f \cdot AF \tag{5}$$

2.10 Statistical analysis

GraphPad Prism v9.4 (GraphPad Software, San Diego, CA) was used to conduct statistical analysis in all cases. A Mantel-Cox Logrank test was used to evaluate differences among survival curves with respect to the sham control group. Changes between individual treatment groups and sham controls for gene expression, cytokine levels, and IHC scores were evaluated *via* Student's t-test. Multiple comparisons between treatment groups were conducted using a two-way analysis of variance (ANOVA) followed by a Tukey's *post hoc* test where the criteria for significance was set to alpha = 0.05 ($p < 0.05$).

3 Results

3.1 Determination of H-FIRE pulsing parameters in an *in vitro* collagen hydrogel tumor scaffold

An H-FIRE waveform is constructed as: positive phase – inter-phase delay – negative phase – inter-pulse delay, with this burst of bipolar pulsed electric fields is repeated until a desired energized-time (100 µs) is reached. Cell death from H-FIRE therapy was investigated for three distinct waveforms: 1) 10-5-10 µs, 2) 5-5-5 µs, 3) 1-5-1 µs. A 3D collagen hydrogel platform was utilized for viability experiments. These hydrogels allow cells to adhere to the collagen matrix and express physiologically relevant morphologies, facilitating characterization of electroporation *in vitro*. H-FIRE therapy was administered, and cell viability was assessed using calcein green and propidium iodide 24 hours after pulsing.

The geometry of the hydrogel was formed such that a linearly varying (constant gradient) electric field is induced across the cells (Figures 2A–C). Rather than quantifying a discrete electric field which elicits cell death, we can describe a sigmoidal relationship between the applied electric field and percent cell death. Numerical methods were used to solve for the electric field distribution along this chip, this was subsequently mapped to the normalized intensity to attain viability plots (Figures 2D, E). Nonlinear regression was conducted to fit the normalized intensity vs. electric field data sets to a sigmoid equation (Equation 6). Here, $I(|E|)$ describes the normalized intensity (I) at a specific electric field magnitude ($|E|$), $EC50$ is the electric field corresponding to 50% viability, and h_m is the slope of the transition.

$$I(|E|) = \frac{100}{1 + 10^{(EC50 - |E|) \cdot h_m}} \tag{6}$$

The fitting parameters of Equation 6 are highlighted in Table 2. Direct comparison of the viability plots demonstrates that longer pulse widths elicit cell death at lower electric fields for both the F98 and DI TNC1 cell lines. Translating the results for *in vivo* ablation,

TABLE 2 F98 and DI TNC cell viability parameters for H-FIRE in collagen hydrogel scaffolds.

Pulse Waveform	Cell line	50% viability, EC50	Slope, h_m
1-5-1 µs	F98 (n = 9) DI TNC1 (n = 11)	961.1 ± 46.0 V/cm 1255.5 ± 122.7 V/cm	$-6.03 \times 10^3 \pm 1.91 \times 10^3$ $-3.83 \times 10^3 \pm 1.04 \times 10^3$
5-5-5 µs	F98 (n = 10) DI TNC1 (n = 8)	845.6 ± 63.3 V/cm 861.3 ± 59.9 V/cm	$-5.55 \times 10^3 \pm 1.35 \times 10^3$ $-4.61 \times 10^3 \pm 0.97 \times 10^3$
10-5-10 µs	F98 (n = 8) DI TNC1 (n = 9)	643.0 ± 22.6 V/cm 667.0 ± 20.4 V/cm	$-7.53 \times 10^3 \pm 0.89 \times 10^3$ $-5.95 \times 10^3 \pm 1.52 \times 10^3$

these results suggest that for given voltage and pulsing parameters, a larger volume of cell death is induced with the 10-5-10 µs waveform in comparison to the others. Interestingly, there is a subtle separation of induced cell death between the healthy DI TNC1 cell line and the malignant F98 cell line using the higher frequency waveform 1-5-1 µs. This result implies H-FIRE can be administered in such a way that cell death is achieved in malignant cells while sparing, to a limited extent, underlying healthy astrocytes.

For the DI TNC1 cell line, the slope of the sigmoid, h_m, indicates large pulse widths incur cell death more efficiently, as $|h_{10\text{-}5\text{-}10}| > |h_{5\text{-}5\text{-}5}| > |h_{1\text{-}5\text{-}1}|$. Ultimately, a balance between the extent of cell death and anticipated nerve excitation was desired. The effects of pulse width on nerve excitation were previously studied demonstrating greater excitation at lower frequency waveforms (36).

Numerical modeling for *in vivo* treatments indicated that the high-dose H-FIRE protocol was estimated to produce 98.7% and 100% coverage of the tumor in ablation strength and BBB disruption strength fields respectively while the low-dose H-FIRE protocol was predicted to produce 6.7% and 100% ablation strength and BBB disruption strength fields respectively (Figure shown in Supplemental Material (Data Sheet 1).

3.2 Validation of Lipodox perfusion into the brain following H-FIRE

Lipodox concentrations are reported in Figure 4. The findings of the study showed that while significantly higher concentrations of Lipodox were still detected in the Lipodox only F98 group ($p< 0.006$), the use of high-dose H-FIRE significantly improved the penetration of Lipodox into the brain tissue compared to all other groups ($p< 0.003$).

3.3 Characterization of the bioluminescence kinetic curve and tumor growth study

First, the kinetics of bioluminescence was quantified, as both the tumor type and tumor implant location are known to affect the bioluminescent kinetics (Figure 5B). The maximum intensity signal was found to be between 20-30 minutes (n=3) following intraperitoneal administration of D-luciferin (Figure 5A).

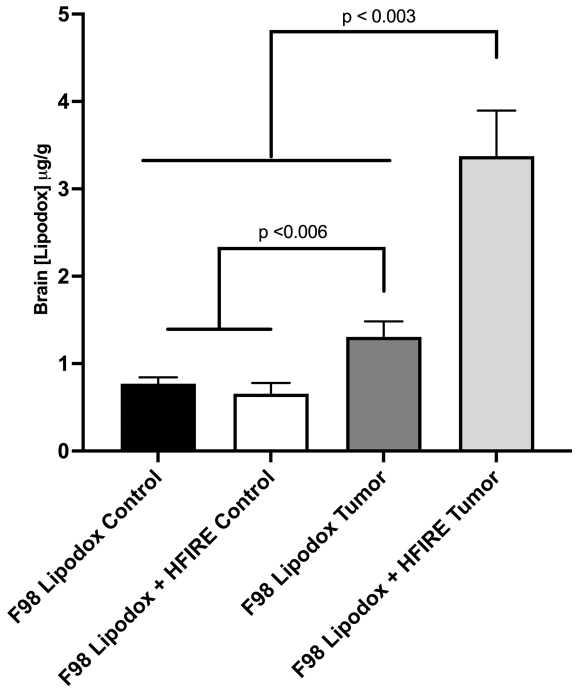

FIGURE 4
Concentrations of Lipodox in bran tissue were measured in four groups (n=3 each) one hour after intraperitoneal injection. All groups received Lipodox injection. The groups include 1) F98 Lipodox Control in which Lipodox concentrations were measured in the normal striatum of the brain contralateral to the tumor, 2) F98 Lipodox + HFIRE Control in which Lipodox concentrations were measured in the homologous, normal striatum of the brain contralateral to the tumor, 3) F98 Lipodox Tumor in which concentrations were measured within the tumor, and 4) F98 Lipodox + HFIRE Tumor in which concentrations were measured within the tumor. Although a detectable difference was noted between the concentrations of Lipodox measured within the healthy part of the brain and within the tumor, H-FIRE treated rodents had a much more significantly elevated concentration in Lipodox concentrations in the tumor. H-FIRE did not increase the concentration of Lipodox in the healthy striatum compared to that of the Lipodox Control.

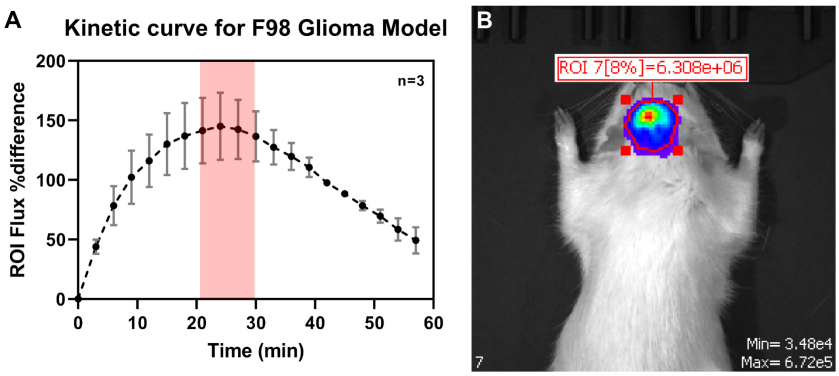

FIGURE 5
(A) Determination of the kinetic curve for quantification of tumor bioluminescent signal during IVIS imaging. The maximum luminescent signal reading was found to be 20-30 miutes following IP administration of D-Luciferin. **(B)** Representative bioluminescent image during the tumor growth kinetic study.

3.4 *In vivo* tumor growth study

We used IVIS bioluminescence, MRI, and H&E (Figures 6A, B) to characterize tumor growth. Day 7 was found to be an optimal time point for treating rodents, as the tumor grew large enough for visualization without surpassing the two-electrode treatment zone or inducing severe neurological decline or death.

3.5 Survival endpoint study

Animals underwent IVIS imaging weekly to monitor progression of tumor growth. While all rodents were inoculated with tumors, the SHAM group did not receive any therapeutic intervention. Representative images of the IVIS signals for SHAM and H-FIRE treated rodents are shown in Figure 7. The SHAM group demonstrated a strong tumor signal throughout the duration of the monitoring period, whereas H-FIRE treated rodents that demonstrated strong tumor signals prior to receiving treatment, demonstrated no relevant signal during follow up imaging, suggesting eradication of the tumor. Photon fluence (φ) with a maximum signal measuring less than 10^4 was considered to be background noise.

Body weight, physical observation (PO) scores, and rodent neurological severity score (RNSS) scores were recorded weekly to monitor potential signs of disease progression. Overall, the animals body weight followed rising trends over the course of the study (data not shown).

The survival curve (Figure 8) demonstrates that H-FIRE significantly lengthened the lives of animals with the F98 glioma tumor (with the exception of the low-dose H-FIRE + DOX group). The groups were each compared for compared survival against the

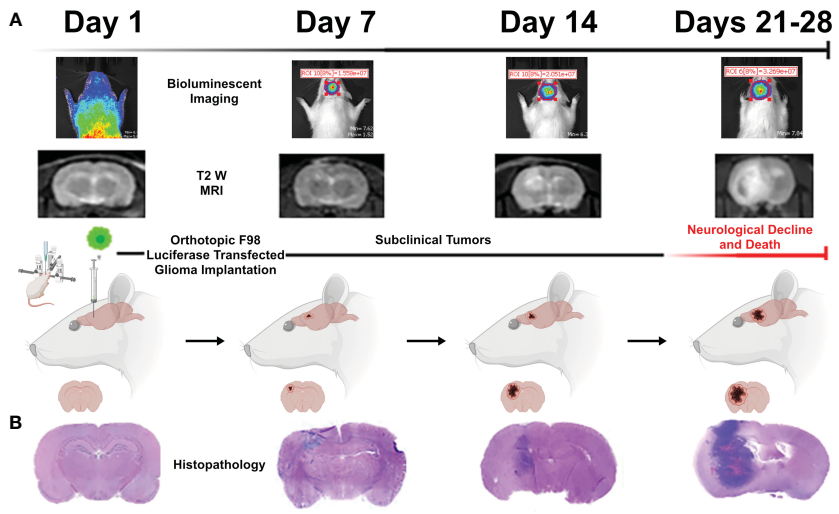

FIGURE 6
Representative images acquired during the tumor growth study *via* **(A)** bioluminescent IVIS imaging, T2W MRI, and **(B)** representative brain histopathology. These three methods were used to quantify tumor growth of untreated rodents over the course of a four-week period to determine the optimal period for treatment intervention (found to be 7 days). Figure created with https://BioRender.com.

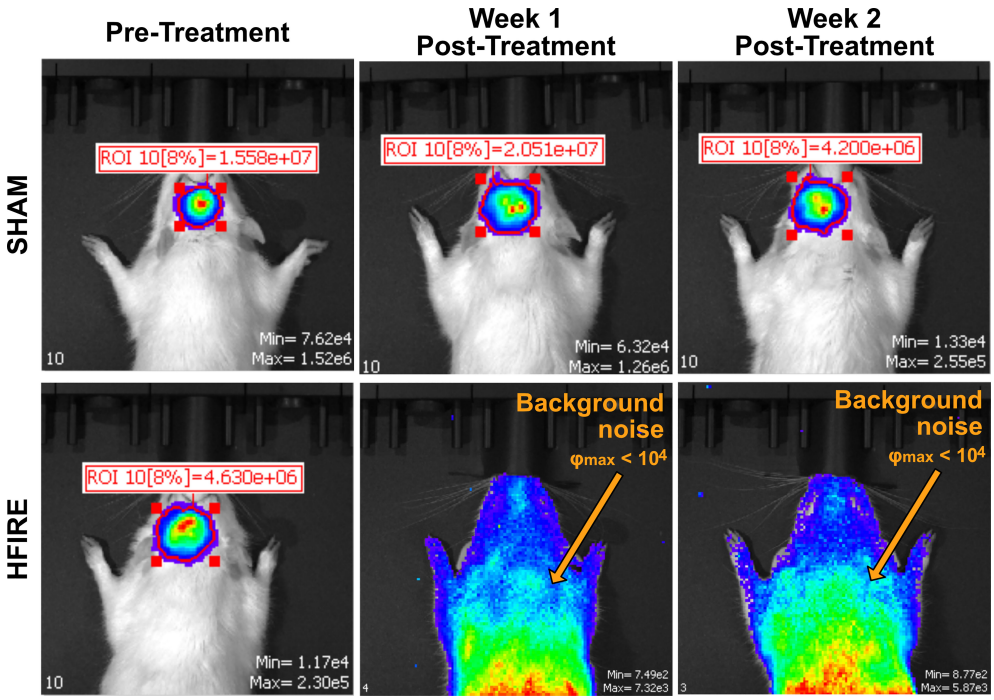

FIGURE 7
Bioluminescent imaging from the IVIS imaging system was used to monitor tumor growth throughout the duration of the study. A representative rodent from the Sham group is shown on the top row while a representative rodent from the high dose H-FIRE therapy group is shown on the bottom row. The individual rodents were imaged at time points 7 days post tumor implantation (pre-treatment), and at time points one and two weeks post treatment. The rodent from the Sham group which, received tumor implantation but no H-FIRE therapy, demonstrates strong presence of the tumor signal throughout the three week period shown, while the tumor bearing rodent receiving H-FIRE therapy demonstrates eradication of the tumor signal one week post treatment. Maximum fluence values under 10^4 were considered background noise and not strong enough to be considered a tumor signal.

sham group, and overall survival fractions were as follows: 50% for high-dose H-FIRE+DOX ($p = 0.044$), 28.6% for high-dose H-FIRE ($p = 0.034$), 20% for low-dose H-FIRE ($p = 0.0214$), 17% for low-dose H-FIRE+DOX (ns; $p = 0.2072$), and 0% for the DOX group (ns; $p = 0.2974$). Statistically greater survival compared to the sham group was seen in high-dose H-FIRE+DOX ($p = 0.044$), high-dose H-FIRE ($p = 0.034$), and low dose H-FIRE ($p = 0.0214$). Low-dose H-FIRE+DOX (ns; $p = 0.2072$) and the DOX only group (ns; $p = 0.2974$) did not show any improvements in survival outcomes. On day 26 post-treatment, all five rats in the Sham group met humane endpoint while 3/6 (50%) high-dose H-FIRE+DOX, 2/7 (29%) high-dose H-FIRE, 1/5 (20%) low-dose H-FIRE, and 1/6 (17%) low-dose H-FIRE+DOX treated rats survived to the conclusion of the trial (day 40).

3.6 Monitoring the Immune response after H-FIRE treatment

Local immune cell infiltration was investigated *via* IHC staining of brain tissue samples collected at the study endpoint (Figure 9). The overall presence of T cells, B cells, and microglia was observed to be greater in the H-FIRE ablation group compared to the sham controls. Furthermore, CD8 cytotoxic T cell infiltration was found to be higher in the H-FIRE ablation group, while the density of CD4 helper T cells and immunosuppressive regulatory T-cells was similar between H-FIRE ablation and sham control groups.

When comparing immune cell infiltrates between the previously defined treatment zones (Section 2.9.2), the proportion of B cells was much higher within the tumor mass (71% in the H-FIRE ablation group vs. 9% in the sham control group), while the proportion of T cells and microglia was higher within the transition zone. Interestingly, when differentiating T cell subtypes, we observed a greater proportion of CD4 helper T cells within the tumor mass (75% in the H-FIRE ablation group vs. 15% in the sham control group), whereas the proportion of cytotoxic T cells and regulatory T cells was greatest within the transition zone of the H-FIRE ablation group.

The present study conducted a comparison of serum cytokine concentrations in rats treated with H-FIRE ablation and H-FIRE BBB disruption. Fourteen cytokines were analyzed, and the results showed that the levels of interferon-gamma (IFNγ) ($p< 0.01$), interleukin-2 (IL-2) ($p< 0.01$), interleukin-6 (IL-6) ($p< 0.01$), and interleukin-17a (IL-17a) ($p< 0.001$) were significantly elevated in rats treated with H-FIRE ablation (Figure 10A). This trend was consistent for IFNγ, IL-2, IL-6 and IL-17a even after the administration of Lipodox chemotherapy, where the levels of these cytokines were increased in rats treated with H-FIRE ablation + Lipodox compared to those treated with H-FIRE BBB disruption + Lipodox. In addition, GM-CSF was found to be

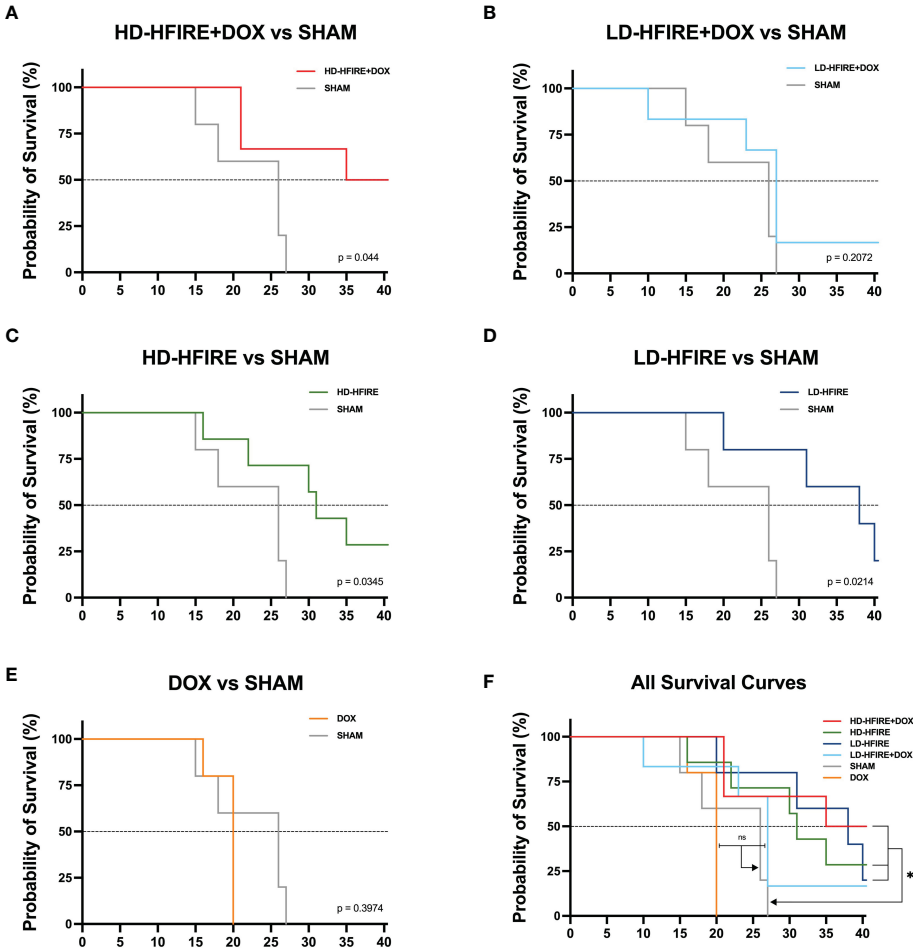

FIGURE 8
Kaplan-Meier survival plots for F98 tumor bearing rats. The **(A)** high-dose H-FIRE+Lipodox (HD-HFIRE+DOX), **(C)** high-dose H-FIRE (HD-HFIRE), and **(D)** low-dose H-FIRE (LD-HFIRE) lived significantly longer than the sham controls ($p < 0.05$). Significance was not noted between the **(B)** low-dose H-FIRE +Lipodox (LD-H-FIRE+DOX) or **(E)** Lipodox only (DOX) groups against the sham. **(F)** Overall, H-FIRE intervention appears to significantly improve overall rodent survival (with the exception of the LD-H-FIRE+DOX group). ns = not significant; *$p < 0.05$.

significantly decreased in rats treated with H-FIRE ablation + Lipodox chemotherapy relative to rats treated with Lipodox alone. Conversely, IL-17a was significantly increased ($p < 0.01$) in the same group of rats. At 24 hours post-H-FIRE ablation, there was a significant increase in the levels of IL-6 ($p < 0.01$), IL-17a ($p < 0.001$) and keratinocyte-derived chemokine (KC) ($p < 0.001$) compared to the sham-treated controls, as shown in Figure 10B. Additionally, tumor necrosis factor-alpha (TNF-α) and vascular endothelial growth factor (VEGF) levels were significantly increased at 10 days post-H-FIRE ablation ($p < 0.05$). There were no significant differences in cytokine concentrations observed between the 24-hour and 10-day post-H-FIRE ablation groups.

Gene expression and pathway analysis indicated significant variations in the expression of genes involved with innate and adaptive immunity between treated F98 rat brains and untreated controls (Figure 11). At 24-hours post-H-FIRE ablation, most analyzed genes were elevated by more than 2-fold in comparison to sham-treated controls. However, only one gene (*Itgam*) was statistically significant ($p < 0.05$). At 10-days post-H-FIRE ablation, significant increases in gene expression were observed in H-FIRE ablation groups in comparison to sham-treated controls. These genes included those related to P/DAMP signaling (e.g., *Il6, Tlr1, Tlr4, Il1b, Il18*), necroptotic tumor cell death (e.g., *Casp1, Casp8, Il1b*), and activation of the adaptive immune system (e.g., *Cd80, Cd8a, Ccr5, Cxcl10*). *Casp1, Casp8, Ccl12, Cd8a, Cxcl10, Il2, Lbp, Tlr1, Tlr3*, and *Tlr4* showed the most significant statistical significance ($p < 0.01$) among the genes upregulated by H-FIRE ablation. In addition, the NF-kappa B (NF-κB) pathway was found to be significantly upregulated relative to sham-controls. NF-κ;B plays an important role in regulating genes associated with inflammation and is responsible for the production of pro-inflammatory cytokines and regulating the development of naive T helper cells into effector T helper cells (Th1, Th2, and Th17 cells), and activated macrophages into the proinflammatory M1 phenotype. The serum cytokine analysis also revealed significant increases in pro-inflammatory cytokines mediated by NF-κ;B following H-FIRE ablation relative to sham controls.

Overall, our results suggest that H-FIRE ablation promotes immune cell infiltration within the tumor microenvironment.

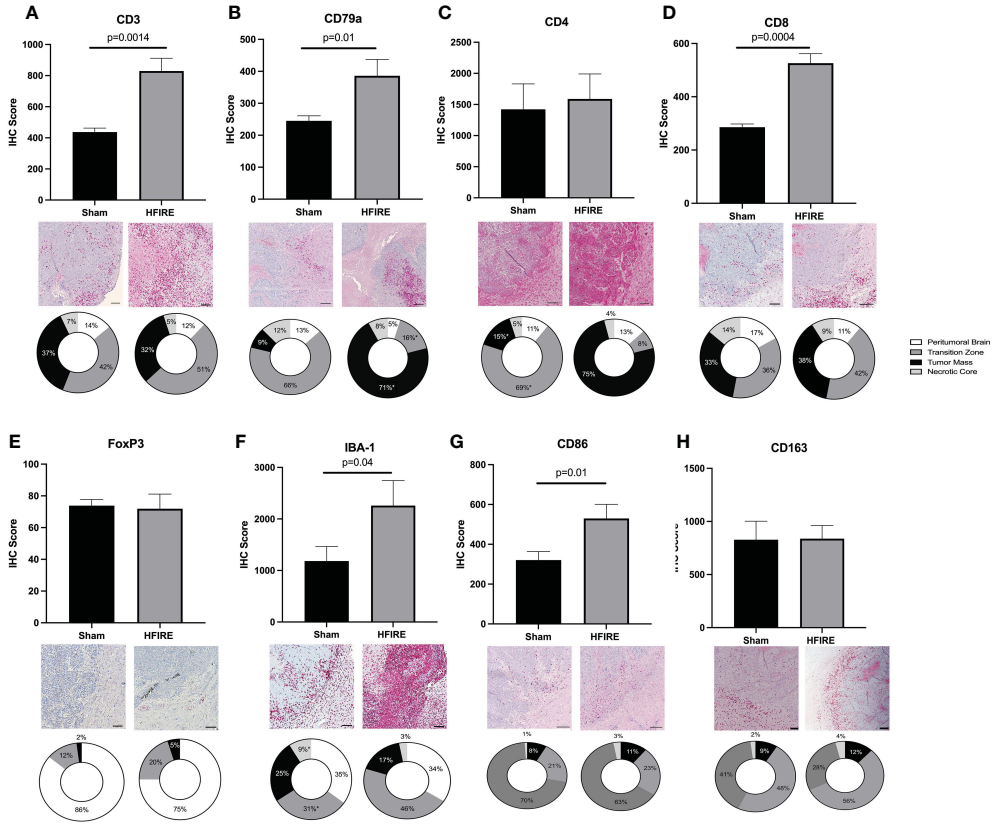

FIGURE 9
Immune cell infiltration after H-FIRE ablation. Brain tissue sections were stained for **(A)** T cells (CD3), **(B)** B cells (CD79a), **(C)** helper T cells (CD4), **(D)** cytotoxic T cells (CD8), **(E)** regulatory T cells (FoxP3), **(F)** macrophages/microglia (Iba-1), **(G)** M1 macrophages (CD86), and **(H)** M2 macrophages (CD163). The proportion of each cell type was studied with regards to proximity to the tumor mass. Immune cell infiltrates were analyzed within the following regions: peritumoral brain, transition zone, tumor mass, and necrotic core. Bar = 150 µm in all panels.

Furthermore, these results allude to a systemic immune response induced by H-FIRE treatment of gliomas.

4 Discussion

Here we have built upon the preclinical studies of first-generation IRE therapy in the brain and have evaluated the efficacy of both monotherapy and combinatorial (liposomal doxorubicin) H-FIRE for GBM. In summary, a three-dimensional collagen hydrogel tissue scaffold was leveraged to investigate H-FIRE cell death in healthy rodent astrocyte (DI TNC1) and rodent malignant glioma cells (F98). This *in vitro* data served to determine the desired pulsing parameters to be implemented *in vivo*. In parallel to this *in vitro* study, the tumor growth characteristics of F98 cells were quantified in a subset of rodents *in vivo* to inform timing of H-FIRE therapy. Thereafter, the survival endpoint study was initiated in six groups of rodents (Table 3) all inoculated with F98 glioma cells. The rodents were monitored for a period up to 40 days post H-FIRE treatment.

As improved overall survival and median survival were seen in all rodents whose treatment protocol included H-FIRE therapy when compared against the sham group, our findings suggest that H-FIRE therapy in the brain extends overall survival time. Meanwhile, the reduction of survival in the DOX only group may indicate that the drug alone induced more toxicity than positive effects. Given that the BBB was not disrupted with this protocol, Lipodox was likely left to systemically circulate, primarily targeting healthy anatomy while the tumor was left to grow. The results from Figure 4 suggest that H-FIRE treatment leads to a higher global concentration of Lipodox in tumors thus, improving its efficacy. However, the authors note that the low-dose H-FIRE protocol was not tested alongside the high-dose protocol in the concentration study. While we note that LD-HFIRE + DOX was not worse than the sham control, there was no statistical improvement—suggesting that the systemic toxicity induced by the Lipodox may have outweighed the benefit of the concentration that was able to penetrate into the brain with the low-dose H-FIRE protocol. From this, we may infer that sufficient BBB disruption was not achieved with this low-dose protocol. The authors recommend that for future investigations, a more comprehensive study of drug penetration into the brain be conducted to confirm that both protocols are adequate for achieving effective drug perfusion. This recommendation is based on the results from Figure 4 which show that the high-dose protocol increases the penetration of Lipodox into the brain tissue, likely leading to the enhanced therapeutic efficacy observed in the HD-HFIRE+DOX group. However, as Lipodox concentration following low-dose H-FIRE was not investigated, we may hypothesize that sufficient Lipodox did not

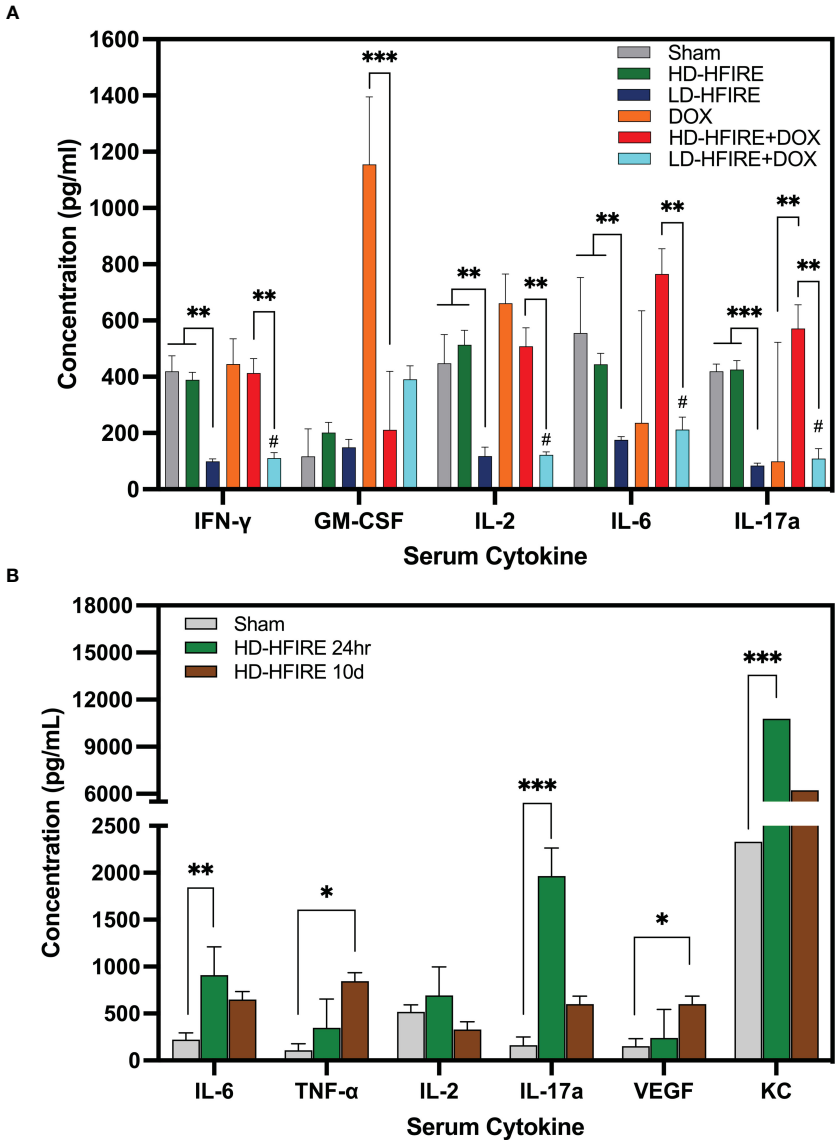

FIGURE 10
(A) Summary of cytokine concentrations across the five treatment groups. Compared to sham-treated controls, IFNγ, IL-2, IL-6, and IL-17a serum cytokine concentrations were significantly decreased following low-dose (BBB disruption) H-FIRE. IFNγ, IL-2, IL-6 and IL-17a were significantly increased following high-dose (ablation) H-FIRE treatment relative to the low-dose (BBB disruption) H-FIRE treatment group. GM-CSF was significantly decreased following treatment with high-dose (ablation) H-FIRE + Lipodox relative to Lipodox alone, whereas IL-17a was significantly increased. **(B)** In a separate group of rodents sacrificed at 24 hours or 10 days post-H-FIRE treatment, IL-6, IL-17a and KC were significantly increased at 24h post-H-FIRE ablation relative to the sham controls, whereas TNF-α and VEGF were significantly increased at 10d post- H-FIRE ablation. (*p< 0.05, **p< 0.01, ***p< 0.001, # group significantly different from sham p<0.01).

enter the brain with this protocol. It is crucial to ensure that the lower-dose protocol is also effective, as it may offer several advantages, including reduced toxicity and improved patient tolerance. Therefore, conducting both high-dose and low-dose drug concentration investigations prior to protocol selection will provide crucial insights into the optimal dosing strategy for Lipodox in the treatment of brain tumors.

Furthermore, our studies demonstrate that H-FIRE can stimulate immune cell infiltration within the tumor microenvironment. H-FIRE-mediated immune responses were assessed *via* IHC performed on treated tissue sections, serum cytokine analysis, and gene expression and pathway analysis. Our results suggest that H-FIRE may be capable of counteracting the immunosuppressive effects of the tumor microenvironment by stimulating pro-inflammatory local and systemic immune responses *via* P/DAMP signaling. In addition, H-FIRE-induced BBB disruption may further facilitate the entry of immune cells into the tumor and activation of the adaptive immune system, which has the potential to induce an anti-tumor response and enhance local tumor control. Additionally, these findings suggest that H-FIRE ablation induces a pro-inflammatory response characterized by the release of various cytokines, which may contribute to tissue damage and regeneration.

The applications of electroporation for BBB disruption are expanding and have demonstrated the potential to further enhance

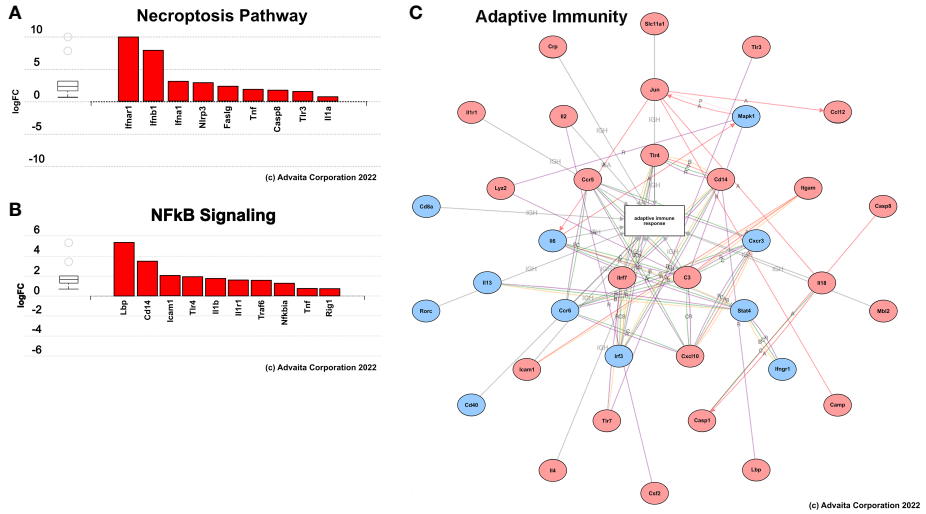

FIGURE 11
Summary of results from pathway analysis performed using iPathwaysGuide. Genes involved in **(A)** necroptosis, **(B)** NFkB signaling, and **(C)** adaptive immune response pathways were significantly upregulated (red) 10 days post-H-FIRE ablation compared to sham-treated controls.

our studies. It is important to note that the mechanistic phenomena of electroporation induced BBB disruption is predominantly due to a loss of tight junction protein integrity caused by endothelial cell cytoskeletal remodeling rather than pore formation in the cellular membrane (37). Studies have suggested that fine tuning electrode configurations as well as the waveform to take on short pulse widths and larger delays may shift toward maximizing BBB disruption field distributions (36). Notably, doxorubicin alone did not improve rodent survival; however, when combined with H-FIRE therapies, improved outcomes were observed, implying that temporary BBB disruption allows for more targeted drug diffusion, potentially reducing the extent of systemic toxicity. Thus, protocols striving for larger BBB disruption may promote improved efficacy of adjuvant liposomal doxorubicin diffusion, allowing for effective targeting of infiltrative cells that have migrated beyond the primary bulk tumor.

Other results have demonstrated the feasibility of applying non-invasive plate electrodes to induce BBB disruption and should be evaluated for combinatorial efficacy (38). These techniques for inducing BBB disruption present the potential for treating not just tumors but also leveraging the power of selectively disrupting the BBB without ablation while still effectively delivering drugs and improving the immune response following the H-FIRE treatments. Leveraging such advantages is not limited to treating gliomas and can be utilized to treat other neurological diseases as well.

Other non-invasive approaches for disrupting the BBB include utilizing focused ultrasound (FUS) in conjunction with microbubbles, however, the skull presents a major challenge for integration of FUS procedures in the brain, as it results in rapid attenuation of sound waves which increases the temperature of the brain limiting the range of safe energy exposures that can be achieved. Additionally, BBB recovery following FUS typically occurs within a few hours, potentially limiting practical treatment windows. Alternatively, convection-enhanced delivery (CED) offers another potential solution for intracranial drug delivery by

TABLE 3 Rodent Cohort Summary.

Name	Tumor (Y/N)	H-FIRE Voltage (V)	Liposomal Doxorubicin (Y/N)	Sample Size (n)	Median Survival (Days)	Overall Survival (%)
Sham	Y	N/A	N	5	26	0
DOX	Y	N/A	Y	5	20	0
Low-dose H-FIRE	Y	180	N	5	38	20
High-dose H-FIRE	Y	525	N	7	31	28.6
Low-dose H-FIRE + DOX	Y	180	Y	6	27	16.7
High-dose H-FIRE + DOX	Y	525	Y	6	37.5	50

bypassing the BBB altogether using a hollow catheter placement directly into the target tissue, and using pressure driven flow to deliver a variety of therapeutic agents. Though effective, CED is limited by the occurrence of perfusate reflux and by the requirement for lengthy treatment sessions due to relatively slow infusion rates. The combination of H-FIRE in conjunction with CED may offer the ability to maximize the success of total therapeutic delivered to the target tissue, as H-FIRE may increase permeability of the targeted tissue allowing for the tissue to absorb therapeutics that would have otherwise been lost to the reflux.

We have demonstrated that H-FIRE monotherapy improves the infiltration of immune cells in the tumor microenvironment. H-FIRE treated tumors have shown higher population of T cells, B cells, and microglia. Out of different T cell subtypes, the cytotoxic T cells have shown an improved infiltration in the analyzed sections. The presence of the immune cells was also analyzed with proximity to the tumor mass. Interestingly, the B cells were found to be the most abundant in the tumor mass. The majority of the other immune cells were found in the transition zone. It is noteworthy that the differences observed here are only analyzed at the endpoint. Since the immune response is a dynamic phenomenon, immune cell abundance may have a different profile at other time points.

For the numerical modeling portion of this study, the induced tumor was assumed to take on the shape of a sphere, where treatment plans were designed to encapsulate the estimated 12mm^3 sphere which was approximated from the tumor growth study. However, it is seen from the histology images (Figure 6B) that the tumors grow in an elliptical fashion rather than spherical. We expect that even if the tumor were to deviate from a perfectly spherical shape, the majority of the tumor would still have been encapsulated within the treatment fields due to the establishment of electrode insertion tracks prior to tumor implantation. The tumor was implanted bisecting the electrode insertion track and placed at the midline of the electrode insertion depth. To this fact, the timepoint of 7 days following tumor implant was suitable for investigation of H-FIRE was chosen because further timepoints would necessitate insertion of ≥ 3 needle electrodes.

From the rodent survival study, we were able to observe that the inclusion of H-FIRE as either a monotherapy or a combinatorial therapy does improve the median survival and overall survival of tumor bearing rodents. While significantly increased median survival ($p=0.0312$) was only seen comparing all rodents receiving H-FIRE therapy (high-dose H-FIRE, low-dose H-FIRE, high-dose H-FIRE+DOX, low-dose H-FIRE+DOX) against the sham group, we note that the highest median survivals were seen in the low-dose H-FIRE, combinatorial high-dose H-FIRE+DOX, and high-dose H-FIRE cohorts, which did not demonstrate statistical significance against the sham group. Therefore, we may infer that low enrollment numbers in each individual cohort contributed to a lack of statistical significance between other groups.

5 Conclusion

Expanding on first-generation IRE therapy brain studies, this study has demonstrated the efficacy of applying H-FIRE as both a monotherapy and as a combinatorial (liposomal doxorubicin) therapy for the treatment of brain tumors. Our results show that H-FIRE mediation in the treatment of rat gliomas significantly improves the median survival while demonstrating a potential for greater overall survival when leveraging it as a combinatorial therapy. While H-FIRE can be effectively used as a monotherapy to target the tumor on its own, the surrounding volumes of BBB disruption that facilitate drug delivery into the brain and the reversible electroporation regions that enhance drug uptake into the cells may further enhance the therapeutic effects. The next step toward the treatment of human patients should involve research into single-needle insertion devices capable of producing large transient BBB disruption.

Data availability statement

The raw data supporting the conclusions of this article will be made available by the authors, without undue reservation.

Ethics statement

The animal study was reviewed and approved by Institutional Animal Care and Use Committee (#19-217).

Author contributions

Conceptualization: SC, ML, BP, NA, YK, JH, SV, RD and JR; Data curation: SC, ML, BP, NA, YK, JG, SS, ST, JH, SV, RD and JR; Formal analysis: SC, ML, BP, NA, RD and JR; Funding acquisition: SV, RD and JR; Investigation: SC, ML, BP, NA, YK, JG, SS, ST, JH, SV, RD and JR; Methodology: SC, ML, BP, YK, ST, JH, SV, RD and JR; Project administration: SC, ML, BP, NA, YK, JH, SV, RD and JR; Resources: SC, ML, BP, NA, YK, JH, SV, RD and JR; Software: SC and ML; Supervision: SC, ML, BP, RD and JR; Validation: SC, ML, BP, NA, RD and JR; Visualization: SC, ML, BP, NA, RD and JR; Writing – original draft: SC and ML; Writing - review and editing: SC, ML, BP, NA, YK, JG, SS, ST, JH, SV, RD and JR; All authors contributed to the article and approved the submitted version.

Funding

This study was supported in part by the NIH P01 (P01CA207206) and the Virginia Research Investment Fund (VRIF). SC is funded by the ICTAS Doctoral Fellowship at Virginia Tech and the P.E.O Scholarship. Additionally, ML is funded by the Cunningham Doctoral Fellowship at Virginia Tech and by the NIH Research Supplement to Promote Diversity in Health-Related Research.

Acknowledgments

The authors would like to acknowledge support from the Institute of Critical Technology and Sciences (ICTAS) and the Center for Engineered Health (CEH) for use of laboratory space and manufacturing technologies.

Conflict of interest

RD, JR, SV, and ML have issued patents and/or patents pending in the area of irreversible electroporation and may receive royalties.

The remaining authors declare that the research was conducted in the absence of any commercial or financial relationships that could be construed as a potential conflict of interest.

Publisher's note

All claims expressed in this article are solely those of the authors and do not necessarily represent those of their affiliated organizations, or those of the publisher, the editors and the reviewers. Any product that may be evaluated in this article, or claim that may be made by its manufacturer, is not guaranteed or endorsed by the publisher.

Supplementary material

The Supplementary Material for this article can be found online at: https://www.frontiersin.org/articles/10.3389/fonc.2023.1171278/full#supplementary-material

References

1. Ostrom QT, Cioffi G, Gittleman H, Patil N, Waite K, Kruchko C, et al. Cbtrus statistical report: primary brain and other central nervous system tumors diagnosed in the united states in 2012–2016. *Neuro-oncology* (2019) 21(Supplement 5):v1–v100. doi: 10.1093/neuonc/noz150

2. Gabathuler R. Approaches to transport therapeutic drugs across the blood–brain barrier to treat brain diseases. *Neurobiol Dis* (2010) 37(1):48–57. doi: 10.1016/j.nbd.2009.07.028

3. Banks WA. From blood–brain barrier to blood–brain interface: new opportunities for cns drug delivery. *Nat Rev Drug Discovery* (2016) 15(4):275–92. doi: 10.1038/nrd.2015.21

4. Joan Abbott N, Patabendige AAK, Dolman DEM, Yusof SR. And David J begley. structure and function of the blood–brain barrier. *Neurobiol Dis* (2010) 37(1):13–25. doi: 10.1016/j.nbd.2009.07.030

5. Iversen LL. *Dopamine handbook*. USA: Oxford University Press (2010).

6. Gernert M, Feja M. Bypassing the blood–brain barrier: direct intracranial drug delivery in epilepsies. *Pharmaceutics* (2020) 12(12):1134. doi: 10.3390/pharmaceutics12121134

7. Tan AC, Ashley DM, López GY, Malinzak M, Friedman HS, Khasraw M. Management of glioblastoma: state of the art and future directions. *CA: Cancer J Clin* (2020) 70(4):299–312. doi: 10.3322/caac.21613

8. Fernandes C, Costa A, Osório L, Lago RC, Linhares P, Carvalho B, et al. Current standards of care in glioblastoma therapy. *Exon Publications* (2017), 197–241. doi: 10.15586/codon.glioblastoma.2017.ch11

9. Hottinger AF, Pacheco P, Stupp R. Tumor treating fields: a novel treatment modality and its use in brain tumors. *Neuro-oncology* (2016) 18(10):1338–49. doi: 10.1093/neuonc/now182

10. Stupp R, Taillibert S, Kanner A, Read W, Steinberg DM, Lhermitte B, et al. Effect of tumor-treating fields plus maintenance temozolomide vs maintenance temozolomide alone on survival in patients with glioblastoma: a randomized clinical trial. *Jama* (2017) 318(23):2306–16. doi: 10.1001/jama.2017.18718

11. Makimoto A, Nishikawa R, Terashima K, Kurihara J, Fujisaki H, Ihara S, et al. Tumor-treating fields therapy for pediatric brain tumors. *Neurol Int* (2021) 13(2):151–65. doi: 10.3390/neurolint13020015

12. Mohammadi AM, Schroeder JL. Laser interstitial thermal therapy in treatment of brain tumors–the neuroblate system. *Expert Rev Med devices* (2014) 11(2):109–19. doi: 10.1586/17434440.2014.882225

13. Mohammadi AM, Hawasli AH, Rodriguez A, Schroeder JL, Laxton AW, Elson P, et al. The role of laser interstitial thermal therapy in enhancing progression-free survival of difficult-to-access high-grade gliomas: a multicenter study. *Cancer Med* (2014) 3(4):971–9. doi: 10.1002/cam4.266

14. Rodriguez A, Tatter SB. Laser ablation of recurrent malignant gliomas: current status and future perspective. *Neurosurgery* (2016) 79(suppl 1):S35–9. doi: 10.1227/NEU.0000000000001442

15. Sloan AE, Ahluwalia MS, Valerio-Pascua J, Manjila S, Torchia MG, Jones SE, et al. Results of the neuroblate system first-in-humans phase i clinical trial for recurrent glioblastoma. *J Neurosurg* (2013) 118(6):1202–19. doi: 10.3171/2013.1.JNS1291

16. Hjouj M, Last D, Guez D, Daniels D, Sharabi S, Lavee J, et al. Mri study on reversible and irreversible electroporation induced blood brain barrier disruption. *PLOS One* (2012) 7:1–9. doi: 10.1371/journal.pone.0042817

17. Lorenzo MF, Thomas SC, Kani Y, Hinckley J, Lee M, Adler J, et al. Temporal characterization of blood–brain barrier disruption with high-frequency electroporation. *Cancers* (2019) 11(12):1850. doi: 10.3390/cancers11121850

18. Fang Z, Chen L, Moser MAJ, Zhang W, Qin Z, Zhang B. Electroporation-based therapy for brain tumors: a review. *J Biomechanical Eng* (2021) 143(10):1–14. doi: 10.1115/1.4051184

19. Gehl J. Electroporation: theory and methods, perspectives for drug delivery, gene therapy and research. *Acta Physiologica Scandinavica* (2003) 177(4):437–47. doi: 10.1046/j.1365-201X.2003.01093.x

20. Wittkampf FHM, Es R, Neven K. Electroporation and its relevance for cardiac catheter ablation. *JACC: Clin Electrophysiology* (2018) 4(8):977–86. doi: 10.1016/j.jacep.2018.06.005

21. Scheffer HJ, Stam AGM, Geboers B, Vroomen LGPH, Ruarus A, Bruijn Bd, et al. Irreversible electroporation of locally advanced pancreatic cancer transiently alleviates immune suppression and creates a window for antitumor t cell activation. *Oncoimmunology* (2019) 8(11):1652532. doi: 10.1080/2162402X.2019.1652532

22. Zhao J, Wen X, Tian L, Li T, Xu C, Wen X, et al. Irreversible electroporation reverses resistance to immune checkpoint blockade in pancreatic cancer. *Nat Commun* (2019) 10(1):1–14. doi: 10.1038/s41467-019-08782-1

23. Brock RM, Beitel-White N, Davalos RV, Allen IC. Starting a fire without flame: the induction of cell death and inflammation in electroporation-based tumor ablation strategies. *Front Oncol* (2020) 10:1235. doi: 10.3389/fonc.2020.01235

24. Chen Y, Moser MAJ, Luo Y, Zhang W, Zhang B. Chemical enhancement of irreversible electroporation: a review and future suggestions. *Technol Cancer Res Treat* (2019) 18:1533033819874128. doi: 10.1177/1533033819874128

25. Arena CB, Sano MB, Rossmeisl JH, Caldwell JL, Garcia PA, Rylander MN, et al. High-frequency irreversible electroporation (h- fire) for non-thermal ablation without muscle contraction. *Biomed Eng Online* (2011) 10(1):1–21. doi: 10.1186/1475-925X-10-102

26. Latouche EL, Arena CB, Ivey JW, Garcia PA, Pancotto TE, Pavlisko N, et al. High-frequency irreversible electroporation for intracranial meningioma: a feasibility study in a spontaneous canine tumor model. *Technol Cancer Res Treat* (2018) 17:1533033818785285. doi: 10.1177/1533033818785285

27. Arena CB, Garcia PA, Sano MB, Olson JD, Rogers-Cotrone T, Rossmeisl JHJr., et al. Focal blood-brain-barrier disruption with high-frequency pulsed electric fields. *Technology* (2014) 2(03):206–13. doi: 10.1142/S2339547814500186

28. Ivey JW, Wasson EM, Alinezhadbalalami N, Kanitkar A, Waldemar Debinski Z, et al. Characterization of ablation thresholds for 3d-cultured patient-derived glioma stem cells in response to high-frequency irreversible electroporation. *Research* (2019) 2019:1–14. doi: 10.34133/2019/8081315

29. Ringel-Scaia VM, Beitel-White N, Lorenzo MF, Brock RM, Huie KE, Coutermarsh-Ott S, et al. High-frequency irreversible electroporation is an effective tumor ablation strategy that induces immunologic cell death and promotes systemic anti-tumor immunity. *EBioMedicine* (2019) 44:112–25. doi: 10.1016/j.ebiom.2019.05.036

30. Agerholm-Larsen B, Iversen HK, Ibsen P, Moller JM, Mahmood F, Jensen KS, et al. Preclinical validation of electrochemotherapy as an effective treatment for brain tumors electrochemotherapy for brain tumors. *Cancer Res* (2011) 71(11):3753–62. doi: 10.1158/0008-5472.CAN-11-0451

31. Sharabi S, Guez D, Daniels D, Cooper I, Atrakchi D, Liraz-Zaltsman S, et al. The application of point source electroporation and chemotherapy for the treatment of glioma: a randomized controlled rat study. *Sci Rep* (2020) 10(1):1–12. doi: 10.1038/s41598-020-59152-7

32. Rossmeisl JH, Herpai D, Quigley M, Cecere TE, Robertson JL, D'Agostino RB, et al. Phase i trial of convection-enhanced delivery of il13ra2 and epha2 receptor targeted cytotoxins in dogs with spontaneous intracranial gliomas. *Neuro-oncology* (2021) 23(3):422–34. doi: 10.1093/neuonc/noaa196

33. Agerholm-Larsen B, Iversen HK, Ibsen P, Moller JM, Mahmood F, Jensen KS, et al. Preclinical validation of electrochemotherapy as an effective treatment for brain tumors electrochemotherapy for brain tumors. *Cancer Res* (2011) 71(11):3753–62. doi: 10.1158/0008-5472.CAN-11-0451

34. Rahman A, Carmichael D, Harris M, Roh JK. Comparative pharmacokinetics of free doxorubicin and doxorubicin entrapped in cardiolipin liposomes. *Cancer Res* (1986) 46(5):2295–9.

35. Rahimi Koshkaki H, Minasi S, Ugolini A, Trevisi G, Napoletano C, Zizzari IG, et al. Immunohistochemical characterization of immune infiltrate in tumor microenvironment of glioblastoma. *J personalized Med* (2020) 10(3):112. doi: 10.3390/jpm10030112

36. Lorenzo MF, Campelo SN, Arroyo JP, Aycock KN, Hinckley J, Arena CB, et al. An investigation for large volume, focal blood-brain barrier disruption with high-frequency pulsed electric fields. *Pharmaceuticals* (2021) 14(12):1333. doi: 10.3390/ph14121333

37. Partridge BR, Kani Y, Lorenzo MF, Campelo SN, Allen IC, Hinckley J, et al. High-frequency irreversible electroporation (H-FIRE) induced blood–brain barrier disruption is mediated by cytoskeletal remodeling and changes in tight junction protein regulation. *Biomedicines* (2022) 10(6):1384. doi: 10.3390/biomedicines10061384

38. Sharabi S, Last D, Daniels D, Fabian ID, Atrakchi D, Bresler Y, et al. Non-invasive low pulsed electrical fields for inducing bbb disruption in mice–feasibility demonstration. *Pharmaceutics* (2021) 13(2):169. doi: 10.3390/pharmaceutics13020169

frontiers | Frontiers in Oncology

TYPE Review
PUBLISHED 19 June 2023
DOI 10.3389/fonc.2023.1192128

OPEN ACCESS

EDITED BY
Konstantinos Gousias,
University of Münster, Germany

REVIEWED BY
Jiao Wang,
Purdue University, United States
Michael C. Burger,
Goethe University Frankfurt, Germany

*CORRESPONDENCE
Hongxin Deng
denghongx@scu.edu.cn

RECEIVED 23 March 2023
ACCEPTED 29 May 2023
PUBLISHED 19 June 2023

CITATION
Xiong Q, Zhu J, Zhang Y and Deng H (2023) CAR-NK cell therapy for glioblastoma: what to do next? *Front. Oncol.* 13:1192128. doi: 10.3389/fonc.2023.1192128

CAR-NK cell therapy for glioblastoma: what to do next?

Qi Xiong, Jiao Zhu, Yong Zhang and Hongxin Deng*

Department of Biotherapy, Cancer Center and State Key Laboratory of Biotherapy, West China Hospital, Sichuan University, Chengdu, China

Glioblastoma is a malignant tumor with the highest morbidity and mortality in the central nervous system. Conventional surgical resection combined with radiotherapy or chemotherapy has a high recurrence rate and poor prognosis. The 5-year survival rate of patients is less than 10%. In tumor immunotherapy, CAR-T cell therapy represented by chimeric antigen receptor-modified T cells has achieved great success in hematological tumors. However, the application of CAR-T cells in solid tumors such as glioblastoma still faces many challenges. CAR-NK cells are another potential adoptive cell therapy strategy after CAR-T cells. Compared with CAR-T cell therapy, CAR-NK cells have similar anti-tumor effects. CAR-NK cells can also avoid some deficiencies in CAR-T cell therapy, a research hotspot in tumor immunity. This article summarizes the preclinical research status of CAR-NK cells in glioblastoma and the problems and challenges faced by CAR-NK in glioblastoma.

KEYWORDS

CAR-NK cells, glioblastoma, natural killer cells, immunotherapy, cell therapy

1 Introduction

Glioblastoma is a malignant tumor with the highest morbidity and mortality in the central nervous system. The incidence of malignant brain tumors is 29.7% in all brain and other central nervous system tumors. Among them, the incidence of glioblastoma is 14.5%, accounting for 48.6% of the incidence of malignant brain tumors, which is the highest incidence of malignant brain tumors (1). According to the WHO tumor grading standard, glioblastoma is the most malignant CNS WHO grade 4 malignant tumor (2). Epidemiological statistics show that the median survival time of patients with glioblastoma is 8 months, and the 5-year survival rate is less than 10%. It is the most lethal malignant brain tumor (1) (3). The traditional treatment of glioblastoma is surgical resection, followed by radiotherapy and chemotherapy. This standard treatment can partially alleviate the disease progression of patients and improve the quality of life of patients. However, over 90% of patients will have tumor recurrence after standard treatment (4) (5). With the breakthrough of immunotherapy technology represented by PD-1 antibody and CAR-T cells, new hope has been brought to treat malignant tumors (6). Various immunotherapy strategies have also been developed to treat glioblastoma (7) (8). CAR-T, namely chimeric antigen receptor T cell. The activated T cells *in vitro* are modified

by the chimeric antigen receptor gene to form CAR-T cells. CAR-T cells target tumor-associated antigens through their expressed chimeric antigen receptors, specifically recognizing and killing tumor cells (9) (10). Due to the excellent anti-tumor effect of CAR-T cells, the United States first approved two CAR-T drugs for treating non-Hodgkin's lymphoma and acute lymphoblastic leukemia in 2017. By March 2023, eight CAR-T drugs on the market worldwide, all for treating hematological malignancies. In terms of clinical trials, as of March 2023, 19 clinical trials of CAR-T in the treatment of glioblastoma were carried out worldwide (https://clinicaltrials.gov/). Although CAR-T has achieved great success in hematological tumors, it still faces many challenges in treating solid tumors such as glioblastoma (11) (12). Studies have shown that T cells in the tumor immune microenvironment of glioblastoma are mainly Treg cells and exhausted cytotoxic T cells (13). Therefore, CAR-T has a natural immunosuppressive effect in the treatment of glioblastoma. Combining CAR-T and immune checkpoint inhibitors such as PD-1 antibodies may be an effective solution strategy (9). However, CAR-T cell therapy may cause side effects such as anti-host immune disease, neurotoxicity and cytokine storm. In addition, CAR-T cell therapy also faces many challenges, such as tumor heterogeneity, off-target effect and low tumor infiltration efficiency (14) (15) (16).

NK cells are an essential part of cellular immunity and have antiviral and anti-tumor effects. NK cell killing target cells depends on the dynamic balance of activating and inhibitory receptors on their cell membranes, without needing antigen pre-sensitization and MHC molecule restrictions (17). Compared with T cells, NK cells have the killing function of tumor cells and play an important role in the shaping of innate immunity and acquired immunity (18) (19). NK cells have the characteristics of universal allogeneic source effector cells. CAR-NK cell uses NK cells as effector cells to express chimeric antigen receptors. After optimization of the chimeric antigen receptor domain, CAR-NK cell can exhibit anti-tumor effects similar to CAR-T cells (20) (21). Clinical studies have reported that the response rate of patients treated with CAR-NK cells reached 73%, and no adverse effects, such as cytokine storm, neurotoxicity and anti-host immune disease occurred during the treatment (22). Compared with CAR-T cell, CAR-NK cell has better safety. As of March 2023, only one clinical trial of CAR-NK cells in the treatment of glioblastoma (NCT03383978). CAR-NK cell is another potential immunotherapy strategy for glioblastoma after CAR-T cell. Based on this, this article reviews the preclinical research progress of CAR-NK in glioblastoma and summarizes the problems and challenges faced by CAR-NK in glioblastoma.

2 Preclinical study of CAR-NK cells in the treatment of glioblastoma

In the preclinical study of CAR-NK cells in glioblastoma, NK cells have multiple sources (Table 1). Tumor-derived cell line NK92 cells are more widely used. In addition, some studies used peripheral blood-derived NK cells as effector cells. The clinical trial of CAR-NK cell in treating glioblastoma (NCT03383978) used NK92 cells as effector cells. Compared with peripheral blood-derived NK cells, NK92 cells are an immortalized cell line derived from tumor patients. The expansion of NK92 cells *in vitro* does not require special culture conditions and is convenient for large-scale preparation (33) (34). In addition, NK92 cells lack the expression of inhibitory receptors KIRs and have low immunogenicity (35). Although tumor-derived NK92 cells have the risk of tumorigenicity, γ-ray irradiation or low-energy electron irradiation can effectively inhibit the proliferation of NK92 cells and maintain their cell activity in the short term. Therefore, CAR-NK cells constructed using NK92 as effector cells have the feasibility of clinical transformation (36) (37) (38). Studies have shown that in the xenograft tumor model of the brain *in situ* glioblastoma in

TABLE 1 Preclinical studies with CAR-NK cells in glioblastoma.

Targets	Sources	Hinge	Transmembrane domain	Costimulatory domain	Ref.
Her2	NK92	CD8α	CD28	CD28-CD3ζ	(23)
EGFR EGFRvIII	NK92	CD8α	CD28	CD28-CD3ζ	(24)
EGFR EGFRvIII	NK92 NKL	CD8α	CD28	CD28-CD3ζ	(25)
EGFRvIII	YTS	c-Myc-tag	DAP12	DAP12	(26)
EGFRvIII	KHYG-1	CD8α	CD28	CD28-4-1BB-CD3ζ	(27)
EGFRvIII	KHYG-1	CD8α	CD28	CD28-4-1BB-CD3ζ	(28)
B7-H3	NK92	CD8α	CD28	CD28-CD3ζ	(29)
EGFR	PB-NK	CD8α	CD28	CD28-CD3ζ	(30)
c-Met AXL	KHYG-1	CD28	CD28	CD28-CD3ζ	(31)
CD73 GD2 NKG2DL	NK92 PBNK	CD8α	CD28	CD28-CD3ζ	(32)

immunodeficient mice, CAR-NK cells constructed with NK92 as effector cells can effectively alleviate the tumor burden of model mice and prolong the survival time of mice (23) (24) (25). Compared with NK92 cells, treating peripheral blood-derived NK cells does not require irradiation of cells, and the risk of tumorigenesis is lower (35). Treatment with chimeric antigen receptors modified by peripheral blood-derived NK cells can also effectively alleviate the tumor burden and prolong the survival of model mice (30) (32). The above studies have shown that NK92 cells and peripheral blood-derived NK cells have good application prospects in glioblastoma. Nevertheless, studies have shown that CAR-NK92 cells have more potent anti-tumor cytotoxicity than CAR-PBNK cells, and CAR-NK92 cells have stronger side effects on non-tumor cells (39). In addition, studies have also found that CAR-NK92 cells secrete higher granzyme A and IL-17A, while CAR-PBNK cells secrete more TNFα, IFNγ and Granulysin cytokines (39). These studies have shown that NK cells from different sources have different characteristics, and it is necessary to select reasonable effector cells in treating glioblastoma with CAR-NK.

In addition, there are also significant differences in chimeric antigen receptors used to modify NK cells, which have been reported from the first generation to the third generation (Table 1). With the development of CAR-T cells, CAR-T cell technology has developed to the fifth generation, of which the second generation CAR-T is the most classic, and the second generation CAR-T is also the most commonly used type in CAR-T clinical trials (40). The second generation of CAR-T cells with CD28 or 4-1BB combined with CD3ζ into chimeric antigen receptor T cells containing two costimulatory domains (14). Among them, CAR-T cells with CD28-CD3ζ costimulatory domain showed faster and more robust signal activity, while CAR-T cells with 4-1BB-CD3ζ costimulatory domain expressed more genes related to T cell memory (41). In terms of anti-tumor effect, CAR-T cells with 4-1BB-CD3ζ costimulatory domain have a stronger anti-tumor effect (42) (43). However, in the study of CAR-NK cells treatment of glioblastoma, chimeric antigen receptors containing CD28-CD3ζ costimulatory domain are mainly used, and some chimeric antigen receptors containing CD28-4-1BB-CD3ζ costimulatory domain are used (Table 1). CAR-NK cells with these two structures can effectively inhibit the progression of glioblastoma in mice (23) (24) (27). The difference between CAR-NK cells with these two structures in anti-glioblastoma is unclear. Studies have shown that CAR-T cells using the CD28-CD3ζ costimulatory domain have a more potent anti-tumor effect than CAR-T cells using the CD28-4-1BB-CD3ζ costimulatory domain (44). Mechanistically, compared to the third-generation CAR-T cells, the second-generation CAR-T cells can activate additional CD3ζ signals, thereby enhancing TCRs signals (45). However, in the ovarian cancer xenograft model, CAR-NK cells with CD28-4-1BB-CD3ζ costimulatory domain have a more potent anti-tumor effect than CAR-NK cells with CD28-CD3ζ costimulatory domain (46). This conclusion is contrary to the above findings in CAR-T. This also reflects the different anti-tumor effects of NK cells and T cells. We may suggest that in the follow-up study of CAR-NK cells, the corresponding chimeric antigen receptors should be rationally designed according to the characteristics of NK cells to optimize the anti-tumor effect of CAR-NK cells, which also provides ideas for the application of CAR-NK in glioblastoma.

3 Targets of CAR-NK cells in the treatment of glioblastoma

Reasonable therapeutic targets are of great significance for the tumor specificity of CAR-NK cell therapy. In the preclinical study of CAR-NK cells in treating glioblastoma, the main therapeutic targets were Her2 and EGFRvIII (Table 1). The primary therapeutic targets in the clinical trials of CAR-T in the treatment of glioblastoma are Her2, EGFRvIII and IL-13Rα (11). In addition, some new glioblastoma therapeutic targets, such as CSPG4, also have good application prospects.

3.1 Her2

Her2 belongs to the human epidermal growth factor receptor family and is a tyrosine kinase receptor on the cell membrane. Her2 does not contain a ligand recognition domain, which activates intracellular downstream signaling pathways by binding to other EGFR family members to form heterodimers. The activation of Her2 affects cell proliferation, differentiation and adhesion (47) (48). High expression of Her2 has been found in various solid tumors such as breast cancer, ovarian cancer and bladder cancer. In addition, Her2 expression is closely related to worse prognosis (49) (50) (51) (52). In early studies, Her2 expression was detected in about 80% of glioblastoma samples (53). However, Her2 expression was not detected in a sample containing 40 cases of glioblastoma (54). In another study, high expression of Her2 was detected in about 40% of 56 glioblastoma samples (23). In a sample study of 107 brain tumors, about 40% of high-grade astrocytomas highly express Her2 (55). The above studies have shown that the expression of Her2 in glioblastoma differs in different patients, which is also closely related to the heterogeneity of tumors (56). Compared with normal tissues, Her2 expression is higher in tumor tissues (57) (58). And Her2 expression is lower in most normal tissues (59).

In 2010, Nabil Ahmed et al. constructed CAR-T cells targeting Her2, which can effectively kill Her2-positive tumor cells derived from glioblastoma patients *in vitro*, effectively inhibit tumor progression in immunodeficient mice and significantly prolong the survival of mice (56). In the subsequent clinical study, after intravenous administration of the CAR-T cells, 7 of the 17 patients enrolled were relieved of tumor progression, and the median survival after treatment was 11.1 months. Although there was no obvious dose-dependent toxicity in this clinical trial, patients after treatment had side effects of headache and spasms (60). This study also suggests that CAR-T cells should further optimize their efficacy and control their negative response in treating solid tumors such as glioblastoma. In a preclinical study of CAR-NK cells, Congcong Zhang et al. analyzed the expression level of Her2 in glioblastoma samples, and high expression of Her2 was detected in about 40% of glioblastomas (23). They used NK92 cells as effector cells to

construct Her2-targeted CAR-NK cells, which can effectively kill Her2-positive glioblastoma cell lines and patient-derived primary glioblastoma cells *in vitro*. In the immunodeficiency mouse model, CAR-NK cells can effectively inhibit tumor growth after treatment. The median survival time of CAR-NK treated mice was 200.5 days, about 3 times longer than that of the control group (23). This study shows that CAR-NK cells targeting Her2 are feasible in treating glioblastoma, and related clinical studies are currently underway (NCT03383978).

3.2 EGFRvIII

EGFR is expressed on the cell membrane surface and is an epidermal growth factor receptor family member. EGFR recognizes and binds to epidermal growth factor, which induces the receptor to form a homodimer or heterodimer. Then the critical tyrosine residues of the intracellular domain of EGFR to be self-phosphorylated, which activates the downstream signal of EGFR and induces cell proliferation and survival (61). Studies have shown that EGFR expression is higher in glioblastoma and lower in normal brain tissue (62) (63). EGFRvIII is the most common EGFR mutant in glioblastoma, and EGFRvIII mutations can be detected in about 20%-40% of malignant gliomas (64) (65). Structurally, the EGFRvIII mutant lacks EGFR exons 2-7, amino acids 6-273, and glycine (66). Functionally, EGFRvIII lacks an extracellular domain. In the absence of ligands, EGFRvIII can constitutively self-activate, thereby activating tumor-promoting signals and enhancing the tumorigenicity of tumor cells (67) (68) (69). Although the expression of EGFRvIII was not significantly correlated with the survival prognosis of glioblastoma patients, patients with high EGFRvIII expression and increased EGFR expression had a poor survival prognosis (70). In addition, EGFRvIII is a mutant specifically expressed in tumor cells, so EGFRvIII is a tumor-specific therapeutic target.

In 2017, Rouke et al. reported the first clinical trial of CAR-T cells targeting EGFRvIII in treating glioblastoma (NCT02209376) (71). A total of 10 patients with recurrent glioblastoma were enrolled in this clinical trial and treated with a single intravenous infusion of CAR-T cells. After treatment, the tumors of 7 patients were analyzed by surgery. The infiltration of CAR-T cells could be detected in all 7 patients, and the expression of EGFRvIII in 5 patients was decreased. However, after CAR-T cell treatment, the tumor microenvironment increased the expression of inhibitory molecules and the infiltration of Treg cells. This clinical trial shows that although intravenous infusion of CAR-T cells can reach the brain tumor site and exert anti-tumor effects, CAR-T cells treatment also needs to solve the problems of the tumor microenvironment and antigen heterogeneity to improve the efficacy of CAR-T cells in the treatment of glioblastoma. In 2019, Goff et al. reported another clinical trial of CAR-T cells targeting EGFRvIII in treating glioblastoma (NCT01454596) (72). In this clinical trial, no tumor regression was observed, 2 of the treated patients had severe hypoxia, and one had death. This clinical trial also reflects that the negative response associated with CAR-T cell therapy is a challenge that cannot be ignored.

In 2015, Sabrina Genßler et al. constructed a dual-specific CAR-NK cell targeting EGFR and EGFRvIII using NK92 as effector cells. The chimeric antigen receptor uses a CD28 and CD3ζ costimulatory domain. In the glioblastoma xenograft model, mice treated with dual-target-specific CAR-NK cells can effectively inhibit tumor growth and prolong the survival time of mice (24). In 2016, Nadja Müller et al. used YTS as an effector cell to overexpress chemokine receptor CXCR4 in CAR-NK cells targeting EGFRvIII, and the chimeric antigen receptor used DAP12 costimulatory domain. In the glioblastoma xenograft model, mice treated with CAR-NK cells also inhibited tumor growth and prolonged survival of mice (26). However, in 2020, Tsutomu Nakazawa et al. used KHYG-1 as an effector cell to construct CAR-NK cells targeting EGFRvIII, and chimeric antigen receptors used CD28,4-1BB and CD3ζ costimulatory domains. *In vitro* experiments, the cells can effectively kill EGFRvIII tumor cells. Still, in the animal model of immunodeficiency mice, the cell therapy cannot inhibit tumor progression and even induces pseudoprogressive pathological features (27). Although clinical trials of CAR-NK cells targeting EGFRvIII are still underway, the above studies have shown that different sources of NK cells and different molecular structures of chimeric antigen receptors can affect the therapeutic effect of CAR-NK cells.

3.3 IL-13Rα2

IL-13Rα2 is expressed on the cell membrane and is a subunit of the IL-13 receptor complex. Under physiological conditions, IL-13 is recruited and recognized by IL-13Rα1, and then IL-13Rα1 binds to IL-4Rα to form a heterodimer, which recruits Jak kinase and activates STAT6, thereby activating intracellular downstream signals (73) (74). Although IL-13Rα1 and IL-13Rα2 have the same binding mode for IL-13, the extracellular recognition domain of IL-13Rα2 has a unique receptor residue, which makes the IL-13 binding pocket of IL-13Rα2 larger, and the spatial complementarity between IL-13Rα2 and IL-13 is higher. Therefore, compared with IL-13Rα1, IL-13Rα2 has a higher affinity for IL-13 (75) (76). However, IL-13Rα2 lacks an intracellular domain and does not have a signal transduction role after recognizing IL-13 (77) (78). Studies have shown that IL-13Rα2 is highly expressed in glioblastoma, but its expression is low in normal brain tissue and other normal tissues. In contrast, patients with high expression of IL-13Rα2 have worse survival prognoses (79) (80) (81). Functionally, IL-13Rα2 competitively binds to IL-13, thereby blocking IL-13Rα1-mediated STAT6 phosphorylation, allowing tumor cells to escape apoptosis, so IL-13Rα2 is also called a pseudoreceptor (82). In addition, high expression of IL-13Rα2 also enhances the migration ability of tumor cells (83). Early clinical studies have shown that targeting IL-13Rα2 in the treatment of glioblastoma safety requirements and is a potential therapeutic target for glioblastoma (84) (85).

In 2015, Christine E. Brown et al. first reported the clinical experimental study of CAR-T targeting IL-13Rα2 in treating glioblastoma (NCT00730613) (86). In this clinical trial, 3 patients

with recurrent glioblastoma were enrolled, and 12 intracranial orthotopic administrations were performed with a maximum dose of 10^8 CAR-T cells. After CAR-T cells treatment, 2 of the 3 patients had a transient anti-tumor response. The expression of IL-13Rα2 in one patient was lower than before treatment, and the volume of tumor necrosis in the other patient was significantly larger after treatment. However, in this clinical study, all patients developed disease recurrence and eventually died after CAR-T treatment, and IL-13Rα2 antigen loss may be a potential mechanism leading to CAR-T cells treatment tolerance. In 2016, Christine E. Brown et al. reported another clinical experimental study of CAR-T cells targeting IL-13Rα2 in treating glioblastoma (NCT02208362) (87). In this study, only one patient with recurrent glioblastoma was enrolled and treated with multiple intracranial *in situ* administrations of CAR-T cells. After treatment, all intracranial and spinal tumors regressed, and no grade 3 or more toxic and side effects occurred during the period. The clinical treatment response lasted for 7.5 months. The above research laid the foundation for CAR-T cells targeting IL-13Rα2 in treating glioblastoma. Compared with CAR-T cells, there is still a lack of CAR-NK cells research reports targeting IL-13Rα2. In fact, in the absence of IFNγ, human NK cells secrete IL-13 cytokines under the stimulation of IL-2 (88) (89). Under the stimulation of IL-12, IL-13 can increase the expression of IFNγ in NK cells (90). In summary, we may suggest that CAR-NK cells targeting IL-13Rα2 can be used in treating glioblastoma in the future, and the problem of tumor escape caused by IL-13Rα2 antigen loss should be solved.

3.4 CSPG4

CSPG4, also known as glial antigen 2 (NG2), is a type I transmembrane protein expressed on the cell membrane and belongs to the chondroitin sulfate proteoglycan family. In tumor tissues, CSPG4 was first found to be highly expressed in melanoma tissues (91). Its expression is closely related to tumor cell proliferation and metastasis (92) (93) (94). CSPG4 is almost not expressed or low in normal tissues, but highly expressed in various solid tumor tissues (95) (96). CSPG4 is a marker of oligodendrocyte progenitor cells. In the state of disease, the expression of CSPG4 may be closely related to the occurrence and development of glioma. CSPG4 can induce cell proliferation, migration and tumor angiogenesis. The expression of CSPG4 can be detected in oligodendroglioma, astrocytoma and glioblastoma (97). Recent studies have shown that CSPG4 is highly expressed in about 50% of glioblastomas, and the expression of CSPG4 can be used as an independent factor for the prognosis of patients. Patients with high expression of CSPG4 have a poorer survival prognosis (98). Compared with tumor-associated antigens such as Her2 and IL-13Rα2, CSPG4 is expressed higher in glioblastoma cells, and CSPG4 is also found to be highly expressed in tumor-associated perivascular cells (99). Although no relevant clinical trials have been carried out, preclinical studies have shown that tumor growth was significantly inhibited in mice treated with CSPG4-specific antibodies (95) (94).

In 2018, Serena Pellegatta et al. constructed CAR-T cells targeting CSPG4. In the patient-derived glioblastoma model constructed by immunodeficient mice. After intratumoral administration of the CAR-T cells, the tumor progression with high expression of CSPG4 and moderate expression of CSPG4 was inhibited, After treatment, the tumor burden of mice decreased, the survival time was significantly prolonged, and about 60% of mice survived in long-term observation (99). Further studies have shown that TNFα secreted by CAR-T cells induces CSPG4 expression in glioblastoma, thereby avoiding tumor escape due to antigen loss (99). The glioblastoma model was constructed in immunodeficient mice in the study based on NK cells. After the combination of NK cells and anti-CSPG4 monoclonal antibody mAb9.2.27, the glioblastoma tumor progression was inhibited and survival time of the mice was significantly prolonged (100). Subsequent studies have shown that activated NK cells secrete IFNγ, activating and recruiting macrophages/microglia to tumor tissues. Activated macrophages/microglia have a killing effect on glioblastoma tumor cells, and their killing ability is even better than NK cells. Moreover, the inhibition of tumors by NK cells and mAb9.2.27 combined treatment depends on the participation of macrophages/microglia (100). The above studies have shown that NK cells targeting CSPG4 are feasible for treating glioblastoma, and there is no relevant report. At the same time, tumor infiltration of macrophages/microglia is also a key factor affecting treatment response, and related combination therapy may be a more effective treatment strategy.

3.5 GD2

Ganglioside is a complex glycolipid on the cell membrane. It mainly exists in the nervous system and is a natural component of the neuronal cell membrane (101) (102). GD2, namely disialoganglioside GD2. In cells, GD2 is synthesized in the endoplasmic reticulum and Golgi apparatus and then transferred to the cell membrane. Functionally, GD2 is closely related to cell adhesion and signal transduction. GD2 plays a crucial role in physiological and pathological processes by driving cell proliferation, angiogenesis and immune escape. The primary pathological significance of GD2 is that it is highly expressed in various malignant tumors (103) (104) (105). In a study of brain tumors, the positive expression of GD2 was found in 80% of diffuse pontine gliomas (106). In addition, glioblastoma tumor stem cells also found positive expression of GD2 (107). In 2021, Malvina Prapa et al. successfully isolated tumor cells from 12 patients with glioblastoma, of which 7 patients had high expression of GD2, and the positive rate of GD2 was more than 80% (108). At the same time, the study also constructed GD2-specific CAR-T cells, and the results showed that GD2-specific CAR-T cells could exert anti-glioma activity *in vivo* and *in vitro*. This study suggests that GD2 is a potential target for CAR-T cells in treating glioblastoma.

In 2022, Robbie G. Majzner et al. first reported a clinical trial of GD2-specific CAR-T cells in treating glioma (NCT04196413) (109). H3K27M mutant glioma cells highly express GD2. Four patients with

H3K27M mutant glioma were enrolled in this clinical trial and treated with intravenous infusion of GD2-specific CAR-T cells. Subsequently, patients who benefited from the treatment continued to infusion GD2-specific CAR-T cells intraventricular. In this clinical trial, 3 of the 4 patients treated with GD2-specific CAR-T showed clinical and radiographic improvement. The results of this study indicate that GD2-specific CAR-T cells have certain clinical benefits in the treatment of glioma. Although there is no report on the treatment of glioblastoma with GD2-specific CAR-NK cells, GD2-specific CAR-NK cells have shown specific anti-tumor effects on neuroblastoma in preclinical studies (110). The above studies suggest that GD2-specific CAR-NK cell is a potential therapeutic strategy for GD2-positive glioblastoma, and related research can be carried out in the future.

4 Challenges of CAR-NK cell therapy for glioblastoma

As mentioned above, CAR-NK cells are feasible for the treatment of glioblastoma. Compared with CAR-T cells, CAR-NK cells have the advantages of safety. Similar to CAR-T cells, CAR-NK cells also need to solve the problems of tumor heterogeneity and tumor immune microenvironment inhibition in treating solid tumors such as glioblastoma. In addition, CAR-NK cells also have challenges such as low preparation efficiency, short survival time *in vivo*, and optimization of anti-tumor activity.

4.1 The immune microenvironment of glioblastoma

As for the blood-brain barrier, the brain has long been considered immune-protected tissue (111). Along with the researches, the brain is now more inclined to be regarded as an immune-specific tissue (112). There are many different types of immune cells in the central nervous system, and they also have functional lymphatic vessels. Glioblastoma is a ‘ cold tumor ‘ due to the lack of lymphocyte infiltration (113). There are mainly four types of cells in the immune microenvironment of glioblastoma, namely: tissue resident cells, such as neurons and astrocytes; myeloid-derived immune cells (Figure 1), such as tissue-resident microglia, bone marrow-derived macrophages (BMDMs), bone marrow-derived DC cells, bone marrow-derived suppressor cells (MDSCs) and neutrophils; the lymphoid-derived immune cells, such as T cells and NK cells; other cells, such as endothelial cells, pericytes, and fibroblasts (114) (115). Weilun Fu et al. used single cell technology to systematically analyze the immune cells in the glioblastoma tumor microenvironment (13). The study found that in the tumor microenvironment of glioblastoma, myeloid-derived immune cells accounted for a relatively high proportion, most of which were tumor-associated macrophages/microglia. In addition, there is a small amount of infiltration of T cells and NK cells in the glioblastoma tumor microenvironment. Still, the T cells are mainly Treg cells, as well as exhausted phenotype helper T cells and cytotoxic T cells, while the NK cells are non-functional NK cells.

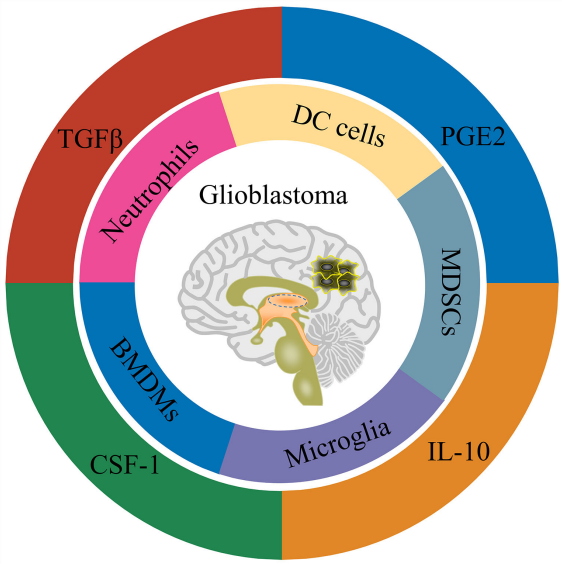

FIGURE 1
Schematic representation of GBM tumor microenvironment.

Consistent with the cell type, there are many immunomodulatory molecules in the tumor microenvironment of glioblastoma, including TGFβ, IL-10, IL-6 and PGE2 (Figure 1). In addition, cells in the glioblastoma tumor microenvironment up-regulate the expression of immune checkpoint receptor-related molecules, such as PD-1/PD-L1, CTLA-4/CD80/CD86 and TIM-3/galectin-9 (115). In summary, glioblastoma is an immunosuppressive ‘cold tumor’, posing great challenges for tumor immunotherapy such as CAR-T and CAR-NK cells. Fortunately, tumor-associated macrophages/microglia are also involved in the anti-tumor effect of NK cell-based immunotherapy (100). In a study of chimeric antigen receptor CAR-NK cells based on NKG2D design, the CAR-NK cells could tolerate the inhibitory effect of TGFβ or soluble MICA/MICB on cytotoxic function in the immune microenvironment. In contrast, the cytotoxicity of wild-type NK cells was inhibited under the condition of TGFβ or soluble MICA/MICB (116). Recent studies have shown that TGFβ signaling is crucial for glioblastoma tumor stem cells escaping NK cell immune surveillance (117). Inhibition of TGFβ signaling or knockout of TGFβ receptor TGFBR2 can prevent NK cell dysfunction and enhance the anti-tumor effect of NK cells on glioblastoma stem cells (117). This study suggests that blocking TGFβ signaling may also improve the anti-tumor effect of CAR-NK cells on glioblastoma. By co-transducing a mutant TGFBR2 (DNR) for B7H3-specific CAR-NK cells, Kajal Chaudhry et al. showed that this co-transducing CAR-NK cells could tolerate the immunosuppressive effect of exogenous TGFβ and further enhance the anti-tumor effect of CAR-NK cells on glioblastoma (118). The above studies suggest that blocking TGFβ signaling is an alternative strategy for CAR-NK cells to glioblastoma therapy. Nevertheless, only a few CAR-NK cell studies have considered the effect of immunosuppressive microenvironment on CAR-NK function. From the perspective of clinical application, more

research should be conducted on how CAR-NK cells overcome the immunosuppressive microenvironment of solid tumors such as glioblastoma in the future.

4.2 The preparation of CAR-NK cells

The preparation of CAR-NK cells includes two parts: the culture of NK cells and the genetic modification of NK cells. These two parts are also the main challenges in CAR-NK cell preparation. At present, the sources of NK cells used to prepare CAR-NK are abundant, mainly from four types of NK cells, namely NK-derived tumor cell line (NK92 et al.), peripheral blood-derived NK cells (PB-NK), umbilical cord blood-derived NK cells (CB-NK) and iPSC-derived NK cells (iPSC-NK). NK cells from different sources have their advantages and disadvantages (Table 2) (14) (35). For example, NK92 cells can be cultured on a large scale and have low immunogenicity, but NK92 is a tumor-derived cell line with a risk of tumorigenicity in clinical applications. PB-NK has a wide range of sources and high safety, but the efficiency of PB-NK culture *in vitro* is low. At present, iPSC-NK is also a research hotspot in the field and has made some breakthroughs (119) (120). Moreover, CAR-NK cells prepared from different sources of NK cells have other functions. Stephan Kloess et al. showed that CAR-NK92 has more potent anti-tumor cytotoxicity than CAR-PB-NK, but CAR-NK92 also has more potent cytotoxicity to non-tumor cells, suggesting that CAR-NK92 may cause side effects of 'on-target' non-tumor cells (39). Herrera et al. showed that CAR-PB-NK had stronger anti-tumor cytotoxicity than CAR-CB-NK, but CAR-CB-NK had stronger proliferation activity (121). In addition to the above-mentioned sources of NK cells, Han-Seop Kim et al. have recently developed a direct somatic reprogramming source of NK cells (drNK). Compared with PB-NK, ES-NK and iPSC-NK cells, drNK is a specific phenotype of $CD56^{bright}CD16^{bright}$NK cells. Compared with CAR-PB-NK, CAR-drNK has a stronger killing effect on tumor cells and tumor stem cells (122). In the preparation cycle, a large amount of drNK can be obtained in 24 days from the initial culture. Therefore, drNK is another potential source of NK cells.

In addition to NK92 cells, NK cells from other sources face the problem of low *in vitro* culture efficiency. At present, the culture of NK cells is divided into two technical routes, one is the feeder cell stimulation culture method, and the other is the non-feeder cell culture method (123) (124). The non-feeder cell culture method activates NK cells through different cytokine combinations and maintains the proliferation of NK cells. The feeder cell method activates NK cells through engineered tumor cells and maintains the proliferation of NK cells under the stimulation of cytokines. Compared with the non-feeder cell culture method, the feeder cell culture method has higher NK cell culture efficiency (124). In the technical route of feeder cell culture method, K562-4-1BBL-mbIL21 was used as feeder cells. After 21 days of culture by Cecele J. Denman et al., NK cells proliferated 31747 times (125), the highest amplification efficiency observed in the literature. Mechanistically, feedeer cell culture provides three necessary signals for NK cell proliferation, namely cell-cell contact, CD137 signal and cytokine signal (126). The feeder cell culture method solves the problem of NK cell culture *in vitro*, but most of the feeder cells used for NK cell culture are tumor-derived cell lines. The NK cells cultured by this method have potential safety risks when reinfusion *in vivo*. Currently, the methods of mitomycin, γ-ray irradiation and freeze-thaw are often used to inactivate feeder cells (127) (128), which alleviates the safety concerns to a certain extent. However, there is a lack of systematic research on the safety evaluation of NK cells by feeder cell culture. Therefore, safe and efficient NK cell culture is still challenging in NK cell therapy.

The genetic modification of NK cells is another challenge. At present, the genetic modification of NK cells mainly includes two methods: electroporation and viral transduction (14). Compared with viral transduction, electroporation is more efficient (129). Lin Xiao et al. used electroporation to transfect NK cells in the study of CAR-NK cells. The transfected nucleic acid was mRNA that overexpressed chimeric antigen receptors, and the transfection efficiency of NK cells in this study was about 100% (130). Although the efficiency of electroporation is high, it will reduce cell viability, and the genetic modification of electroporation is transient. Despite this, there have been many successful reports on electroporation technology in CAR-T cells preparation (131) (132)

TABLE 2 Comparison of NK cells from different sources.

NK Cells	Advantages	Disadvantages
NK92	1. Easy to culture *in vitro*. 2. Low expression of inhibitory receptors KIRs. 3. Low immunogenicity.	1. Lack of activating receptors. 2. Tumor-derived cells. 3. Risk of EBV infection.
PB-NK	1. Mature phenotype. 2. High safety.	1. Low amplification efficiency *in vitro*. 2. Short survival time *in vivo*.
CB-NK	1. Rich source. 2. High safety.	1. Low amplification efficiency *in vitro*. 2. Short survival time *in vivo*. 3. High expression of inhibitory receptor NKG2A. 4. Lack of ADCC function.
iPSC-NK	1. Rich source. 2. Cloning screening can be carried out. 3. Facilitate genetic modification. 4. Low expression of inhibitory receptors KIRs.	1. High expression of inhibitory receptor NKG2A. 2. Short survival time *in vivo*.

(133). Therefore, electroporation technology will also make a breakthrough in CAR-NK cells. Currently, viral transduction is still widely used in CAR-NK cell research, and viral transduction is also a recognized method in CAR-T cell applications. Since the widely used pseudovirus is VSV-G envelope protein lentivirus, the cell receptor of VSV-G is LDLR, and the expression of LDLR in NK cells is low, which also leads to the low transduction efficiency of VSV-G envelope protein lentivirus on NK cells (134). To solve this problem, researchers have tried to use viruses with different envelope proteins to modify NK cells, among which RD114 envelope protein retrovirus and BaEV envelope protein lentivirus are more successful (134) (135). The typical cell receptor of these two envelope proteins is ASCT2, which is highly expressed in activated NK cells (134). Compared with RD114, the cell receptor of BaEV contains another receptor ASCT1, so the efficiency of BaEV envelope protein lentivirus transduction of NK cells is higher (136). However, NK cells are a class of natural antiviral immune cells that have a natural resistance to viral transduction, which is one of the reasons for the low efficiency of viral transduction of NK cells. Tolga Sutlu et al. used the BX795 inhibitor to block TBK1/IKKε, which can partially inhibit the antiviral response of NK cells, thereby increasing the viral transduction efficiency by 3.8 times (137). Peter Chockley et al. obtained a similar conclusion using inhibitors such as BX795, that is, blocking TBK1/IKKε can improve the efficiency of virus transduction of NK cells (138). The genetic modification efficiency of NK cells was effectively improved by modifying the envelope protein and blocking TBK1/IKKε. However, future research still needs to address the problems of low virus packaging efficiency and cytotoxicity of inhibitors such as BX795.

4.3 The persistence of CAR-NK cells

The short survival time of NK cells *in vivo* is a significant challenge for adoptive NK cell therapy. In clinical studies of adoptive NK cell therapy, NK cells survive within 2 weeks *in vivo* (139) (140) (141). The short residence time of NK cells in the body can bring safety advantages, but it also limits the therapeutic efficiency of NK cells. At present, cytokines such as IL-2 and IL-15 are often used to prolong the survival time of NK cells *in vivo* (123). In the study of CAR-NK cells, to extend the survival time of CAR-NK cells *in vivo* and improve its therapeutic efficiency, the same strategy will be used, that is, IL-2 or IL-15 adjuvant therapy (20) (142) (143) (144) (145) (146). Although IL-2 is more widely used, IL-15 may be more effective in maintaining NK cell survival *in vivo*. Elizabeth L. Siegler et al. evaluated the survival of CAR-NK cells *in vivo* under cytokine support therapy. Animal experiments were designed to give IL-15 support therapy 1-7 days after CAR-NK cells treatment and IL-2 support therapy 1-21 days after CAR-NK cells treatment. The proportion of NK cells in peripheral blood, spleen and ascites was detected at different times after CAR-NK cells treatment. The results showed that the proportion of NK cells in various tissues reached the maximum on the day10 and then gradually decreased (20). This study indicates that IL-15 has a higher efficiency in maintaining the survival of NK cells *in vivo* than IL-2. Similarly, Enli Liu et al. constructed CAR-NK cells with endogenous expression of IL-15, and continuously detected the peripheral blood of CAR-NK cells treated mice. It was found that CAR-NK cells continued to survive in the peripheral blood at a high proportion until day 49, and a certain proportion of CAR-NK cells could still be detected on the 75th day after treatment (146). This study further confirmed that IL-15 can effectively maintain the survival of NK cells *in vivo*.

Although cytokines can prolong the survival time of NK cells *in vivo*, cytokine support therapy may also bring corresponding side effects. It has been confirmed that systemic IL-2 treatment can induce the activation of Treg cells and bring serious vascular leakage syndrome and neurotoxicity and other side effects (147) (148) (149). Systemic administration of IL-15 mainly affects NK cells, γδ cells and CD8 memory T cells, but IL-15 can cause symptoms such as hypotension and thrombocytopenia in a dose-dependent manner and can lead to a decrease in neutrophils (150). Compared with IL-2, IL-15 is a safer choice (151) (152). However, the systemic toxicity of IL-15 cannot be ignored. Recent studies have shown that after CAR-NK cells co-express IL-15, mice treated with the CAR-NK cells can cause systemic toxicity in animal models of acute lymphoblastic leukemia. Although CAR-NK cells have the most potent anti-tumor effect *in vivo*, the survival of mice has not been significantly improved (153). In summary, IL-15 has a significant advantage in maintaining the survival of NK cells *in vivo*, but the systemic toxicity caused by IL-15 cannot be ignored. To make better use of this characteristic of IL-15, the safe dosage and administration mode of IL-15 can be further studied in the future. In addition to natural cytokines, directional modified IL-2 cytokines have a high affinity for IL-2Rβ receptors and can specifically activate T cells (154) (155). Studies have shown that EPO/TPO can improve the survival of NK cells *in vivo* and enhance their anti-tumor activity (156). At present, there are few reports on the continued survival of CAR-NK cells. We may suggest that the future can focus on this progress.

4.4 The anti-tumor activity of CAR-NK cells

The classical chimeric antigen receptor contains four components: extracellular antigen recognition domain, hinge region, transmembrane domain and intracellular domain (Figure 2). The antigen recognition domain is usually composed of single chain antibody (scFv). The hinge region is used to connect the antigen recognition domain and the transmembrane domain. Its length plays an vital role in the formation of immune synapses by effector cells. Currently, the hinge region of CAR-NK cells primarily uses the hinge region fragment of CD8α, while the transmembrane domain of CAR-NK cells mainly uses the transmembrane domain fragment of CD28. Compared with the above components, the intracellular costimulatory domain of chimeric antigen receptors is essential for the activation and function of effector cells. Currently, the main costimulatory domain used in CAR-NK cell research is CD28-CD3ζ (14) (157). CD28-CD3ζ is one of the intracellular costimulatory domains often used in classical second-generation CAR-T cells. With the

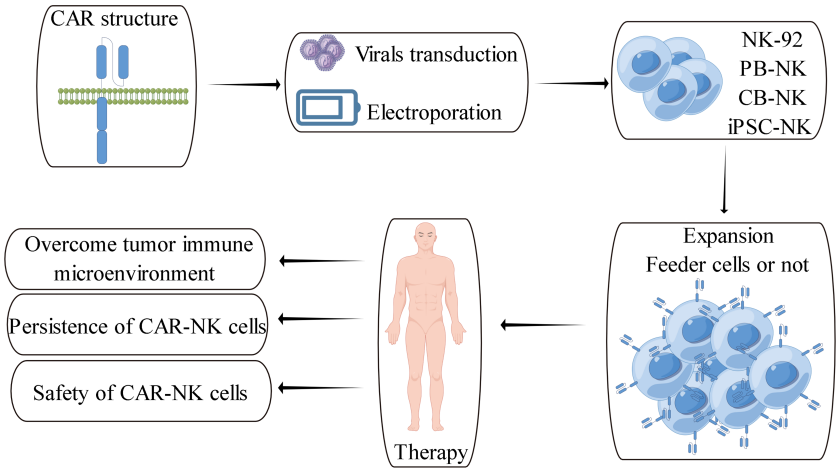

FIGURE 2
Schematic overview of CAR-NK cell therapy and its challenges (157).

deepening of CAR-NK cells research, more and more evidence shows that it is not the best choice to construct CAR-NK cells directly using CAR-T-derived chimeric antigen receptors (14). The activation of NK cells and T cells are quite different. The activation of T cells mainly depends on their specific TCR receptors, while the activation of NK cells depends on various activating receptors expressed on their cell membranes (18). Therefore, it is necessary to rationally design chimeric antigen receptors based on the characteristics of NK cells, and CAR-NK cells based on rational design have also made positive research progress.

Through a comprehensive analysis of NK cell activating receptors, Ece Canan Sayitoglu et al. found that NK cells overexpressing DNAM1 or NKG2D can enhance the killing effect of NK cells on tumor cells (158). DNAM1 is an activating receptor expressed on the cell membrane of NK cells, which activates NK cells after recognizing ligands CD155 and CD112 (159) (160). DNAM1 is a type I transmembrane protein. Ming-Ru Wu et al. linked DNAM1 to the intracellular costimulatory domain of CD3ζ to form a chimeric receptor. By comparison, NK cells expressing chimeric receptors have a better killing effect on tumor cells than NK cells expressing wild-type DNAM1 receptors. However, NK cells expressing chimeric receptors will reduce their anti-tumor effects after adding a costimulatory domain CD28, OX40 or 4-1BB between DNAM1 and CD3ζ (161). In 2020, Yao Huang et al.added 2B4 costimulatory domain between DNAM1 and CD3ζ. Compared with CD3ζ, CD28-CD3ζ, DNAM1-CD3ζ and 2B4-CD3ζ, CAR-NK expressing DNAM1-2B4-CD3ζ chimeric antigen receptor has the best anti-tumor effect (162). The above studies have shown that the expression of DNAM1 can enhance the anti-tumor effect of NK cells. In the construction of chimeric antigen receptors, DNAM1-2B4-CD3ζ is an ideal choice, and further research can be carried out on this basis.

In addition to DNAM1, Ece Canan Sayitoglu et al. also confirmed that NK cells overexpressing NKG2D can enhance the killing effect of NK cells on tumor cells (158). NKG2D is an activating receptor expressed on the cell membrane of NK cells, and its ligands are MICA, MICB and ULBPs (163) (164). Unlike type I transmembrane proteins such as CD28, 4-1BB, DNAM1 and CD3ζ, NKG2D belongs to type II transmembrane protein. Compared with type I transmembrane protein, the transmembrane expression of type II transmembrane protein does not require the guidance of signal peptide, and the C-terminal of type II transmembrane protein is outside the cell membrane. Therefore, two different strategies exist for modifying chimeric receptors based on NKG2D. First, without changing the characteristics of NKG2D type II transmembrane protein, the added costimulatory domain is connected to the N-terminus of NKG2D, or the extracellular recognition domain is linked to the C-terminus of NKG2D. Robin Parihar et al. linked an intracellular costimulatory domain of CD3ζ to the N-terminus of NKG2D. Unlike unmodified NK cells, NK cells modified with this chimeric receptor have more potent anti-tumor effects. Moreover, NK cells modified with this chimeric receptor can tolerate the interference of TGFβ and soluble MICA/MICB on the anti-tumor effect of NK cells in the immune microenvironment (116). Using a similar strategy, Changjiang Guo et al. connected a 4-1BB costimulatory domain to the N-terminus of NKG2D. Compared with the chimeric receptor without the 4-1BB costimulatory domain, NK cells modified with this chimeric receptor have more potent anti-tumor effects. This study also confirmed that modifying the C-terminal extracellular recognition domain of NKG2D would directly determine the function of chimeric receptors when using this strategy to modify NKG2D (165).

Another modification strategy for NKG2D is to use only the transmembrane domain of NKG2D, and design it from scratch according to type I transmembrane protein design method. The signal peptide, recognition domain and hinge region are linked at the N-terminus of the transmembrane domain of NKG2D, and different costimulatory domains are linked at the C-terminus of the transmembrane domain of NKG2D. NKG2D induces cell activation by forming a heterohexamer with DAP10, and the binding of NKG2D to DAP10 depends on the arginine on the NKG2D transmembrane domain (166) (167). Therefore, this strategy effectively retains the functional domain of NKG2D, namely the

transmembrane domain. More representative is a 2018 study by Ye Li et al. (20). The study used this strategy to add different combinations of costimulatory domains at the C-terminus of the NKG2D transmembrane domain. The chimeric antigen receptor with costimulatory domain 2B4 and CD3ζ have the best anti-tumor effect after modifying NK cells, and its anti-tumor effect is better than that of NK cells expressing T-CAR binding antigen receptors. In the tumor xenograft model of immunodeficient mice, compared with CAR-T cell therapy, mice treated with CAR-NK cells had longer survival. It is worth noting that when the different domains of the chimeric antigen receptor were functionally verified, the inactivation mutation of CD3ζ did not significantly reduce the killing effect of CAR-NK on tumor cells. In another study, Lin et al. compared DAP12 with CD3ζ and found that NK cells using DAP12 costimulatory domain chimeric antigen receptor had more potent anti-tumor effect than those using CD3ζ costimulatory domain chimeric antigen receptor (130). This study suggests that DAP12 is more suitable for designing chimeric antigen receptors than CD3ζ in constructing NK cell chimeric antigen receptors. The above studies have shown that NKG2D is a vital receptor to enhance the anti-tumor activity of NK cells no matter which strategy is used. When modifying NKG2D, the properties of its type II transmembrane protein should be fully considered for reasonable design and strict verification.

It is worth noting that both DNAM1 and NKG2D can effectively enhance their anti-tumor activity when combined with 2B4 in the construction of chimeric antigen receptors. When 2B4 is not combined with DNAM1 or NKG2D, the design of chimeric antigen receptors based on 2B4 can also improve the anti-tumor activity of NK cells. In 2019, Yingxi Xu et al. compared 2B4-CD3ζ with 4-1BB-CD3ζ. This study showed that NK cells using 2B4 costimulatory domain chimeric antigen receptors had more potent anti-tumor effects (168). In 2021, Ilias Christodoulou et al. also confirmed the same conclusion, that is, compared with 4-1BB-CD3ζ, NK cells using 2B4 costimulatory domain chimeric antigen receptor have more potent anti-tumor effect (153). Therefore, 2B4 is also a vital candidate receptor when designing NK cell chimeric antigen receptors.

In summary, the rational design of NK cell chimeric antigen receptors is of great significance for improving the anti-tumor activity of CAR-NK cells. DNAM1, NKG2D and 2B4 are essential candidates for rational design. In addition, the mechanism of the combined action between different domains of chimeric antigen receptors also needs to be further elucidated.

4.5 The safety of CAR-NK cells

Compared with CAR-T cell therapy, CAR-NK cell therapy is more safe (14). In 2018, Ye Li et al. used iPSC-derived NK cells as effector cells to construct mesothelin-targeted CAR-NK cells for treating human ovarian cancer (20). In this preclinical study, the survival time of mice treated with CAR-NK cells was significantly prolonged, and no apparent cytokine storm was detected during the treatment. As a control, CAR-T cell therapy slightly improved the survival of mice. The survival rate of mice in the CAR-T cells treatment group was significantly lower than that in the CAR-NK cells treatment group. In the same year, Enli Liu et al. used umbilical cord blood-derived NK cells as effector cells to construct CAR-NK cells targeting CD19 for treating lymphoblastic leukemia (146). In this preclinical study, the survival time of mice treated with CAR-NK cells was significantly prolonged. After 10 months of treatment, pathological examination of lymph nodes, spleen and bone marrow of mice showed no abnormal proliferation of CAR-NK cells. Subsequently, in 2020, Enli Liu et al. reported the clinical results of umbilical cord blood CAR-NK cells in treating lymphoblastic leukemia (22). A total of 11 patients were enrolled in this clinical trial. After CAR-NK cell administration, 8 patients showed a therapeutic response, of which 7 patients were completely relieved. After CAR-NK cells treatment, there was no treatment-related cytokine storm, neurotoxicity and anti-host disease, and the levels of inflammatory factors such as IL-6 did not exceed the baseline level. The above studies have shown that CAR-NK treatment has safety advantages.

The concerns about the safety of CAR-NK cells come from two aspects. First, NK-derived tumor cell lines are used as effector cells in many preclinical and even some clinical studies (14), and there is a risk of tumorigenicity. The current solution is to use gamma-ray irradiation and other methods to treat NK-derived tumor cell lines to maintain cell activity and inhibit their proliferation. In 2017, Paulina Nowakowska et al. constructed the preparation of clinical-grade CAR-NK92 cells. This study used NK-derived tumor cell line NK92 cell as effector cells. The prepared CAR-NK92 cells were irradiated with 10 Gy gamma-ray irradiation. This study showed that CAR-NK92 cells lost the ability of cell proliferation after irradiation, and CAR-NK92 cells could maintain their cell activity and function within 24 h after treatment (36). In 2020, Qian Liu et al. further studied the irradiation dose. In this study, CAR-NK92-MI cells were also irradiated with different doses of gamma rays. Compared with 10 Gy irradiation dose, CAR-NK92-MI cells irradiated with 5 Gy irradiation dose showed better anti-tumor ability in mice, and the survival of mice was improved more significantly (38). Compared with gamma-ray irradiation, treating CAR-NK92 cells with low-energy electron irradiation can also effectively inhibit the proliferation of CAR-NK92 cells, and has less effect on the whole gene expression level of cells (37).

Although methods such as gamma-ray irradiation can effectively inhibit the proliferation activity of NK-derived tumor cell lines, different NK-derived tumor cell lines have different functions in anti-tumor effects. Tsutomu Nakazawa et al. used NK-derived tumor cell line KHYG-1 as an effector cell to construct CAR-NK cells. In the glioblastoma animal model, the tumor progression of mice treated with CAR-NK cells was not inhibited, and even pseudoprogression occurred. In addition, the CAR-NK cells were co-cultured with tumor cells *in vitro*. High levels of IL-6 expression were detected, and IL-6 is one of the markers of cytokine storms (27). Therefore, in constructing CAR-NK cells using NK-derived tumor cell lines, in addition to inactivating cells such as irradiation to inhibit their tumorigenicity, the differences in anti-tumor effects between different NK-derived tumor cell lines and the resulting safety issues should be considered.

In some studies of CAR-NK cells, cytokines such as IL-2 are used to prolong the survival of CAR-NK cells *in vivo* and enhance the function of CAR-NK cells. Therefore, another concern about the safety of CAR-NK cells is the systemic toxicity these cytokines may bring to the body. Compared with IL-2, IL-15 is a safer choice (151) (152). Enli Liu et al.co-expressed IL-15 in CAR-NK cells to improve the anti-tumor effect of CAR-NK and prolong the residence time of CAR-NK cells *in vivo* (146). However, recent studies have shown that in animal models of CAR-NK cells co-expressing IL-15 in treating acute lymphoblastic leukemia, mice treated with CAR-NK cells can cause systemic toxicity. Although the CAR-NK cells have the most potent anti-tumor effect *in vivo*, the survival time of mice has not been significantly improved (153). In fact, in order to enhance the safety of CAR-NK cells, Enli Liu et al. introduced a suicide gene as a safety switch while co-expressing IL-15 (146). Therefore, the relatively safe IL-15 also needs to consider its potential safety issues. We may suggest that future research should rationally design CAR-NK cells treatment programs to enhance the anti-tumor effect of NK cells while overcoming the systemic toxicity of these cytokines.

5 Summary and prospect

Glioblastoma is a malignant tumor with the highest morbidity and mortality in the central nervous system. The survival time of patients is short, and the 5-year survival rate is less than 10%. Immunotherapy represents a promising class of glioblastoma treatment methods, such as tumor vaccines, immune checkpoint inhibitors, combination therapy and adoptive immunotherapy. Immunotherapy has carried out clinical research on glioblastoma (169). In adoptive cell immunotherapy, CAR-NK cell is another potential adoptive cell therapy strategy after CAR-T cell. Compared with CAR-T cells, CAR-NK cells do not cause similar adverse effects of CAR-T cell, such as cytokine storm and anti-host immune disease and has higher safety. In addition, the constructed CAR-NK cells retained the natural anti-tumor response of NK cells while allowing NK cells to specifically target tumors. CAR-NK cells with specific optimization have anti-tumor effects equivalent to CAR-T cells (20). At present, CAR-NK cell has achieved some positive therapeutic effects in preclinical studies of glioblastoma (Table 1), and clinical studies of CAR-NK cells targeting Her2 in the treatment of glioblastoma are also underway (NCT03383978).

However, CAR-NK cell treatment of glioblastoma also needs to address the inhibition in the immunosuppressive microenvironment of glioblastoma. For example, TGFβ in the immunosuppressive microenvironment is a classic immunomodulatory molecule. TGFβ plays a tumor-promoting role by inhibiting the anti-tumor activity of T cells and NK cells (170). In addition, CAR-NK cell faces challenges in terms of low preparation efficiency, short survival time *in vivo*, optimization of anti-tumor activity and safety. Fortunately, there are some solutions to these challenges of CAR-NK cell, such as the efficient preparation of CAR-NK cells *in vitro* by feeder-cells method or cytokine-assisted therapy to prolong the survival time of CAR-NK cells *in vivo*. Although these solutions are imperfect, they also lay the foundation for further research on CAR-NK cell therapy. In conclusion, CAR-NK cell is feasible in treating glioblastoma and a safe and effective cell therapy strategy. Future research should focus on optimizing the anti-tumor effect of CAR-NK and overcoming the tumor immunosuppressive microenvironment of solid tumors such as glioblastoma. CAR-NK has begun to see the dawn, and the future can be expected.

Author contributions

QX drafted and proofread the manuscript. HD and JZ proofread the manuscript. YZ drew the picture of the manuscript. All authors contributed to the article and approved the submitted version.

Funding

This work was supported by grants from 1.3.5 project for disciplines of excellence, West China Hospital, Sichuan University (ZYGD20003).

Acknowledgments

The authors would like to thank all the reviewers who participated in the review.

Conflict of interest

The authors declare that the research was conducted in the absence of any commercial or financial relationships that could be construed as a potential conflict of interest.

Publisher's note

References

1. Ostrom QT, Patil N, Cioffi G, Waite K, Kruchko C, Barnholtz-Sloan JS, et al. CBTRUS statistical report: primary brain and other central nervous system tumors diagnosed in the united states in 2013–2017. *Neuro-oncology* (2020) 22(Supplement_1): iv1–iv96. doi: 10.1093/neuonc/noaa200

2. Louis DN, Perry A, Reifenberger G, Brat DJ, Cree IA, Figarella-Branger D, et al. The 2016 world health organization classification of tumors of the central nervous system: a summary. . *Acta neuropathologica* (2016) 131(6):803–20. doi: 10.1007/s00401-016-1545-1

3. Wild CP, Weiderpass E, Stewart BW. World cancer report: cancer research for cancer prevention. *Lyon France: Int Agency Res Cancer* (2020) 1):1–611.

4. Daubon T, Hemadou A, Romero Garmendia I, Saleh M. Glioblastoma immune landscape and the potential of new immunotherapies. *Front Immunol* (2020) 11:2495. doi: 10.3389/fimmu.2020.585616

5. Minniti G, Niyazi M, Alongi F, Navarria P, Belka C. Current status and recent advances in reirradiation of glioblastoma. *Radiat Oncol* (2021) 16(1):36. doi: 10.1186/s13014-021-01767-9

6. Guha P, Heatherton KR, O'Connell KP, Alexander IS, Katz SC. Assessing the future of solid tumor immunotherapy. *Biomedicines* (2022) 10(3):655. doi: 10.3390/biomedicines10030655

7. Sampson JH, Maus MV, June CH. Immunotherapy for brain tumors. *J Clin Oncol* (2017) 35(21):2450–6. doi: 10.1200/JCO.2017.72.8089

8. Bausart M, Préat V, Malfanti A. Immunotherapy for glioblastoma: the promise of combination strategies. *J Exp Clin Cancer research: CR* (2022) 41(1):35. doi: 10.1186/s13046-022-02251-2

9. Shen SH, Woroniecka K, Barbour AB, Fecci PE, Sanchez-Perez L, Sampson JH, et al. CAR T cells and checkpoint inhibition for the treatment of glioblastoma. *Expert Opin Biol Ther* (2020) 20(6):579–91. doi: 10.1080/14712598.2020.1727436

10. Hupperetz C, Lah S, Kim H, Kim CH. CAR T cell immunotherapy beyond haematological malignancy. *Immune network* (2022) 22(1):e6. doi: 10.4110/in.2022.22.e6

11. Feldman L, Brown C, Badie B. Chimeric antigen receptor (CAR) T cell therapy for glioblastoma. *Neuromolecular Med* (2022) 2021:1–6. doi: 10.1007/s12017-021-08689-5

12. Yoo HJ, Harapan BN. Chimeric antigen receptor (CAR) immunotherapy: basic principles, current advances, and future prospects in neuro-oncology. *Immunologic Res* (2021) 69(6):471–86. doi: 10.1007/s12026-021-09236-x

13. Fu W, Wang W, Li H, Jiao Y, Huo R, Yan Z, et al. Single-cell atlas reveals complexity of the immunosuppressive microenvironment of initial and recurrent glioblastoma. *Front Immunol* (2020) 11:835. doi: 10.3389/fimmu.2020.00835

14. Pfefferle A, Huntington ND. You have got a fast CAR: chimeric antigen receptor NK cells in cancer therapy. *Cancers* (2020) 12(3):706. doi: 10.3390/cancers12030706

15. Rafiq S, Hackett CS, Brentjens RJ. Engineering strategies to overcome the current roadblocks in CAR T cell therapy. *Nat Rev Clin Oncol* (2020) 17(3):147–67. doi: 10.1038/s41571-019-0297-y

16. Gumber D, Wang LD. Improving CAR-T immunotherapy: overcoming the challenges of T cell exhaustion. *EBioMedicine* (2022) 77:103941. doi: 10.1016/j.ebiom.2022.103941

17. Morvan MG, Lanier LL. NK cells and cancer: you can teach innate cells new tricks. *Nat Rev Cancer* (2016) 16(1):7–19. doi: 10.1038/nrc.2015.5

18. Bald T, Krummel MF, Smyth MJ, Barry KC. The NK cell–cancer cycle: advances and new challenges in NK cell–based immunotherapies. *Nat Immunol* (2020) 21(8):835–47. doi: 10.1038/s41590-020-0728-z

19. Gasteiger G, Rudensky AY. Interactions between innate and adaptive lymphocytes. *Nat Rev Immunol* (2014) 14(9):631–9. doi: 10.1038/nri3726

20. Li Y, Hermanson DL, Moriarity BS, Kaufman DS. Human iPSC-derived natural killer cells engineered with chimeric antigen receptors enhance anti-tumor activity. *Cell Stem Cell* (2018) 23(2):181–92. doi: 10.1016/j.stem.2018.06.002

21. Pan K, Farrukh H, Chittepu VCSR, Xu H, Pan CX, Zhu Z, et al. CAR race to cancer immunotherapy: from CAR T, CAR NK to CAR macrophage therapy. *J Exp Clin Cancer research: CR* (2022) 41(1):119. doi: 10.1186/s13046-022-02327-z

22. Liu E, Marin D, Banerjee P, Macapinlac HA, Thompson P, Basar R, et al. Use of CAR-transduced natural killer cells in CD19-positive lymphoid tumors. *New Engl J Med* (2020) 382(6):545–53. doi: 10.1056/NEJMoa1910607

23. Zhang C, Burger MC, Jennewein L, Genßler S, Schönfeld K, Zeiner P, et al. ErbB2/HER2-specific NK cells for targeted therapy of glioblastoma. *J Natl Cancer Institute* (2016) 108(5):djv375. doi: 10.1093/jnci/djv375

24. Genßler S, Burger MC, Zhang C, Oelsner S, Mildenberger I, Wagner M, et al. Dual targeting of glioblastoma with chimeric antigen receptor-engineered natural killer cells overcomes heterogeneity of target antigen expression and enhances antitumor activity and survival. *Oncoimmunology* (2016) 5(4):e1119354. doi: 10.1080/2162402X.2015.1119354

25. Han J, Chu J, Chan WK, Zhang J, Wang Y, Cohen JB, et al. CAR-engineered NK cells targeting wild-type EGFR and EGFRvIII enhance killing of glioblastoma and patient-derived glioblastoma stem cells. *Sci Rep* (2015) 5(1):1–13. doi: 10.1038/srep11483

26. Müller N, Michen S, Tietze S, Töpfer K, Schulte A, Lamszus K, et al. Engineering NK cells modified with an EGFRvIII-specific chimeric antigen receptor to overexpress CXCR4 improves immunotherapy of CXCL12/SDF-1α-secreting glioblastoma. *J immunotherapy* (2015) 38(5):197. doi: 10.1097/CJI.0000000000000082

27. Nakazawa T, Murakami T, Natsume A, Nishimura F, Morimoto T, Matsuda R, et al. KHYG-1 cells with EGFRvIII-specific CAR induced a pseudoprogression-like feature in subcutaneous tumours derived from glioblastoma-like cells. *Anticancer Res* (2020) 40(6):3231–7. doi: 10.21873/anticanres.14304

28. Murakami T, Nakazawa T, Natsume A, Nishimura F, Nakamura M, Matsuda R, et al. Novel human NK cell line carrying CAR targeting EGFRvIII induces antitumor effects in glioblastoma cells. *Anticancer Res* (2018) 38(9):5049–56. doi: 10.21873/anticanres.12824

29. Grote S, Chan KC-H, Baden C, Hans B, Mihály S, Leonie F, et al. CD276 as a novel CAR NK-92 therapeutic target for neuroblastoma. *Adv In Cell And Gene Ther* (2021) 4(1):e105. doi: 10.1002/acg2.105

30. Ma R, Lu T, Li Z, Teng KY, Mansour AG, Yu M, et al. An oncolytic virus expressing IL-15/IL-15Rα combined with off-the-shelf EGFR-CAR NK cells targets glioblastoma. *Cancer Res* (2021) 81(13):3635–48. doi: 10.1158/0008-5472.CAN-21-0035

31. Kang CH, Kim Y, Lee SM, Choi SU, Park CH. Development of antigen-specific chimeric antigen receptor KHYG-1 cells for glioblastoma. *Anticancer Res* (2021) 41(4):1811–9. doi: 10.21873/anticanres.14947

32. Wang J, Toregrosa-Allen S, Elzey BD, Utturkar S, Lanman NA, Bernal-Crespo V, et al. Multispecific targeting of glioblastoma with tumor microenvironment-responsive multifunctional engineered NK cells. *Proc Natl Acad Sci* (2021) 118(45):e2107507118. doi: 10.1073/pnas.2107507118

33. Gong JH, Maki G, Klingemann HG. Characterization of a human cell line (NK-92) with phenotypical and functional characteristics of activated natural killer cells. *Leukemia* (1994) 8(4):652–8.

34. Zhang L, Meng Y, Feng X, Han Z. CAR-NK cells for cancer immunotherapy: from bench to bedside. *biomark Res* (2022) 10(1):12. doi: 10.1186/s40364-022-00364-6

35. Lin C, Zhang J. Reformation in chimeric antigen receptor based cancer immunotherapy: redirecting natural killer cell. *Biochim Biophys Acta (BBA)-Reviews Cancer* (2018) 1869(2):200–15. doi: 10.1016/j.bbcan.2018.01.005

36. Nowakowska P, Romanski A, Miller N, Odendahl M, Bonig H, Zhang C, et al. Clinical grade manufacturing of genetically modified, CAR-expressing NK-92 cells for the treatment of ErbB2-positive malignancies. *Cancer Immunology Immunotherapy* (2018) 67(1):25–38. doi: 10.1007/s00262-017-2055-2

37. Walcher L, Kistenmacher A-K, Sommer C, Böhlen S, Ziemann C, Dehmel S, et al. Low energy electron irradiation is a potent alternative to gamma irradiation for the inactivation of (CAR-) NK-92 cells in ATMP manufacturing. *Front Immunol* (2021) 12. doi: 10.3389/fimmu.2021.684052

38. Liu Q, Xu Y, Mou J, Tang K, Fu X, Li Y, et al. Irradiated chimeric antigen receptor engineered NK-92MI cells show effective cytotoxicity against CD19+ malignancy in a mouse model. *Cytotherapy* (2020) 22(10):552–62. doi: 10.1016/j.jcyt.2020.06.003

39. Kloess S, Oberschmidt O, Dahlke J, Vu XK, Neudoerfl C, Kloos A, et al. Preclinical assessment of suitable natural killer cell sources for chimeric antigen receptor natural killer–based "Off-the-Shelf" acute myeloid leukemia immunotherapies. *Hum Gene Ther* (2019) 30(4):381–401. doi: 10.1089/hum.2018.247

40. MacKay M, Afshinnekoo E, Rub J, Hassan C, Khunte M, Baskaran N, et al. The therapeutic landscape for cells engineered with chimeric antigen receptors. *Nat Biotechnol* (2020) 38(2):233–44. doi: 10.1038/s41587-019-0329-2

41. Salter AI, Ivey RG, Kennedy JJ, Voillet V, Rajan A, Alderman EJ, et al. Phosphoproteomic analysis of chimeric antigen receptor signaling reveals kinetic and quantitative differences that affect cell function. *Sci Signaling* (2018) 11(544):eaat6753. doi: 10.1126/scisignal.aat6753

42. Ying Z, He T, Wang X, Zheng W, Lin N, Tu M, et al. Parallel comparison of 4-1BB or CD28 co-stimulated CD19-targeted CAR-T cells for b cell non-hodgkin's lymphoma. *Mol Therapy-Oncolytics* (2019) 15:60–8. doi: 10.1016/j.omto.2019.08.002

43. Du H, Hirabayashi K, Ahn S, Kren NP, Montgomery SA, Wang X, et al. Antitumor responses in the absence of toxicity in solid tumors by targeting B7-H3 via chimeric antigen receptor T cells. *Cancer Cell* (2019) 35(2):221–37. doi: 10.1016/j.ccell.2019.01.002

44. Abate-Daga D, Lagisetty KH, Tran E, Zheng Z, Gattinoni L, Yu Z, et al. A novel chimeric antigen receptor against prostate stem cell antigen mediates tumor destruction in a humanized mouse model of pancreatic cancer. *Hum Gene Ther* (2014) 25(12):1003–12. doi: 10.1089/hum.2013.209

45. Ramello MC, Benzaïd I, Kuenzi BM, Lienlaf MM, Kandell WM, Santiago DN, et al. An immunoproteomic approach to characterize the CAR interactome and signalosome. *Sci Signaling* (2019) 12(568):eaap9777. doi: 10.1126/scisignal.aap9777

46. Ao X, Yang Y, Li W, Tan Y, Guo W, Ao L, et al. Anti-αFR CAR-engineered NK-92 cells display potent cytotoxicity against αFR-positive ovarian cancer. *J Immunotherapy* (2019) 42(8):284. doi: 10.1097/CJI.0000000000000286

47. Lupu R, Colomer R, Kannan B, Lippman ME. Characterization of a growth factor that binds exclusively to the erbB-2 receptor and induces cellular responses. *Proc Natl Acad Sci* (1992) 89(6):2287–91. doi: 10.1073/pnas.89.6.2287

48. Krishnamurti U, Silverman JF. HER2 in breast cancer: a review and update. *Adv anatomic Pathol* (2014) 21(2):100–7. doi: 10.1097/PAP.0000000000000015

49. Cai Y, Wang J, Zhang L, Wu D, Yu D, Tian X, et al. Expressions of fatty acid synthase and HER2 are correlated with poor prognosis of ovarian cancer. *Med Oncol* (2015) 32(1):1–6. doi: 10.1007/s12032-014-0391-z

50. Yan M, Schwaederle M, Arguello D, Millis SZ, Gatalica Z, Kurzrock R, et al. HER2 expression status in diverse cancers: review of results from 37,992 patients. *Cancer Metastasis Rev* (2015) 34(1):157–64. doi: 10.1007/s10555-015-9552-6

51. Minner S, Jessen B, Stiedenroth L, Burandt E, Köllermann J, Mirlacher M, et al. Low level HER2 overexpression is associated with rapid tumor cell proliferation and

poor prognosis in prostate cancer. *Clin Cancer Res* (2010) 16(5):1553–60. doi: 10.1158/1078-0432.CCR-09-2546

52. Slamon DJ, Godolphin W, Jones LA, Holt JA, Wong SG, Keith DE, et al. Studies of the HER-2/neu proto-oncogene in human breast and ovarian cancer. *science* (1989) 244(4905):707–12. doi: 10.1126/science.2470152

53. Liu G, Ying H, Zeng G, Wheeler CJ, Black KL, Yu JS, et al. HER-2, gp100, and MAGE-1 are expressed in human glioblastoma and recognized by cytotoxic T cells. *Cancer Res* (2004) 64(14):4980–6. doi: 10.1158/0008-5472.CAN-03-3504

54. Haynik DM, Roma AA, Prayson RA. HER-2/neu expression in glioblastoma multiforme. *Appl Immunohistochemistry Mol Morphology* (2007) 15(1):56–8. doi: 10.1097/01.pai.0000213133.09160.da

55. Ramezani M, Siami S, Rezaei M, Khazaei S, Sadeghi M. An immunohistochemical study of HER2 expression in primary brain tumors. *BioMedicine* (2020) 10(1):21. doi: 10.37796/2211-8039.1001

56. Ahmed N, Salsman VS, Kew Y, Shaffer D, Powell S, Zhang YJ, et al. HER2-specific T cells target primary glioblastoma stem cells and induce regression of autologous experimental tumors. *Clin Cancer Res* (2010) 16(2):474–85. doi: 10.1158/1078-0432.CCR-09-1322

57. Camp RL, Dolled-Filhart M, King BL, Rimm DL. Quantitative analysis of breast cancer tissue microarrays shows that both high and normal levels of HER2 expression are associated with poor outcome. *Cancer Res* (2003) 63(7):1445–8.

58. Lin Y-J, Mashouf LA, Lim M. CAR T cell therapy in primary brain tumors: current investigations and the future. *Front Immunol* (2022) 13:817296. doi: 10.3389/fimmu.2022.817296

59. Press MF, Cordon-Cardo C, Slamon DJ. Expression of the HER-2/neu proto-oncogene in normal human adult and fetal tissues. *Oncogene* (1990) 5(7):953–62.

60. Ahmed N, Brawley V, Hegde M, Bielamowicz K, Kalra M, Landi D, et al. Her2-specific chimeric antigen receptor–modified virus-specific t cells for progressive glioblastoma: a phase 1 dose-escalation trial. *JAMA Oncol* (2017) 3(8):1094–101. doi: 10.1001/jamaoncol.2017.0184

61. Zandi R, Larsen AB, Andersen P, Stockhausen MT, Poulsen HS. Mechanisms for oncogenic activation of the epidermal growth factor receptor. *Cell signalling* (2007) 19 (10):2013–23. doi: 10.1016/j.cellsig.2007.06.023

62. Parsons DW, Jones S, Zhang X, Lin JC, Leary RJ, Angenendt P, et al. An integrated genomic analysis of human glioblastoma multiforme. *Science* (2008) 321 (5897):1807–12. doi: 10.1126/science.1164382

63. Salomon DS, Brandt R, Ciardiello F, Normanno N. Epidermal growth factor-related peptides and their receptors in human malignancies. *Crit Rev oncology/hematology* (1995) 19(3):183–232. doi: 10.1016/1040-8428(94)00144-I

64. Aldape KD, Ballman K, Furth A, Buckner JC, Giannini C, Burger PC, et al. Immunohistochemical detection of EGFRvIII in high malignancy grade astrocytomas and evaluation of prognostic significance. *J Neuropathology Exp Neurol* (2004) 63 (7):700–7. doi: 10.1093/jnen/63.7.700

65. Biernat W, Huang H, Yokoo H, Kleihues P, Ohgaki H. Predominant expression of mutant EGFR (EGFRvIII) is rare in primary glioblastomas. *Brain Pathol* (2004) 14 (2):131–6. doi: 10.1111/j.1750-3639.2004.tb00045.x

66. Sugawa N, Ekstrand AJ, James CD, Collins VP. Identical splicing of aberrant epidermal growth factor receptor transcripts from amplified rearranged genes in human glioblastomas. *Proc Natl Acad Sci* (1990) 87(21):8602–6. doi: 10.1073/pnas.87.21.8602

67. Fan Q-W, Cheng CK, Gustafson WC, Charron E, Zipper P, Wong RA, et al. EGFR phosphorylates tumor-derived EGFRvIII driving STAT3/5 and progression in glioblastoma. *Cancer Cell* (2013) 24(4):438–49. doi: 10.1016/j.ccr.2013.09.004

68. Huang H-JS, Nagane M, Klingbeil CK, Lin H, Nishikawa R, Ji XD, et al. The enhanced tumorigenic activity of a mutant epidermal growth factor receptor common in human cancers is mediated by threshold levels of constitutive tyrosine phosphorylation and unattenuated signaling. *J Biol Chem* (1997) 272(5):2927–35. doi: 10.1074/jbc.272.5.2927

69. Furnari FB, Cloughesy TF, Cavenee WK, Mischel PS. Heterogeneity of epidermal growth factor receptor signalling networks in glioblastoma. *Nat Rev Cancer* (2015) 15(5):302–10. doi: 10.1038/nrc3918

70. Shinojima N, Tada K, Shiraishi S, Kamiryo T, Kochi M, Nakamura H, et al. Prognostic value of epidermal growth factor receptor in patients with glioblastoma multiforme. *Cancer Res* (2003) 63(20):6962–70.

71. O'Rourke DM, Nasrallah MP, Desai A, Melenhorst JJ, Mansfield K, Morrissette JJD, et al. A single dose of peripherally infused EGFRvIII-directed CAR T cells mediates antigen loss and induces adaptive resistance in patients with recurrent glioblastoma. *Sci Trans Med* (2017) 9(399):eaaa0984. doi: 10.1126/scitranslmed.aaa0984

72. Goff SL, Morgan RA, Yang JC, Sherry RM, Robbins PF, Restifo NP, et al. Pilot trial of adoptive transfer of chimeric antigen receptor transduced T cells targeting EGFRvIII in patients with glioblastoma. *J immunotherapy* (2019) 42(4):126. doi: 10.1097/CJI.0000000000000260

73. LaPorte SL, Juo ZS, Vaclavikova J, Colf LA, Qi X, Heller NM, et al. Molecular and structural basis of cytokine receptor pleiotropy in the interleukin-4/13 system. *Cell* (2008) 132(2):259–72. doi: 10.1016/j.cell.2007.12.030

74. Kelly-Welch AE, Hanson EM, Boothby MR, Keegan AD. Interleukin-4 and interleukin-13 signaling connections maps. *Science* (2003) 300(5625):1527–8. doi: 10.1126/science.1085458

75. Arima K, Sato K, Tanaka G, Kanaji S, Terada T, Honjo E, et al. Characterization of the interaction between interleukin-13 and interleukin-13 receptors. *J Biol Chem* (2005) 280(26):24915–22. doi: 10.1074/jbc.M502571200

76. Lupardus PJ, Birnbaum ME, Garcia KC. Molecular basis for shared cytokine recognition revealed in the structure of an unusually high affinity complex between IL-13 and IL-13Rα2. *Structure* (2010) 18(3):332–42. doi: 10.1016/j.str.2010.01.003

77. Caput D, Laurent P, Kaghad M, Lelias JM, Lefort S, Vita N, et al. Cloning and characterization of a specific interleukin (IL)-13 binding protein structurally related to the IL-5 receptor α chain. *J Biol Chem* (1996) 271(28):16921–6. doi: 10.1074/jbc.271.28.16921

78. Donaldson DD, Whitters MJ, Fitz LJ, Neben TY, Finnerty H, Henderson SL, et al. The murine IL-13 receptor α2: molecular cloning, characterization, and comparison with murine IL-13 receptor α1. *J Immunol* (1998) 161(5):2317–24. doi: 10.4049/jimmunol.161.5.2317

79. Thaci B, Brown CE, Binello E, Werbaneth K, Sampath P, Sengupta S, et al. Significance of interleukin-13 receptor alpha 2–targeted glioblastoma therapy. *Neuro-oncology* (2014) 16(10):1304–12. doi: 10.1093/neuonc/nou045

80. Brown CE, Warden CD, Starr R, Renate S, Xutao D, Behnam B, et al. Glioma IL13Rα2 is associated with mesenchymal signature gene expression and poor patient prognosis. *PloS One* (2013) 8(10):e77769. doi: 10.1371/journal.pone.0077769

81. Joshi BH, Plautz GE, Puri RK. Interleukin-13 receptor α chain: a novel tumor-associated transmembrane protein in primary explants of human malignant gliomas. *Cancer Res* (2000) 60(5):1168–72.

82. Rahaman SO, Sharma P, Harbor PC, Aman MJ, Vogelbaum MA, Haque SJ, et al. IL-13Rα2, a decoy receptor for IL-13 acts as an inhibitor of IL-4-dependent signal transduction in glioblastoma cells. *Cancer Res* (2002) 62(4):1103–9.

83. Newman JP, Wang GY, Arima K, Guan SP, Waters MR, Cavenee WK, et al. Interleukin-13 receptor alpha 2 cooperates with EGFRvIII signaling to promote glioblastoma multiforme. *Nat Commun* (2017) 8(1):1–17. doi: 10.1038/s41467-017-01392-9

84. Iwami K, Shimato S, Ohno M, Okada H, Nakahara N, Sato Y, et al. Peptide-pulsed dendritic cell vaccination targeting interleukin-13 receptor α2 chain in recurrent malignant glioma patients with HLA-a* 24/A* 02 allele. *Cytotherapy* (2012) 14(6):733–42. doi: 10.3109/14653249.2012.666633

85. Kunwar S, Prados MD, Chang SM, Berger MS, Lang FF, Piepmeier JM, et al. Direct intracerebral delivery of cintredekin besudotox (IL13-PE38QQR) in recurrent malignant glioma: a report by the cintredekin besudotox intraparenchymal study group. *J Clin Oncol* (2007) 25(7):837–44. doi: 10.1200/JCO.2006.08.1117

86. Brown CE, Badie B, Barish ME, Weng L, Ostberg JR, Chang WC, et al. Bioactivity and safety of IL13Rα2-redirected chimeric antigen receptor CD8+ T cells in patients with recurrent glioblastoma. *Clin Cancer Res* (2015) 21(18):4062–72. doi: 10.1158/1078-0432.CCR-15-0428

87. Brown CE, Alizadeh D, Starr R, Weng L, Wagner JR, Naranjo A, et al. Regression of glioblastoma after chimeric antigen receptor T-cell therapy. *New Engl J Med* (2016) 375(26):2561–9. doi: 10.1056/NEJMoa1610497

88. Hoshino T, Winkler-Pickett RT, Mason AT, Ortaldo JR, Young HA. IL-13 production by NK cells: IL-13-producing NK and T cells are present *in vivo* in the absence of IFN-γ. *J Immunol* (1999) 162(1):51–9. doi: 10.4049/jimmunol.162.1.51

89. Loza MJ, Peters SP, Zangrilli JG, Perussia B. Distinction between IL-13+ and IFN-γ+ natural killer cells and regulation of their pool size by IL-4. *Eur J Immunol* (2002) 32(2):413–23. doi: 10.1002/1521-4141(200202)32:2<413::AID-IMMU413>3.0.CO;2-X

90. Ohayon DE, Krishnamurthy D, Brusilovsky M, Waggoner SN. IL-4 and IL-13 modulate natural killer cell responses under inflammatory conditions. *J Immunol* (2017) 198(1_Supplement):194.11. doi: 10.4049/jimmunol.198.Supp.194.11

91. Pluschke G, Vanek M, Evans A, Dittmar T, Schmid P, Itin P, et al. Molecular cloning of a human melanoma-associated chondroitin sulfate proteoglycan. *Proc Natl Acad Sci* (1996) 93(18):9710–5. doi: 10.1073/pnas.93.18.9710

92. Beard RE, Zheng Z, Lagisetty KH, Burns WR, Tran E, Hewitt SM, et al. Multiple chimeric antigen receptors successfully target chondroitin sulfate proteoglycan 4 in several different cancer histologies and cancer stem cells. *J immunotherapy Cancer* (2014) 2(1):1–11. doi: 10.1186/2051-1426-2-25

93. Wang X, Wang Y, Yu L, Sakakura K, Visus C, Schwab JH, et al. CSPG4 in cancer: multiple roles. *Curr Mol Med* (2010) 10(4):419–29. doi: 10.2174/156652410791316977

94. Hafner C, Breiteneder H, Ferrone S, Thallinger C, Wagner S, Schmidt WM, et al. Suppression of human melanoma tumor growth in SCID mice by a human high molecular weight-melanoma associated antigen (HMW-MAA) specific monoclonal antibody. *Int J Cancer* (2005) 114(3):426–32. doi: 10.1002/ijc.20769

95. Rivera Z, Ferrone S, Wang X, Jube S, Yang H, Pass HI, et al. CSPG4 as a target of antibody-based immunotherapy for malignant mesothelioma. *Clin Cancer Res* (2012) 18(19):5352–63. doi: 10.1158/1078-0432.CCR-12-0628

96. Geldres C, Savoldo B, Hoyos V, Caruana I, Zhang M, Yvon E, et al. T Lymphocytes redirected against the chondroitin sulfate proteoglycan-4 control the growth of multiple solid tumors both *in vitro* and *in vivo*. *Clin Cancer Res* (2014) 20 (4):962–71. doi: 10.1158/1078-0432.CCR-13-2218

97. Schiffer D, Mellai M, Boldorini R, Bisogno I, Grifoni S, Corona C, et al. The significance of chondroitin sulfate proteoglycan 4 (CSPG4) in human gliomas. *Int J Mol Sci* (2018) 19(9):2724. doi: 10.3390/ijms19092724

98. Svendsen A, Verhoeff JJC, Immervoll H, Brøgger JC, Kmiecik J, Poli A, et al. Expression of the progenitor marker NG2/CSPG4 predicts poor survival and resistance to ionising radiation in glioblastoma. *Acta neuropathologica* (2011) 122(4):495–510. doi: 10.1007/s00401-011-0867-2

99. Pellegatta S, Savoldo B, Di Ianni N, Corbetta C, Chen Y, Patané M, et al. Constitutive and TNFα-inducible expression of chondroitin sulfate proteoglycan 4 in glioblastoma and neurospheres: implications for CAR-T cell therapy. *Biochem Biophys Res Commun* (2013) 441:514–8. doi: 10.1126/scitranslmed.aao2731

100. Poli A, Wang J, Domingues O, Planagumà J, Yan T, Rygh CB, et al. Targeting glioblastoma with NK cells and mAb against NG2/CSPG4 prolongs animal survival. *Oncotarget* (2013) 4(9):1527. doi: 10.18632/oncotarget.1291

101. Sonnino S, Chiricozzi E, Grassi S, Mauri L, Prioni S, Prinetti A, et al. Gangliosides in membrane organization. *Prog Mol Biol Trans Sci* (2018) 156:83–120. doi: 10.1016/bs.pmbts.2017.12.007

102. Schnaar RL. Gangliosides of the vertebrate nervous system. *J Mol Biol* (2016) 428(16):3325–36. doi: 10.1016/j.jmb.2016.05.020

103. Liu Z, Zhou J, Yang X, Liu Y, Zou C, Lv W, et al. Safety and antitumor activity of GD2-specific 4SCAR-T cells in patients with glioblastoma. *Mol Cancer* (2023) 22 (1):3. doi: 10.1186/s12943-022-01711-9

104. Nazha B, Inal C, Owonikoko TK. Disialoganglioside GD2 expression in solid tumors and role as a target for cancer therapy. *Front Oncol* (2020) 10:1000. doi: 10.3389/fonc.2020.01000

105. Shao C, Anand V, Andreeff M, Battula VL. Ganglioside GD2: a novel therapeutic target in triple-negative breast cancer. *Ann New York Acad Sci* (2022) 1508(1):35–53. doi: 10.1111/nyas.14700

106. Mount CW, Majzner RG, Sundaresh S, Arnold EP, Kadapakkam M, Haile S, et al. Potent antitumor efficacy of anti-GD2 CAR T cells in H3-K27M(+) diffuse midline gliomas. *Nat Med* (2018) 24(5):572–9. doi: 10.1038/s41591-018-0006-x

107. Woo SR, Oh YT, An JY, Kang BG, Nam DH, Joo KM, et al. Glioblastoma specific antigens, GD2 and CD90, are not involved in cancer stemness. *Anat Cell Biol* (2015) 48(1):44–53. doi: 10.5115/acb.2015.48.1.44

108. Prapa M, Chiavelli C, Golinelli G, Grisendi G, Bestagno M, Di Tinco R, et al. GD2 CAR T cells against human glioblastoma. *NPJ Precis Oncol* (2021) 5(1):93. doi: 10.1038/s41698-021-00233-9

109. Majzner RG, Ramakrishna S, Yeom KW, Patel S, Chinnasamy H, Schultz LM, et al. GD2-CAR T cell therapy for H3K27M-mutated diffuse midline gliomas. *Nature* (2022) 603(7903):934–41. doi: 10.1038/s41586-022-04489-4

110. Mitwasi N, Feldmann A, Arndt C, Koristka S, Berndt N, Jureczek J, et al. "UniCAR"-modified off-the-shelf NK-92 cells for targeting of GD2-expressing tumour cells. *Sci Rep* (2020) 10(1):2141. doi: 10.1038/s41598-020-59082-4

111. Ransohoff RM, Engelhardt B. The anatomical and cellular basis of immune surveillance in the central nervous system. *Nat Rev Immunol* (2012) 12(9):623–35. doi: 10.1038/nri3265

112. Sampson JH, Gunn MD, Fecci PE, Ashley DM. Brain immunology and immunotherapy in brain tumours. *Nat Rev Cancer* (2020) 20(1):12–25. doi: 10.1038/s41568-019-0224-7

113. Huang Y, Kim B, Chan CK, Hahn SM, Weissman IL, Jiang W, et al. Improving immune–vascular crosstalk for cancer immunotherapy. *Nat Rev Immunol* (2018) 18 (3):195–203. doi: 10.1038/nri.2017.145

114. De Leo A, Ugolini A, Veglia F. Myeloid cells in glioblastoma microenvironment. *Cells* (2021) 10(1):18. doi: 10.3390/cells10010018

115. Fanelli GN, Grassini D, Ortenzi V, Pasqualetti F, Montemurro N, Perrini P, et al. Decipher the glioblastoma microenvironment: the first milestone for new groundbreaking therapeutic strategies. *Genes* (2021) 12(3):445. doi: 10.3390/genes12030445

116. Parihar R, Rivas C, Huynh M, Omer B, Lapteva N, Metelitsa LS, et al. NK cells expressing a chimeric activating receptor eliminate MDSCs and rescue impaired CAR-T cell activity against solid tumors. *Cancer Immunol Res* (2019) 7(3):363–75. doi: 10.1158/2326-6066.CIR-18-0572

117. Shaim H, Shanley M, Basar R, Daher M, Gumin J, Zamler DB, et al. Targeting the αv integrin/TGF-β axis improves natural killer cell function against glioblastoma stem cells. *J Clin Invest* (2021) 131(14):e142116. doi: 10.1172/JCI142116

118. Chaudhry K, Geiger A, Dowlati E, Lang H, Sohai DK, Hwang EI, et al. Co-Transducing B7H3 CAR-NK cells with the DNR preserves their cytolytic function against GBM in the presence of exogenous TGF-β. *Mol Ther Methods Clin Dev* (2022) 27:415–30. doi: 10.1016/j.omtm.2022.10.010

119. Zhu H, Kaufman DS. An improved method to produce clinical-scale natural killer cells from human pluripotent stem cells. *Methods Mol Biol* (2019) 2048:107–19. doi: 10.1007/978-1-4939-9728-2_12

120. Goldenson BH, Hor P, Kaufman DS. iPSC-derived natural killer cell therapies - expansion and targeting. *Front Immunol* (2022) 13:841107. doi: 10.3389/fimmu.2022.841107

121. Herrera L, Santos S, Vesga MA, Anguita J, Martin-Ruiz I, Carrascosa T, et al. Adult peripheral blood and umbilical cord blood NK cells are good sources for effective CAR therapy against CD19 positive leukemic cells. *Sci Rep* (2019) 9(1):1–10. doi: 10.1038/s41598-019-55239-y

122. Kim H-S, Kim JY, Seol B, Song CL, Jeong JE, Cho YS, et al. Directly reprogrammed natural killer cells for cancer immunotherapy. *Nat Biomed Eng* (2021) 5(11):1360–76. doi: 10.1038/s41551-021-00768-z

123. Shimasaki N, Jain A, Campana D. NK cells for cancer immunotherapy. *Nat Rev Drug Discovery* (2020) 19(3):200–18. doi: 10.1038/s41573-019-0052-1

124. Cho D, Campana D. Expansion and activation of natural killer cells for cancer immunotherapy. *Korean J Lab Med* (2009) 29(2):89–96. doi: 10.3343/kjlm.2009.29.2.89

125. Denman CJ, Senyukov VV, Somanchi SS, Phatarpekar PV, Kopp LM, Johnson JL, et al. Membrane-bound IL-21 promotes sustained ex vivo proliferation of human natural killer cells. *PloS One* (2012) 7(1):e30264. doi: 10.1371/journal.pone.0030264

126. Vidard L, Dureuil C, Baudhuin J, Vescovi L, Durand L, Sierra V, et al. CD137 (4-1BB) engagement fine-tunes synergistic IL-15–and IL-21–driven NK cell proliferation. *J Immunol* (2019) 203(3):676–85. doi: 10.4049/jimmunol.1801137

127. Harada H, Saijo K, Watanabe S, Tsuboi K, Nose T, Ishiwata I, et al. Selective expansion of human natural killer cells from peripheral blood mononuclear cells by the cell line, HFWT. *Japanese J Cancer research: Gann* (2002) 93(3):313–9. doi: 10.1111/j.1349-7006.2002.tb02174.x

128. Bae DS, Lee JK. Development of NK cell expansion methods using feeder cells from human myelogenous leukemia cell line. *Blood Res* (2014) 49(3):154–61. doi: 10.5045/br.2014.49.3.154

129. Boissel L, Betancur M, Lu W, Wels WS, Marino T, Van Etten RA, et al. Comparison of mRNA and lentiviral based transfection of natural killer cells with chimeric antigen receptors recognizing lymphoid antigens. *Leukemia lymphoma* (2012) 53(5):958–65. doi: 10.3109/10428194.2011.634048

130. Xiao L, Cen D, Gan H, Sun Y, Huang N, Xiong H, et al. Adoptive transfer of NKG2D CAR mRNA-engineered natural killer cells in colorectal cancer patients. *Mol Ther* (2019) 27(6):1114–25. doi: 10.1016/j.ymthe.2019.03.011

131. Yoshikawa T, Wu Z, Inoue S, Kasuya H, Matsushita H, Takahashi Y, et al. Genetic ablation of PRDM1 in antitumor T cells enhances therapeutic efficacy of adoptive immunotherapy. *Blood* (2022) 139(14):2156–72. doi: 10.1182/blood.2021012714

132. Stadtmauer EA, Fraietta JA, Davis MM, Cohen AD, Weber KL, Lancaster E, et al. CRISPR-engineered T cells in patients with refractory cancer. *Science* (2020) 367 (6481):eaba7365. doi: 10.1126/science.aba7365

133. Nahmad AD, Reuveni E, Goldschmidt E, Tenne T, Liberman M, Horovitz-Fried M, et al. Frequent aneuploidy in primary human T cells after CRISPR-Cas9 cleavage. *Nat Biotechnol* (2022) 40(12):1807–13. doi: 10.1101/2021.08.20.457092

134. Bari R, Granzin M, Tsang KS, Roy A, Krueger W, Orentas R, et al. A distinct subset of highly proliferative and lentiviral vector (LV)-transducible NK cells define a readily engineered subset for adoptive cellular therapy. *Front Immunol* (2019) 2001. doi: 10.3389/fimmu.2019.02001

135. Kelly PF, Vandergriff J, Nathwani A, Nienhuis AW, Vanin EF. Highly efficient gene transfer into cord blood nonobese diabetic/severe combined immunodeficiency repopulating cells by oncoretroviral vector particles pseudotyped with the feline endogenous retrovirus (RD114) envelope protein. *Blood J Am Soc Hematol* (2000) 96 (4):1206–14.

136. Colamartino ABL, Lemieux W, Bifsha P, Nicoletti S, Chakravarti N, Sanz J, et al. Efficient and robust NK-cell transduction with baboon envelope pseudotyped lentivector. *Front Immunol* (2019) 10:2873. doi: 10.3389/fimmu.2019.02873

137. Sutlu T, Nyström S, Gilljam M, Stellan B, Applequist SE, Alici E, et al. Inhibition of intracellular antiviral defense mechanisms augments lentiviral transduction of human natural killer cells: implications for gene therapy. *Hum Gene Ther* (2012) 23(10):1090–100. doi: 10.1089/hum.2012.080

138. Chockley P, Patil SL, Gottschalk S. Transient blockade of TBK1/IKKε allows efficient transduction of primary human natural killer cells with vesicular stomatitis virus G-pseudotyped lentiviral vectors. *Cytotherapy* (2021) 23(9):787–92. doi: 10.1016/j.jcyt.2021.04.010

139. Miller JS, Soignier Y, Panoskaltsis-Mortari A, McNearney SA, Yun GH, Fautsch SK, et al. Successful adoptive transfer and *in vivo* expansion of human haploidentical NK cells in patients with cancer. *Blood* (2005) 105(8):3051–7. doi: 10.1182/blood-2004-07-2974

140. Romee R, Rosario M, Berrien-Elliott MM, Wagner JA, Jewell BA, Schappe T, et al. Cytokine-induced memory-like natural killer cells exhibit enhanced responses against myeloid leukemia. *Sci Trans Med* (2016) 8(357):357ra123–357ra123. doi: 10.1126/scitranslmed.aaf2341

141. Bachanova V, Cooley S, Defor TE, Verneris MR, Zhang B, McKenna DH, et al. Clearance of acute myeloid leukemia by haploidentical natural killer cells is improved using IL-2 diphtheria toxin fusion protein. *Blood J Am Soc Hematol* (2014) 123 (25):3855–63. doi: 10.1182/blood-2013-10-532531

142. Zhu H, Blum RH, Bernareggi D, Ask EH, Wu Z, Hoel HJ, et al. Metabolic reprograming via deletion of CISH in human iPSC-derived NK cells promotes *in vivo* persistence and enhances anti-tumor activity. *Cell Stem Cell* (2020) 27(2):224–37. doi: 10.1016/j.stem.2020.05.008

143. Zhang Q, Tian K, Xu J, Zhang H, Li L, Fu Q, et al. Synergistic effects of cabozantinib and EGFR-specific CAR-NK-92 cells in renal cell carcinoma. *J Immunol Res* (2017) 2017:6915912. doi: 10.1155/2017/6915912

144. Zhang Q, Xu J, Ding J, Liu H, Li H, Li H, et al. Bortezomib improves adoptive carbonic anhydrase IX–specific chimeric antigen receptor–modified NK92 cell therapy in mouse models of human renal cell carcinoma. *Oncol Rep* (2018) 40(6):3714–24. doi: 10.3892/or.2018.6731

145. Lu C, Guo C, Chen H, Zhang H, Zhi L, Lv T, et al. A novel chimeric PD1-NKG2D-41BB receptor enhances antitumor activity of NK92 cells against human lung

cancer H1299 cells by triggering pyroptosis. *Mol Immunol* (2020) 122:200–6. doi: 10.1016/j.molimm.2020.04.016

146. Liu E, Tong Y, Dotti G, Shaim H, Savoldo B, Mukherjee M, et al. Cord blood NK cells engineered to express IL-15 and a CD19-targeted CAR show long-term persistence and potent antitumor activity. *Leukemia* (2018) 32(2):520–31. doi: 10.1038/leu.2017.226

147. Skrombolas D, Frelinger JG. Challenges and developing solutions for increasing the benefits of IL-2 treatment in tumor therapy. *Expert Rev Clin Immunol* (2014) 10(2):207–17. doi: 10.1586/1744666X.2014.875856

148. Chavez AR, de V, Buchser W, Basse PH, Liang X, Appleman LJ, Maranchie JK, et al. Pharmacologic administration of interleukin-2: inducing a systemic autophagic syndrome? *Ann New York Acad Sci* (2009) 1182(1):14–27. doi: 10.1111/j.1749-6632.2009.05160.x

149. Jiang T, Zhou C, Ren S. Role of IL-2 in cancer immunotherapy. *Oncoimmunology* (2016) 5(6):e1163462. doi: 10.1080/2162402X.2016.1163462

150. Conlon KC, Lugli E, Welles HC, Rosenberg SA, Fojo AT, Morris JC, et al. Redistribution, hyperproliferation, activation of natural killer cells and CD8 T cells, and cytokine production during first-in-human clinical trial of recombinant human interleukin-15 in patients with cancer. *J Clin Oncol* (2015) 33(1):74. doi: 10.1200/JCO.2014.57.3329

151. Berger C, Berger M, Hackman RC, Gough M, Elliott C, Jensen MC, et al. Safety and immunologic effects of IL-15 administration in nonhuman primates. *Blood J Am Soc Hematol* (2009) 114(12):2417–26. doi: 10.1182/blood-2008-12-189266

152. Yang Y, Lundqvist A. Immunomodulatory effects of IL-2 and IL-15; implications for cancer immunotherapy. *Cancers* (2020) 12(12):3586. doi: 10.3390/cancers12123586

153. Christodoulou I, Ho WJ, Marple A, Ravich JW, Tam A, Rahnama R, et al. Engineering CAR-NK cells to secrete IL-15 sustains their anti-AML functionality but is associated with systemic toxicities. *J immunotherapy Cancer* (2021) 9(12):e003894. doi: 10.1136/jitc-2021-003894

154. Zhang Q, Hresko ME, Picton LK, Su L, Hollander MJ, Nunez-Cruz S, et al. A human orthogonal IL-2 and IL-2Rβ system enhances CAR T cell expansion and antitumor activity in a murine model of leukemia. *Sci Trans Med* (2021) 13(625):eabg6986. doi: 10.1126/scitranslmed.abg6986

155. Aspuria P-J, Vivona S, Bauer M, Semana M, Ratti N, McCauley S, et al. An orthogonal IL-2 and IL-2Rβ system drives persistence and activation of CAR T cells and clearance of bulky lymphoma. *Sci Trans Med* (2021) 13(625):eabg7565. doi: 10.1126/scitranslmed.abg7565

156. Chanswangphuwana C, Allan DSJ, Chakraborty M, Reger RN, Childs RW. Augmentation of NK cell proliferation and anti-tumor immunity by transgenic expression of receptors for EPO or TPO. *Mol therapy: J Am Soc Gene Ther* (2021) 29(1):47–59. doi: 10.1016/j.ymthe.2020.09.023

157. Gong Y, Klein Wolterink RGJ, Wang J, Bos GMJ, Germeraad WTV. Chimeric antigen receptor natural killer (CAR-NK) cell design and engineering for cancer therapy. *J Hematol Oncol* (2021) 14(1):1–35. doi: 10.1186/s13045-021-01083-5

158. Sayitoglu EC, Georgoudaki A-M, Chrobok M, Ozkazanc D, Josey BJ, Arif M, et al. Boosting natural killer cell-mediated targeting of sarcoma through DNAM-1 and NKG2D. *Front Immunol* (2020) 11:40. doi: 10.3389/fimmu.2020.00040

159. Huang Z, Qi G, Miller JS, Zheng SG. CD226: an emerging role in immunologic diseases. *Front Cell Dev Biol* (2020) 8:564. doi: 10.3389/fcell.2020.00564

160. Shibuya A, Shibuya K. DNAM-1 versus TIGIT: competitive roles in tumor immunity and inflammatory responses. *Int Immunol* (2021) 33(12):687–92. doi: 10.1093/intimm/dxab085

161. Wu M-R, Zhang T, Alcon A, Sentman CL. DNAM-1-based chimeric antigen receptors enhance T cell effector function and exhibit *in vivo* efficacy against melanoma. *Cancer Immunology Immunotherapy* (2015) 64(4):409–18. doi: 10.1007/s00262-014-1648-2

162. Huang Y, Zeng J, Liu T, Xu Q, Song X, Zeng J. DNAM1 and 2B4 costimulatory domains enhance the cytotoxicity of anti-GPC3 chimeric antigen receptor-modified natural killer cells against hepatocellular cancer cells *in vitro*. *Cancer Manage Res* (2020) 12:3247. doi: 10.2147/CMAR.S253565

163. Lazarova M, Wels WS, Steinle A. Arming cytotoxic lymphocytes for cancer immunotherapy by means of the NKG2D/NKG2D-ligand system. *Expert Opin Biol Ther* (2020) 20(12):1491–501. doi: 10.1080/14712598.2020.1803273

164. Siemaszko J, Marzec-Przyszlak A, Bogunia-Kubik K. NKG2D natural killer cell receptor-a short description and potential clinical applications. *Cells* (2021) 10(6):1420. doi: 10.3390/cells10061420

165. Guo C, Wang X, Zhang H, Zhi L, Lv T, Li M, et al. Structure-based rational design of a novel chimeric PD1-NKG2D receptor for natural killer cells. *Mol Immunol* (2019) 114:108–13. doi: 10.1016/j.molimm.2019.07.009

166. Garrity D, Call ME, Feng J, Wucherpfennig KW. The activating NKG2D receptor assembles in the membrane with two signaling dimers into a hexameric structure. *Proc Natl Acad Sci* (2005) 102(21):7641–6. doi: 10.1073/pnas.0502439102

167. Molfetta R, Quatrini L, Santoni A, Paolini R. Regulation of NKG2D-dependent NK cell functions: the yin and the yang of receptor endocytosis. *Int J Mol Sci* (2017) 18(8):1677. doi: 10.3390/ijms18081677

168. Xu Y, Liu Q, Zhong M, Wang Z, Chen Z, Zhang Y, et al. 2B4 costimulatory domain enhancing cytotoxic ability of anti-CD5 chimeric antigen receptor engineered natural killer cells against T cell malignancies. *J Hematol Oncol* (2019) 12(1):1–13. doi: 10.1186/s13045-019-0732-7

169. Mehta RS, Rezvani K. Chimeric antigen receptor expressing natural killer cells for the immunotherapy of cancer. *Front Immunol* (2018) 9:283. doi: 10.3389/fimmu.2018.00283

170. Derynck R, Turley SJ, Akhurst RJ. TGFβ biology in cancer progression and immunotherapy. *Nat Rev Clin Oncol* (2021) 18(1):9–34. doi: 10.1038/s41571-020-0403-1

frontiers | Frontiers in Oncology

TYPE Review
PUBLISHED 12 July 2023
DOI 10.3389/fonc.2023.1183059

OPEN ACCESS

EDITED BY
Theophilos Tzaridis,
Sanford Burnham Prebys Medical Discovery Institute, United States

REVIEWED BY
Mohsin Wahid,
Dow University of Health Sciences, Pakistan
Christine Mehner,
Mayo Clinic Florida, United States

*CORRESPONDENCE
Hongcai Wang
Roger0412@126.com
Jingyun Ma
majingyun198401@126.com

RECEIVED 09 March 2023
ACCEPTED 16 May 2023
PUBLISHED 12 July 2023

CITATION
Xie Z, Chen M, Lian J, Wang H and Ma J (2023) Glioblastoma-on-a-chip construction and therapeutic applications. *Front. Oncol.* 13:1183059. doi: 10.3389/fonc.2023.1183059

Glioblastoma-on-a-chip construction and therapeutic applications

Zuorun Xie, Maosong Chen, Jiangfang Lian, Hongcai Wang* and Jingyun Ma*

The Affiliated Lihuili Hospital of Ningbo University, Ningbo, Zhejiang, China

Glioblastoma (GBM) is the most malignant type of primary intracranial tumor with a median overall survival of only 14 months, a very poor prognosis and a recurrence rate of 90%. It is difficult to reflect the complex structure and function of the GBM microenvironment *in vivo* using traditional *in vitro* models. GBM-on-a-chip platforms can integrate biological or chemical functional units of a tumor into a chip, mimicking *in vivo* functions of GBM cells. This technology has shown great potential for applications in personalized precision medicine and GBM immunotherapy. In recent years, there have been efforts to construct GBM-on-a-chip models based on microfluidics and bioprinting. A number of research teams have begun to use GBM-on-a-chip models for the investigation of GBM progression mechanisms, drug candidates, and therapeutic approaches. This review first briefly discusses the use of microfluidics and bioprinting technologies for GBM-on-a-chip construction. Second, we classify non-surgical treatments for GBM in pre-clinical research into three categories (chemotherapy, immunotherapy and other therapies) and focus on the use of GBM-on-a-chip in research for each category. Last, we demonstrate that organ-on-a-chip technology in therapeutic field is still in its initial stage and provide future perspectives for research directions in the field.

KEYWORDS

glioblastoma, organ-on-a-chip, microfluidics, bioprinting, chemotherapy, immunotherapy

1 Introduction

Glioblastoma (GBM) is the most common primary malignancy of the brain, accounting for approximately 57% of all gliomas and 48% of all primary malignancies of the brain (1). It is the most aggressive glial tumor type with characteristics including a proclivity for necrosis, uncontrolled cellular proliferation, diffuse infiltration, increased angiogenesis, and widespread genomic heterogeneity (2). Despite recent advances in comprehensive treatment for GBM, including surgery, radiotherapy, and systemic therapies such as chemotherapy and targeted therapy, as well as supportive care, the overall prognosis and long-term survival rates of GBM patients remain poor (3). The most commonly used post-operative treatment regimen for GBM internationally is the 'Stupp'

regimen, in which temozolomide (TMZ) treatment concurrent with radiotherapy is followed by TMZ adjuvant chemotherapy. A progression-free survival of 6.9 months and median overall survival of 14.6 months have been reported in newly diagnosed GBM patients treated with the Stupp regimen (4).However, there is an urgent need for more patient-specific precision therapeutic approaches for GBM to improve overall survival and quality of life of GBM patients.

Numerous studies have shown that inter-tumor and intra-tumor heterogeneity in GBM are the main reasons for unsatisfactory clinical and pre-clinical trial results (5–8). Successful targeting of GBM heterogeneity requires insight into the factors that drive sub-clonal variation, such as vascularity, hypoxia and inflammation (9). This can be achieved by advanced *in vitro* GBM models includingboth GBM tumor and normal brain tissues. However, traditional Petri-dish-based assays do not fully represent the complexity of tumors, limiting their potential use to determine predictive functional biomarkers. Organ-on-a-chip (OoC) is a revolutionary novel technology that has been developed rapidly in the past decade. Using OoC technology, human functional units constituting tissues and organs can be simulated ex vivo on microscopic cell and tissue culture vehicles, including the basic components and elements necessary for functional units, such as multicellular components, extracellular matrix (ECM) and physicochemical microenvironmental factors (10–13). OoC can compensate for the disadvantages of previous cell culture methods owing to various advantages unmatched by those of traditional methods, including three-dimensional (3D) dynamic culture, controlled physicochemical stimulation, low cost, high throughput and high reliability (14). Moreover, OoC can be used to monitor cell biology changes in real time when combined with imaging instruments, helping to better record cell behavior changes during disease states and the full range of responses to drugs. As a versatile platform, OoC can cope with challenges regarding tumor sample collection and analysis and has made considerable contributions to multiple research fields, including oncogenesis, tumor metastasis, treatment verification, drug resistance and screening, with a particularly significant role in precision oncology (15).

In recent years, OoC with microfluidics and 3D bioprinting has been used to model the GBM tumor microenvironment (TME); this technology is termed 'GBM-on-a-chip' (16, 17). GBM-on-a-chip can mimic the functional units of GBM tumors *in vitro*, replicating the cellular composition and anatomical structure of both the target tumor and normal brain tissues, effectively simulating *in vivo* biochemical stimuli and biophysical factors to achieve precise regulation of complex factors in the GBM TME in a spatio-temporal controllable manner (18). GBM-on-a-chip can provide bionic support at the cellular and tissue levels and has been widely used to investigate biological mechanisms and therapeutics in GBM with great potential for applications in personalized precision medicine and immunotherapy (19).

In this review, we present the microfluidics and bioprinting technologies that are currently used to construct GBM-on-a-chip models. We also review recent studies of the use of GBM-on-a-chip in a variety of treatments including chemotherapy, immunotherapy and other therapies (phototherapy, magnetic hyperthermia therapy, and focused ultrasound therapy). By describing the applications of these GBM-on-a-chip models in GBM investigation, we provide a broad perspective on the progress and future of the technology.

2 The GBM microenvironment and construction technologies for *in vitro* GBM-on-a-chip models

2.1 The GBM microenvironment

The TME is closely related to tumorigenesis, tumor development, and metastasis (20). In recent years, the TME has emerged as a significant participating factor and therapeutic target in GBM. The GBM TME, which refers to the sum of the internal and external environments in which GBM occurs and develops, is a complex and variable system that differs from the microenvironment in which normal brain cells and tissues are located (21). The GBM TME includes numerous cellular systems mainly represented by immune cells (tumor-associated macrophages, monocytes, and microglia (TAMs), neutrophils, regulatory T cells and bone marrow myeloid-derived suppressor cells), GBM cells, glioma stem cells, astrocytes and endothelial cells, as well as brain blood vessels, the lymphatic system, neurons, and the ECM which is essential for the microenvironment stability (22, 23) (Figure 1). As well as, hypoxia in the central tumor tissues, a high degree of epithelial–mesenchymal transition, high cell motility and invasive ability, disruption of the function of the blood-brain barrier (BBB), increased molecular permeability, and susceptibility to brain edema are all significant biological features of the GBM TME (24).

Overall, GBM is closely linked to the GBM TME. GBM can release cell signaling molecules to influence the TME by promoting tumor angiogenesis and inducing immune tolerance, while immune cells within the TME influence GBM cell growth and development (25). Furthermore, the non-tumor elements of the TME have a clear role in promoting GBM cell proliferation and invasion (26). The presence of the GBM TME enhances the capacity for GBM cell proliferation, migration and immune escape, thereby promoting the development of GBM. There is a relationship between the genetics of tumors and the complexity of their surrounding microenvironment. In view of the unsatisfactory results of current treatments for GBM, extensive and in-depth investigation into mechanisms of GBM development in the TME especially the relationship between the complexity of the surrounding TME and tumor genetics, is probably needed to provide new targets and new therapeutic regimens for GBM treatments (27).

2.2 GBM-on-a-chip models based on microfluidics

Most organ- or tumor-on-a-chip systems, such as GBM-on-a-chip models, are constructed using microfluidics technology, and the majority of microfluidic devices have been fabricated through

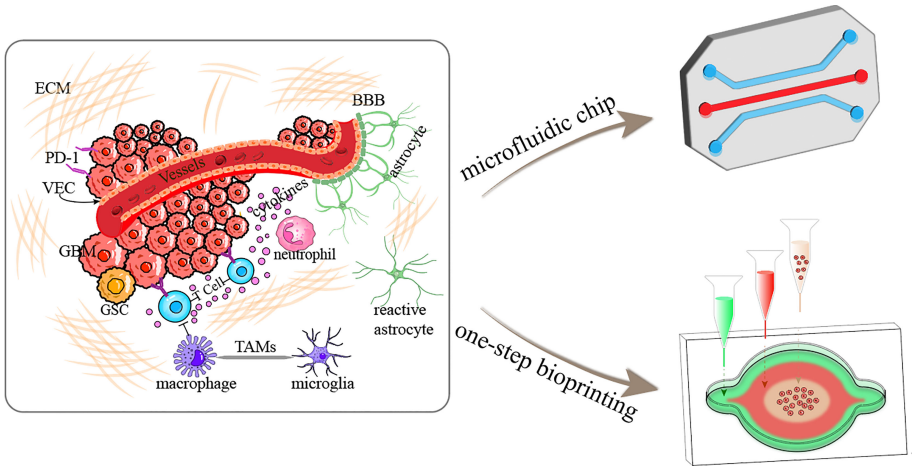

FIGURE 1
Schematic diagram illustrating the GBM tumor microenvironment and construction of GBM-on-a-chip based on microfluidics and one-step bioprinting. ECM, extracellular matrix; BBB, blood-brain barrier; PD-1, programmed cell death protein 1; VEC, vascular endothelial cell; GSC, glioma stem cell; TAMs, tumor-associated microglia and macrophages.

photolithography and soft lithography (28, 29). The main polymeric material used to manufacture microfluidic chips is polydimethylsiloxane (PDMS), which offers advantages in terms of transparency, biocompatibility, flexibility, gas permeability, and resolution, giving it a dominant position in the field (30).

Olubajo et al. used standard photolithography and wet etching techniques to fabricate a microfluidic chip featuring inlet and outlet channels (Figure 2A) (31). This chip was designed to cultivate 128 GBM tumor samples from 33 distinct patients in an *in vitro* fluid flow environment. The system was equipped with continuous nutrient circulation and waste removal, allowing for an average cultivation period of 72 h. The tissue viability as analyzed by flow cytometry was 61.1% in tissue maintained on the microfluidic platform after 72 h, compared with 68.9% for fresh tissue, demonstrating that patient-derived GBM tissue could be successfully maintained within the microfluidic chip to model biological processes and tissue structures of tumors for the mechanistic and therapeutic investigation in GBM. In another study, Dou et al. used soft lithography to create a polyacrylamide hydrogel-based GBM model that could precisely generate orthogonal chemical stimulation and controllable stiffness gradients to investigate the biological behaviors of GBM cells (Figure 2B) (32). They reported that the morphology, migration, and reactive oxygen species level of GBM cells could be regulated by increasing hydrogel stiffness, whereas the epidermal growth factor gradient could accelerate cell migration. Liu et al. developed a microfluidic device by photolithography to co-culture U87-MG cells and human umbilical vein endothelial cells (HUVECs) within a macroporous gelatin transglutaminase hydrogel to mimic a tumor-microvascular environment according to physiological conditions for studying antioxidants effects of GBM cells *in vitro* (33). Antioxidant diffusion from the HUVEC formed vessel lumen to U87-MG cells reflected the drug transportation and permeation functions of the tumor vessel.

In conclusion, microfluidics enable reproduction of the GBM TME with a reduced size chip, in particular, combination of the BBB with the tumor tissue. However, such chips usually need to be integrated with other devices as they do not have the capacity for entire laboratory operations. Moreover, the low manufacturing efficiency of PDMS-based microfluidic devices makes them unsuitable for mass production, limiting the commercialization of microfluidic systems.

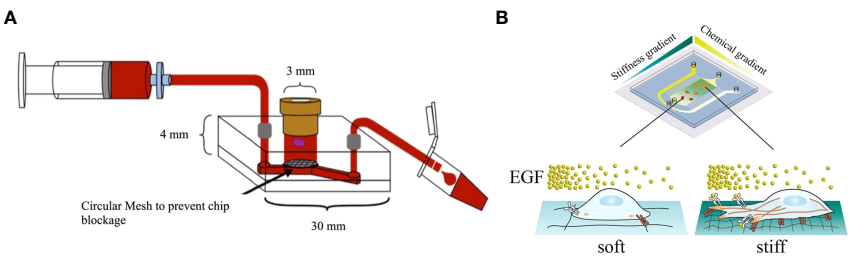

FIGURE 2
GBM-on-a-chip models constructed by microfluidic technology. **(A)** Schematic diagram of a microfluidic culture device setup (31). **(B)** Image of a microfluidic system allowing stiffness and chemical gradients simultaneously (32). Reproduced with permission from (31, 32).

2.3 GBM-on-a-chip models based on 3D bioprinting

As well as microfluidics, bioprinting can be used to develop refined GBM-on-a-chip models, allowing simultaneous 3D printing of specific elements such as various types of cells and ECM mimetic materials directly onto a cell-compatible substrate that can be used to form vascular networks and reproduce the heterogeneous TME (34). Furthermore, researchers can collect cells from GBM patients and construct *in vitro* tumor-on-a-chip models with biochemical and biophysical properties of GBM, which can replicate the structure of their counterparts *in vivo* and the corresponding genetics of GBM patients.

In recent years, GBM models bioprinted with a unique combination of cells and bioinks have been increasingly used for further research into biological mechanisms of GBM and pre-clinical studies of GBM therapies. As an example, a GBM tumor was printed within a hydrogel system containing macrophages by extrusion-based bioprinting to build a bionic GBM TME for the investigation of the effects of infiltrating immune cells on GBM cell behavior and drug responses (35). In addition, 3D bioprinting was used to develop a novel vascularized GBM-on-a-chip model to mimic the pathophysiological conditions of GBM tumors and the surrounding vascular microenvironment, showing that gravitational force has a significant role in GBM mechanical regulation (36). Heinrich et al. constructed a 3D bioprinted GBM model to investigate the interactions between macrophages and GBM cells and for testing of drugs targeting this interaction (Figure 3A) (37). This GBM model was bioprinted using a bioink encapsulating RAW264.7 (a mouse macrophages cell line), and GL261 (mouse GBM cells) implanted with bioink used to fill the cavity, where the construct was subsequently photo-crosslinked.

Such 3D bioprinting can also be used to construct a patient-specific GBM-on-a-chip with patient derived GBM cells and viable bioinks to better mimic the GBM TME. For example, Yi et al. constructed a GBM-on-a-chip model based on extrusion-based bioprinting for the testing of tumor-killing drug candidates and screening of effective treatments for GBM patients resistant to standard drug therapy (Figure 3B) (16). In this work, patient-derived GBM cells, HUVECs, and brain-derived ECM were printed into a separated concentric ring structure of cancer stroma that could mimic the structural, biochemical, and biophysical features of the GBM tumor while maintaining a radial oxygen gradient, representing the heterogeneous ecology of GBM. In another study, Neufeld et al. used 3D bioprinting to develop a perfusable GBM model that could reproduce various *in vivo* features of GBM including growth kinetics, invasiveness, and genetic characteristics, and was used to test drug response (Figure 3C) (38). The heterogenic TME was reproduced using a fibrin-based GBM bioink containing patient-derived GBM cells, astrocytes and microglia, and perfusable blood vessels were simulated using a sacrificial bioink coated with brain pericytes and HUVECs. These 3D bioprinted models demonstrate the promising potential of advanced bio-manufacturing techniques in the investigation of GBM.

Compared with GBM cell lines such as U87 that have been criticized for not accurately representing the genetic and molecular characteristics of GBM in patients, GBM models bioprinted using patient-derived cells are more credible and personalized. Although they are limited by the development of applicable bioinks that satisfactorily mimic the GBM TME, these advanced biomanufacturing techniques show promise in for applications in the study of GBM. Further work is required to develop novel bioink materials and formulations for the construction of more

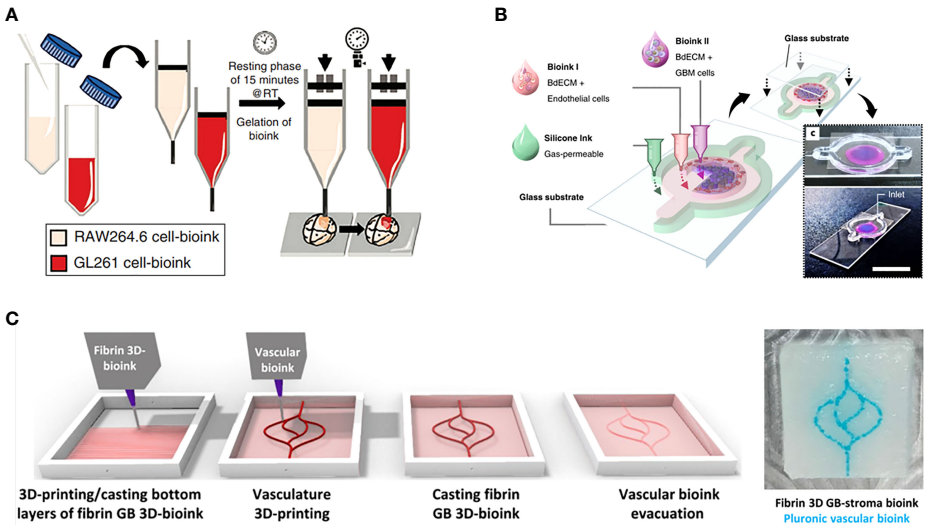

FIGURE 3
GBM-on-a-chip models constructed by one-step 3D bioprinting. **(A)** Schematic images of 3D-bioprinted mini-brain with two GelMA-gelatin bioinks containing macrophages and GBM cells (37). **(B)** 3D bioprinted GBM-on-a-chip with construction of a concentric ring structure by using various bioinks and other materials (16). **(C)** The process for 3D-bioprinting the vascularized GBM model with 3D-bioprinted vascular bioink containing GBM tumor cells and stromal cells (38). Reproduced with permission from (16, 37, 38).

representative GBM models based on bioprinting rather than small animal models.

3 GBM-on-a-chip for therapeutic applications

3.1 GBM-on-a-chip for the study of chemotherapy drugs

Chemotherapy, a treatment that kills tumor cells through the use of chemicals, can prolong progression-free survival and overall survival in GBM patients. GBM tumors grow rapidly and easily recur; thus aggressive and effective individualized chemotherapy would be valuable. *In vitro* GBM-on-a-chip models can assist in identifying the sensitivity of patients to specific drugs, screening different drug combinations and guiding treatment decisions.

3.1.1 GBM-on-a-chip for the study of single-agent TMZ

TMZ, an alkylating agent with antitumor activity, methylates the O6 or N7 positions of guanine residues on DNA molecules and exerts cytotoxic effects through mismatch repair of methylated adducts (39, 40). It is the first-line chemotherapy drug for GBM.

To investigate the capacity of TMZ to inhibit invasion and induce programmed cell death, Samiei et al. created a multi-compartment microfluidic device in which U87 and U251-MG cells were cultured, including side channels for nutrients and drugs to be delivered to the cells and stroma compartments for culture of GBM cells (Figure 4Ai) (41). U87 and U251 GBM cells cultured in the 3D environment were significantly less sensitive to the drugs compared with those cultured in monolayer systems, and TMZ-induced autophagy and TMZ -induced apoptosis were observed. As shown in Figure 4Aii, there was a decrease in the invasiveness of U87 and U251 GBM cells after treatment with TMZ, and the number of invasive cells decreased with increasing TMZ dose. Ozturk et al. used extrusion-based bioprinting to construct a microfluidic platform allowing long-term culture and drug delivery with two perfused vascular channels between which a patient-derived GBM tumor spheroid was placed for monitoring and assessment of GBM cell responses to TMZ treatment (Figure 4B) (42). As shown in Figure 4Bi, a plexiglass perfusion chamber contained the 3D tissue composed of vascular channels, and a GBM spheroid was bioprinted and cultured under medium perfusion. The inner channel surface of the vascular channels was replicated by injecting HUVECs in suspension into the channels. Overgrowth of GBM cells was found to hinder the efficacy of long-term TMZ treatment, and cell metabolic activity in the GBM spheroid decreased over time with increasing TMZ dose, demonstrating that some GBM cells remain invasive after long-term TMZ treatment. As shown in Figure 4Bii, after treatment with TMZ for 14 days, the GBM cells had regressed and the tumor core had shrunk, however, after 31 days of TMZ treatment, the restoration of invasiveness in some GBM cells that survived the treatment strongly promoted cell drug resistance even with continuing TMZ treatment. The main focus of conventional evaluation methods is the effect of drugs on cell viability or metabolism. By contrast, Zhang et al. used the microfluidic trypsin treatment method to analyze the effect of TMZ on single-cell adhesion of U87 GBM cells, proposing that the ability to regulate cell adhesion was also a significant aspect in drug evaluation (43). According to the results, the inhibitory effect of TMZ on U87 GBM cell adhesion strength after 6 h adhesion became stronger over time, suggesting that the efficacy of TMZ is time dependent. Lactic acid was added to the culture medium to mimic the acidic TME, which was demonstrated to effectively inhibit the effects of TMZ and promote TMZ resistance of U87 GBM cells.

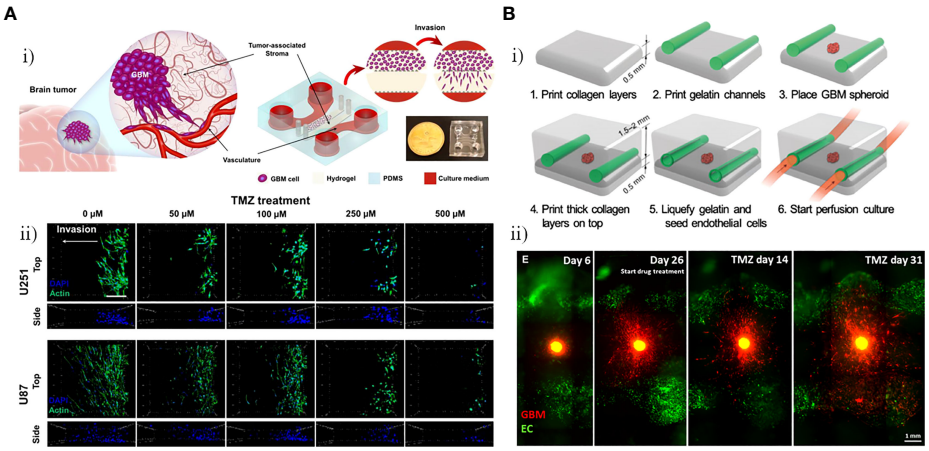

FIGURE 4
GBM-on-chips for the study of single-agent TMZ. **(A)** Investigation of the capacity of TMZ to inhibit invasion and induce programmed cell death in the GBM-on-a-chip model (41). **(i)** GBM-on-a-chip including side channels for nutrients and drugs to be delivered to cells and stroma compartments for culture of GBM cells. **(ii)** Evaluation of effects of different concentrations of TMZ on cytoskeleton of the U251 and U87 cells in the GBM-on-a-chip model. **(B)** Analysis of *in vitro* 3D-bioprinted GBM-on-a-chip model under long-term TMZ treatment (42). Schematic images of 3D-bioprinted GBM model and experimental results. **(i)** Process for 3D-bioprinting GBM model containing a GBM spheroid and vascular channels. **(ii)** Invasive behavior of patient-derived GBM cells at different stages (before TMZ treatment, day 26 when TMZ treatment was started, and 14 days and 31 days after TMZ treatment). Reproduced with permission from (41, 42).

3.1.2 GBM-on-a-chip for the study of TMZ-based combination chemotherapy

Akay et al. constructed a GBM-on-a-chip platform with the aim of assessing the drug response of GBM cells to varying concentrations of two types of clinical anti-tumor agents, TMZ and bevacizumab (BEV) (Figure 5A) (44). The chip included two inlets and one outlet by which seven microfluidic channels were connected (Figure 5Ai). Small hydrogel-based gaps between each channel prevented the diffusion of any small drug molecules through the channel. After 7 days culture of primary human derived GBM cells from three different patients as 3D GBM spheroids, 7.5 μM BEV solution and 600μM TMZ solution were respectively applied into the GBM spheroids through the left and right channels. Single-agent TMZ was more effective than single-agent BEV as a the human GBM cell treatment, whereas TMZ in combination with BEV worked more effectively compared with mono-TMZ (Figure 5Aii). Ma et al. developed a detachable and assembled microfluidic device consisting of a glass cover plate coated with PDMS and a microfluidic chip constructed form PDMS, into which a multicellular spherical matrix system was integrated to mimic *in vivo* conditions. The aim was to investigate the invasive behavior of GBM cells and the anti-invasion effects of resveratrol (Res, a traditional Chinese medicine), TMZ, and the Res + TMZ combination on GBM (46). Compared with single-agent TMZ, Res in combination with TMZ treatment at the same concentration promoted the efficacy of TMZ against GBM cells, and single-agent Res also exhibited significant anti-cancer effects. These results confirmed the previous theory proposing that Res has anti-invasive and anti-proliferative effects on GBM, as well as amplifying the anti-cancer effect of TMZ against GBM (47, 48). Jie et al. developed a bionic intestine-liver-GBM system for evaluation of combination drug treatments in GBM (Figure 5B) (45). As effective drugs for GBM chemotherapy require the ability to penetrate the BBB and maintain pharmacological activity after metabolism in the liver, these factors have a significant role in determining the pharmacological activity of many drugs for GBM. In the microfluidic chip, Caco-2 cells were cultured in the upper layer, into which a hollow fiber was embedded to replicate an artificial intestine to deliver drugs. HepG2 cells and U251 cells were respectively cultured within two horizontally aligned olivary chambers of the bottom chamber to mimic liver metabolism and the GBM tissue (Figure 5Bi). After intestinal absorption and liver metabolism simulated by the intestine-liver metabolic model, Irinotecan (CPT-11), TMZ, and cyclophosphamide (CP) were applied as single- and double-drug combination therapies for GBM cells. Compared with single-drug treatments, the CPT-11 and TMZ combination showed a marked improvement in efficacy (Figures 5Bii, iii). When used to treat U251 cells, this combination was more effective than the CPT-11 and CP combination as well as the TMZ and CP combination.

3.1.3 GBM-on-a-chip for the study of non-TMZ chemotherapy

Fan et al. developed a 3D microfluidic chip for culture of U87 GBM cells, constructed using a photopolymerizable polyethylene glycol diacrylate (PEGDA) hydrogel, to test a combination drug

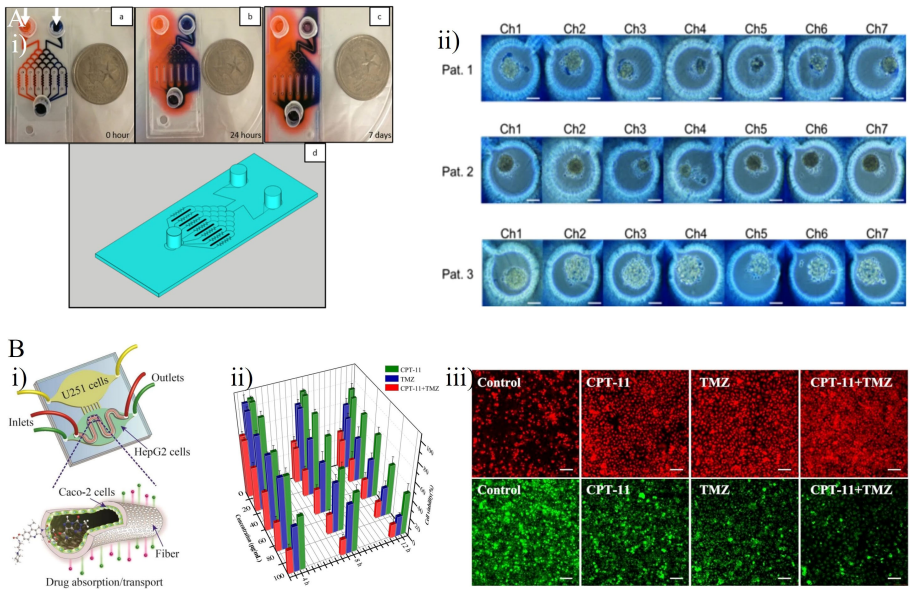

FIGURE 5
GBM-on-chips for drug studies of TMZ-based combination chemotherapy. **(A)** Patient- specific GBM-on-a-chip for testing of drug candidates (including TMZ and BEV) (44). **(i)** Two dyes were loaded into two inlets of this chip to characterize the gradients of two solutions generated in seven microfluidic channels. **(ii)** Cells loaded with 0.4% trypan blue for semi-quantitative cell viability after 7 days of drug administration. **(B)** An intestine-liver-GBM biomimetic microfluidic system for evaluating drug combination (including CPT-11, TMZ, and CP) in GBM (45). **(i)** The hollow fiber integrated microfluidic chip co-cultured Caco-2 cells, HepG2 cells, and U251 cells to simulate *in vivo* pharmacokinetic processes. **(ii)** Inhibitory effects of single- and double-drug combinations (CPT-11 and TMZ) on U251 cells after 4 h, 8 h, and 12 h treatment. **(iii)** Effects of single- and double-drug combinations on apoptosis of U251 cells. Intracellular reactive oxygen species generation (red) and glutathione reduction (green). Reproduced with permission from (44, 45).

therapy consisting of Pitavastatin and Irinotecan (Figure 6A) (49). This platform with three inlets and one outlet that included a top glass cover plate, a bottom glass cover plate, and a middle layer composed of PEGDA hydrogel, could drive diffusion *via* a concentration gradient to regulate the release of chemicals. It also provided a large number of miniature culture chambers in which high-throughput GBM spheroids could be formed (Figure 6Ai). This enabled massive parallel testing of responses to multiple drugs with simultaneous administration in a 3D biologically compatible microenvironment. The results indicated that the Pitavastatin and Irinotecan combination worked more effectively compared with individual agent treatments, with drug efficacy measured based on the cell viability of GBM spheroids (Figure 6Aii). In another study, Liu et al. constructed a microfluidic device in which U251 GBM cells were cultured under various conditions to evaluate the efficacy of vincristine (VCR) and bleomycin (BLM) against GBM cells at six different concentrations (Figure 6B) (50). After 4 days high concentration (100 μg/mL) treatment, decreases in the tumor size and number of tumor cells were observed in both the VCR and the BLM group. Compared with BLM, VCR worked more effectively, killing more than 80% of U251 cells and reducing tumor size by 49%, whereas BLM killed about 66% of U251 cells and reduced tumor size by 30% (Figure 6Bii). Recently, Rahimifard et al. created a microfluidic platform to evaluate the effects of pyrazino[1,2-a] benzimidazole derivatives on patient-derived GBM cells (51). New pyrazino[1,2-a] benzimidazole derivatives were found to have obvious anti-cancer properties and COX-II inhibitory effects (52). GBM cells were exposed to subtoxic concentrations of 2,6-dimethyl pyrazino[1,2-a] benzimidazole (L1 6.5μM) and 3,4,5-trimethoxy pyrazino[1,2-a] benzimidazole (L2 42.5μM). Both L1 and L2 exhibited anti-proliferative and anti-migration properties against GBM cells, and both retarded the formation of 3D GBM spheroids.

As GBM tumors inevitably recur after surgery and radiation treatment, chemotherapy plays an important part in killing the remaining GBM cells. However, the BBB prevents the entry of adequate chemotherapeutic drugs into the cerebral circulation brain, limiting the effects of systemic chemotherapy against GBM. To overcome this limitation, there is a need for a patient-specific *in vitro* model using OoC technology that accurately represents the GBM TME, especially the BBB. Such patient-specific models could be used to screen the most appropriate drug combinations for individuals. However, owing to its lack of capacity to reflect neurotoxicity and other adverse effects on patients, the model would need to be integrated with multiple biological systems that can recapitulate the complex functionalities of different human tissues or organs so as to simulate the physiology of the patient with a high degree of fidelity. Thus, researchers could search for better chemotherapeutics to target GBM while reducing drug-induced injury.

3.2 GBM-on-a-chip for immunotherapeutic investigation

GBM is highly heterogeneous, and extrinsic components of tumor cells that are inherent to the brain, as well as intrinsic mechanisms of tumor cells that assist immune evasion make the GBM TME extremely challenging to cope with (53). Reducing the barrier to immunosuppression by targeting the tumor stroma may provide an opportunity to treat GBM. The immunotherapies for GBM currently be investigated using GBM-on-a-chip models can be broadly classified into immunotherapies targeting TAMs, immune checkpoint blockade (ICB) therapy, and chimeric antigen receptor T cells (CAR-T) therapy.

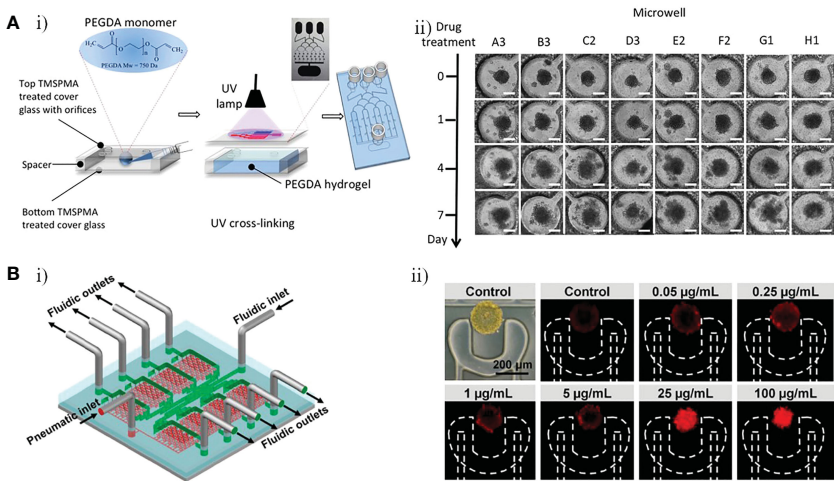

FIGURE 6
GBM-on-a-chip for drug studies of non-TMZ chemotherapy. **(A)** PEGDA hydrogel-based GBM-on-a-chip for evaluation of anti-cancer drugs (Pitavastatin and Irinotecan) (49). **(i)** Illustration of the construction of final hydrogel-based microfluidic device with microchannels and microwells. **(ii)** Images of GBM tumor spheroids in the microwells before (day 0) and after (days 1, 4, and 7) combinatorial drug treatment. **(B)** Microfluidic platform for monitoring tumor response to vincristine and bleomycin (50). **(i)** Representative schematic of a recyclable microfluidic platform. **(ii)** Effects of different concentrations of vincristine on tumor cell death after 4 days of treatment. Reproduced with permission from (49, 50).

3.2.1 Immunotherapy targeting TAMs

TAMs can secrete a variety of enzymes, reactive oxygen species, growth factors, and cytokines that contribute directly and/or indirectly to tumor proliferation, invasion and angiogenesis in GBM (54). Thus, they have an essential role in the formation of the immunosuppressive GBM TME (55, 56). Although a large number of studies have demonstrated that TAMs can promote the invasion and proliferation of GBM (57–60), the specific mechanisms by which TAMs interact with GBM cells are not known and whether they are involved in GBM recurrence and the nature of their interactions with tumor stem cells are still unclear. Therefore, in-depth study of the relationship between TAMs and GBM cells may provide the basis for immunotherapy targeting TAMs.

Gu et al. established three microfluidic assays, which they refer to as co-migration assays, based on a microfluidic device that can be used for the investigation of the bi-directional relationship between GBM cells and microglia (61). Microglia exhibited both anti-tumor and pro-tumor activities, suppressing early tumor growth by their phagocytosis and killing ability, then participating in tumor invasion and proliferation in the malignant stage to promote the tumor progression of GBM. Hong et al. developed a 3D microfluidic co-culture device to investigate the effects of microRNA (miR)-124-loaded extracellular vesicles (EVs) by recreating the interaction between microglia and GBM cells (Figure 7A) (62). U373-MG cells and microglia were co-cultured with miR-124 EVs for 4 days (Figure 7Ai). The miR-124 EVs exhibited inhibitory effects on the proliferation and metastasis of GBM and suppressed microglial M2 polarization *via* STAT3 regulation, providing initial evidence for the use of miR-124 EVs to develop a novel therapeutic strategy. The miR-124 EV treatment also suppressed tumor progression and anti-tumor immune responses, leading to enhanced intratumoral infiltration of natural killer (NK) cells (Figure 7Aii). Similarly, Cui et al. created a biomimetic and microfluidic-based model to mimic macrophage-associated immunosuppression and tumor angiogenesis in GBM and to investigate the antitumor function of macrophages (65). The results indicated that the regulation of tumor angiogenesis in GBM may involve TGF-β1 (soluble immunosuppressive cytokine) and surface endothelial-macrophage interactions, whereas perivascular macrophage-endothelial interactions are involved in regulating pro-angiogenic activity *via* the integrin (αvβ3). Using this GBM-on-a-chip model, a novel dual αvβ3 and TGF-β1 blockade was found to suppress tumor neovascularization of GBM by simultaneously targeting endothelial-macrophage interactions and macrophage-associated immunosuppression.

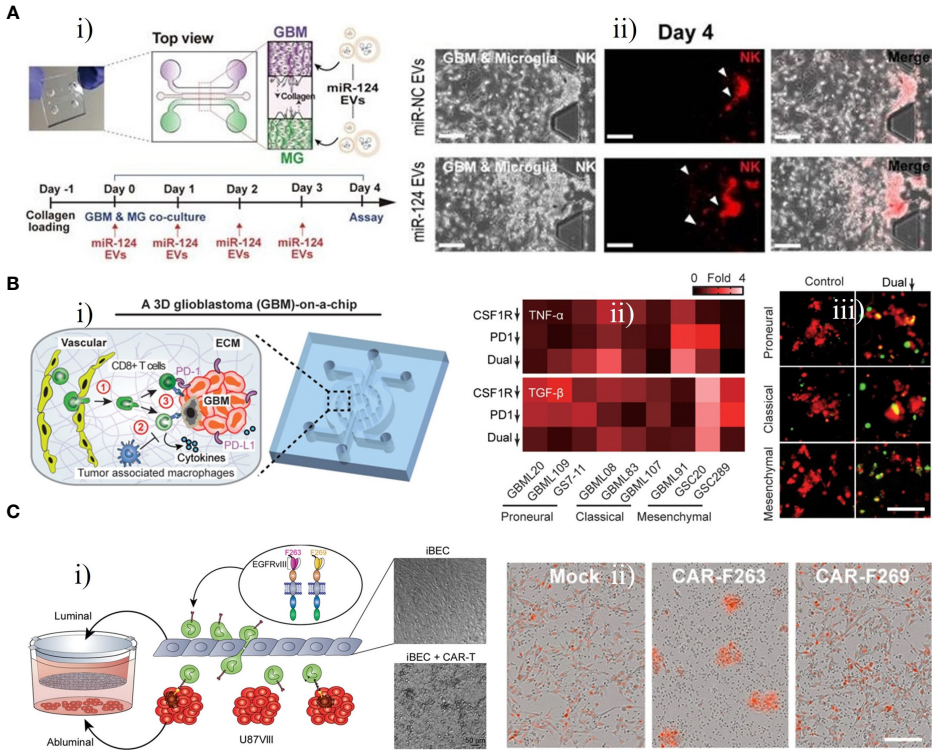

FIGURE 7
GBM-on-chips for investigation of immunotherapy. **(A)** Microfluidic co-culture device for investigating inhibition of tumor progression by miR-124 EVs (62). **(i)** Co-culture of microglia U373MG cells with miR-124 EVs for 4 days. **(ii)** On day 4, NK cells in the microfluidic device were treated with miR-negative control EVs or miR-124 EVs. **(B)** GBM- on-a-chip model of the TME for optimizing anti-PD-1 immunotherapy (63). **(i)** Schematic image of a patient-specific GBM-on-a-chip to recreate the immunosuppressive TME. **(ii)** Quantified cytokine levels showing significantly increased and decreased expression of TNF-α and TGF-β with dual inhibition therapy. **(iii)** Relative to the control group, co-blockade of PD-1 and CSF-1R resulted in more apoptotic GBM cells (green nuclei). **(C)** Transwell BBB and U87vIII co-culture model for pre-clinical evaluation of GBM-targeting CAR-T (64). **(i)** Schematic illustration of the construction of transwell BBB and U87vIII co-culture microfluidic device. **(ii)** CAR–T mediated cytotoxicity of U87vIII cells, with CAR-F263 showing a faster and stronger U87vIII killing response. Reproduced with permission from (62–64).

3.2.2 ICB therapy

ICB therapy has achieved great success in the treatment of advanced tumors of various types, including melanoma, lymphoma, lung cancer, and kidney cancer, with significant improvements in median overall survival in recent years (66–69). Immune checkpoint inhibitors are known to promote the transition from a normal immune system to enhanced immune activation (70). The potential benefits of ICB therapy for GBM patients have attracted significant interest in recent years; however, the efficacy has been unsatisfactory to date (71).

Cui et al. developed a patient-specific GBM-on-a-chip platform for analyzing the heterogeneity of immunosuppressive TMEs and optimizing anti-programmed cell death protein 1 (PD-1, an immune checkpoint inhibitor) immunotherapy against various GBM subtypes (Figure 7B) (63). This platform was used to culture brain microvascular endothelial cells simulating a 3D brain microvascular environment, human macrophage-derived TAMs, molecularly distinct patient-derived GBM cells, and human primary CD8+ T cells in a biomimetic 3D brain ECM to mimic the interaction between an immune system and GBM cells (Figure 7Bi). Various subtypes of GBM exhibited diverse CD8+ T-cell dynamics, and a CSF-1R inhibitor could enhance the efficacy of the PD-1 inhibitor, revealing that immunotherapeutic efficacy for GBM may be improved by immune checkpoint inhibitors targeting PD-1 combined with inhibitors targeting TAM-associated CSF-1R signalling (Figures 7Bii, iii). This patient-specific GBM-on-a-chip platform provided a means of screening personalized immunotherapies for GBM patients. The team further designed an in silico immuno-oncology model to analyze GBM immune interactions based on patient-specific immunological characteristics and measurements of end-point data from the GBM-on-a-chip system mentioned above. This model could dynamically and comprehensively analyze the multiple mechanisms of TAM-associated immunosuppression against anti-PD-1 immunotherapy. It was further demonstrated that immune responses in GBM patients could be enhanced by co-targeting TAM-associated CSF-1R signalling and PD-1 checkpoints, especially in GBM patients who did not respond to single ICB therapy targeting PD-1 (72).

3.2.3 CAR-T therapy

CAR-T therapy, a revolutionary cellular immunotherapy by which T cells are genetically modified, has been approved for specific haematological malignancies and shows potential to target a variety of solid tumors (73). EGFRvIII, a variant of the epidermal growth factor receptor (EGFR), is expressed only in tumors and represents a tumor antigen that can be targeted by CAR-T in GBM (74).

Huang et al. created a microfluidic platform based on a transwell BBB and U87vIII co-culture system for assessment of BBB extravasation of U87MG cells expressing tumor-specific mutant protein EGFRvIII (U87vIII) targeted by CAR-T (Figure 7C) (64). Control mock T cells, and CAR-F263 and CAR-F269 with different tonic signalling profiles (two anti-EGFRvIII-targeting CAR-T cells) were applied to the luminal side (Figure 7Ci). After 48 h treatment, the cell viability of the U87vIII cells decreased significantly, and activated CAR-F263 showed robust cytotoxicity against U87vIII cells. Compared with CAR-F263, CAR-F269 exhibited approximately quadruple lower efficiency in killing U87vIII cells with a similar cytotoxic profile (Figure 7Cii). These results demonstrate the potential of this platform in deciphering the effects of CAR-T on post-barrier target cells with concomitant toxicity and the mechanisms of BBB disruption induced by CAR-T.

In recent years, OoC technology has proved able to almost fully reproduce the GBM tumor immune microenvironment and has become a potent tool for investigation of GBM immunotherapy. However, as microfluidic chips are usually constructed using artificially engineered materials, they may not exactly replicate the real TME. Moreover, there are many geneogenous immunizing cells and adaptive immunizing cells, and the absence of one cellular component or incorrect cellular proportions may result in differences compared with the natural tumor immune microenvironment. Thus, standardization is urgently required to enable researchers to build homogenous models with standard methods that can reproduce the complexity of the GBM tumor immune microenvironment in the future.

3.3 GBM-on-a-chip for other therapies

3.3.1 Phototherapy

Phototherapy comprises two main approaches: photodynamic therapy (PDT), and photothermal therapy (PTT). PDT can cause local chemical damage to target lesions under specific light irradiation, using a photosensitizer to produce large amounts of reactive oxygen radicals that can kill tumor cells. PTT causes local thermal damage when the photothermal agent is irradiated by light at a specific wavelength, causing it to heat up and consequently kill tumor cells (75). The use of photosensitizers is a key component of PDT, whereas there is no need for an exogenous photothermal contrast agent to increase efficiency in PTT.

PDT requires three key elements, namely, a photosensitizer, oxygen, and light, to comprehensively improve its efficacy (76, 77). Lou et al. developed a microfluidic chip for high-throughput PDT assays for analysis of the efficacy of PDT against C6 cells under different treatment parameters: photosensitizer concentration, oxygen level and light level (Figure 8A) (78). In this chip, three layers– a gas layer, cell layer and liquid filter layer– were stacked in a glass substrate in which C6 cells were cultured and exposed to PDT under different conditions (Figure 8Ai). Subsequently, live/dead fluorescence staining was used to monitor cell viability, and integrated control of three key microenvironmental factors in the microfluidic system was used to comprehensively evaluate the efficacy of photosensitizer. As shown in Figure 8Aii, the PDT efficacy and number of dead C6 cells increased as the levels of the three factors increased. Yoon et al. synthesized methylene blue (MB)-conjugated polyacrylamide nanoparticles (PAA NPs) with a polyethylene glycol dimethacrylate (PEGDMA, Mn 550) cross-linker to improve the efficacy of PDT (80). A micro-fluidic system was developed to reliably and quantitatively measure the efficacy of PDT with MB–PEGDMA PAA NPs. The survival of C6 cells was measured with different light illumination time periods for

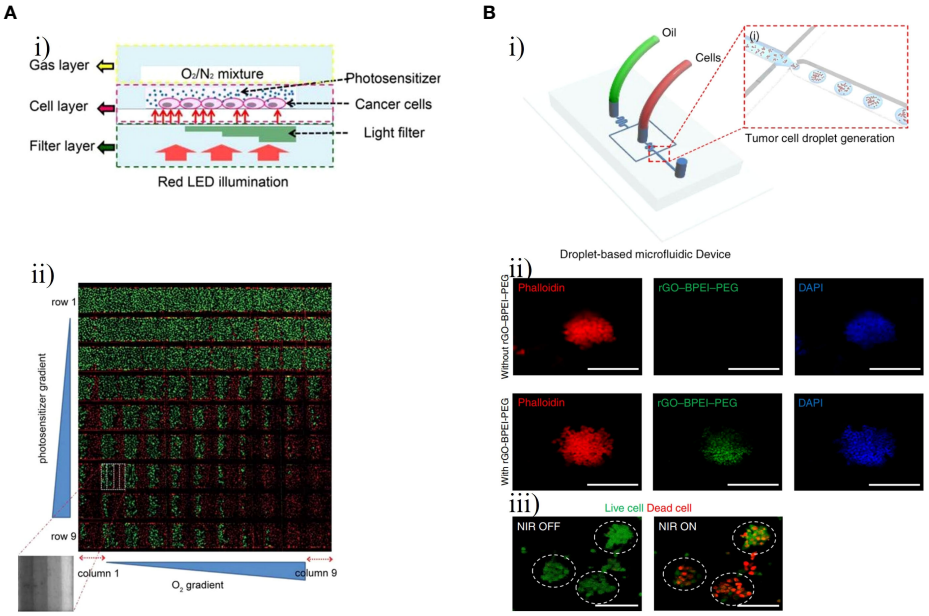

FIGURE 8
GBM-on-chips for phototherapy. **(A)** GBM-on-a-chip system for PDT screening with control of various treatment parameters (78). **(i)** Schematic illustration of the chip with control of three basic elements (photosensitizer, oxygen, and light). **(ii)** Fluorescence image of C6 cell viability after PDT treatment with horizontal channels and vertical columns. **(B)** Droplet-based GBM-on-a-chip platform for applications in PTT. **(i)** Schematic representation of the microfluidic device that generated uniformly sized 3D GBM spheroids (79). **(ii)** Fluorescent microscopic images of GBM spheroids with and without rGO-BPEI-PEG nanocomposites. **(iii)** Fluorescent microscopic images of GBM spheroids with and without NIR laser management. Reproduced with permission from (78, 79).

a given MB–PEGDMA PAA NP dose; the optimal results were obtained at half maximum inhibition time under light illumination. Batches of nanoparticles were tested with three different MB loadings simultaneously on the PDT chip to determine of their cell killing efficacy.

PTT uses the light-to-heat ability of photothermal agents to enhance the heating of cells and tissues in a localized region. Cell death occurs almost instantaneously owing to protein denaturation and destruction of plasma membranes at tissue temperatures greater than 60°C, which are usually reached with PTT (81). Lee et al. constructed a photo-crosslinkable hydrogel microfluidic co-culture GBM-on-a-chip model using two-step photolithography techniques to investigate tumor metastasis and evaluate the efficacy of PTT against metastatic U87-MG cells and MCF7 human breast carcinoma cells (82). Based on the photothermal near-infrared (NIR) laser conversion function of gold nanoparticles, a new type of tumor photothermal therapy called gold nanoparticle mediated NIR thermal therapy has emerged. This has the advantages of being non-invasive and evading drug resistance and has a wide range of applications in the field of tumor thermal therapy (83, 84). After NIR laser irradiation, the viability of MCF7 and U87MG cells treated with 20 v/v% gold nanorods significantly decreased from about 90% to less than 10%, demonstrating that this treatment combination could decrease the viability of cancer cells. Lee et al. further created a droplet-based microfluidic device to evaluate the effect of PTT with a reduced graphene oxide-branched polyethyleneimine-polyethylene glycol (rGO-BPEI-PEG) nanocomposite on 3D GBM spheroids and to demonstrate the application of the 3D GBM spheroids for testing of drug response (Figure 8B) (79). Carbon-based nanomaterials such as rGO have unique advantages including environmental friendliness, low cost, high photothermal conversion capability, high thermal stability, and biocompatibility and are widely used in the field of photothermal devices. This microfluidic chip included two inlets for the oil phase and the aqueous phase with cultured U87-MG cells (Figure 8Bi). The aqueous droplets with GBM cells, the size of which could be controlled by the number of cells, were generated by a microfluidic junction producing shear forces. After 4 h of treatment with different concentrations of rGO-BPEI-PEG nanocomposites, the viability of GBM spheroids declined from 91% to 55% following NIR laser irradiation (Figures 8Bii, iii).

3.3.2 Magnetic hyperthermia therapy

Magnetic hyperthermia therapy (MHT) is a novel type of anti-tumor physical therapy, that takes advantage of the thermal effects of magnetic nanoparticles (MNPs) with an alternating magnetic field (AMF) and the fact that tumor cells are less heat-tolerant than normal cells. The AMF is used to selectively kill tumor cells while MNPs are injected into the tumor site (85, 86). Mamani et al. created an 'MHT-on-a-chip' model based on OoC technology to mimic GBM tumors, with MNPs dispersed in aqueous medium into cavities of the chip for the MHT application (Figure 9A) (87). The microfluidic platform included two compartments separated by a porous interface that allowed cell-to-cell interactions and cell culture in a 3D environment and microchannels allowing fluid to flow throughout the medium (Figure 9Ai). Through administering a flow of MNPs targeting GBM cells, this platform could mimic the dynamic TME *in vivo*. The MHT assay was performed after C6 cells

had been 3D cultured in the chip for 48 h. MNPs consisting of magnetite coated with aminosilane were used to evaluate the efficacy of MHT in C6 cells. After 30 min of magnetic hyperthermia using the MNPs, nearly all GBM cells in the GBM-on-a-chip model were killed. (Figure 9Aii).

3.3.3 Focused ultrasound

The technical principle of focused ultrasound (FUS) is to use ultrasound to penetrate human tissue without damage with a focus on the target lesion. This produces a thermal effect, force effect, and cavitation effect, resulting in direct or indirect regulation and treatment of the lesion area (89). Ultrasound delivered through the skull can be focused on a tumor for targeted ablation or used to open the BBB for delivery of drugs (90). To investigate the potential of FUS in combination with nanomedicines for treatment of GBM, Zervantonakis et al. designed a multi-layer acoustofluidic platform in which F98 rat cells were cultured in a 3D microenvironment (Figure 9B) (88). This platform consisted of a microfluidic chip with optical transparency and a FUS system with a closed-loop controller (Figure 9Bi). Temperature-sensitive liposomal carriers released DOX nanoparticles upon FUS-induced heating, resulting an increase in cellular drug uptake in the region focalized by FUS. Compared with isolated treatment groups, DOX-induced GBM cell death was increased and GBM cell proliferation in the 3D microenvironment was reduced following this treatment (Figure 9Bii). These results demonstrated that acoustofluidics can be used to precisely control drug release and monitor localized cell responses, and to target tumor cells regionally without causing damage to adjacent normal cells.

Phototherapy is a promising therapeutic option for cancer. To date, 5-Aminolevulinic acid-PDT has been approved by the Food and Drug Administration (FDA) for GBM treatment and has shown promising outcomes. However, its effectiveness is limited by the ability of the NIR laser to penetrate into deep brain regions. Therefore, future research should focus on increasing penetration depth in order to enhance the applicability of phototherapy. A number of challenges still need to be overcome before MHT can be applied to GBM clinical treatment, although there have been enormous advances in MHT research over the decades. For example, owing to a lack of specificity, MNPs could accumulate in healthy tissues as well as at the GBM tumor site, which might cause damage to surrounding structures. Moreover, MHT may not completely ablate the GBM tumor, leading to tumor recurrence. More research is also needed to provide sufficient clinical data to support its effectiveness and safety. A combination of phototherapy, MHT, and immunotherapy with an all-in-one microfluidic platform might be an option to achieve synergistic effects. Combined with FUS, drug-loaded microbubbles can temporally increase the permeability of the BBB and can be released at specific locations, enabling targeted delivery into the brain. However, there could be a sterile inflammatory response when the BBB is opened by FUS. In the future, emphasis should be placed on control of ultrasound parameters and the optimization of microbubble types and injection doses to achieve efficient drug delivery.

4 Conclusions and future perspectives

Bionic characteristics of the GBM TME, including cell-to-cell and cell-to-ECM interactions, capillaries, the BBB, and oxygen concentration gradients, can be reproduced by component construction and 3D cell arrangement with microfluidics and bioprinting in GBM-on-a-chip models. These models have considerable potential applications in studies of chemotherapy, immunotherapy, and other GBM therapies. GBM-on-a-chip models have been used to study the interactions between GBM

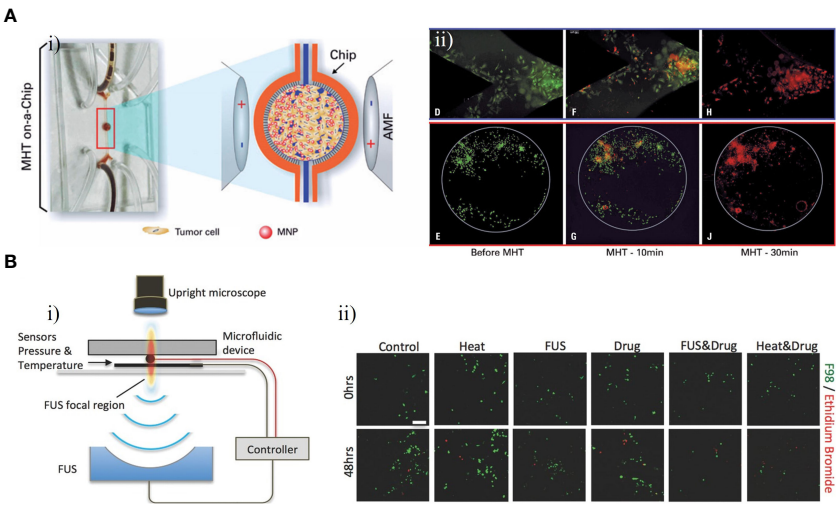

FIGURE 9
GBM-on-chips for MHT and FUS. **(A)** Microfluidic chip for evaluation of MHT (87). **(i)** In the central cavity, magnetic nanoparticles interacted with GBM cells and were then submitted an AMF. **(ii)** Viability assay for C6 cells, showing live cells before MHT and after 10 min and 30 min of MHT. **(B)** Acoustofluidic platform for controlled drug release and chemotherapy response targeting GBM (88). **(i)** Schematic illustration of the closed-loop FUS-microfluidic integrated device for drug release in GBM cells. **(ii)** Viable F98 cells and dead cells were observed before (0 h) and after (48 h) the experiment. Reproduced with permission from (87, 88).

TABLE 1 Examples of glioblastoma-on-a-chip models for therapeutic applications.

Therapeutic Approaches	Targets	Cell Sources	Main Materials	Technologies	Ref.
Chemotherapy	TMZ	U87-MG, U251-MG	PDMS	Microfluidic chip and soft lithography	(41)
Chemotherapy	TMZ	HUVECs, Patient's primary GBM	Collagen hydrogel precursor and Gelatin from porcine skin	Three dimensional bioprinting	(42)
Chemotherapy	TMZ	U87-MG	PDMS	Microfluidic chip and soft lithography	(43)
Chemotherapy	TMZ and BEV	Patient's primary GBM	PEGDA hydrogel	Microfluidic chip and photolithography	(44)
Chemotherapy	TMZ and Res	U87-MG	PDMS	Microfluidic chip and soft lithography	(46)
Chemotherapy	TMZ, CP and CPT-11	Caco-2, HepG2, U251-MG	PDMS and hollow fiber	Microfluidic chip and soft lithography	(45)
Chemotherapy	Pitavastatin and Irinotecan	U87-MG	PEGDA hydrogel	Microfluidic chip and soft lithography	(49)
Chemotherapy	Vincristine and Bleomycin	U251-MG	PDMS	Microfluidic chip and soft lithography	(50)
Chemotherapy	Pyrazino[1,2-a] benzimidazole derivatives	Patient's primary GBM	PDMS	Microfluidic chip and soft lithography	(51)
Immunotherapy	GBM and Microglia	microglial BV-2 cells, C6	PDMS	Microfluidic chip and soft lithography	(61)
Immunotherapy	GBM and Microglia	U373-MG, U87-MG, Patient's primary GBM and microglia, NK-92	PDMS	Microfluidic chip and soft lithography	(62)
Immunotherapy	Macrophage antitumor	GL261, CT-2A, RAW264.7, ATCC	PDMS	Microfluidic chip and soft lithography	(65)
Immunotherapy	anti-PD-1 immunotherapy	Patient's primary GBM, hBMVECs, TAM, CD8+T-cell	PDMS	Microfluidic chip and soft lithography	(63)
Immunotherapy	anti-PD-1 immunotherapy	Patient's primary GBM, hBMVECs, TAM, CD8+T-cell	PDMS	Microfluidic chip and soft lithography	(72)
Immunotherapy	CAR-T	U87-MG Human's primary T cells	Collagen and Fibronectin	NR	(64)
Photodynamic therapy (PDT)	PDT by MB combined with hypoxic conditions	C6	PDMS	Microfluidic chip and soft lithography	(78)
PDT	PDT by MB-PEGDMA PAA NPs	C6	PDMS	Microfluidic chip and soft lithography	(80)
Photothermal therapy (PTT)	PTT by gold nanorods	U87-MG, MCF7	PDMS	Microfluidic chip and soft lithography	(82)
PTT	PTT by rGO-BPEI-PEG	U87-MG	PDMS	Microfluidic chip and soft lithography	(79)

(Continued)

TABLE 1 Continued

Therapeutic Approaches	Targets	Cell Sources	Main Materials	Technologies	Ref.
Magnetic hyperthermia therapy (MHT)	MHT by iron oxide coated with aminosilane	C6	PDMS	Microfluidic chip and soft lithography	(87)
Focused ultrasound (FUS)	FUS and doxorubicin-TS-liposomes	F98-GFP, Bend3	PDMS	Microfluidic chip and soft lithography	(88)

TMZ, temozolomide; U87-MG and U251-MG, two types of glioblastoma cell lines; PDMS, Polydimethylsiloxane; HUVECs, human umbilical vein endothelial cells; BEV, bevacizumab; PEGDA, poly(ethylene) glycol diacrylate; Res, Resveratrol; CP, cisplatin; CPT-11, irinotecan; HepG2, liver hepatocellular carcinoma cell line; Caco-2, colorectal adenocarcinoma cell line; C6, rat glioblastoma cell line; U373-MG, glioblastoma astrocytoma cell line; GL261, CT-2A, mouse glioblastoma cell lines; hBMVECs, human brain microvascular endothelial cells; RAW264.7, ATCC, mouse macrophage cells; CAR-T, chimeric antigen receptor T-cell; MB–PEGDMA PAA NPs, methylene blue conjugated polyacrylamide nanoparticles with a polyethylene glycol dimethacrylate cross-linker; MCF7, breast cancer cell line; rGO-BPEI-PEG, reduced graphene oxide-branched polyethyleneimine-polyethylene glycol; TS, temperature-sensitive; F98-GEP, glioblastoma cell line; Bend3, endothelial cell line of mouse brain.

cells and the brain microenvironment, demonstrating that GBM cells can alter the behavior of other cells in the brain, whereas the microenvironment can also influence the behavior of GBM cells. GBM-on-a-chip models have also been used to test the effects of different drugs and treatments on GBM cells in a more realistic microenvironment than those provided by traditional cell culture models. The efficacy of different drug delivery methods, such as nanoparticles and liposomes, can also be tested using GBM-on-a-chip models. However, the development of OoC technology in therapeutic fields is still in its initial stage. At present, GBM-on-a-chip models may not fully replicate the complex interactions between different cell types and the ECM that occur in the brain. Moreover, the models may not be able to capture the high heterogeneity of GBM that can vary greatly in terms of its genetic makeup and response to treatment, which could limit their usefulness in developing personalized treatment strategies for GBM patients. In the future, there is a need to build on the breakthrough of GBM-on-a-chip technology and develop more complex and bionic humanized GBM-on-a-chip models with more complex structure and function. There are still many new technologies in electrical and optical disciplines that can potentially be combined with GBM-on-a-chip, which would broaden the technical field of GBM therapy. For instance, optical-based bioprinting techniques enable rapid construction of GBM-on-a-chip models with continuous automated production. Combined with nanotechnology, GBM-on-a-chip platforms have the potential to regulate nanodrug delivery in response to electrical stimulation to facilitate targeted therapies, PPT, and PDT. Recently, the FDA has removed the requirement for animal testing prior to human clinical trials. This could represent an opportunity for OoC technology to usher in rapid development and replace animal models. One of the main advantages of OoC technology is that it can provide more accurate results than animal models. For example, a personalized GBM-on-a-chip platform can be used to develop patient-specific precision strategies and identify the best drug combination to optimize treatment outcomes in the broader GBM patient population. In the future, researchers could integrate GBM-on-a-chip with multi-organ chips to model the intersection of different biological systems. This could recapitulate organ-level physiology and pathophysiology of GBM patient, and leveraging computational modelling in combination with experimental data generated using this platform could lead to the development of effective new drugs with low side-effects and the discovery of novel therapeutic targets in GBM. As the technology continues to improve and become more widely adopted, it has the potential to transform the field of drug development and toxicology testing, while also reducing the need for animal testing.

Table 1 summarizes the therapeutic approaches, targets, cell sources, main materials and technologies of the GBM-on-a-chip models for therapy applications that are discussed in this review.

Author contributions

Conceptualization, JM and ZX; writing—original draft preparation, ZX; writing—review and editing, JM and HW; supervision, MC, and JF. All authors contributed to the article and approved the submitted version.

Funding

This work was supported by the Ningbo Natural Science Foundation (grant no. 2022J252), the Ningbo Municipal Bureau of Science and Technology (grant no. 2021S172) and NINGBO Medical and Health Leading Academic Discipline Project (grant no. 2022-F04).

Acknowledgments

The authors express their gratitude to Dr. Yang Zhou for providing valuable assistance in revising the manuscript. Dr. Zhou's constructive comments greatly enhanced the quality of the manuscript.

Conflict of interest

The authors declare that the research was conducted in the absence of any commercial or financial relationships that could be construed as a potential conflict of interest.

Publisher's note

References

1. Ostrom QT, Gittleman H, Truitt G, Boscia A, Kruchko C, Barnholtz-Sloan JS. CBTRUS statistical report: primary brain and other central nervous system tumors diagnosed in the united states in 2011-2015. *Neuro Oncol* (2018) 20(suppl_4):iv1–iv86. doi: 10.1093/neuonc/noy131

2. Kesari S. Understanding glioblastoma tumor biology: the potential to improve current diagnosis and treatments. *Semin Oncol* (2011) 38(Suppl 4):S2–10. doi: 10.1053/j.seminoncol.2011.09.005

3. Taphoorn MJ, Sizoo EM, Bottomley A. Review on quality of life issues in patients with primary brain tumors. *Oncologist* (2010) 15(6):618–26. doi: 10.1634/theoncologist.2009-0291

4. Stupp R, Mason WP, Van Den Bent MJ, Weller M, Fisher B, Taphoorn MJ, et al. Radiotherapy plus concomitant and adjuvant temozolomide for glioblastoma. *N Engl J Med* (2005) 352(10):987–96. doi: 10.1056/NEJMoa043330

5. Gangoso E, Southgate B, Bradley L, Rus S, Galvez-Cancino F, McGivern N, et al. Glioblastomas acquire myeloid-affiliated transcriptional programs *via* epigenetic immunoediting to elicit immune evasion. *Cell* (2021) 184(9):2454–2470 e26. doi: 10.1016/j.cell.2021.03.023

6. Aldape K, Brindle KM, Chesler L, Chopra R, Gajjar A, Gilbert MR, et al. Challenges to curing primary brain tumours. *Nat Rev Clin Oncol* (2019) 16(8):509–20. doi: 10.1038/s41571-019-0177-5

7. Qazi MA, Vora P, Venugopal C, Sidhu SS, Moffat J, Swanton C, et al. Intratumoral heterogeneity: pathways to treatment resistance and relapse in human glioblastoma. *Ann Oncol* (2017) 28(7):1448–56. doi: 10.1093/annonc/mdx169

8. Meyer M, Reimand J, Lan X, Head R, Zhu X, Kushida M, et al. Single cell-derived clonal analysis of human glioblastoma links functional and genomic heterogeneity. *Proc Natl Acad Sci USA* (2015) 112(3):851–6. doi: 10.1073/pnas.1320611111

9. Prager BC, Bhargava S, Mahadev V, Hubert CG, Rich JN. Glioblastoma stem cells: driving resilience through chaos. *Trends Cancer* (2020) 6(3):223–35. doi: 10.1016/j.trecan.2020.01.009

10. Ingber DE. Human organs-on-chips for disease modelling, drug development and personalized medicine. *Nat Rev Genet* (2022) 23(8):467–91. doi: 10.1038/s41576-022-00466-9

11. Vunjak-Novakovic G, Ronaldson-Bouchard K, Radisic M. Organs-on-a-chip models for biological research. *Cell* (2021) 184(18):4597–611. doi: 10.1016/j.cell.2021.08.005

12. Perrett S, Buell AK, Knowles TPJ. *Biological and bio-inspired nanomaterials: properties and assembly mechanisms* Vol. 1174. Singapore: Springer Nature (2019).

13. Zhang B, Korolj A, Lai BFL, Radisic M. Advances in organ-on-a-chip engineering. *Nat Rev Mater* (2018) 3(8):257–78. doi: 10.1038/s41578-018-0034-7

14. Park SE, Georgescu A, Huh D. Organoids-on-a-chip. *Science* (2019) 364 (6444):960–5. doi: 10.1126/science.aaw7894

15. Ayuso JM, Virumbrales-Muñoz M, Lang JM, Beebe DJ. A role for microfluidic systems in precision medicine. *Nat Commun* (2022) 13(1):3086. doi: 10.1038/s41467-022-30384-7

16. Yi HG, Jeong YH, Kim Y, Choi YJ, Moon HE, Park SH, et al. A bioprinted human-glioblastoma-on-a-chip for the identification of patient-specific responses to chemoradiotherapy. *Nat BioMed Eng* (2019) 3(7):509–19. doi: 10.1038/s41551-019-0363-x

17. Xiao Y, Kim D, Dura B, Zhang K, Yan R, Li H, et al. Ex vivo dynamics of human glioblastoma cells in a microvasculature-on-a-Chip system correlates with tumor heterogeneity and subtypes. *Adv Sci (Weinh)* (2019) 6(8):1801531. doi: 10.1002/advs.201801531

18. Lin Z, Luo G, Du W, Kong T, Liu C, Liu Z. Recent advances in microfluidic platforms applied in cancer metastasis: circulating tumor cells' (CTCs) isolation and tumor-On-A-Chip. *Small* (2020) 16(9):e1903899. doi: 10.1002/smll.201903899

19. Takebe T, Zhang B, Radisic M. Synergistic engineering: organoids meet organs-on-a-Chip. *Cell Stem Cell* (2017) 21(3):297–300. doi: 10.1016/j.stem.2017.08.016

20. Spano D, Zollo M. Tumor microenvironment: a main actor in the metastasis process. *Clin Exp Metastasis* (2012) 29(4):381–95. doi: 10.1007/s10585-012-9457-5

21. Turley SJ, Cremasco V, Astarita JL. Immunological hallmarks of stromal cells in the tumour microenvironment. *Nat Rev Immunol* (2015) 15(11):669–82. doi: 10.1038/nri3902

22. Bikfalvi A, Da Costa CA, Avril T, Barnier JV, Bauchet L, Brisson L, et al. Challenges in glioblastoma research: focus on the tumor microenvironment. *Trends Cancer* (2023) 9(1):9–27. doi: 10.1016/j.trecan.2022.09.005

23. Klemm F, Maas RR, Bowman RL, Kornete M, Soukup K, Nassiri S, et al. Interrogation of the microenvironmental landscape in brain tumors reveals disease-specific alterations of immune cells. *Cell* (2020) 181(7):1643–1660 e17. doi: 10.1016/j.cell.2020.05.007

24. Hanahan D, Weinberg RA. Hallmarks of cancer: the next generation. *Cell* (2011) 144(5):646–74. doi: 10.1016/j.cell.2011.02.013

25. Birocchi F, Cusimano M, Rossari F, Beretta S, Rancoita PMV, Ranghetti A, et al. Targeted inducible delivery of immunoactivating cytokines reprograms glioblastoma microenvironment and inhibits growth in mouse models. *Sci Transl Med* (2022) 14 (653):eabl4106. doi: 10.1126/scitranslmed.abl4106

26. Grossen A, Smith K, Coulibaly N, Arbuckle B, Evans A, Wilhelm S, et al. Physical forces in glioblastoma migration: a systematic review. *Int J Mol Sci* (2022) 23(7):4055. doi: 10.3390/ijms23074055

27. Klemm F, Joyce JA. Microenvironmental regulation of therapeutic response in cancer. *Trends Cell Biol* (2015) 25(4):198–213. doi: 10.1016/j.tcb.2014.11.006

28. Puryear Iii JR, Yoon JK, Kim Y. Advanced fabrication techniques of microengineered physiological systems. *Micromachines (Basel)* (2020) 11(8):730.

29. Ishahak M, Hill J, Amin Q, Wubker L, Hernandez A, Mitrofanova A, et al. Modular microphysiological system for modeling of biologic barrier function. *Front Bioeng Biotechnol* (2020) 8:581163. doi: 10.3389/fbioe.2020.581163

30. Lee H-J, Yoon T-H, Park J-H, Perumal J, Kim D-P. Characterization and fabrication of polyvinylsilazane glass microfluidic channels *via* soft lithographic technique. *J Ind Eng Chem* (2008) 14(1):45–51. doi: 10.1016/j.jiec.2007.06.002

31. Olubajo F, Achawal S, Greenman J. Development of a microfluidic culture paradigm for ex vivo maintenance of human glioblastoma tissue: a new glioblastoma model? *Transl Oncol* (2020) 13(1):1–10. doi: 10.1016/j.tranon.2019.09.002

32. Dou J, Mao S, Li H, Lin JM. Combination stiffness gradient with chemical stimulation directs glioma cell migration on a microfluidic chip. *Anal Chem* (2020) 92 (1):892–8. doi: 10.1021/acs.analchem.9b03681

33. Liu H, Jie M, He Z, Li HF, Lin JM. Study of antioxidant effects on malignant glioma cells by constructing a tumor-microvascular structure on microchip. *Anal Chim Acta* (2017) 978:1–9. doi: 10.1016/j.aca.2017.05.009

34. Depalma TJ, Sivakumar H, Skardal A. Strategies for developing complex multi-component *in vitro* tumor models: highlights in glioblastoma. *Adv Drug Delivery Rev* (2022) 180:114067. doi: 10.1016/j.addr.2021.114067

35. Tang M, Xie Q, Gimple RC, Zhong Z, Tam T, Tian J, et al. Three-dimensional bioprinted glioblastoma microenvironments model cellular dependencies and immune interactions. *Cell Res* (2020) 30(10):833–53. doi: 10.1038/s41422-020-0338-1

36. Silvani G, Basirun C, Wu H, Mehner C, Poole K, Bradbury P, et al. A 3D-bioprinted vascularized glioblastoma-on-a-Chip for studying the impact of simulated microgravity as a novel pre-clinical approach in brain tumor therapy (Adv. therap. 11/2021). *Advanced Ther* (2021) 4:2170033. doi: 10.1002/adtp.202170033

37. Heinrich MA, Bansal R, Lammers T, Zhang YS, Michel Schiffelers R, Prakash J. 3D-bioprinted mini-brain: a glioblastoma model to study cellular interactions and therapeutics. *Adv Mater* (2019) 31(14):e1806590. doi: 10.1002/adma.201806590

38. Neufeld L, Yeini E, Reisman N, Shtilerman Y, Ben-Shushan D, Pozzi S, et al. Microengineered perfusable 3D-bioprinted glioblastoma model for in vivo mimicry of tumor microenvironment. *Sci Adv* (2021) 7(34):eabi9119. doi: 10.1126/sciadv.abi9119

39. Zhang J, Stevens MF, Laughton CA, Madhusudan S, Bradshaw TD. Acquired resistance to temozolomide in glioma cell lines: molecular mechanisms and potential translational applications. *Oncology* (2010) 78(2):103–14. doi: 10.1159/000306139

40. Sarkaria JN, Kitange GJ, James CD, Plummer R, Calvert H, Weller M, et al. Mechanisms of chemoresistance to alkylating agents in malignant glioma. *Clin Cancer Res* (2008) 14(10):2900–8. doi: 10.1158/1078-0432.CCR-07-1719

41. Samiei E, Seyfoori A, Toyota B, Ghavami S, Akbari M. Investigating programmed cell death and tumor invasion in a three-dimensional (3D) microfluidic model of glioblastoma. *Int J Mol Sci* (2020) 21(9):3162. doi: 10.3390/ijms21093162

42. Ozturk MS, Lee VK, Zou H, Friedel RH, Intes X, Dai G. High-resolution tomographic analysis of *in vitro* 3D glioblastoma tumor model under long-term drug treatment. *Sci Adv* (2020) 6(10):eaay7513. doi: 10.1126/sciadv.aay7513

43. Zhang Q, Mao S, Li W, Huang Q, Feng S, Hong Z, et al. Microfluidic adhesion analysis of single glioma cells for evaluating the effect of drugs. *Sci China Chem* (2020) 63(6):865–70. doi: 10.1007/s11426-020-9734-7

44. Akay M, Hite J, Avci NG, Fan Y, Akay Y, Lu G, et al. Drug screening of human GBM spheroids in brain cancer chip. *Sci Rep* (2018) 8(1):15423. doi: 10.1038/s41598-018-33641-2

45. Ma J, Li N, Wang Y, Wang L, Wei W, Shen L, et al. Engineered 3D tumour model for study of glioblastoma aggressiveness and drug evaluation on a detachably assembled microfluidic device. *BioMed Microdevices* (2018) 20(3):80. doi: 10.1007/s10544-018-0322-4

46. Filippi-Chiela EC, Thomé MP, Bueno E Silva MM, Pelegrini AL, Ledur PF, Garicochea B, et al. Resveratrol abrogates the temozolomide-induced G2 arrest leading to mitotic catastrophe and reinforces the temozolomide-induced senescence in glioma cells. *BMC Cancer* (2013) 13:147. doi: 10.1186/1471-2407-13-147

47. Castino R, Pucer A, Veneroni R, Morani F, Peracchio C, Lah TT, et al. Resveratrol reduces the invasive growth and promotes the acquisition of a long-lasting differentiated phenotype in human glioblastoma cells. *J Agric Food Chem* (2011) 59(8):4264–72. doi: 10.1021/jf104917q

48. Jie M, Mao S, Liu H, He Z, Li HF, Lin JM. Evaluation of drug combination for glioblastoma based on an intestine-liver metabolic model on microchip. *Analyst* (2017) 142(19):3629–38. doi: 10.1039/C7AN00453B

49. Fan Y, Nguyen DT, Akay Y, Xu F, Akay M. Engineering a brain cancer chip for high-throughput drug screening. *Sci Rep* (2016) 6:25062. doi: 10.1038/srep25062

50. Liu W, Xu J, Li T, Zhao L, Ma C, Shen S, et al. Monitoring tumor response to anticancer drugs using stable three-dimensional culture in a recyclable microfluidic platform. *Anal Chem* (2015) 87(19):9752–60. doi: 10.1021/acs.analchem.5b01915

51. Rahimifard M, Bagheri Z, Hadjighassem M, Jaktaji RP, Behroodi E, Haghi-Aminjan H, et al. Investigation of anti-cancer effects of new pyrazino[1,2-a]benzimidazole derivatives on human glioblastoma cells through 2D in vitro model and 3D-printed microfluidic device. *Life Sci* (2022) 28(302):120505. doi: 10.1016/j.lfs.2022.120505

52. Azami Movahed M, Daraei B, Shahosseini S, Esfahanizadeh M, Zarghi A. Design, synthesis, and biological evaluation of new pyrazino[1,2-a] benzimidazole derivatives as selective cyclooxygenase (COX-2) inhibitors. *Arch Pharm (Weinheim)* (2019) 352(2):e1800265.

53. Tomaszewski W, Sanchez-Perez L, Gajewski TF, Sampson JH. Brain tumor microenvironment and host state: implications for immunotherapy. *Clin Cancer Res* (2019) 25(14):4202–10. doi: 10.1158/1078-0432.CCR-18-1627

54. Hoelzinger DB, Demuth T, Berens ME. Autocrine factors that sustain glioma invasion and paracrine biology in the brain microenvironment. *J Natl Cancer Inst* (2007) 99(21):1583–93. doi: 10.1093/jnci/djm187

55. Bloch O, Crane CA, Kaur R, Safaee M, Rutkowski MJ, Parsa AT. Gliomas promote immunosuppression through induction of B7-H1 expression in tumor-associated macrophages. *Clin Cancer Res* (2013) 19(12):3165–75. doi: 10.1158/1078-0432.CCR-12-3314

56. Li W, Graeber MB. The molecular profile of microglia under the influence of glioma. *Neuro Oncol* (2012) 14(8):958–78. doi: 10.1093/neuonc/nos116

57. Dzaye O, Hu F, Derkow K, Haage V, Euskirchen P, Harms C, et al. Glioma stem cells but not bulk glioma cells upregulate IL-6 secretion in Microglia/Brain macrophages *via* toll-like receptor 4 signaling. *J Neuropathol Exp Neurol* (2016) 75 (5):429–40. doi: 10.1093/jnen/nlw016

58. Vinnakota K, Hu F, Ku MC, Georgieva PB, Szulzewsky F, Pohlmann A, et al. Toll-like receptor 2 mediates microglia/brain macrophage MT1-MMP expression and glioma expansion. *Neuro Oncol* (2013) 15(11):1457–68. doi: 10.1093/neuonc/not115

59. Coniglio SJ, Segall JE. Review: molecular mechanism of microglia stimulated glioblastoma invasion. *Matrix Biol* (2013) 32(7-8):372–80. doi: 10.1016/j.matbio.2013.07.008

60. Markovic DS, Vinnakota K, Chirasani S, Synowitz M, Raguet H, Stock K, et al. Gliomas induce and exploit microglial MT1-MMP expression for tumor expansion. *Proc Natl Acad Sci U.S.A.* (2009) 106(30):12530–5. doi: 10.1073/pnas.0804273106

61. Gu R, Zhang X, Zhang G, Tao T, Yu H, Liu L, et al. Probing the bi-directional interaction between microglia and gliomas in a tumor microenvironment on a microdevice. *Neurochem Res* (2017) 42(5):1478–87. doi: 10.1007/s11064-017-2204-1

62. Hong S, You JY, Paek K, Park J, Kang SJ, Han EH, et al. Inhibition of tumor progression and M2 microglial polarization by extracellular vesicle-mediated microRNA-124 in a 3D microfluidic glioblastoma microenvironment. *Theranostics* (2021) 11(19):9687–704. doi: 10.7150/thno.60851

63. Cui X, Morales RT, Qian W, Wang H, Gagner JP, Dolgalev I, et al. Hacking macrophage-associated immunosuppression for regulating glioblastoma angiogenesis. *Biomaterials* (2018) 161:164–78. doi: 10.1016/j.biomaterials.2018.01.053

64. Nakamura Y, Namikawa K, Kiniwa Y, Kato H, Yamasaki O, Yoshikawa S, et al. Efficacy comparison between anti-PD-1 antibody monotherapy and anti-PD-1 plus anti-CTLA-4 combination therapy as first-line immunotherapy for advanced acral melanoma: a retrospective, multicenter study of 254 Japanese patients. *Eur J Cancer* (2022) 176:78–87. doi: 10.1016/j.ejca.2022.08.030

65. Reck M, Rodriguez-Abreu D, Robinson AG, Hui R, Csőszi T, Fülöp A, et al. Pembrolizumab versus chemotherapy for PD-L1-Positive non-Small-Cell lung cancer. *N Engl J Med* (2016) 375(19):1823–33. doi: 10.1056/NEJMoa1606774

66. Topalian SL, Hodi FS, Brahmer JR, Gettinger SN, Smith DC, McDermott DF, et al. Safety, activity, and immune correlates of anti-PD-1 antibody in cancer. *N Engl J Med* (2012) 366(26):2443–54. doi: 10.1056/NEJMoa1200690

67. Brahmer JR, Tykodi SS, Chow LQ, Hwu WJ, Topalian SL, Hwu P, et al. Safety and activity of anti-PD-L1 antibody in patients with advanced cancer. *N Engl J Med* (2012) 366(26):2455–65. doi: 10.1056/NEJMoa1200694

68. Preusser M, Lim M, Hafler DA, Reardon DA, Sampson JH. Prospects of immune checkpoint modulators in the treatment of glioblastoma. *Nat Rev Neurol* (2015) 11 (9):504–14. doi: 10.1038/nrneurol.2015.139

69. Arrieta VA, Iwamoto F, Lukas RV, Sachdev S, Rabadan R, Sonabend AM. Can patient selection and neoadjuvant administration resuscitate PD-1 inhibitors for glioblastoma? *J Neurosurg* (2019) 132(5):1667–72. doi: 10.3171/2019.9.JNS192523

70. Cui X, Ma C, Vasudevaraja V, Serrano J, Tong J, Peng Y, et al. Dissecting the immunosuppressive tumor microenvironments in glioblastoma-on-a-Chip for optimized PD-1 immunotherapy. *Elife* (2020) 9:e52253. doi: 10.7554/eLife.52253

71. Zhang Z, Liu L, Ma C, Cui X, Lam RHW, Chen W. An in silico glioblastoma microenvironment model dissects the immunological mechanisms of resistance to PD-1 checkpoint blockade immunotherapy. *Small Methods* (2021) 5(6):2100197. doi: 10.1002/smtd.202100197

72. Hong M, Clubb JD, Chen YY. Engineering CAR-T cells for next-generation cancer therapy. *Cancer Cell* (2020) 38(4):473–88. doi: 10.1016/j.ccell.2020.07.005

73. Faulkner C, Palmer A, Williams H, Wragg C, Haynes HR, White P, et al. EGFR and EGFRvIII analysis in glioblastoma as therapeutic biomarkers. *Br J Neurosurg* (2015) 29(1):23–9. doi: 10.3109/02688697.2014.950631

74. Huang J, Li YB, Charlebois C, Nguyen T, Liu Z, Bloemberg D, et al. Application of blood brain barrier models in pre-clinical assessment of glioblastoma-targeting CAR-T based immunotherapies. *Fluids Barriers CNS* (2022) 19(1):38. doi: 10.1186/s12987-022-00342-y

75. Li X, Lovell JF, Yoon J, Chen X. Clinical development and potential of photothermal and photodynamic therapies for cancer. *Nat Rev Clin Oncol* (2020) 17 (11):657–74. doi: 10.1038/s41571-020-0410-2

76. Donohoe C, Senge MO, Arnaut LG, Gomes-da-Silva LC. Cell death in photodynamic therapy: from oxidative stress to anti-tumor immunity. *Biochim Biophys Acta Rev Cancer* (2019) 1872(2):188308. doi: 10.1016/j.bbcan.2019.07.003

77. Kwiatkowski S, Knap B, Przystupski D, Saczko J, Kędzierska E, Knap-Czop K, et al. Photodynamic therapy - mechanisms, photosensitizers and combinations. *BioMed Pharmacother* (2018) 106:1098–107. doi: 10.1016/j.biopha.2018.07.049

78. Lou X, Kim G, Yoon HK, Lee YE, Kopelman R, Yoon E. A high-throughput photodynamic therapy screening platform with on-chip control of multiple microenvironmental factors. *Lab Chip* (2014) 14(5):892–901. doi: 10.1039/c3lc51077h

79. Yoon HK, Lou X, Chen YC, Koo Lee YE, Yoon E, Kopelman R. Nano-photosensitizers engineered to generate a tunable mix of reactive oxygen species, for optimizing photodynamic therapy, using a microfluidic device. *Chem Mater* (2014) 26 (4):1592–600. doi: 10.1021/cm403505s

80. Knavel EM, Brace CL. Tumor ablation: common modalities and general practices. *Tech Vasc Interv Radiol* (2013) 16(4):192–200. doi: 10.1053/j.tvir.2013.08.002

81. Lee JM, Seo HI, Bae JH, Chung BG. Hydrogel microfluidic co-culture device for photothermal therapy and cancer migration. *Electrophoresis* (2017) 38(9-10):1318–24. doi: 10.1002/elps.201600540

82. Sikdar D, Rukhlenko ID, Cheng W, Premaratne M. Optimized gold nanoshell ensembles for biomedical applications. *Nanoscale Res Lett* (2013) 8(1):142. doi: 10.1186/1556-276X-8-142

83. Raji V, Kumar J, Rejiya CS, Vibin M, Shenoi VN, Abraham A. Selective photothermal efficiency of citrate capped gold nanoparticles for destruction of cancer cells. *Exp Cell Res* (2011) 317(14):2052–8. doi: 10.1016/j.yexcr.2011.04.010

84. Lee JM, Choi JW, Ahrberg CD, Choi HW, Ha JH, Mun SG, et al. Generation of tumor spheroids using a droplet-based microfluidic device for photothermal therapy. *Microsyst Nanoeng* (2020) 6:52. doi: 10.1038/s41378-020-0167-x

85. Mahmoudi K, Bouras A, Bozec D, Ivkov R, Hadjipanayis C. Magnetic hyperthermia therapy for the treatment of glioblastoma: a review of the therapy's history, efficacy and application in humans. *Int J Hyperthermia* (2018) 34(8):1316–28. doi: 10.1080/02656736.2018.1430867

86. Kaczmarek K, Hornowski T, Dobosz B, Józefczak A. Influence of magnetic nanoparticles on the focused ultrasound hyperthermia. *Mater (Basel)* (2018) 11 (9):1607. doi: 10.3390/ma11091607

87. Mamani JB, Marinho BS, Rego GNA, Nucci MP, Alvieri F, Santos RSD, et al. Magnetic hyperthermia therapy in glioblastoma tumor on-a-Chip model. *Einstein (Sao Paulo)* (2020) 18:eAO4954.

88. Phenix CP, Togtema M, Pichardo S, Zehbe I, Curiel L. High intensity focused ultrasound technology, its scope and applications in therapy and drug delivery. *J Pharm Pharm Sci* (2014) 17(1):136–53. doi: 10.18433/J3ZP5F

89. Etame AB, Diaz RJ, Smith CA, Mainprize TG, Hynynen K, Rutka JT. Focused ultrasound disruption of the blood-brain barrier: a new frontier for therapeutic delivery in molecular neurooncology. *Neurosurg Focus* (2012) 32(1):E3. doi: 10.3171/2011.10.FOCUS11252

90. Zervantonakis IK, Arvanitis CD. Controlled drug release and chemotherapy response in a novel acoustofluidic 3D tumor platform. *Small* (2016) 12(19):2616–26. doi: 10.1002/smll.201503342

frontiers | Frontiers in Oncology

TYPE Original Research
PUBLISHED 23 November 2023
DOI 10.3389/fonc.2023.1235212

OPEN ACCESS

EDITED BY
Konstantinos Gousias,
University of Münster, Germany

REVIEWED BY
Matthias Krammer,
Academic Teaching Hospital Munich Bogenhausen (Technical University Munich), Germany
Jose Pedro Lavrador,
King's College Hospital NHS Foundation Trust, United Kingdom

*CORRESPONDENCE
Franziska Staub-Bartelt
franziska.staub-bartelt@med.uni-duesseldorf.de

RECEIVED 05 June 2023
ACCEPTED 30 October 2023
PUBLISHED 23 November 2023

CITATION
Staub-Bartelt F, Rapp M and Sabel M (2023) Feasibility of intraoperative neuromonitoring and cortical/subcortical mapping in patients with cerebral lesions of highly functional localizations—pathway to case adapted monitoring and mapping procedures. *Front. Oncol.* 13:1235212. doi: 10.3389/fonc.2023.1235212

Feasibility of intraoperative neuromonitoring and cortical/subcortical mapping in patients with cerebral lesions of highly functional localizations—pathway to case adapted monitoring and mapping procedures

Franziska Staub-Bartelt*, Marion Rapp and Michael Sabel

Department of Neurosurgery, University Hospital Duesseldorf, Duesseldorf, Germany

Background: Intraoperative neuromonitoring (IONM) and mapping procedures *via* direct cortical stimulation (DCS) are required for resection of eloquently located cerebral lesions. In our neurooncological department, mapping and monitoring are used either combined or separately for surgery of functional lesions. The study aims to provide a practical insight into strengths and pitfalls of intraoperative neuromonitoring and mapping in supratentorial functionally located infiltrating lesions.

Methods: IONM and mapping techniques performed in eloquent located brain tumors were analyzed with a focus on neurological outcome and resection results obtained *via* MRI. Additionally, the surgeons' view on obligatory techniques was explored retrospectively immediately after surgery. To evaluate the impact of the described items, we correlated intraoperative techniques in various issues.

Results: Majority of the 437 procedures were performed as awake surgery (53%). Monopolar stimulation was used in 348 procedures and correlated with a postoperative temporary neurological deficit. Bipolar stimulation was performed in 127 procedures, particularly on tumors in the left hemisphere for language mapping. Overall permanent deficit was seen in 2% of the patients; neither different mapping or monitoring modes nor stimulation intensity, localization, or histopathological findings correlated significantly with permanent deficits. Evaluation of post-OP MRI revealed total resection (TR) in 209 out of 417 cases. Marginal residual volume in cases where total resection was assumed but MRI failed to proof TR was found (0.4 ml). Surgeons' post-OP evaluation of obligatory techniques matched in 73% with the techniques actually used.

Conclusion: We report 437 surgical procedures on highly functional located brain lesions. Resection without permanent deficit was adequately achievable in 98% of the procedures. Chosen mapping or monitoring techniques mostly depended on localization and vascular conflicts but also in some procedures on availability of resources, which was emphasized by the post-OP surgeons' evaluation. With the present study, we aimed to pave the way to á la carte choice of monitoring and or mapping techniques, reflecting the possibilities of even supratotal resection in eloquent brain tumor lesions and the herewith increased need for monitoring and limiting resources.

KEYWORDS

intraoperative monitoring, brain mapping, brain tumor, eloquent location, supratentorial brain tumor

Introduction

Surgical gross total resection represents the gold standard according to therapeutical approaches of infiltrating brain tumors. The aim of the surgical intervention is an achievement of complete removal of the tumor as seen on the MRI scan and described as gross total resection in the literature in order to extend survival of the patients as this is directly linked to an extended overall survival in high-grade glioma patients (1–3). For low-grade glioma, it is well known that a residual tumor volume and extent of resection can predict the progression-free survival and time to malignant transformation (4, 5) as well as overall survival. Surgical resection in brain metastasis has also been the object of partly critical investigation. For this brain tumor entity too, surgical resection was found to be a significant factor for longer survival and preservation of functional status in many studies comparing the surgical approach and radiation therapy or radiation therapy alone. Patients that underwent surgery before radiation, regardless of the type of radiation (whole-brain or stereotactic radiosurgery), showed a significant longer patient survival and higher Karnofsky Performance Scale Scores (6, 7).

Thus, surgical therapy represents a main step in therapeutical concepts for cerebral lesions of different etiologies.

The most common highly functional supratentorial cerebral lesions comprise areas of motor and speech function. An important feature of gliomas and to some extent metastasis is the infiltrating zone. Here, functional tissue is infiltrated by malignant cells. Surgical intervention in this zone would inherently result in neurological/neurocognitive deficits, a non-resection in potential earlier recurrence. Thus, a possible definition of "eloquent" localization could be the ability to correlate a defined neurological/neurocognitive deficit with the destruction of this tissue by progression of the tumor or resection.

Maximum but safe resection is the superior aim in brain tumor surgery. In order to achieve the aimed resection but also to preserve functional status, as well as to provide the patient with optimal conditions for adjuvant therapies, intraoperative neuromonitoring and mapping using direct cortical and subcortical stimulation techniques have been well-established procedures in resection of tumors relating to motor pathways or speech areas and fiber tracts (8–12). In addition to motor and speech function, neurocognitive integrity has more and more become a target for intraoperative testing over the last few years (13–15).

There are different methods used for intraoperative monitoring (IOM) of neurological function. Transcranial electric stimulation (TES) can be used for motor-evoked potentials (TES-MEP) for monitoring of motor pathway integrity. Additionally, somatosensory-evoked potential (SSEP) monitoring to watch over sensory function can be performed. MEP monitoring can also be performed *via* direct cortical stimulation (DCS) by placing a strip electrode (SE) on the precentral gyrus allowing a continuous control of neurological motor function in asleep patients. DCS is also carried out by the usage of handheld monopolar or bipolar stimulation probes (16, 17), which enables the surgeon to map the functionality of the tissue. Bipolar stimulation is commonly used for awake mapping procedures, whereas monopolar mapping is particularly used for motor mapping for tumors located near or around motor pathways even though speech mapping is also performed at least on a research basis *via* monopolar mapping stimulation (18, 19). In summary, to date there are several options for mapping and monitoring procedures available, from which the surgeon can choose for special indications.

Over the past two decades, we have implemented the mentioned technical methods as well as awake and asleep resection protocols at our department. Instead of choosing one method over the other, we preoperatively determine what we think is the most suitable technique for preservation of neurological function. For reevaluation of the decisions, the present study was conceived in which we analyzed clinical and intraoperative data of 437 procedures in 400 patients that underwent surgery of eloquent brain lesions during a period of 4 years and complemented these data with subjective evaluations of the decisions made preoperatively by the surgeons that had performed surgery. All patients underwent surgery using either a single or combination of different mentioned intraoperative neuromonitoring and mapping

methods. Additionally, we combined asleep and awake procedures. With this study, we aim to provide a deeper insight into strengths and pitfalls of intraoperative neuromonitoring and mapping in supratentorial eloquent brain tumors, especially gliomas and the hereby used methods at our institution.

Patients and methods

In this single-center analysis (screening period 01/2019–01/23), we performed evaluation of intraoperatively collected data of neuromonitoring and mapping procedures in patients undergoing surgery for eloquently located supratentorial brain lesions. We complemented these data with sociodemographic data, clinical findings of preoperative and postoperative neurological status up to 6 months postoperative, and MRI studies for residual volume evaluation and neuropathological diagnosis. The study was approved by the local ethical committee (Study Number 2022-2242). Reporting of this study was according to the strengthening of the reporting of observational studies in epidemiology (STROBE) guidelines for observational studies (Supplementary Material).

Patients

Inclusion criteria for the present analysis were (1) surgical intervention in patients >18 years between January 2019 and January 2023. (2) Intraoperative monitoring and/or mapping devices were used. (3) The addressed lesion was located supratentorial. Procedures for posterior fossa or spine surgery were excluded. Availability of IONM or mapping data was also taken into consideration as to some extent some data were missing in some of the cases. However, missing of few data of individuals did not lead to exclusion. The number of procedures is given for all single analyses.

Data collection

General data

Sociodemographic data, neuropathological results, and information on medical/surgical history, if applicable, were taken from the local patient administration system. Surgical history was divided into four categories: (1) primary surgery, (2) recurrent surgery with neuropathological confirmation of recurrent disease, (3) recurrent surgery without neuropathological confirmation of recurrent disease, (4) 2nd-look surgery.

Neuropathological results if obtained before introduction of WHO 5 Classifications of Central Nervous System Tumors 2021 (20) were adapted according to the new classification.

Neurological outcome

Patients underwent initial neurological examination at timepoint of admission; this was defined as timepoint "pre-operative". Postsurgery patients underwent multiple examination, especially in case of any new neurological deficit. For the present analyses, we consistently used the examination at timepoint of dismission for definition of timepoint "postoperative". Furthermore, patients with new neurological deficit in the postoperative state were followed up at around 3 months ("3-month FU") and 6 months (6-month FU). Neurological examination was performed by different specially trained team members who also carried out awake procedure preparation and awake procedure testing intraoperatively. Our protocol includes a detailed questionnaire about general condition and health-related problems as well as a detailed neurological examination of cranial nerves, motoric and sensory testing, and, if applicable, speech testing as described further on.

Monitoring and mapping data

Monitoring and mapping data were obtained using the following technical devices with a described standard setup for different monitoring/mapping techniques.

ISIS Xpert and C2 Xplore (inomed Medizintechnik GmbH, Emmendingen, Germany, NeuroExplorer Software Version 6).

monitoring
- SSEP (ISIS only)
- TES-MEP (ISIS only)
- DCS MEP (ISIS only, four to six contact subdural strips).

mapping
- Cortical and subcortical with monopolar probe
- cortical and subcortical with bipolar probe

In cases where the C2 Xplore device was used, amperage of bipolar stimulation is given in the numbers of ISIS Xpert device as there are other technical nuances between those devices leading to different settings. For better comparison, we standardized the data obtained.

Ojemann Cortical Stimulator (Integra LifeSciences)

mapping
- Cortical and subcortical with bipolar probe

Awake status

Additionally, surgical protocols were screened for stimulation details and information on awake status and time of awake condition if applicable. Awake status was divided into following subcategories: "awake," "not adequately awake," "not awake". In cases where awake surgery was planned but not conducted due to non-compliance of patients or other reasons ("not adequately awake"), the procedure was categorized in awake surgery status for statistical analyses.

More detailed technical data such as monitoring/mapping devices and technical setups are reported in the Supplementary Information.

Choice of adequate mapping/monitoring or speech testing

At patients' presentation and when indication for surgery is set due to radiological and or clinical findings, we take a deep look into MRI scans and decide as a team of the leading surgeon and assistant surgeon as well as monitoring staff which technique to use in this special case. There has to be careful consideration of clinical and technical examination results in order to choose the right methods for the particular cases. The day before surgery, team members of the neurooncological team will talk to the patient through the procedure and perform neurological examination of the patient with evaluation of cranial nerves, motor and sensibility deficits, and general symptoms as headaches and perform a quick screening of speech disturbances. If there are any conspicuousness about speech deficits in the screening, the whole testing battery that we defined at our department is useful for efficient speech testing is performed. Details about the speech testing are described below.

Language testing

When language testing was performed, different tests were conducted with some items taken from Aachen Aphasia Test (21). Baseline testing was performed the day before surgery in order to have comparable data for intraoperative testing. Furthermore, all patients underwent postoperative testing at least at one time point in the postoperative state until they were discharged.

The following dimensions of language skills were tested pre-intra- and postoperatively in order to evaluate patients' speech affection:

Spontaneous speech

Patients are motivated to talk about a topic of their choice. This is done to test semantic aspects of the patients' speech, articulation, phonology, and syntax in general.

Token test

Testing language comprehension by showing and matching geometrical shapes of different sizes and colors.

Free reading

By reading the written language comprehension is tested.

Picture naming

Analysis of the designation of images of colors, objects, or actions.

Pyramids and palm trees test

Test for semantic memory used to detect language impairment. The test uses iconic images to determine the degree to which a subject can access meaning from pictures and words.

Surgeons' postoperative evaluation

In order to compare chosen methods with a postoperative reevaluation, we retrospectively performed inquiries of surgeons concerning assessment of obligatory monitoring/mapping in the present case. Obligatory modes were divided into the following 13 categories: monopolar stimulation, bipolar stimulation, combination monopolar/SSEP/MEP, combination monopolar SSEP/MEP/SE, combination monopolar/bipolar, combination monopolar/bipolar/SSEP/MEP, combination monopolar/bipolar/SSEP/MEP/SE, combination bipolar SSEP/MEP/SE, SSEP/MEP/SE only, monitoring/mapping (m/m) not needed, m/m not applicable/no resection, used methods inconclusive.

The chosen method for each specific case served as preoperative evaluation and was not documented separately.

Procedures were led by three senior surgeons with each more than 10–25 years of experience in the field of brain tumor surgery and intraoperative monitoring/mapping procedures. Senior surgeons were accompanied by residents with different experiences in brain tumor surgery.

Residual volume (MRI)

For evaluation of residual tumor volume, results of postoperative conducted MRIs were screened. All MRIs were carried out within 72 h postsurgery. We defined four groups for result description:

(1) intraoperatively defined macroscopic total resection and total resection in postoperative MRI, (2) intraoperatively defined macroscopic total resection and residual tumor volume in postoperative MRI, (3) intraoperatively defined macroscopic residual tumor volume and residual tumor volume in postoperative MRI, and (4) no MRI. Residual volume was either calculated by the reporting radiologist or if missing by the study team under usage of a volumetry tool in the local radiology information system (SECTRA Workstation 101, IDS7, Version 24.1, Sectra AB, Sweden, 2022). Results of residual tumor volume are stated in milliliters. Residual volumes less than 0.1 ml were defined as total resection.

Statistical analyses

All statistical analyses were conducted using IBM SPSS Statistics Version 26 (IBM Corporation, USA). Obtained results were statistically analyzed by using chi-square test for nominal variables. Group comparison was performed by univariate analyses of variance by (ANOVA), and *post-hoc* tests were adjusted using Bonferroni correction. Additionally, we carried out correlation calculation under usage of Pearson correlation. Statistical cutoff stated as p-value for all results was set at 0.05.

Results

General data

Overall, we included 437 surgical procedures in 400 patients (47% women, n = 188; 53% men, n = 212) over a period of 48 months in the present analyses. There were 27 patients who underwent surgery twice and five patients who had triple surgery during the observation period.

The mean age of patients at surgery was 56.6 years [± SD 14.9, range 20–90 years]. If patients underwent more than one surgical procedure, age at first recorded surgery was enclosed in the reported data.

68% of surgeries were primary cases (n = 296). One-third were recurrent surgeries with neuropathological confirmation of recurrent disease (n = 121). In 3% (n=12), recurrent surgery revealed no recurrent disease but showed other diagnoses, for example radio necrosis or reactive tissue changes. Eight (2%) procedures were labeled as second-look surgery in patients with significant residual tumor volume in postoperative MRIs due to different reasons.

One patient underwent primary surgery without mapping/monitoring and showed residual volume in the postoperative MRI; therefore, second-look surgery was advised. Four patients showed different impairments under subcortical stimulation (one patient anomia with 2 mA bipolar subcortical stimulation, one patient >70% deterioration in the picture naming test as well as under subcortical bipolar stimulation, one patient who underwent monopolar subcortical mapping with a 2-mA resection limit achieved, and one patient who showed a significant increase in SSEP latencies and therefore resection had to be stopped).

In two patients, primary surgery was finished under expectance of total resection with no link to functional limits. One patient underwent primary surgery under expectance of debulking as resection could only be achieved under speech monitoring, but speech testing preoperatively showed too much effect for reliable intraoperative testing. After recovery from primary surgery, awake surgery was evaluated as soon as possible; therefore, a second-look surgery with indented total resection was performed.

A total of 235 procedures were performed on lesions in the left hemisphere (54%), 196 were right-hemispheric tumors (45%), and 6 were located elsewhere (1%, rostrum, splenium, bifrontal).

Majority of neuropathological diagnoses were high-grade glioma (glioblastoma, IDH-wild type, MGMT methylation positive or negative) with 191 procedures (43.7%). IDH-mutant astrocytoma (WHO 1–4) and cerebral metastases were each diagnosed in 86 procedures (19.7%). Oligodendroglioma, IDH-mutant 1p/19q co-deletion (WHO 2 + 3), was diagnosed in 38 procedures (8.7%).

For a summary of cohorts' complete general data results, please refer to Table 1.

TABLE 1 Summary of cohorts' general data.

AGE (y)	
Mean	56.6 [SD ± 14.9]
Range	20–90
	n = 400
SEX	
Female	188
Male	212
DIAGNOSIS	
Astrocytoma IDH-mutant (2-3)	80
Astrocytoma IDH-mutant (4)	6
Glioblastoma, IDH-wild type (4) MGMT –	105
Glioblastoma, IDH-wild type (4) MGMT +	86
Oligodendroglioma (2-3)	38
Diffuse hemispheric glioma	1
Cerebral metastasis	86
Aggressive NHL	7
Meningioma	1
Atypical meningioma	4
High-grade neuroepithelial tumor	1
Low-grade neuroepithelial tumor	3
Dysembrioplastic neuroepithelial tumor	1
Ganglioglioma	2
Radiation necrosis	2
Reactive tissue changes	10
Chronic inflammatory tissue changes	1
Florid inflammatory demyelinating	
CNS lesion	1
Cerebral toxoplasmosis	2
SURGICAL HISTORY	
Primary surgery	296
Recurrent surgery with diagnosis of	121
recurrent disease	
Recurrent surgery without diagnosis of	12
recurrent disease	
Second look	8
LOCALIZATION	
Left hemisphere	235
Right hemisphere	196
Other	6

Awake status

Overall, 53% (n = 233) of procedures were conducted as awake surgery or were at least planned as awake surgery. Out of 233 planned awake procedures, 36 were categorized as "not awake adequately" (15%). Most frequent localizations for awake surgery in left hemispheric tumors were frontal, temporal, fronto-temporal, and parietal lesions, in the right hemisphere most commonly right parietal tumors followed by temporal and frontal lesions. Patients that underwent planned awake surgery were significantly younger

compared with the non-awake patients with a mean age of 52.3 years in the awake group vs. 60.2 years in the non-awake group ($p < 0.001$, Figure 1A).

Awake status and duration of awake status differed significantly according to the hemisphere. While lesions located in the left hemisphere were more frequently planned and conducted as awake procedure ($p < 0.001$, Figure 1B), the duration of the awake phase was significantly longer when performed on lesions in the right hemisphere (left = 69.6 min [± SD 25.2] vs. right = 80.8 min [± SD 27.1], $p = 0.023$, Figure 1C).

Intraoperative monitoring/stimulation data

TES-MEP and SSEP monitoring

SSEP monitoring was conducted in 234 and TES-MEP in 260 procedures. The range of stimulation for the present cohort for left and right medianus SSEP monitoring was 0.8–20 mA and for tibilias SSEP on the right side 0.5–30 mA and for the left side 1.7–30 mA. For MEP monitoring, maximum stimulation of 220 mA at a band-pass filter between 250 and 500 Hz or a maximum of 100 mA at 500 Hz was used. For upper extremities, the range of stimulation was 40 to 80 mA and for lower extremities 60–110 mA in the present cohort.

SSEP and MEP monitoring *via* SE was conducted in 172 cases (Figure 2). SSEP monitoring was significantly more frequently used in left hemispheric lesions (n = 136 vs. 94, $p = 0.007$), whereas usage of TES-MEP did not significantly differ concerning localization (Figure 3). SSEP monitoring was significantly more often used in asleep surgery status ($p < 0.001$ SSEP, Figure 4).

Furthermore, we analyzed EEG documentation for intraoperative seizures; EEG data were available for 260 patients. Seizures were observed in 22 patients either *via* EEG only or by EEG and clinical determination (8%). There were 13 patients with seizure occurrence (59%) who underwent an awake procedure. Preoperative seizure did not increase the risk for intraoperative seizures ($p = 0.854$), but bipolar stimulation significantly correlated with occurrence of intraoperative seizures ($p = 0.008$) whereas monopolar stimulation did not.

Monopolar/bipolar mapping

Monopolar mapping was conducted in 348 procedures (Figure 2). Stimulation ranged from 0.5 to 20 mA. Epidural stimulation in 127 cases (36%) was conducted with a mean current of 10.6 mA [± SD 4.2]. In the vast majority of surgeries, a cortical stimulation was performed with 329 cases (96%) and a mean current of 7.6 mA [± SD 4.4]; subcortical stimulation was

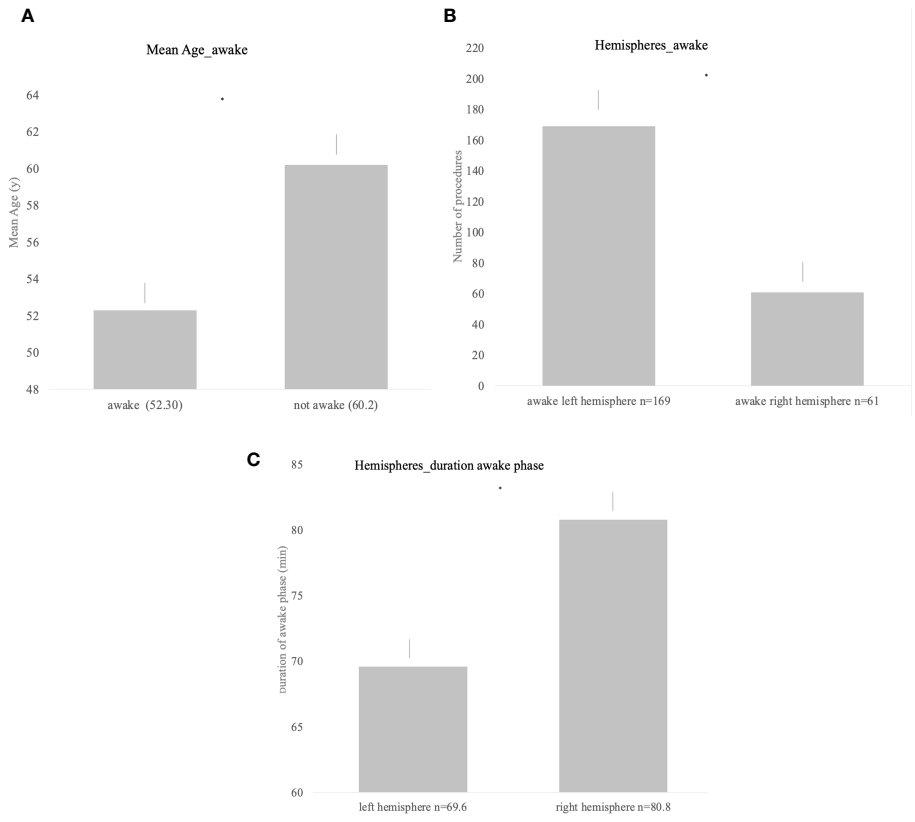

FIGURE 1
(A) Significant difference in the mean age and awake status ($p < 0.001$). **(B)** Awake status for procedures of both hemispheres; left hemispheric lesions were significantly more often operated under awake settings ($p < 0.001$). **(C)** Duration of the awake phase for both hemispheres showing significantly longer awake duration in right hemispheric lesions ($p = 0.0023$).

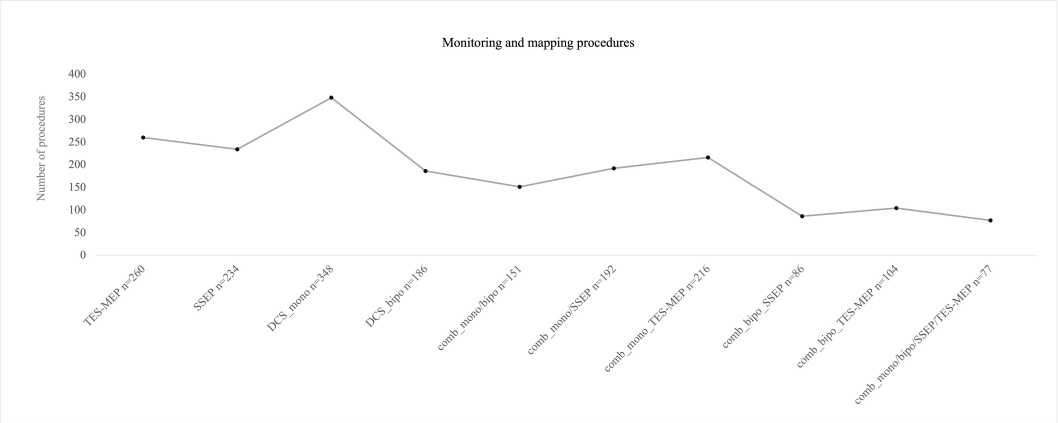

FIGURE 2
Number of procedures for different monitoring/mapping modes that were used intraoperatively. Mostly monopolar stimulation was used. The combination ("comb") of monopolar and bipolar mapping plus monitoring was the least combination that was used intraoperatively.

found in 302 surgeries (87%) with a mean current of 3.4 mA [± SD 3.2], ranging from 0.2 to 20 mA.

The proportion of awake procedures in monopolar mapping procedures was 52% with 181 cases (Figure 4).

There were 186 procedures conducted under usage of bipolar stimulation (Figure 2). Bipolar cortical mapping was found in 91% (n = 169) with a mean current of 2.2 mA [± SD 1.4, range 1–3 mA] and subcortical stimulation in 73% (n = 136) with a mean current of 2.1 mA [± SD 1.0, range 0.8–3 mA]. In the awake setting, 169 patients underwent bipolar stimulation (91%, Figure 4). If clinical evaluation, in case of awake surgery, or MEP/SSEP monitoring allowed so, resection was stopped at a minimum of 1 mA when performing subcortical mapping.

In 151 cases, both monopolar and bipolar stimulation were performed, thereof a total of 91% (n = 136) proceeded in an awake setting (Figure 2).

During both mapping procedures, awake surgery status was more frequently planned than asleep procedures (monopolar stimulation $p = 0.026$, bipolar stimulation $p \leq 0.001$, Figure 4).

Localization did not correlate significantly with use of monopolar mapping; however, bipolar mapping was used more frequently for left hemispheric tumors ($p \leq 0.001$, Figure 3).

Surgeons' evaluation of obligatory stimulation mode

Most frequently monopolar mapping (n= 172), bipolar mapping (n= 98), and combination of monopolar/bipolar mapping (n= 85) were designated as obligatory stimulation modes. In only 10 procedures, combination of all mapping and monitoring techniques was seen as obligatory (four lesions left frontal, temporal and fronto-temporal, six lesions right fronto-parietal, parietal and fronto-temporal); however, SSEP/MEP monitoring was seen obligatory in around 16% of all procedures, independently from mapping procedures that were performed, but most commonly in right hemispheric lesions with monopolar stimulation combined with SSEP/MEP monitoring.

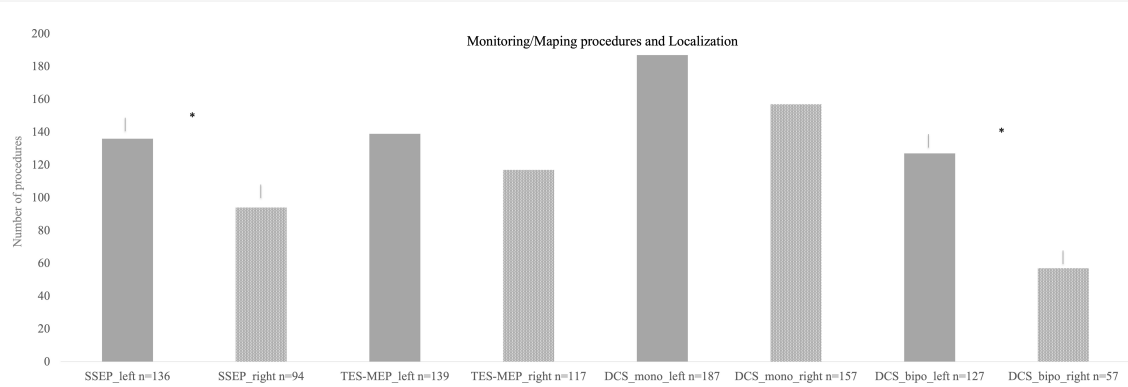

FIGURE 3
Different monitoring and mapping procedures separated according to localization. Monopolar stimulation was mostly used on left hemispheric lesions followed by monopolar stimulation on right hemispheric procedures. The least used method was bipolar stimulation for right hemispheric lesions. * = significant results.

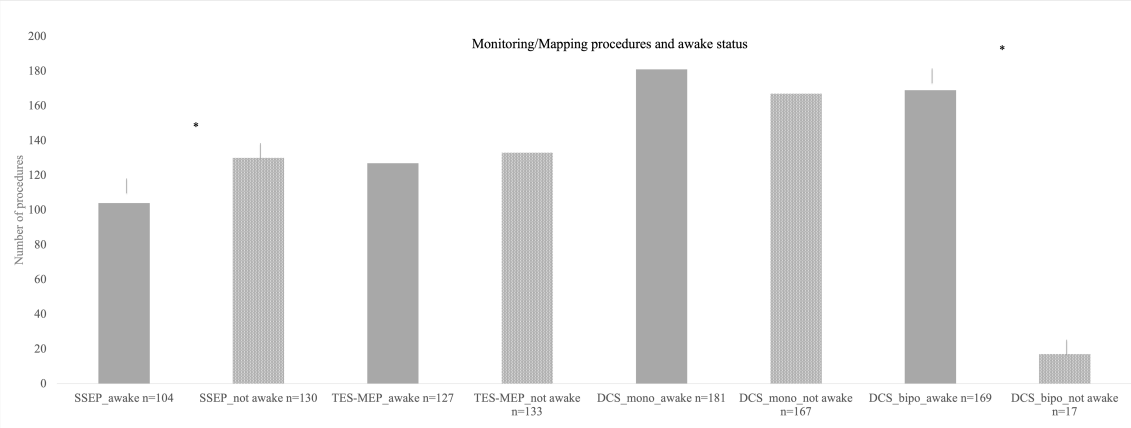

FIGURE 4
Different monitoring and mapping procedures here parted in accordance by awake status. Here, also monopolar mapping was most commonly used either awake or asleep with no significant difference in number of procedures. Bipolar stimulation in the asleep status was used least in the cohort. * = significant results.

In eight cases, SSEP/MEP monitoring only was evaluated as required without any mapping procedure. Three procedures were performed without any requirement of monitoring or mapping due to intraoperative non-functional localization (0.7%). Two surgeries were terminated without any intervention. In one procedure, all methods used were rated as inconclusive with no benefit for safe resection (Figure 5).

A significant correlation between localization of tumor and postoperative stated obligatory stimulation modus was found ($p = < 0.001$).

Monopolar obligatory mapping was found to be essential in right hemispheric tumors more often than left hemispheric ones; on the contrary, bipolar mapping and combination of monopolar/bipolar mapping were evaluated as essential more often on left hemispheric lesions.

Incongruency of the obligatory method according to surgeons' evaluation and the intraoperatively used method was more often seen with obligatory bipolar mapping (23% bipolar mapping, 10% for monopolar mapping).

Clinical outcome

In 279 cases, preoperative deficits were noticed (64%), mostly motor deficits (n = 70), speech disorders (n = 58), affection of vision and or cranial nerves (n = 28), and behavioral changes (n = 28). Additionally, preoperative seizures were observed in 49 cases (11%).

A new postoperative neurological impairment was seen in 57 patients (13%, Figure 6); seven patients died shortly after resection. However, deaths were not directly related to surgical complications. Majority of neurological deficits (61%) were seen after procedures on left hemispheric tumors, and right hemispheric surgeries led to postoperative new deficits in 35% of the cases. 4% occurred in other locations.

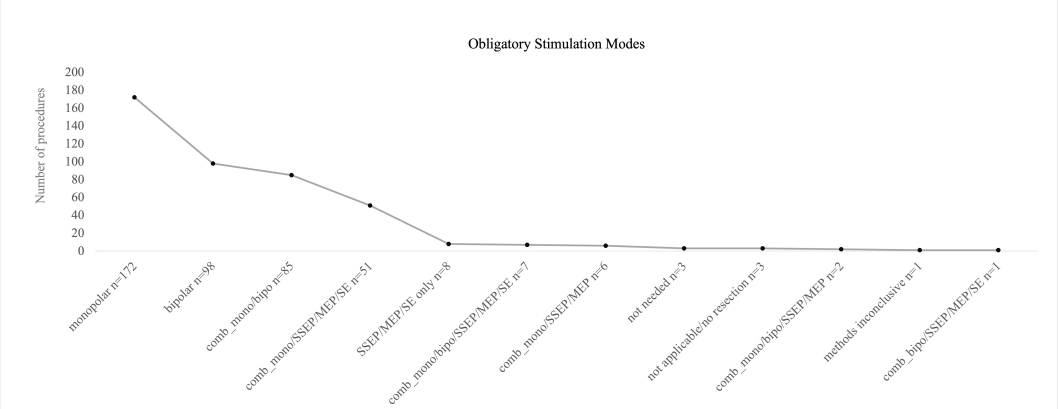

FIGURE 5
Postoperative evaluation of obligatory mapping or monitoring modes by the operating surgeon. Monopolar, bipolar, and a combination of both mapping procedures were mostly stated as "obligatory" for the preceding surgery. Full technical equipment with a combination of mapping and monitoring was less frequently recalled as obligatory.

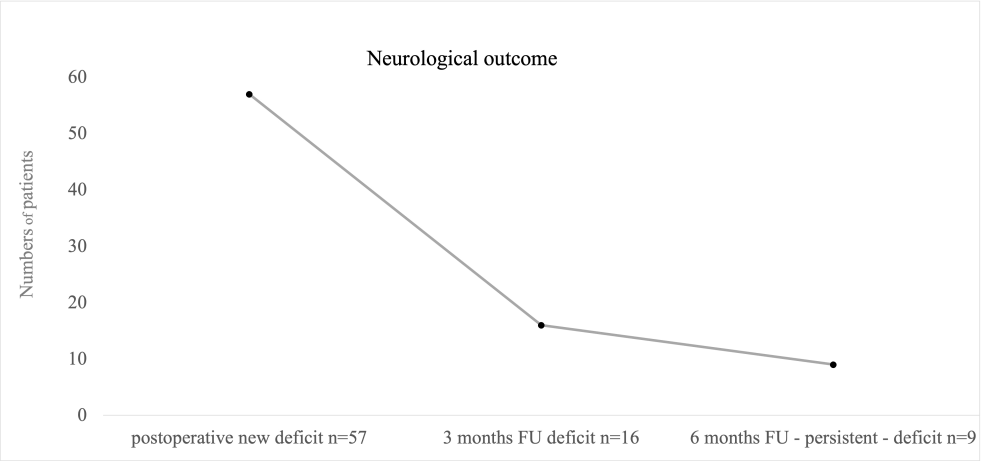

FIGURE 6
Illustrating cases with postoperative and persistent new neurological deficits. We defined "persistent deficit" as neurological impairment after 6 months postoperative. Nine patients suffered from persistent deficits after surgical intervention; mostly permanent speech disorders were seen.

A total of 24 patients suffered from high-grade hemiparesis, one patient showed sensory deficits as new and leading symptoms, 22 patients presented a new speech disorder affecting either sensory or motoric aspects of speech, and global aphasia as the combination of both was seen in one patient. Three patients presented new impairment in facial motoric or vision. Six patients had a combined deficit of speech and motor function.

At first follow-up after 3 months postoperative, persistent neurological deficits in 16 cases out of 56 were reported (4%, n = 411, Figure 6). At 6 months of follow-up, neurological deficits were still seen after nine procedures, an overall of 2% concerning all procedures, and were defined as permanent deficit by that time (n= 406, Figure 6) with five patients with persistent motor impairment and four speech disturbances. Overall, 13 patients had died within 6 months postsurgery (2%).

Permanent deficits occurred independently from diagnosis ($p = 0.958$) or localization ($p = 0.271$). Significantly increased risk of death was seen in cases with preoperative neurological deficit ($p = 0.030$). Surgical status "awake" significantly correlated with direct postoperative speech deficits not motor deficits ($p = 0.003$). Overall evaluation of persistent deficit after 6 months however revealed no significant influence by awake or asleep status ($p = 0.593$).

Correlation of stimulation/monitoring modes and postoperative neurological deficit revealed no significant results for SSEP monitoring ($p = 0.341$), TES-MEP ($p = 0.659$), and bipolar stimulation ($p = 0.061$), but monopolar stimulation with $p = 0.007$. Permanent deficit at 6 months did also only significantly correlate with usage of monopolar stimulation ($p = 0.012$). At last, neurological impairment and obligatory stimulation mode turned out to be not significantly related ($p = 0.109$).

We examined postoperative MRI scans of patients who experienced new neurological impairments after surgery. In our analysis, we identified indications of infarction or postoperative bleeding in 21 MRI scans (comprising 17 cases of infarction and 4 cases of bleeding). Notably, most infarctions were very and relatively small (n = 15) and are not assumed to be a potential reason for neurological impairment. In two patients, the infarction may have contributed to their postoperative and later permanent deficits. In a specific case, a patient exhibited a basal ganglia infarction and subsequently experienced postoperative motor deficits. Additionally, in the second patient, a relatively extensive territorial infarction occurred, leading to motor deficits as well.

Resection results

For evaluation of resection results, 417 MRIs were available. In 20 cases, postoperative MRI was renounced due to biopsy-only procedures or postoperative bleeding with no reasonable MRI results expected. In 50% of the procedures, a total resection was achieved (n = 209); in 149 (36%) procedures, an already intraoperatively expected residual volume was proven by postoperative MRI, mostly in left fronto-temporal and straight left temporal lesions. In 14% of the cases, intraoperative evaluation of total resection failed proof by postoperative MRI. Overall, 268 surgeries were evaluated as total resection procedures by the surgeons; however, in 59 cases, postoperative MRI revealed residual tumor volume in those cases with a mean residual volume of 0.41 ml [± SD 0.73, range 0.1–4.8 ml] (Figure 7).

Discussion

The present study summarizes neurological outcome and resection results of 437 procedures as well as risk factors for neurological impairment after surgical procedures in eloquent brain areas when combining all modalities of monitoring and mapping procedures for tumor resection of infiltrating lesions.

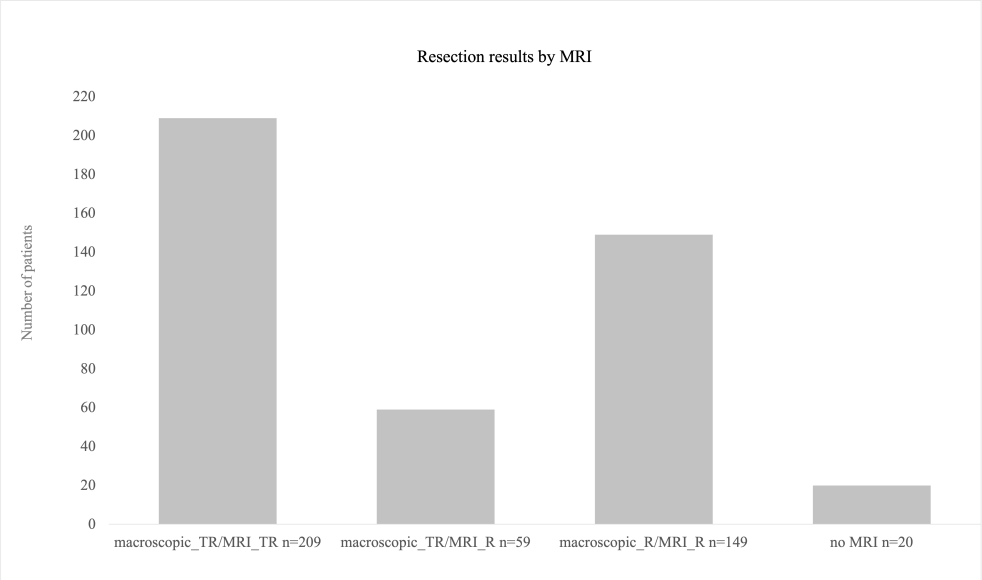

FIGURE 7
Resection results as obtained by postoperative MRI scans. A total of 209 procedures were finished with total resection. In 59 cases, surgeons' evaluation was total resection intraoperatively but nevertheless post-OP MRI revealed residual volume (mean 0.4 ml). A total of 20 procedures were biopsies only where no MRI postoperatively was conducted.

Stimulation procedures and neurological outcome

Monopolar stimulation was conducted in the vast majority of procedures. Motor pathway mapping with cortical and subcortical monopolar stimulation was performed on lesions in both hemispheres with no significant difference. This technique is widely used for intraoperative mapping of the motor cortex (M1) and cortico-spinal tract (22, 23). Mapping of motor functions can also be carried out using bipolar stimulation (12, 24); however, it is by far not as reliable as monopolar-induced MEPs or TES-MEP.

In our clinic, bipolar stimulation for motor mapping was only performed additionally to monopolar cortical mapping in cases when monopolar mapping revealed MEP answers in more than one gyrus or if obtained MEPs showed some inconsistences. Bipolar mapping was significantly more often used on left hemispheric lesions for language mapping procedures, which is also described as standard procedure in the literature (11, 25); however, for language mapping, patients need to be awake during surgery. In our cohort, the majority of procedures were performed in the awake status and hereof the majority of lesions were located on the left hemisphere. SSEP monitoring was also used more often in left hemispheric lesions, which the authors think is a result of the majority of lesions located left hemispheric; at least 54% of the procedures were performed on lesions located in the left hemisphere. 31% of the right hemispheric lesions were also operated on in the awake status. Our group mainly addressed right hemispheric lesions under monopolar stimulation in the awake status when fine motor skills or complex motor tasks had to be monitored during surgery.

Major focus when choosing individual mapping and or monitoring modes lies in the neurological outcome. Maximum resection results shall be achieved under maximum safe circumstances concerning motor and speech integrity of the patient. New neurological deficits after brain surgery negatively affect quality of life in glioma patients, which has been discussed more frequently in the past years to be defined as an important prognostic factor (26), and can contribute to a shorter overall survival at least in patients with glioblastoma (27). Furthermore, a delay in adjuvant therapies due new postoperative motor impairment contributes to a decrease in life expectancy. Thus, there is consensus about focusing on preservation of functional integrity during surgical therapy of brain tumors especially high-grade gliomas, as they cannot be cured by surgery (28).

In our study with a large number of procedures, we only found permanent new neurological deficits in 2% of the procedures. Viagano et al. published similar results with new permanent deficits in 1.9% of patients when combining TES and DCS high-frequency stimulation in asleep procedures for tumors affecting motor pathways (29). Rossi et al. studied outcomes in 102 patients with tumors affecting the motor cortex when using different stimulation paradigms for high-frequency stimulation. In the standard approach group, using the same paradigm for monopolar stimulation as we did in our study, also 2% of the patients suffered from permanent neurological impairment (30). A meta-analysis including 90 publications with over 8,000 glioma patients revealed slightly more permanent neurological deficits with 3.4% of surgeries under mapping procedures in eloquent procedures (31). The same result with 3.4% new deficits were achieved in a study by Gogos et al. (16), comprising 58 patients with diagnosed glioma and lesions located near motor pathways.

In patients with direct postoperative neurological impairment, we found two patients in which intraoperatively an increase of SSEP

latencies was seen. In three patients, speech testing showed difficulties due to lack of patients' compliance resolving in a new deficit in the postoperative phase. In the other cases, there were no warning signs such as loss of SSEP or MEP signals, but majority of patients that underwent surgery in the awake status showed fine impairment during intraoperative testing; therefore, resection was stopped under careful consideration of the clinical findings.

None of the patients with permanent deficits underwent surgery with special intraoperative monitoring or mapping events. Five patients suffered from speech disorders, and four patients suffered from new high-grade hemiparesis. Two patients showed minor territorial infarcts in the postoperative MRI; it must be assumed that these were causal for the new and then in the follow-up also permanent neurological deficit (hemiparesis).

There are two questions to be raised in the light of the certainly very low persistent deficits in our cohort. On the one hand, the question is whether the cohorts' localizations really were as functional as assumed from the MRI. We found that only in 0.7% of the procedures, there were only negative mapping results or there was no MEP or SSEP signal to be obtained during the surgical procedure. The authors concluded that in these cases, the tumor was not functionally located. However, this is a very small number given more than 99% of the surgeries with positive feedback and useful monitoring/mapping procedures as evaluated postoperatively by the surgeons. On the other hand, heterogeneity of our cohort might have contributed to the slightly better result as there are different growth and therefore infiltration patterns between tumor entities resulting in different complexities of functional preservation during resection. Infiltrating tumors might be relevantly of higher risk for postoperative deficits due to difficulties in resection limits. In our cohort, the infiltrating tumors were the majority, but there were a not insignificant number of patients with tumor entities that are known for not infiltrating but extruding growth patterns, which is different to the meta-analysis of de Witt et al. as they only enclosed glioma patients with infiltrating growth patterns. In order to evaluate the significance of neuropathological diagnoses, we correlated diagnoses with neurological outcome and found no significant correlation. Thus, for our cohort, we did not see a link from diagnoses to infiltration patterns, resection, and permanent deficits.

When searching for determinants that contributed to the patients' outcome, we found that surgical procedures on left hemispheric lesions were more often noticed to cause postoperative neurological deficits than right hemispheric procedures. Nevertheless, this did not result in permanent new neurological deficits at 6 months FU. However, nine patients suffered from permanent deficit after 6 months post-op, four had recurrent surgery, and five underwent primary surgery. 67% were left hemispheric lesions with five patients suffering from speech disorder and one patient suffering from motor impairment in a left-parietal lesion. Interestingly, we found a strong correlation of preoperative neurological deficit and death within the first 6 months postsurgery.

In our study, majority of left hemispheric lesions were operated in the awake status. Awake procedures are discussed to improve safety of resection (24, 32). Although we found that there was a significant correlation between awake surgical status and direct postoperative speech deficit, which was not seen for motor impairment, in our cohort and this correlation was seen independently from the localization of the lesion, the overall 6-month evaluation of persistent deficits was not significantly influenced by the surgical status. Early postoperative overall neurological deterioration was only seen when using monopolar stimulation; all other monitoring or mapping techniques did not significantly influence the neurological outcome. However, again this finding was not verifiable at the 6-month FU and might have been influenced by the circumstance that monopolar stimulation has been used in nearly 80% of the procedures compared with only 38% bipolar stimulation; we think that the wider exposure of monopolar stimulation might have increased the probability of postoperative effect. Other statistically significant cofounders were not found.

Intraoperative seizures

Intraoperative seizures induced by DCS are commonly seen and discussed complications in the literature. Studies provide a wide range of stimulation-induced seizures with reported rates in the low single-digit up to more than 50%, leading to an increase of neurological postoperative impairment (33–35). Part of the discussion are predictors for intraoperative seizures. Preoperative seizures tend to be risk factors for stimulation-induced intraoperative seizures (24, 33, 36). In our cohort, we recorded seizures in 8% of the procedures, with none of the patients suffering from preoperative seizures. All patients were therapy-naïve concerning anticonvulsants. We were not able to reproduce findings of correlation between preoperative and intraoperative seizures; however, in our cohort bipolar stimulation expectedly correlated with incidence of stimulation-induced seizures, whereas stimulation intensity did not significantly influence the incidence of intraoperative seizures.

Evaluation of surgeons

One of the major aims of this study was to correlate preoperatively chosen monitoring or mapping techniques with postoperative evaluation of the techniques used by the surgeon. We found that in 73% procedures, the postoperative evaluation of obligatory stimulation mode matched the preoperatively defined methods to be used intraoperatively. The localization of the tumor correlated with postoperative surgeons' evaluation, and as expected, monopolar obligatory mapping was found to be essential more often in right hemispheric lesions, whereas bipolar mapping and combined monopolar/bipolar mapping were more often evaluated as essential for tumors in the left hemisphere. Interestingly, SSEP/MEP monitoring only or in combination with DCS was only seen obligatory in 15% with a rising number of obligatory evaluations after engagement of new monitoring staff from 11 procedures that were evaluated as obligatory monitored by SSEP/MEP to 25 procedures (per year). The authors discussed that and found that

there either must be a bias due to availability of more monitoring staff or procedures became more demanding with high-risk vascular involvement. Nevertheless, there was no correlation between stated obligatory stimulation mode and postoperative neurological outcome. Interestingly, more incongruence between the evaluated obligatory method and actual technique used was seen with bipolar mapping. This might be a result of non-adequate awake patients with left hemispheric lesions that needed to undergo bipolar mapping due to localization, but mapping or adequate testing was not able to be performed due to noncompliance to awake situation or seizures at the beginning.

Resection result

The extent of resection and its impact on overall survival (OS) in patients suffering from glioma are widely discussed. Different thresholds for impact on OS were published ranging from 60% to 98% (37–40). Also, in oligodendroglioma and metastasis, the extent of resection seems to have a significant impact on survival (41, 42).

Total resection, meaning no detectable contrast enhancement in the post-OP MRI, was achieved in 50% of the procedures. There were 20 procedures performed as biopsy without post-OP MRI. In 149 (36%) procedures, the functional limit was achieved intraoperatively, as defined by monitoring and or mapping results. In 59 (14%) procedures, surgeons assumed total resection but post-OP MRI showed residual tumor volume with a very low mean residual volume of 0.41 ml and a maximum residual volume of 4.8 ml in one case. In our cohort, total resection was achieved in arguably fewer cases than in comparable publications (31), but there are some points that led to this result. Firstly, functional limits were achieved intraoperatively, in more than one-third of procedures. Achievement of total resection would have meant neurological deterioration for the patient, something that has to be avoided in the light of survival benefits. Secondly, using intraoperative tools for functional preservation and then deciding intraoperatively to maximize resection regardless of the mapping results would fail the surgical aim. Thirdly, in the procedures that were evaluated as total resection but nonetheless showed residual volume in the post-OP MRI, residual volume was marginal with a mean of 0.4 ml. Concerning comparable publications, a residual tumor volume up to 8 cm^3 could be acceptable for an effect on survival that can still be achieved at least for gliomas (40). Furthermore, with this study, we searched for impacts on resection results but found that there was no significant correlation either between monitoring/mapping results or between the resection result and neurological outcome. However, we did not analyze survival data of the present cohort. Nevertheless, in consideration of already published literature, we assume that the very much marginal residual volume did not have any negative impact on patients' OS.

Limitation

The lacking survival data might be a limitation to the study in order to comprehend the given resection results. Nonetheless, as this was not the focus of the present analysis, the authors renounced this fractional analysis. Additionally in some cases, information on stimulation modes or thresholds could not be obtained from all sources that were available to the authors. However, as there were only minor missing data, we do not think that this would have affected the results significantly.

In the context of determining and evaluating the extent of resection in patients with glioblastoma, another limitation might be the lack of an assessment of the influence of 5-ALA on the resection. However, a meaningful statistical analysis in the reported cohort was not feasible because all patients with suspected or confirmed brain tumors, and at least at the beginning of the observation period, patients suspected of cerebral metastasis, received 5-ALA. Therefore, group comparisons regarding the extent of resection for this cohort were not applicable. We clearly assume that, as reported in the literature, resection under 5-ALA had a positive impact on conduction of resection. However, it is important to consider that the current cohort consists of highly functionally located tumors. Even though resection was performed under fluorescence guidance, and residual fluorescence may have been visible, functional assessment was more decisive for the extent of resection.

Conclusion

In the light of the important role of surgical procedures in the therapy process for brain tumor lesions and the superior aim to preserve functionality of the patients, adequate planning of intraoperative required monitoring or mapping techniques is of highest priority. Deciding which intraoperative mapping and or monitoring procedure is best for the patient is highly individual. The choice of a certain technique mainly depends on localization and experience of the surgeon. With the present study, we demonstrate operability of highly functional infiltrating brain lesions of various localizations without major neurological impairment under usage of IONM and mapping techniques. We were able to give an overview of pitfalls and strengths of the different technical procedures and if, respectively, how they correlate with postoperative neurological outcome and resection results. Furthermore, we retrospectively included the surgeons' view and evaluated the impact of a possibly existing mismatch between preoperative and postoperative assessment of individual technical considerations for each procedure. With this evaluation, we were able to show that certain techniques might not be useful for every case and in the light of optimalization of resources not required for safe resections in every cases. These results shall contribute to a practical but high-quality decision-making process for every surgeon addressing eloquent brain lesions.

Data availability statement

The raw data supporting the conclusions of this article will be made available by the authors, without undue reservation.

Ethics statement

The studies involving humans were approved by Ethikkommission Düsseldorf, Heinrich-Heine Universität. The studies were conducted in accordance with the local legislation and institutional requirements. The ethics committee/institutional review board waived the requirement of written informed consent for participation from the participants or the participants' legal guardians/next of kin because Local laws permit usage of clinical data that was obtained during routine procedures without informed consent.

Author contributions

FS-B contributed to the design and implementation of the research, performed data collection and designed statistical analysis of the results and wrote the manuscript. MR contributed to the design of the research and data collection and to the writing of the manuscript. MS designed and directed the project and contributed to the writing of the manuscript. All authors contributed to the article and approved the submitted version.

Funding

The author(s) declare financial support was received for the research, authorship, and/or publication of this article. The first author will receive funding of the publication fee. This funding is subject to acceptance of the manuscript. Invoice will be paid by university directly.

Acknowledgments

The statistical analyses were performed with the support of Oliver Radke, Heinrich-Heine University Düsseldorf.

Conflict of interest

The authors declare that the research was conducted in the absence of any commercial or financial relationships that could be construed as a potential conflict of interest.

Publisher's note

Supplementary material

The Supplementary Material for this article can be found online at: https://www.frontiersin.org/articles/10.3389/fonc.2023.1235212/full#supplementary-material

References

1. Stummer W, Reulen HJ, Meinel T, Pichlmeier U, Schumacher W, Tonn JC, et al. Extent of resection and survival in glioblastoma multiforme: identification of and adjustment for bias. *Neurosurgery* (2008) 62(3):564–76. doi: 10.1227/01.neu.0000317304.31579.17

2. Sanai N, Polley MY, McDermott MW, Parsa AT, Berger MS. An extent of resection threshold for newly diagnosed glioblastomas. *J Neurosurg* (2011) 115(1):3–8. doi: 10.3171/2011.2.JNS10998

3. Brown TJ, Brennan MC, Li M, Church EW, Brandmeir NJ, Rakszawski KL, et al. Association of the extent of resection with survival in glioblastoma: A systematic review and meta-analysis. *JAMA Oncol* (2016) 2(11):1460–9. doi: 10.1001/jamaoncol.2016.1373

4. Berger MS, Deliganis AV, Dobbins J, Keles GE. The effect of extent of resection on recurrence in patients with low grade cerebral hemisphere gliomas. *Cancer* (1994) 74(6):1784–91. doi: 10.1002/1097-0142(19940915)74:6<1784::AID-CNCR2820740622>3.0.CO;2-D

5. Smith JS, Chang EF, Lamborn KR, Chang SM, Prados MD, Cha S, et al. Role of extent of resection in the long-term outcome of low-grade hemispheric gliomas. *J Clin Oncol* (2008) 26(8):1338–45. doi: 10.1200/JCO.2007.13.9337

6. Prabhu RS, Press RH, Patel KR, Boselli DM, Symanowski JT, Lankford SP, et al. Single-fraction stereotactic radiosurgery (SRS) alone versus surgical resection and SRS for large brain metastases: A multi-institutional analysis. *Int J Radiat Oncol Biol Phys* (2017) 99(2):459–67. doi: 10.1016/j.ijrobp.2017.04.006

7. Patchell RA, Tibbs PA, Walsh JW, Dempsey RJ, Maruyama Y, Kryscio RJ, et al. A randomized trial of surgery in the treatment of single metastases to the brain. *N Engl J Med* (1990) 322(8):494–500. doi: 10.1056/NEJM199002223220802

8. Ferracci FX, Duffau H. Improving surgical outcome for gliomas with intraoperative mapping. *Expert Rev Neurother* (2018) 18(4):333–41. doi: 10.1080/14737175.2018.1451329

9. Keles GE, Lundin DA, Lamborn KR, Chang EF, Ojemann G, Berger MS. Intraoperative subcortical stimulation mapping for hemispherical perirolandic gliomas located within or adjacent to the descending motor pathways: evaluation of morbidity and assessment of functional outcome in 294 patients. *J Neurosurg* (2004) 100(3):369–75. doi: 10.3171/jns.2004.100.3.0369

10. Kombos T, Suess O, Ciklatekerlio O, Brock M. Monitoring of intraoperative motor evoked potentials to increase the safety of surgery in and around the motor cortex. *J Neurosurg* (2001) 95(4):608–14. doi: 10.3171/jns.2001.95.4.0608

11. Bello L, Gallucci M, Fava M, Carrabba G, Giussani C, Acerbi F, et al. Intraoperative subcortical language tract mapping guides surgical removal of gliomas involving speech areas. *Neurosurgery* (2007) 60(1):67–80. discussion 80-62. doi: 10.1227/01.NEU.0000249206.58601.DE

12. Duffau H, Capelle L, Denvil D, Sichez N, Gatignol P, Taillandier L, et al. Usefulness of intraoperative electrical subcortical mapping during surgery for low-grade gliomas located within eloquent brain regions: functional results in a consecutive series of 103 patients. *J Neurosurg* (2003) 98(4):764–78. doi: 10.3171/jns.2003.98.4.0764

13. Tomasino B, Guarracino I, Ius T, Skrap M. Continuous real-time neuropsychological testing during resection phase in left and right prefrontal brain tumors. *Curr Oncol* (2023) 30(2):2007–20. doi: 10.3390/curroncol30020156

14. Duffau H. Awake surgery for nonlanguage mapping. *Neurosurgery* (2010) 66(3):523–8. discussion 528-529. doi: 10.1227/01.NEU.0000364996.97762.73

15. Ruis C. Monitoring cognition during awake brain surgery in adults: A systematic review. *J Clin Exp Neuropsychol* (2018) 40(10):1081–104. doi: 10.1080/13803395.2018.1469602

16. Gogos AJ, Young JS, Morshed RA, Avalos LN, Noss RS, Villanueva-Meyer JE, et al. Triple motor mapping: transcranial, bipolar, and monopolar mapping for supratentorial glioma resection adjacent to motor pathways. *J Neurosurg* (2020) 134(6):1728–37. doi: 10.3171/2020.3.JNS193434

17. Seidel K, Szelényi A, Bello L. Chapter 8 - Intraoperative mapping and monitoring during brain tumor surgeries. In: Nuwer MR, MacDonald DB, editors. *Handbook of Clinical Neurology*. Amsterdam: Elsevier (2022). p. 133–49.

18. Schucht P, Seidel K, Jilch A, Beck J, Raabe A. A review of monopolar motor mapping and a comprehensive guide to continuous dynamic motor mapping for resection of motor eloquent brain tumors. *Neurochirurgie* (2017) 63(3):175–80. doi: 10.1016/j.neuchi.2017.01.007

19. Verst SM, de Aguiar PHP, Joaquim MAS, Vieira VG, Sucena ABC, Maldaun MVC. Monopolar 250-500Hz language mapping: Results of 41 patients. *Clin Neurophysiol Pract* (2019) 4:1–8. doi: 10.1016/j.cnp.2018.11.002

20. Louis DN, Perry A, Wesseling P, Brat DJ, Cree IA, Figarella-Branger D, et al. The 2021 WHO classification of tumors of the central nervous system: a summary. *Neuro Oncol* (2021) 23(8):1231–51. doi: 10.1093/neuonc/noab106

21. Huber W, Poeck K, Willmes K. The aachen aphasia test. *Adv Neurol* (1984) 42:291–303.

22. Schucht P, Seidel K, Beck J, Murek M, Jilch A, Wiest R, et al. Intraoperative monopolar mapping during 5-ALA-guided resections of glioblastomas adjacent to motor eloquent areas: evaluation of resection rates and neurological outcome. *Neurosurg Focus* (2014) 37(6):E16. doi: 10.3171/2014.10.FOCUS14524

23. Bello L, Riva M, Fava E, Ferpozzi V, Castellano A, Raneri F, et al. Tailoring neurophysiological strategies with clinical context enhances resection and safety and expands indications in gliomas involving motor pathways. *Neuro Oncol* (2014) 16 (8):1110–28. doi: 10.1093/neuonc/not327

24. Hervey-Jumper SL, Li J, Lau D, Molinaro AM, Perry DW, Meng L, et al. Awake craniotomy to maximize glioma resection: methods and technical nuances over a 27-year period. *J Neurosurg* (2015) 123(2):325–39. doi: 10.3171/2014.10.JNS141520

25. Ojemann G, Ojemann J, Lettich E, Berger M. Cortical language localization in left, dominant hemisphere. An electrical stimulation mapping investigation in 117 patients. 1989. *J Neurosurg* (2008) 108(2):411–21. doi: 10.3171/JNS/2008/108/2/0411

26. Cheng JX, Zhang X, Liu BL. Health-related quality of life in patients with high-grade glioma. *Neuro Oncol* (2009) 11(1):41–50. doi: 10.1215/15228517-2008-050

27. McGirt MJ, Mukherjee D, Chaichana KL, Than KD, Weingart JD, Quinones-Hinojosa A. ASSOCIATION OF SURGICALLY ACQUIRED MOTOR AND LANGUAGE DEFICITS ON OVERALL SURVIVAL AFTER RESECTION OF GLIOBLASTOMA MULTIFORME. *Neurosurgery* (2009) 65(3):463–70. doi: 10.1227/01.NEU.0000349763.42238.E9

28. Weller M, van den Bent M, Preusser M, Le Rhun E, Tonn JC, Minniti G, et al. EANO guidelines on the diagnosis and treatment of diffuse gliomas of adulthood. *Nat Rev Clin Oncol* (2021) 18(3):170–86. doi: 10.1038/s41571-020-00447-z

29. Viganò L, Callipo V, Lamperti M, Rossi M, Conti Nibali M, Sciortino T, et al. Transcranial versus direct electrical stimulation for intraoperative motor-evoked potential monitoring: Prognostic value comparison in asleep brain tumor surgery. *Front Oncol* (2022) 12:963669. doi: 10.3389/fonc.2022.963669

30. Rossi M, Nibali MC, Viganò L, Puglisi G, Howells H, Gay L, et al. Resection of tumors within the primary motor cortex using high-frequency stimulation: oncological and functional efficiency of this versatile approach based on clinical conditions. *J Neurosurg* (2019) p:1. doi: 10.3171/2019.5.JNS19453

31. De Witt Hamer PC, Robles SG, Zwinderman AH, Duffau H, Berger MS. Impact of intraoperative stimulation brain mapping on glioma surgery outcome: a meta-analysis. *J Clin Oncol* (2012) 30(20):2559–65. doi: 10.1200/JCO.2011.38.4818

32. Taylor MD, Bernstein M. Awake craniotomy with brain mapping as the routine surgical approach to treating patients with supratentorial intraaxial tumors: a prospective trial of 200 cases. *J Neurosurg* (1999) 90(1):35–41. doi: 10.3171/jns.1999.90.1.0035

33. Roca E, Pallud J, Guerrini F, Panciani PP, Fontanella M, Spena G. Stimulation-related intraoperative seizures during awake surgery: a review of available evidences. *Neurosurg Rev* (2020) 43(1):87–93. doi: 10.1007/s10143-019-01214-0

34. Spena G, Schucht P, Seidel K, Rutten GJ, Freyschlag CF, D'Agata F, et al. Brain tumors in eloquent areas: A European multicenter survey of intraoperative mapping techniques, intraoperative seizures occurrence, and antiepileptic drug prophylaxis. *Neurosurg Rev* (2017) 40(2):287–98. doi: 10.1007/s10143-016-0771-2

35. Ulkatan S, Jaramillo AM, Tellez MJ, Kim J, Deletis V, Seidel K. Incidence of intraoperative seizures during motor evoked potential monitoring in a large cohort of patients undergoing different surgical procedures. *J Neurosurg* (2017) 126(4):1296–302. doi: 10.3171/2016.4.JNS151264

36. Boetto J, Bertram L, Moulinié G, Herbet G, Moritz-Gasser S, Duffau H. Low rate of intraoperative seizures during awake craniotomy in a prospective cohort with 374 supratentorial brain lesions: electrocorticography is not mandatory. *World Neurosurg* (2015) 84(6):1838–44. doi: 10.1016/j.wneu.2015.07.075

37. Grabowski MM, Recinos PF, Nowacki AS, Schroeder JL, Angelov L, Barnett GH, et al. Residual tumor volume versus extent of resection: predictors of survival after surgery for glioblastoma. *J Neurosurg* (2014) 121(5):1115–23. doi: 10.3171/2014.7.JNS132449

38. Chaichana KL, Jusue-Torres I, Navarro-Ramirez R, Raza SM, Pascual-Gallego M, Ibrahim A, et al. Establishing percent resection and residual volume thresholds affecting survival and recurrence for patients with newly diagnosed intracranial glioblastoma. *Neuro Oncol* (2014) 16(1):113–22. doi: 10.1093/neuonc/not137

39. Lacroix M, Abi-Said D, Fourney DR, Gokaslan ZL, Shi W, DeMonte F, et al. A multivariate analysis of 416 patients with glioblastoma multiforme: prognosis, extent of resection, and survival. *J Neurosurg* (2001) 95(2):190–8. doi: 10.3171/jns.2001.95.2.0190

40. Coburger J, Segovia J, Ganslandt O, Ringel F, Wirtz CR, Renovanz M. Counseling patients with a glioblastoma amenable only for subtotal resection: results of a multicenter retrospective assessment of survival and neurologic outcome. *World Neurosurg* (2018) 114:e1180–5. doi: 10.1016/j.wneu.2018.03.173

41. Kinslow CJ, Garton ALA, Rae AI, Marcus LP, Adams CM, McKhann GM, et al. Extent of resection and survival for oligodendroglioma: a U.S. population-based study. *J Neurooncol* (2019) 144(3):591–601. doi: 10.1007/s11060-019-03261-5

42. Winther RR, Hjermstad MJ, Skovlund E, Aass N, Helseth E, Kaasa S, et al. Surgery for brain metastases-impact of the extent of resection. *Acta Neurochir (Wien)* (2022) 164(10):2773–80. doi: 10.1007/s00701-021-05104-7

frontiers | Frontiers in Oncology

TYPE Original Research
PUBLISHED 23 November 2023
DOI 10.3389/fonc.2023.1229747

OPEN ACCESS

EDITED BY
Konstantinos Gousias,
University of Münster, Germany

REVIEWED BY
Lefteris Zacharia,
University of Nicosia, Cyprus
Nihal Karakas,
Istanbul Medipol University, Türkiye
Rosendo Luria-Perez,
Children's Hospital of Mexico Federico Gomez, Mexico

*CORRESPONDENCE
Benjamin J. Umlauf
benjamin.umlauf@austin.utexas.edu

RECEIVED 26 May 2023
ACCEPTED 26 October 2023
PUBLISHED 23 November 2023

CITATION
Shipley A, Frampton G, Davies BW and Umlauf BJ (2023) Generating *Shigella* that internalize into glioblastoma cells. *Front. Oncol.* 13:1229747. doi: 10.3389/fonc.2023.1229747

Generating *Shigella* that internalize into glioblastoma cells

Austin Shipley[1], Gabriel Frampton[1], Bryan W. Davies[2,3] and Benjamin J. Umlauf[1,4]*

[1]Department of Neurosurgery, Dell Medical School, The University of Texas at Austin, Austin, TX, United States, [2]Department of Molecular Biosciences, The University of Texas at Austin, Austin, TX, United States, [3]John Ring LaMontagne Center for Infectious Diseases, The University of Texas at Austin, Austin, TX, United States, [4]Mulva Clinic for the Neurosciences, The University of Texas at Austin, Austin, TX, United States

Introduction: The use of microorganisms as drug delivery systems to treat cancer has expanded recently, including FDA approval of certain viruses as oncolytics. Microorganisms have several unique benefits compared to traditional pharmacologic agents including dose independence, the ability to produce therapeutic proteins locally within the tumor, and simplicity of administration. However, current microbial delivery systems such as AAV9 and herpes virus have limited cassette sizes, minimal cancer cell selectivity, and low innate cytotoxicity. To address these issues, we sought to generate a strain of *Shigella flexneri* to selectively internalize into glioblastoma (GBM) brain tumor cells as an initial step to generating a bacterial-based drug delivery system.

Methods: We generated *S. flexneri* that selectively internalize into GBM cells using iterative co-cultured assays.

Results: After 50 rounds of co-culture, the new strain infected 95 percent of GBM cells in 2 hours. GBM-infecting Shigella demonstrate a 124-fold preference for internalizing in nine different GBM cell lines compared to Normal Astrocytes (NA) controls. Additionally, we developed an in-cell western to identify GBM-infecting Shigella clones that preferentially internalize in patient samples without iterative co-culture. Finally, we demonstrate internalization into GBM cells is mediated via a factor modified by myristoylation.

Discussion: In conclusion, here we present a novel bacterial platform that preferentially internalizes in brain tumor cells. This system provides numerous potential benefits over current interventions and other microbial strategies for treating brain tumors.

KEYWORDS

***Shigella*, glioblastoma, drug delivery, microbial factories, myristoylation**

Introduction

Microorganism-based drug delivery systems are emerging as a promising approach to treating solid tumors (1–4). Most strategies focus on using a virus (for example, herpes simplex virus) to directly lyse malignant cells and/or edit the cancer genome through gene therapy (4–11). While current microbial delivery methods have the potential to radically improve outcomes compared to traditional chemotherapy, inherent features of these viruses such as small cassette size, low cancer cell selectivity, and poor innate cytotoxicity have limited the use of this class of therapeutics (11). To address these issues, we generated an intracellular bacterium to serve as the basis of a drug delivery system to use as a novel therapeutic platform to treat brain tumors in the future (12–14).

Glioblastoma (GBM) is the most common malignant, primary brain tumor observed in adults, and patients diagnosed with GBM demonstrate a median survival of only 15 months (15, 16). The standard of care for GBM is gross total surgical resection, if possible, followed by radiation and chemotherapy. Even with complete surgical resection of the tumor and adjuvant chemotherapy, these tumors reoccur, ultimately resulting in mortality (15–19).

The basis for our system is *Shigella flexneri*, a gram-negative intracellular bacterium similar to the viruses discussed above. Importantly, *Shigella* has a type 3 secretion system capable of administering toxic proteins into the host cell cytosol (12, 20, 21),, and multiple tools exist to improve the safety of the bacterium. Further, *Shigella* has an unlimited cassette space to encode therapeutic proteins (22–24). Thus, this system has multiple potential benefits compared to current oncolytic virus platforms. Additionally, a recent report demonstrated that co-administration of attenuated *Salmonella* and neutrophil-derived doxorubicin nanoparticles significantly reduced the tumor burden in an orthotopic, murine model of glioblastoma (25). Here, we examined the safety profile of the parental and GBM-infecting *S. flexneri* strain, generated *Shigella* that selectively internalizes into GBM cells via iterative co-culture, and identified that a myristoylation enzyme is essential for internalization into GBM cells. In summary, this manuscript describes the generation and initial testing of the GBM-infecting *Shigella* platform that can be used in the future as a drug delivery system to treat brain tumors post-surgical resection.

Materials and methods

Origin and culture of *S. flexneri* strain 2475 serotype 2a

S. flexneri strain 2475 serotype 2a was grown from frozen Davies lab stocks that were originally a gift from Shelley M. Payne. Unique *Shigella* culture conditions were used for each assay described below. Generally, *Shigella* was streaked out from frozen stocks onto Tryptic Soy Broth (TSB) (30 g/L) + agar (15 g/L), and Congo Red (100 mg/L) sterile plates and incubated overnight at 30°C or 37°C. Individual colonies were expanded in sterile Tryptic Soy Broth (30 g/L) using a shaking incubator (250 rpm) at 30°C.

Shiga toxin protein detection

At 24 hours prior to testing, *Shigella* was streaked out from the frozen stock onto TSB (30 g/L) + Congo Red (0.01% w/v) plates and incubated overnight at 37°C. Colonies were picked and grown for approximately 2 hours (OD_{650} = 0.6) (13). Samples were tested according to the manufacturer's protocol for ImmunoCard STAT!® EHEC (Cat#: 751630). Band intensity was measured using ImageJ.

Detecting shiga toxin DNA

A single *Shigella* colony was picked using a pipet tip and resuspended in 20 µL nuclease-free water. A colony was incubated for 10 min at 95°C and then centrifuged at 1,000 rcf for 1 min to remove membrane components.

Supernatant at a volume of 5 µL was used as the template for a PCR assay to quantify the presence of DNA encoding for Shiga toxin(s). Potential DNA regions were amplified with the Phusion taq polymerase kit (HF buffer, 20 cycles) using previously described primers that are specific for Shiga toxin 1 (Stx1 – primer pair: ATGTCAGAGGGATAGATCCA and TATAGCTACT GTCACCAGACAAT), Shiga toxin 2 (Stx2 – primer pair: AGTTCTGCGTTTTGTCACTGTC and CGGAAGCAC ATTGCTGATT), or positive control virulence factor F (virF – primer pair: AGCTCAGGCAATGAAACTTTGAC and TGGGCTTGATATTCCGATAAGTC) (26). Bands were identified by staining gel with SYBR Green dye (1:10,000 dilution) and imaging using a blue light transilluminator. Band intensity was quantified using the publicly available ImageJ software analysis suite.

MsbB gene deletions

Genes were deleted as previously described using standard Lambda red recombineering methods with minor modifications (22, 27). *S. flexneri* was streaked onto TSB agar plates with 0.01% Congo Red and grown at 37°C overnight. The next day, 96 red colonies of *Shigella* were picked using a filtered p200 pipet tip. Each colony was added into 400 µL of TSB in a deep-well block plate and incubated at 37°C, 250 rpm, until an OD_{650} of 0.6 was reached (approximately 2.5 to 3 hours). *Shigella* suspensions were combined and pelleted into a 50-mL conical tube. After washing three times with 25 mL of 10% glycerol, *Shigella* was resuspended in 5 mL of 10% glycerol. *Shigella* was electroporated with 200 ng of pRedTKI plasmid DNA (Addgene Plasmid #51628) and recovered in TSB for 1 hour at 30°C, followed by plating on TSB + 50 µg/mL Kan agar plates with 0.01% Congo Red overnight. The pRedTKI plasmid introduces the Lambda red genes necessary for homologous recombination along with conferring Kan resistance.

Shigella + pRedTKI colonies were picked and incubated at 30°C, 250 rpm, until an OD_{650} of 0.6 was reached (approximately 3 hours); during the last 30 min of incubation, L-arabinose was added at 10 mmol/L to induce the Lambda red recombination genes along with 50 µg/mL kanamycin to maintain transmission of the

pRedTKI plasmid. Bacteria were pelleted in a 50-mL conical tube by centrifugation at 4,000 × *g*, transferred to a 1.5-mL Eppendorf tube, washed three times with 500 µL of 10% glycerol, and resuspended in 50 µL of 10% glycerol. Using an electroporation cuvette with a 2 mm gap, *Shigella* were transfected via electroporation with 200 ng of I-SceI-flanking resistance cassette with 70-bp homology adjacent to the gene to be deleted. The cassette for MsbB1 was as follows: TGGTGCGGGGCAAGTTGTGCCGCTACACTATCACCAGA TTGATTTTTGCCTTATCCGAAACTGGAAAAGCTAGG GATAACAGGGTAATATGGAGAAAAAAATCACTGG ATATACCACCGTTGATATATCCCAATGGCATCG TAAAGAACATTTTGAGGCATTTCAGTCAGTTGCTCAATGT ACCTATAACCAGACCGTTCAGCTGGATATTACGGCC TTTTTAAAGACCGTAAAGAAAAATAAGCACAAGTTTT ATCCGGCCTTTATTCACATTCTTGCCCGCCTGA TGAATGCTCATCCGGAATTACGTATGGCAATGAA AGACGGTGAGCTGGTGATATGGGATAGTGTTC ACCCTTGTTACACCGTTTTCCATGAGCAAACTG AAACGTTTTCATCGCTCTGGAGTGAATACCACGACGATT TCCGGCAGTTTCTACACATATATTCGCAAGATGTG GCGTGTTACGGTGAAAACCTGGCCTATTTCCCTAAAGGG TTTATTGAGAATATGTTTTTCGTCTCAGCCA ATCCCTGGGTGAGTTTCACCAGTTTTGATTTA AACGTGGCCAATATGGACAACTTCTTCGCCCCCGT TTTCACCATGGGCAAATATTATACGCAAGGCGACAAG GTGCTGATGCCGCTGGCGATTCAGGTTCATCATGCCGTTT GTGATGGCTTCCATGTCGGCAGAATGCT TAATGAATTACAACAGTACTGCGATGAGTGGCAGGGCG GGGCGTAATAGGGATAACAGGGTATAAAAGCCT CTCGCGAGGAGAGGCCTTCGCCTGATGATAAGTTCAAGTT TGCTTCAGAATATTCGAAATCT.

The cassette for MsbB2 was as follows: AATTAAGGTTAG ATGTATTCTCTGAATAAAATATTAATGATGATTATGGTAG GGGCATTCGCACTAAATATAGGGATAACAGGGTAA TATGGAGAAAAAAATCACTGGATATACCACCGTT GATATATCCCAATGGCATCGTAAAGAACATTTT GAGGCATTTCAGTCAGTTGCTCAATGTACCTATA ACCAGACCGTTCAGCTGGATATTACGGCCTTTTTA AAGACCGTAAAGAAAAATAAGCACAAGTTTTATC CGGCCTTTATTCACATTCTTGCCCGCCTGATGAATGC TCATCCGGAATTACGTATGGCAATGAAAGACGGTGAG CTGGTGATATGGGATAGTGTTCACCCTTGTTACACCGTT TTCCATGAGCAAACTGAAACGTTTTCATCGCTCTGGAGTG AATACCACGACGATTTCCGGCAGTTTCTACACATATA TTCGCAAGATGTGGCGTGTTACGGTGAAAACCTGGCCTA TTTCCCTAAAGGGTTTATTGAGAATATGTTTTTCGTCTC AGCCAATCCCTGGGTGAGTTTCACCAGTTTTGATTTA AACGTGGCCAATATGGACAACTTCTTCGCCC CCGTTTTCACCATGGGCAAATATTATACGCAAG GCGACAAGGTGCTGATGCCGCTGGCGATTCAG GTTCATCATGCCGTTTGTGATGGCTTCCATGTCGGCAGAA TGCTTAATGAATTACAACAGTACTGCGATGAGTGGCAGG GCGGGGCGTAATAGGGATAACAGGGTAATAATTAT AAAGTACAGGTATTTCCACTAGTTGTTTCTTACAGG TTACCAATCGAAACACATCCCCCTTCCG.

The primer pair for identifying MsbB1 was TTGAACTTATCATCAGGCGAAGGCCTC and CGGCTTTTTTTATTTGGTGCGGGG, and that for MsbB2 was CTGCTATCCGCTCTTTGGATGCA and CTACACAGTCCTCCGTGCCAA. Electroporated *Shigella* was allowed to recover in Super Optimal broth with Catabolite repression (SOC) for 3 hours at 30°C and plated on TSB + 50 µg/mL Kan + 12.5 µg/mL chloramphenicol (Cam) agar plates with 0.01% Congo Red overnight.

To complete the gene deletion protocol, a single colony of *Shigella* + pRedTKI + Cam resistance cassette was incubated at 30°C, 250 rpm, until an OD_{650} of 0.6 (approximately 3 hours) in 3 mL TSB + 50 µg/mL Kan + 20 mmol/L isopropyl β-D-1-thiogalactopyranoside (IPTG) to induce I-SceI expression to excise the Cam resistance gene. A sample of liquid culture was seeded onto TSB + 50 µg/mL Kan + agar plates with 0.01% Congo Red and incubated overnight. Modifications were verified by PCR.

Internalization assay

Tissue culture

GBM cell lines were obtained from Dr. John Kuo (GSC 112, 15, 109, 114, 124, 113, 115, and 99) or ATCC (U-251 MG, Cat#: 09063001, Lot#: 17K073). Normal astrocytes were purchased from Lonza (Cat#: CC-2565) and grown according to the manufacturer's protocol without antibiotics. Mammalian cells were grown in tissue culture-treated T25 or T75 flasks in low-glucose Dulbecco's modified Eagle's medium (DMEM) with 10% fetal bovine serum (FBS), GlutaMAX, and 1% sodium pyruvate (without pen/strep) (28–30). Cells were split at 1:3 using Accutase (Innovative Cell Technologies, San Diego, CA, USA; Cat#: AT104) to remove cells from tissue culture plastic when >80% confluent. Cells were washed two times with complete media before replating. Neurons were harvested from rats using a typical protocol and maintained using a previously described culture protocol (31). Briefly, the hippocampus from mice was isolated via dissection, placed in a digestion solution consisting of L-cysteine, NaOH, $CaCl_2$, DNAse I, EDTA, and papain for 35 min, and then inactivated in serum media. Cells then underwent trituration, were strained through a 100-µm cell strainer, and were centrifuged for 5 min at 200 × *g*, 4°C. The supernatant was aspirated, and cells were counted and replated at 750,000 cells/mL. Neurobasal media at a volume of 2 mL with B-27 supplement, GlutaMAX, and 1.25% FBS was added to a culture plate. Thirty percent of the media was replaced twice per week. After 3 days of culture, 5-fluoro-2′-deoxyuridine (FUDR) was added to remove dividing cells. All mammalian cells were cultured at 37°C, 5% CO_2.

Co-culture assay

Mammalian cells were maintained in culture as described above. At 24 hours prior to co-culture assays, the media was changed without removing cells from the tissue culture flask. Cells grown to 80% confluency in a T25 flask were used for each round of co-culture.

S. flexneri was streaked on TSB agar plates with 0.01% Congo Red and grown at 37°C overnight. The next day, 96 red colonies of *Shigella* were picked using a filtered p200 pipet tip and added to individual wells of a deep-well block plate that contained 400 µL of TSB. The deep-well block plate was incubated at 37°C, 250 rpm, until an OD_{650} of 0.6 was reached (approximately 2.5 to 3 hours). A control well was used to estimate the *Shigella* growth rate. After reaching the mid-log phase (0.6 OD_{650}), individual wells were pooled, and the *Shigella* was concentrated to 2×10^8 cfu/mL (OD_{650} of 1.0 = 8.0×10^8). Next, 250 µL of *Shigella* concentrate was added to ~5 mL of GBM, normal astrocyte (NA), or rNeuron media. *Shigella*-containing media at a volume of 5 mL was added to the T25 cell culture flask containing mammalian cells. The T25 culture flask was centrifuged at 200 × *g* for 10 min and then incubated at 37°C, 5% CO_2, for 30 min. After 30 min, culture media was removed by aspiration. The T25 flask was washed four times using 5 mL of phosphate-buffered saline (PBS) for 1 min with gentle agitation. Next, 5 mL of mammalian culture media containing 20 µg/mL of gentamicin was added to the T25 flask. The T25 flask was incubated at 37°C, 5% CO_2, for an additional 90 min. After 90 min, the media was aspirated, and cells were washed four times with PBS, 1 min per wash, with gentle agitation.

After the final wash, 1 mL of Accutase (Innovative Cell Technologies; Cat#: AT104) was added to the T25 flask. The T25 flask was incubated at 37°C, 5% CO_2, until GBM, NA, or rNeuron cells detached from the plate. Mammalian cell membranes were mechanically disrupted by pulling the cell suspension through a 27Ga needle 10 times. The mammalian cell lysate was centrifuged at 1,000 × *g* for 2 min to pellet any membrane-associated (but not internalized) *Shigella*. Mammalian cell lysate at a volume of 20 µL was plated onto a TSB + 0.01% Congo Red agar plate and grown at 37°C overnight. Individual colonies were expanded and frozen in 25% glycerol or used directly for the next round of co-culture assays.

Confocal fluorescence microscopy

Tissue culture

At 24 hours prior to internalization, GBM cells were grown to ~80% confluence using the protocol described above in the mammalian cell culture section on Poly-D-Lysine, No. 1.5 glass-bottom dishes (MatTek, Ashland, MA, USA; Cat#: P35GC-1.5-14-C).

An individual *Shigella* colony was picked, grown to the mid-log phase, and co-cultured with mammalian cells in the microscopy dish using the protocol described above in the co-culture assay section. After the final wash, cells were fixed with 4% paraformaldehyde (PFA) (Electron Microscopy Sciences, Hatfield, PA, USA; Cat#: 50-980-487) for 10 min and then washed three times with PBS.

For membrane + DNA imaging

PBS staining solution at a volume of 1 mL containing wheat germ agglutinin-fluorescein (WGA; 1:2,000, Vector Laboratories, Burlingame, CA, USA; Cat#: FL-1021) and Hoechst 33342 (1:800, Invitrogen, Carlsbad, CA, USA; Cat#: H3570) was added to the fixed cells and incubated for 15 min. Cells were washed three times with PBS. After the final wash, 1 mL of PBS was added to the dish so cells did not dry out during imaging. Cells were imaged using a 60× objective on a Nikon Eclipse Ti2 confocal microscope. Images were processed and analyzed using the publicly available ImageJ software package.

For *Shigella* antibody staining

Cells were permeabilized by adding 1 mL of 0.1% Triton X-100 in PBS for 5 min. Blocking buffer at a volume of 1 mL (PBS + 30 mg/mL bovine serum albumin (BSA) + 5% donkey serum + 0.1% Triton X-100) was added to each dish, and the cells were incubated at 4°C overnight. The next day, cells were washed three times with PBS. Next, cells were incubated with an anti-*Shigella* antibody (1:200, Abcam, Cambridge, UK; Cat#: ab65282) in 1 mL PBS + 30 mg/mL BSA + 0.1% Triton X-100 for 90 min at room temperature. After incubation, cells were washed three times with PBS. Next, cells were incubated with anti-rabbit Alexa Fluor 488 secondary (1:1,000, Invitrogen; Cat#: A21206) in PBS + 30 mg/mL BSA + 5% donkey serum + 0.1% Triton X-100 (1-mL total volume) for 60 min. Cells were washed three times with PBS. Next, cells were incubated with Phalloidin Dye 594 (1:1,000, Abnova, Taipei, Taiwan; Cat#: U0292) and Hoechst 33342 (1:800, Invitrogen; Cat#: H3570) in PBS (1-mL total volume) for 15 min. Cells were imaged using a 60× objective on a Nikon Eclipse Ti2 confocal microscope. Images were processed and analyzed using the publicly available ImageJ software package.

In-cell western

Cell culture

At 24 hours prior to internalization, GBM or NA cells were grown to 80% confluence as described in the mammalian tissue culture section above on a tissue culture-treated, black well, clear bottom, 96-well tissue culture plate.

Co-culture

Individual *Shigella* colonies were picked and expanded as described above in a deep block 96-well plate. *Shigella* culture at a volume of 40 µL from a single well was added to 200 µL of GBM or NA media previously plated into each well of the clear-bottom, black, 96-well plate. The 96-well plate was centrifuged at 200 × *g* for 10 min and then incubated at 37°C, 5% CO_2, for 30 min. Culture media was removed after 30 min by dumping the supernatant into a sterile glass dish containing bleach. The plate was washed four times with PBS using a similar method to remove the supernatant. Next, 200 µL of mammalian cell media containing 20 µg/mL gentamicin was added to each well. The plate was incubated at 37°C, 5% CO_2, for 90 min. After incubation, the plate was washed four times with PBS. Cells were fixed by adding 200 µL of 4% PFA to each well and incubating for 10 min. The plate was washed three times with PBS. Cells were permeabilized by adding 200 µL of PBS containing 0.1% Triton X-100 to each well for 5 min. Blocking buffer containing 1% BSA and 1% donkey serum was added to each well, and the plate

was incubated at 4°C overnight. The next day, the plate was washed three times with PBS. The plate was incubated with anti-*Shigella* antibody (1:200, Abcam; Cat#; ab65282) in PBS + 30 mg/mL BSA + 0.1% Triton X-100 (100 µL per well) for 90 min. The plate was washed with PBS three times. Finally, each well was incubated with IR_{800}CW anti-rabbit secondary (1:10,000, LI-COR, Lincoln, NE, USA; Cat#: D20119-05) in PBS + 30 mg/mL BSA + 5% donkey serum + 0.1% Triton X-100 for 60 min. The plate was washed three times with PBS and imaged on a LI-COR Fc scanner using a 2-min medium resolution scan. A standard curve of *Shigella* was used on each plate to convert the IR_{800} signal to the number of bacteria per well. It was important to ensure that the moles of anti-*Shigella* antibody greatly exceeded the moles of *Shigella* to ensure the saturated binding assumption was valid in order to quantify the number of bacteria per well.

Statistical methods

Data are generally presented as means with standard deviation. All validation experiments were conducted with a minimum of two independent replicates. For microscopy experiments, a minimum of three fields were quantified from at least two independent experiments. Significant differences between *Shigella* internalization in cell lines were determined using ANOVA with a 1% false discovery rate used as the threshold for significance. For microscopy assays, ANOVA was used to determine differences between groups with a 5% false discovery rate used as the threshold for significance.

Results

Overall scheme for generating *Shigella* that internalizes in brain tumor cells

As described in Figure 1A, we developed a scheme to identify *Shigella* clones that preferentially internalize into brain tumors using iterative co-culture assays. Briefly, *S. flexneri*, an intracellular bacterium, was streaked onto agar plates. Clones containing the virulence factor needed to survive inside mammalian cells were expanded and incubated with a brain tumor cell line, U-251 GBM. Bacteria that internalized into GBM cells were harvested and used for additional rounds of co-culture.

Identification of an *S. flexneri* strain suitable for GBM internalization

In order to identify a *Shigella* strain that is safe to use as a therapeutic platform, we identified a strain that did not contain Shiga toxins. We probed *S. flexneri* strain 2475 serotype 2a for DNA regions encoding Shiga toxins using previously described primers. As expected, we did not observe a band at the expected size for the PCR product (Supplementary Figure 1) (26, 32, 33). Quantification of this region demonstrated 15- and 21-fold less intense signal compared to positive control PCR for virF. We also quantified levels of Shiga toxin 1 and 2 proteins in *S. flexneri* strain 2475 serotype 2a prior to co-culture using a rapid test commercially available detecting kit (Figure 1B). The parental *Shigella* strain was negative for both Stx1 and Stx2, relative to a positive control included in the kit, under normal conditions and when treated with mitomycin C to induce the lytic cycle of potential Stx-producing prophage. Finally, whole genome sequencing indicated there were no Shiga toxin encoding regions in the virulence plasmid or genome (Supplementary Figure 4).

Generating *Shigella* that internalizes into a GBM cell line

As described in Figure 1, *Shigella* clones were incubated with U-251 GBM cells. Internalized clones were selected and carried forward to the next round of co-culture. Thus, *Shigella* clones that internalized in GBM cells were enriched iteratively to generate a population of GBM internalizing *Shigella*. To monitor the degree of enrichment of *Shigella* clones that internalized in GBM cells during the selection process, we performed fluorescence microscopy and counted the number of *Shigella* internalized in GBM cells as the co-culture experiments progressed. As shown in Figure 2A, internalized *Shigella* appear as rod-like structures within the boundaries of the U251 GBM cell membrane (demarcated by wheat germ agglutinin) when stained with a DNA intercalating dye Hoechst 33342 (rendered blue). The number of GBM cells demonstrating an internalized bacterium increased after each round of *Shigella* co-culture, starting with 5% ± 2.5% in round 10 and enriching to 95% ± 1% by round 50 of co-culture. The percentage of GBM cells with an internalized bacterium was calculated by taking three randomly selected fields and dividing the total number of infected cells by the total number of U-251 cells present (Figure 2B). The number of individual *Shigella* bacteria present inside each infected cell also increased as the rounds of co-culture progressed (Figure 2C). In round 5, only one to two bacteria were present in an infected cell. By round 50, an average of 20 ± 5.5 bacteria were present within each infected GBM cell.

As demonstrated in Figure 2D, individual GBM-infecting *Shigella* clones were expanded, and then an internalization assay was performed using patient-derived GSC 112 GBM cells and NA cells. Cells were fixed, permeabilized, and subjected to a quantitative in-cell western using an anti-*Shigella* antibody and an IR_{800} signal as a readout. A *Shigella* standard curve was used to convert the fluorescent signal to the amount of *Shigella* in each well. Out of 96 total clones, 85 clones internalized below detectable levels in NA cells. All 96 clones demonstrated increased internalization in GSC 112 cells compared to NA cells. The average number of bacteria internalized into GSC 112 over the entire 96-well plate was 2.6 bacteria per GSC 112 cell. Values ranged from 10.367 to 0.06 bacteria per GSC 112 cell.

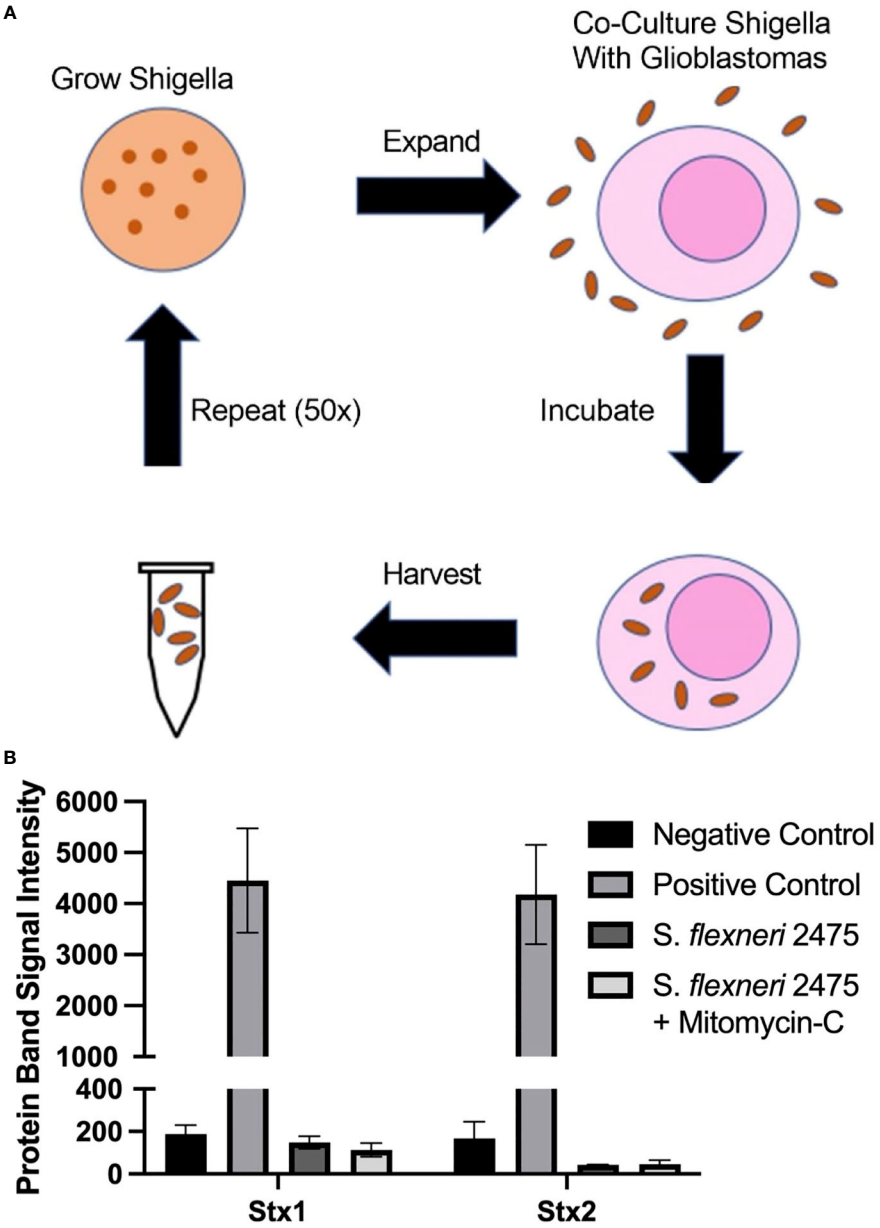

FIGURE 1
Scheme to generate GBM-infecting *Shigella* and verification of safety. **(A)** Scheme to select *Shigella flexneri* that preferentially internalize into glioblastomas. **(B)** The absence of Shiga toxin proteins in the parental strain of *Shigella* (*S. flexneri* 2475 serotype 2A) was measured using a Shiga toxin detection kit prior to co-culture. Lack of Shiga toxins was confirmed during normal growth conditions and with mitomycin C (Mito) induction. Band intensity corresponding to Stx1, Stx2, or controls is plotted for each group. GBM, glioblastoma.

GBM-infecting bacteria retain *Shigella* virulence plasmid

U-251 cells were infected with round 50 GBM-infecting Shigella. Cells were fixed and then stained with an anti-Shigella antibody targeting the lipopolysaccharide (LPS), phalloidin-AF594, and Hoechst 33342 then imaged via confocal microscopy. The DNA rod-like structures observed inside GBM cells throughout this study co-localized with an anti-Shigella antibody (Figure 3A). Quantification of these images is presented in Figure 3B; a greater than 1,000-fold increase was observed in Shigella fluorescent signal in round 50 GBM-infecting Shigella (0.909 ± 0.110 rfu) compared to non-internalizing or other negative controls (non-internalizing (R0) = 0.002 ± 0.001 Escherichia coli 0.002 ± 0.001 no bacteria 0.001 ± 0.0). Additionally, GBM-infecting Shigella plated on TSB + 0.01% Congo Red agar plates uptake Congo Red (indicated by red colonies) similar to non-internalizing Shigella starting bacteria (positive control). A closely related E. coli (negative control) did not uptake the red dye as expected (Figure 3C). In addition, the Shiga toxin detection assay was repeated, and it is demonstrated in Supplementary Figure 2 that GBM-infecting Shigella still did not express Shiga toxins under normal growth conditions or when induced with mitomycin C.

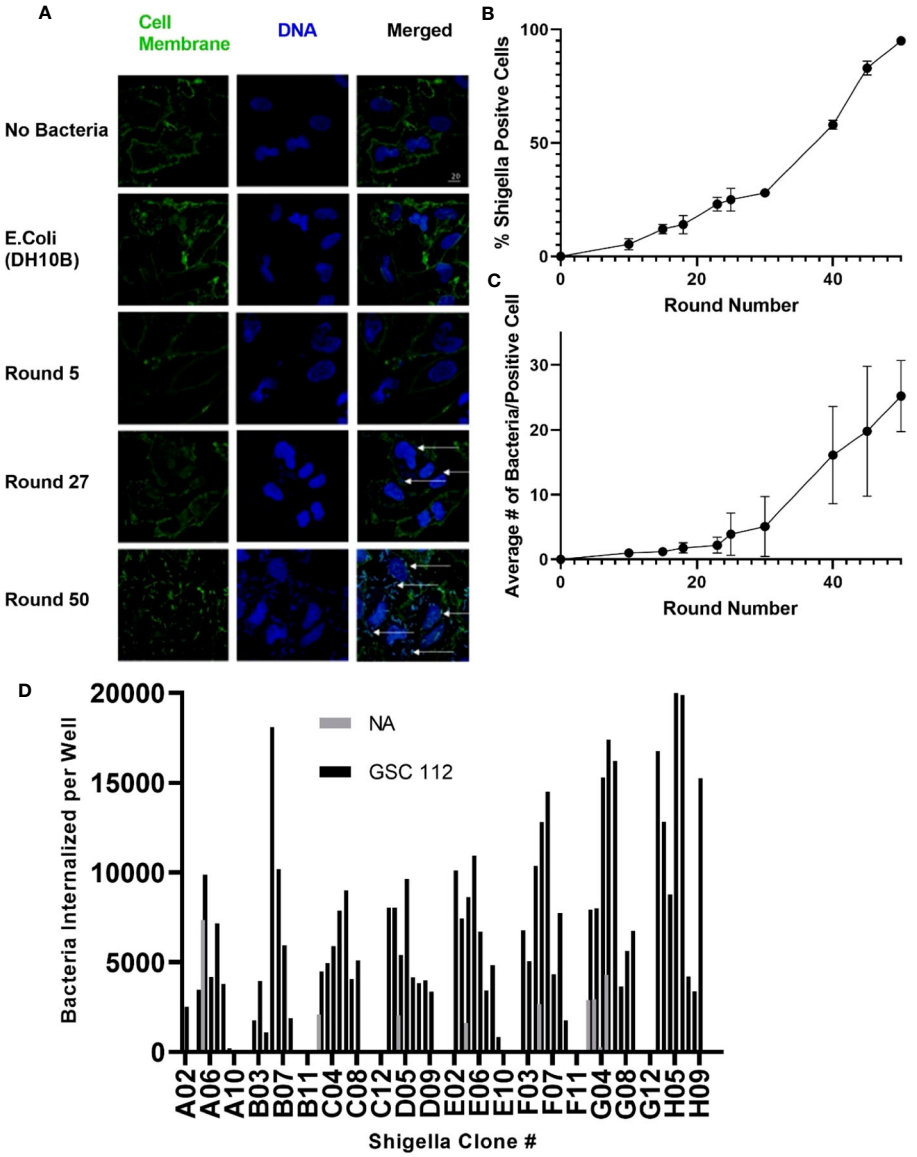

FIGURE 2
Generating *Shigella* that internalizes into a GBM cell line. *Shigella* was incubated in U-251 cells *in vitro*. Internalized *Shigella* was isolated and amplified. This process was repeated 50 times, as indicated by round number. **(A)** Confocal fluorescence microscopy of internalized *Shigella* in U-251 cells. *Shigella* was incubated with U-251 GBM cells, fixed, and stained with Hoechst 33342 for DNA (blue) and wheat germ agglutinin (WGA) for cell membranes (green). White arrows indicate individual *Shigella*. The scale bar indicates 20 µm. **(B)** The percentage of U-251 cells with internalized *Shigella* identified via microscopy is plotted over 50 rounds of co-culture with a minimum of three fields counted per round. **(C)** The mean number of *Shigella* rods per U-251 cell, with at least one *Shigella* rod inside the cell membrane, is plotted over 50 rounds of internalization. Three fields were counted for each round. **(D)** GBM-infecting *Shigella* were streaked, individual colonies expanded, and single colonies incubated with GSC 112 GBM cells. After incubation, the amount of internalized *Shigella* was quantified using an in-cell western. The number of *Shigella* internalized into GSC 112 and NA is plotted for 96 individual GBM-infecting *Shigella* clones. Clones exhibiting below detectable levels of the bacterial signal are represented as zero. GBM, glioblastoma; TSB, Tryptic Soy Broth; NA, normal astrocyte.

GBM-infecting *Shigella* preferentially internalizes in GBM cells compared to normal astrocyte controls

Next, GBM-infecting *Shigella* was incubated with a panel of patient-derived GBM cell lines, as well as normal astrocytes and normal rat neurons, to quantify both the breadth and specificity of this platform to internalize in adult malignant brain tumors. Nine patient-derived glioblastoma stem cell (GSC) lines were incubated with GBM-infecting *Shigella*. Internalized *Shigella* was harvested and plated to count the number of internalized bacteria per group. GSC 115 showed the highest internalization at 123,800 bacteria/5 × 10^5 GBM cells. To demonstrate the specificity of the platform, GBM-infecting *Shigella* were incubated with normal astrocytes and internalized bacteria counted. Approximately 383 bacteria internalized/~300 NA cells (two separate patient cell lines) were

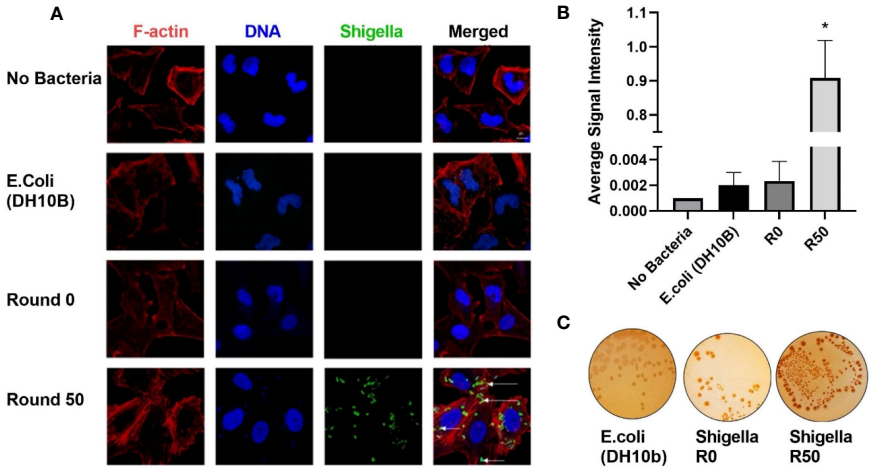

FIGURE 3
GBM-infecting *Shigella* retain *Shigella flexneri* phenotype. **(A)** GBM-infecting *Shigella* or control were incubated with U-251 GBM cells. Gentamycin and washing eliminated non-internalized bacteria. Cells were fixed, stained with Hoechst 33342 for DNA (blue), Phalloidin for F-Actin (red), anti-*Shigella* antibody (ab65282), and counterstained with anti-rabbit Alexa Fluor 488 (green) to visualize *Shigella* via fluorescence confocal microscopy. Scale bars indicate 20 μm, and white arrows highlight *Shigella*. **(B)** The average signal intensity of *Shigella* fluorescence is quantified and plotted (*$p < 0.05$ by ANOVA, n = 3 individual fields/group). **(C)** *Shigella* isolated from GBM cells was plated on TSB + Congo Red agar plates. Representative plates are shown. Red colonies demonstrate that GBM-infecting *Shigella* can still process Congo Red dye, indicating retention of virulence plasmid. GBM, glioblastoma.

observed. Figure 4A shows the colony counts recovered after internalization for each GSC or NA cell line. A one-way ANOVA of the colony counts indicated that seven out of the nine GSC cell lines demonstrated significantly higher internalization ($p < 0.01$) compared to NA. Figure 4C depicts the fold change between each GSC cell line relative to NA. The average fold increase was 123 ± 110; GSC 115 demonstrated the highest internalization with a 373 ± 59.5-fold increase compared to NA.

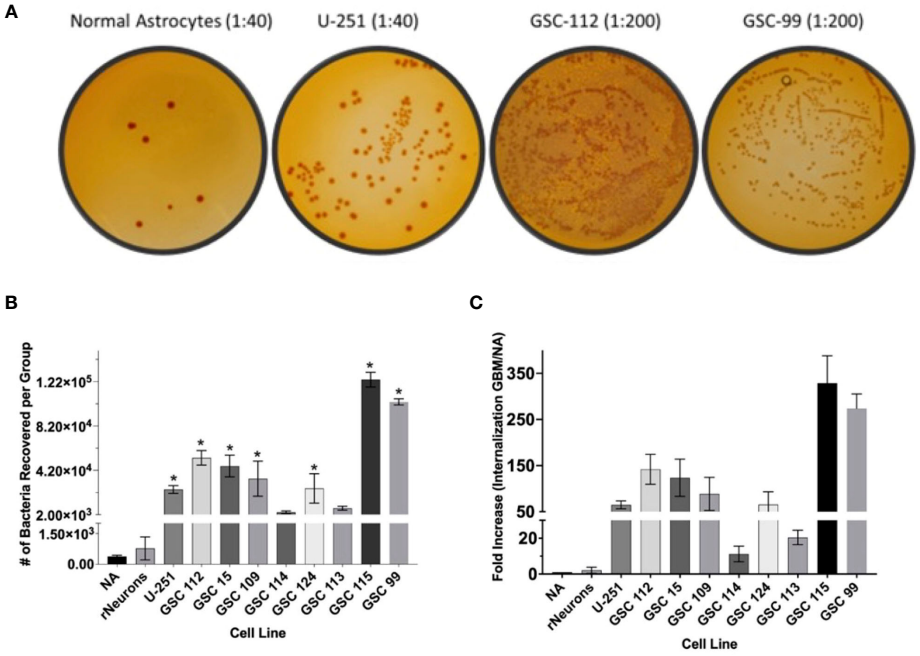

FIGURE 4
GBM-infecting *Shigella* preferential internalization into GBM cells compared to normal astrocyte controls. Internalized GBM-infecting *Shigella* was quantified in a panel of GBM cell lines, two unique normal astrocyte (NA) cell preparations, and rat neurons. **(A)** GBM-infecting Shigella was incubated with either GBM or normal astrocyte cells. Internalized Shigella was recovered and plated on TSB + Congo Red plates to quantify internalized bacteria. Representative images are demonstrated in panel **(A)** Dilutions depicted for NA and U-251 cells is 1/40. All GSC cell lines are diluted 1/200. **(B)** Shigella recovered from each cell line is plotted and compared to normal astrocytes (*$p < 0.01$ via multi-comparison corrected ANOVA). **(C)** The fold change of internalization for each GBM cell line compared to NA is plotted. The average fold change over all GBM cell lines was 123 ± 21.2 (standard error of the mean), and GSC 115 displayed the greatest fold change of 322 ± 34.3. GBM, glioblastoma; TSB, Tryptic Soy Broth.

Whole genome characterization of GBM-infecting *Shigella*

We performed whole genome sequencing on GBM-infecting *Shigella* and compared the data to those of the parental strain. We identified 177 mutations in 46 genes (Supplementary Figure 3 and Supplementary Table 1). Seventeen mutations were in genes related to metabolism/homeostasis, 13 genes were involved in DNA regulation, seven genes were involved in transcriptional regulation, six mutations were in genes associated with stress response, and three mutations occurred in genes with unknown function. Importantly, we identified no mutations that would affect the virulence or safety of the novel bacterium.

Membrane anchored factor in novel *Shigella* strain mediates internalization in GBM cells

We removed MsbB1 and MsbB2 myristoylation factors from the round 50 GBM-infecting *Shigella* using recombineering (Supplementary Figure 4). As expected from previous reports (34–37), removal of the myristoylation enzymes lowered the TLR4 detection relative to unmodified *Shigella* ($p < 0.05$ via ANOVA, Supplementary Figure 5). Interestingly, removing MsbB1 also decreased the recovery of *Shigella* that internalized into GBM cells from an average of 2.82×10^4 to 320 bacteria per group ($p < 0.05$ via ANOVA). Removal of both MsbB1 and MsbB2 completely abrogated internalization to an average of <1 bacterium recovered. Confocal imaging of GBM cells treated with either R50, MsbB1 KO, or MsbB1 and MsbB2 KO demonstrate a significant decrease in cells internalizing *Shigella* (Figure 5). After MsbB1 was removed, the percentage of *Shigella*-positive cells dropped from 95% to 25% ($p < 0.05$ via ANOVA). Quantifying the fluorescent *Shigella* signal indicated that MsbB1 removal reduced the mean signal to 0.425 rfu compared to 6.16 rfu for R50 (~14.5-fold decrease in signal). Removal of both MsbB1 and MsbB2 resulted in 0% of cells with a *Shigella* internalized and a fluorescent signal of 0.009 rfu (~684-fold decrease). GBM cells that did demonstrate *Shigella* internalization after removal of myristoylation factor MsbB1 had similar numbers of internalized *Shigella* compared to R50. The growth curves of R50, MsbB1 KO, and MsbB1 and MsbB2 KO *Shigella* are presented in Supplementary Figure 6.

Discussion

In this study, we demonstrated a method to generate *S. flexneri* clones that selectively internalize into GBM cell lines. We first

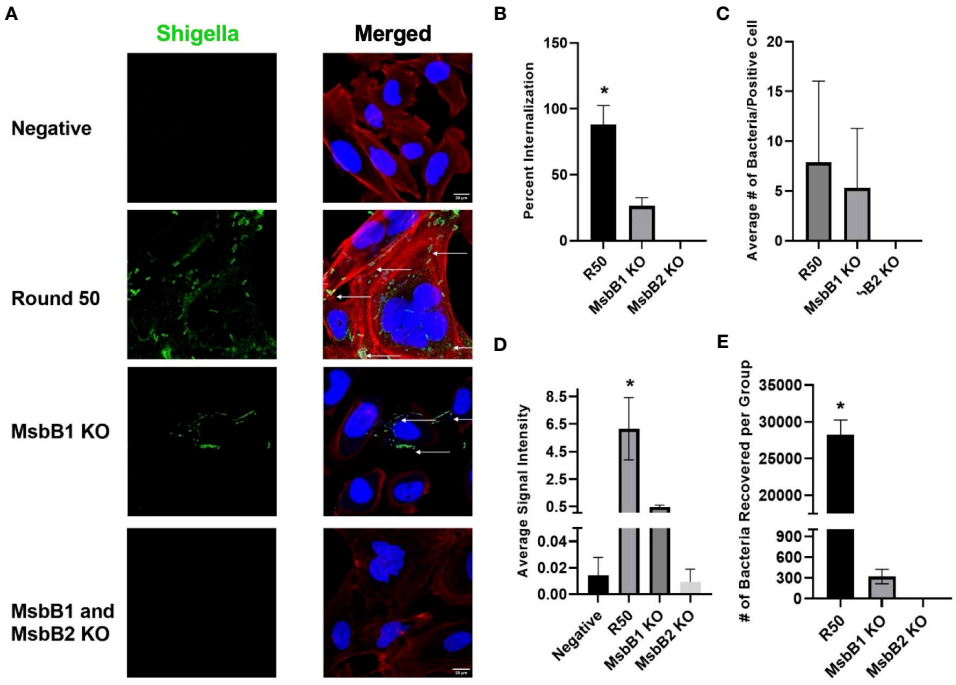

FIGURE 5
Characterization of GBM-infecting *Shigella*. **(A)** GBM-infecting *Shigella*, GBM-infecting *Shigella* MsbB1 and MsbB2 knock-out, and control *Shigella* were incubated with U-251 GBM cells. Gentamycin and washing eliminated non-internalized bacteria. Cells were fixed, stained with Hoechst 33342 for DNA (blue), Phalloidin for F-Actin (red), anti-*Shigella* antibody (ab65282), and counterstained with Alexa Fluor 488 (green) to visualize *Shigella* using confocal fluorescence microscopy. **(B)** The percentage of U-251 cells with internalized *Shigella* identified via microscopy is plotted. **(C)** The mean number of *Shigella* rods per U-251 cell, with at least one *Shigella* rod inside the cell membrane. **(D)** The average signal intensity of *Shigella* fluorescence is quantified and plotted (*$p < 0.05$ by ANOVA, n = 3 individual fields/group). **(E)** GBM-infecting *Shigella* or MsbB1 and MsbB2 knock-out *Shigella* are incubated with GBM cells. Internalized *Shigella* was recovered and plated on TSB + Congo Red plates to quantify internalized bacteria. GBM, glioblastoma; TSB, Tryptic Soy Broth.

selected a strain of *Shigella* that does not express Shiga toxins to improve the safety profile of the platform (12). After only 50 rounds of co-culture with GBM cells, *Shigella* clones demonstrated a high propensity for internalizing into GBM cells. We observed less than one cell per field with internalized *Shigella* after five rounds of co-culture compared to 95% of cells infected with multiple bacteria after 50 rounds of co-culture. GBM-infecting *Shigella* retained LPS surface markers and the virulence plasmid throughout the co-culture process. Finally, we developed an in-cell western screen to complement the co-culture assays to improve patient specificity of the platform without further co-culture assays. In-cell western screening provides the opportunity to personalize this platform quickly for each patient tumor or to identify an optimal GBM-infecting *Shigella* clone for GBM cell lines that cannot be reliably cultured for 50 rounds of co-culture assays.

Previous studies have used microorganisms as delivery vehicles for GBM and other brain tumors (1–8, 10, 11, 38). Most studies, including those advancing to clinical trials, have focused on using a virus to deliver a therapeutic to the tumor (4). While these studies have potential advantages over traditional chemotherapy, using a virus as a therapeutic factory presents challenges. Namely, most viruses have limited specificity for GBM cells, small cassette sizes, and safety concerns (39). GBM-infecting *Shigella* still replicates inside a mammalian cell, similar to the current virus strategies (14). However, the larger size and complexity of *Shigella* allow for rapid identification of clones that preferentially internalize into GBM (it typically takes hundreds of passages with a given cell type to change the tropism of a virus) (40, 41). A recent report described systemic administration of attenuated *Salmonella* to immunodeficient animals bearing orthotopic glioblastoma, resulting in *Salmonella* accumulation in hypoxic regions of the tumor. While this report relied on neutrophil-derived doxorubicin particles to mediate tumor regression, this study further demonstrates the propensity of bacteria to infect glioblastoma (25). Additionally, the large genome and DNA editing resources available for *Shigella* allow for any sized cassette to be permanently integrated into the genome (22, 27). Thus, almost any combination of therapeutic proteins is available for researchers to identify the optimal combination of therapeutics for treating GBM. Further, *Shigella* contains the equipment to ensure that therapeutic proteins are delivered directly into the cytosol of infected GBM cells via a type three secretion system (12, 20). In terms of safety, the potential for large cassette sizes allows for improved safety controls, as bacterial therapeutics factories can be programmed to self-destruct and/or suicide switches can be added ab lib into the platform (22, 24, 27). Finally, GBM-infecting *Shigella* remains sensitive to beta-lactams, so simple administration of penicillin or other blood–brain barrier-permeable antibiotics, including additional beta-lactams, vancomycin, aminoglycosides, fluoroquinolones (particularly moxifloxacin and levofloxacin), doxycycline, or polymyxins, can serve as master suicide switch(es) to immediately halt GBM-infecting *Shigella* activity in the case of adverse events such as fever or general infection (42). It is important to note that despite selecting a strain of *Shigella* with high sensitivity to antibiotics, it is possible that GBM-infecting *Shigella* could potentially become antibiotic-resistant, impacting the safety of our proposed drug delivery platform.

This study focused on developing *Shigella* to internalize into GBM cells as a foundation for a drug delivery system. We envision this platform serving as a tool for neurosurgeons to clean the margins of a GBM post-resection. GBM-infecting *Shigella* could be administered into the surgical cavity before closing to infect and eradicate cancerous cells in the invasive margin that cause disease recurrence. This approach bypasses the need for systemic administration and reduces the potential for internalization into off-target cells in the body. However, many steps are required before GBM-infecting *Shigella* are suitable for a drug delivery platform including stabilizing genetic material, controlling the bacterial population, ensuring intracellular replication, modulating immunogenicity, and weaponizing the system with cytotoxic proteins such as ribosome toxins (gelonin), cytokines (IL-2 and TNF), and autophagy-inducing proteins (caspases) (43–46). Additionally, further understanding of GBM-infecting *Shigella* on the tumor microenvironment including replication, macrophage polarization, and innate inflammation is essential to translating this novel platform into a drug delivery system.

Our data indicate that a myristoylated factor mediates the selective internalization of GBM-infecting *Shigella* into GBM cells. Removal of MsbB1 and MsbB2 myristoylation enzymes completely abrogates the internalization of GBM-infecting *Shigella* in GBM cells. Previous reports indicate that removing MsbB genes does not impair the internalization of *Shigella* in intestinal cells, the typical target of wild-type *Shigella* or *Salmonella* Typhimurium invasion into tumor cells (47–49). Further, a group reported removal of a single MsbB does not impair *Shigella* internalization in HeLa cells, and double knock-out only reduces internalization by 50% (50). Our data indicate ~75% reduction in internalization with single MsbB and 100% reduction (complete) of internalization with double MsbB knock-out, indicating that this mechanism may be unique for GBM-infecting *Shigella* to internalize in GBM cells (50). Our data are congruent with those of previous studies that removed MsbB genes to "detoxify" LPS. These studies indicated that MsbB enzymes interact with late acyltransferases to affect the branching of LPS to reduce the innate immunogenicity of LPS by lowering TLR4 engagement (35, 51–54). We also observed reduced TLR4 activity in MsbB knock-outs, and the sequencing data indicate the removal of only those two enzymes. Further, GBM cells that did internalize MsbB1 KO *Shigella* did so at a similar rate to R50 GBM-infecting *Shigella*, indicating that this effect is not a function of the reduced growth rate observed with MsbB knock-outs. Thus, we conclude that myristoylation (presumably to anchor a factor that mediates internalization to the bacterial membrane) is essential for GBM-infecting *Shigella* to internalize into GBM cells. However, our data do not indicate what that factor is. Whole genome sequencing did not identify obvious mutations in MsbB genes or a known myristoylated protein; however, future RNA-sequencing, epigenetic, and/or proteomic studies of *Shigella* membrane-bound proteins could identify factors with differential copy number, alterations in promoters, and/or *de-novo* localization to bacterial membranes that are driving the observed changes in *Shigella* internalization in GBM cells. These studies can be narrowed bioinformatically by eliminating proteins of interest that do not contain an N-terminal glycine (either directly after synthesis or after

post-translational cleavage) that is required for modification with myristic acid (55). Identifying this factor could allow for the deletion of enzymes upstream of MsbB that still modulate LPS TLR4 engagement without abrogating internalization in GBM cells. Controlling innate immunogenicity could complement typical anti-cancer strategies such as arming GBM-infecting *Shigella* with immunomodulators, toxins, or other cytotoxic factors to increase the selective cytotoxic potential of this platform. Finally, other groups have utilized bacteria as a therapeutic agent to treat cancer, implying that this could be translatable to the clinic in the future when coupled with the correct cytotoxic payloads and safety measures (43, 56, 57). Finally, identifying these factors will be essential to understanding the mechanism of how GBM-infecting *Shigella* is preferentially internalizing in GBM cells compared to normal glia and neurons. Studies of GBM cells indicate abnormal patterns of glycosylation, lipids, and membrane proteins on the apical plasma membranes compared to non-malignant brain cells, which may interact with the myristoylated factor to provide the high specificity of internalization that we observed in this study (58–60).

In the future, we propose identifying GBM-infecting *Shigella* clones that preferentially internalize into a given patient's GBM. As demonstrated in Figure 2D, we created an in-cell western to rapidly identify personalized GBM-infecting *Shigella* clones for a given patient tumor without further rounds of co-culture. This allows for the identification of clones that internalize into patient cell lines that cannot undergo multiple rounds of passaging or samples directly resected from the operating room. We propose expanding these studies to develop a pipeline capable of generating a personalized GBM-infecting *Shigella* therapy for each patient afflicted with a brain tumor. Additionally, weaponizing GBM-infecting *Shigella* with multiple modalities and safety controls in the future will allow testing the benefits of this platform compared to other microorganism strategies for treating brain tumors (43, 56). Finally, we propose identifying the myristoylated factor(s) driving the internalization of GBM-infecting *Shigella* into brain tumor cells to simultaneously improve the efficacy, specificity, and safety of our novel platform.

In conclusion, here, we presented the idea and proof-of-concept for generating GBM-infecting *Shigella* that selectivity internalizes into brain tumors compared to normal brain tissue. This platform demonstrates numerous potential benefits compared to existing microorganism platforms including high selectivity, unlimited cassette space, and the potential to improve the safety profile. Future studies with GBM-infecting *Shigella* will demonstrate the utility of this platform to benefit patients suffering from malignant brain tumors.

Data availability statement

The datasets presented in this study can be found in online repositories. The names of the repository/repositories and accession number(s) can be found in the article/Supplementary Material.

Ethics statement

Ethical approval was not required for the studies on humans in accordance with the local legislation and institutional requirements because only commercially available established cell lines were used. Ethical approval was not required for the studies on animals in accordance with the local legislation and institutional requirements because only commercially available established cell lines were used.

Author contributions

AS designed assays and wrote the manuscript, GF designed assays and edited the manuscript, BD conceptualized the study and edited the manuscript, and BU conceptualized the study, designed assays, and wrote the manuscript. All authors contributed to the article and approved the submitted version.

Funding

The author(s) declare financial support was received for the research, authorship, and/or publication of this article. This study received financial support from the Mulva Clinic for the Neurosciences (BU).

Acknowledgments

We want to thank Julia Bastin and Dr. Lief Fenno for providing rat neurons for this study.

Conflict of interest

The authors declare that the research was conducted in the absence of any commercial or financial relationships that could be construed as a potential conflict of interest.

Publisher's note

Supplementary material

The Supplementary Material for this article can be found online at: https://www.frontiersin.org/articles/10.3389/fonc.2023.1229747/full#supplementary-material

References

1. Dighe OR, Korde P, Bisen YT, Iratwar S, Kesharwani A, Vardhan S, et al. Emerging recombinant oncolytic poliovirus therapies against Malignant glioma: A review. *Cureus* (2023) 15:e34028. doi: 10.7759/cureus.34028

2. Vorobyev PO, Kochetkov DV, Chumakov PM, Zakirova NF, Zotova-Nefedorova SI, Vasilenko KV, et al. 2-deoxyglucose, an inhibitor of glycolysis, enhances the oncolytic effect of coxsackievirus. *Cancers (Basel)* (2022) 14:5611. doi: 10.3390/cancers14225611

3. Suryawanshi YR, Schulze AJ. Oncolytic viruses for Malignant glioma: on the verge of success? *Viruses* (2021) 13:1294. doi: 10.3390/v13071294

4. Lu VM, Shah AH, Vallejo FA, Eichberg DG, Luther EM, Shah SS, et al. Clinical trials using oncolytic viral therapy to treat adult glioblastoma: a progress report. *Neurosurg Focus* (2021) 50:E3. doi: 10.3171/2020.11.FOCUS20860

5. Aldrak N, Alsaab S, Algethami A, Bhere D, Wakimoto H, Shah K, et al. Oncolytic herpes simplex virus-based therapies for cancer. *Cells* (2021) 10:1541. doi: 10.3390/cells10061541

6. Qiao J, Dey M, Chang AL, Kim JW, Miska J, Ling A, et al. Intratumoral oncolytic adenoviral treatment modulates the glioma microenvironment and facilitates systemic tumor-antigen-specific T cell therapy. *Oncoimmunology* (2015) 4:e1022302. doi: 10.1080/2162402X.2015.1022302

7. Bauzon M, Hermiston T. Armed therapeutic viruses - a disruptive therapy on the horizon of cancer immunotherapy. *Front Immunol* (2014) 5:74. doi: 10.3389/fimmu.2014.00074

8. Tsiatas M, Mountzios G, Curigliano G. Future perspectives in cancer immunotherapy. *Ann Trans Med* (2016) 4:273. doi: 10.21037/atm.2016.07.14

9. Steel JC, Morrison BJ, Mannan P, Abu-Asab MS, Wildner O, Miles BK, et al. Immunocompetent syngeneic cotton rat tumor models for the assessment of replication-competent oncolytic adenovirus. *Virology* (2007) 369:131–42. doi: 10.1016/j.virol.2007.07.022

10. Chiocca EA, Rabkin SD. Oncolytic viruses and their application to cancer immunotherapy. *Cancer Immunol Res* (2014) 2:295–300. doi: 10.1158/2326-6066.CIR-14-0015

11. Shende P, Basarkar V. Recent trends and advances in microbe-based drug delivery systems. *Daru* (2019) 27:799–809. doi: 10.1007/s40199-019-00291-2

12. Wei J, Goldberg MB, Burland V, Venkatesan MM, Deng W, Fournier G, et al. Complete genome sequence and comparative genomics of *Shigella flexneri* serotype 2a strain 2457T. *Infect Immun* (2003) 71:2775–86. doi: 10.1128/IAI.71.5.2775-2786.2003

13. Payne SM. Laboratory cultivation and storage of *Shigella*. *Curr Protoc Microbiol* (2019) 55:e93. doi: 10.1002/cpmc.93

14. Koestler BJ, Ward CM, Payne SM. *Shigella* pathogenesis modeling with tissue culture assays. *Curr Protoc Microbiol* (2018) 50:e57. doi: 10.1002/cpmc.57

15. Stupp R, Taillibert S, Kanner A, Read W, Steinberg DM, Lhermitte B, et al. Effect of tumor-treating fields plus maintenance temozolomide vs maintenance temozolomide alone on survival in patients with glioblastoma: A randomized clinical trial. *JAMA* (2017) 318:2306–16. doi: 10.1001/jama.2017.18718

16. Siegel RL, Miller KD, Jemal A. Cancer statistics. *CA Cancer J Clin* (2020) 70:7–30. doi: 10.3322/caac.21590

17. Hanif F, Muzaffar K, Perveen K, Malhi SM, Simjee Sh U. Glioblastoma Multiforme: A Review of its Epidemiology and Pathogenesis through Clinical Presentation and Treatment. *Asian Pac J Cancer Prev* (2017) 18:3–9. doi: 10.22034/APJCP.2017.18.1.3

18. McGranahan T, Therkelsen KE, Ahmad S, Nagpal S. Current state of immunotherapy for treatment of glioblastoma. *Curr Treat Options Oncol* (2019) 20:24. doi: 10.1007/s11864-019-0619-4

19. Stupp R, Mason WP, van den Bent MJ, Weller M, Fisher B, Taphoorn MJB, et al. Radiotherapy plus concomitant and adjuvant temozolomide for glioblastoma. *New Engl J Med* (2005) 352:987–96. doi: 10.1056/NEJMoa043330

20. Strockbine NA, Jackson MP, Sung LM, Holmes RK, O'Brien AD. Cloning and sequencing of the genes for Shiga toxin from *Shigella* dysenteriae type 1. *J Bacteriol* (1988) 170:1116–22. doi: 10.1128/jb.170.3.1116-1122.1988

21. Koestler BJ, Fisher CR, Payne SM. Formate promotes *Shigella* intercellular spread and virulence gene expression. *mBio* (2018) 9:e01777-18. doi: 10.1128/mBio.01777-18

22. Herod A, Ryu J, Rohde J. Lambda red recombineering in *Shigella flexneri*. *Methods Mol Biol* (2022) 2523:9–21. doi: 10.1007/978-1-0716-2449-4_2

23. Datsenko KA, Wanner BL. One-step inactivation of chromosomal genes in Escherichia coli K-12 using PCR products. *Proc Natl Acad Sci USA* (2000) 97:6640–5. doi: 10.1073/pnas.120163297

24. Yang J, Sun B, Huang H, Jiang Y, Diao L, Chen B, et al. High-efficiency scarless genetic modification in Escherichia coli by using lambda red recombination and I-SceI cleavage. *Appl Environ Microbiol* (2014) 80:3826–34. doi: 10.1128/AEM.00313-14

25. Mi Z, Yao Q, Qi Y, Zheng J, Liu J, Liu Z, et al. Salmonella-mediated blood-brain barrier penetration, tumor homing and tumor microenvironment regulation for enhanced chemo/bacterial glioma therapy. *Acta Pharm Sin B* (2023) 13:819–33. doi: 10.1016/j.apsb.2022.09.016

26. Belanger SD, Boissinot M, Menard C, Picard FJ, Bergeron MG. Rapid detection of Shiga toxin-producing bacteria in feces by multiplex PCR with molecular beacons on the smart cycler. *J Clin Microbiol* (2002) 40:1436–40. doi: 10.1128/JCM.40.4.1436-1440.2002

27. Morrison BA, Shain DH. An AMP nucleosidase gene knockout in Escherichia coli elevates intracellular ATP levels and increases cold tolerance. *Biol Lett* (2008) 4:53–6. doi: 10.1098/rsbl.2007.0432

28. Weichert JP, Clark PA, Kandela IK, Vaccaro AM, Clarke W, Longino MA, et al. Alkylphosphocholine analogs for broad-spectrum cancer imaging and therapy. *Sci Trans Med* (2014) 6:240ra275–240ra275. doi: 10.1126/scitranslmed.3007646

29. Clark PA, Al-Ahmad AJ, Qian T, Zhang RR, Wilson HK, Weichert JP, et al. Analysis of cancer-targeting alkylphosphocholine analog permeability characteristics using a human induced pluripotent stem cell blood-brain barrier model. *Mol Pharmaceutics* (2016) 13:3341–9. doi: 10.1021/acs.molpharmaceut.6b00441

30. Zorniak M, Clark PA, Leeper HE, Tipping MD, Francis DM, Kozak KR, et al. Differential expression of 2',3'-cyclic-nucleotide 3'-phosphodiesterase and neural lineage markers correlate with glioblastoma xenograft infiltration and patient survival. *Clin Cancer Res* (2012) 18:3628–36. doi: 10.1158/1078-0432.CCR-12-0339

31. Fenno LE, Levy R, Yizhar O. Molecular optimization of rhodopsin-based tools for neuroscience applications. *Methods Mol Biol* (2022) 2501:289–310. doi: 10.1007/978-1-0716-2329-9_14

32. Gray MD, Lampel KA, Strockbine NA, Fernandez RE, Melton-Celsa AR, Maurelli AT. Clinical isolates of Shiga toxin 1a-producing *Shigella flexneri* with an epidemiological link to recent travel to Hispaniola. *Emerg Infect Dis* (2014) 20:1669–77. doi: 10.3201/eid2010.140292

33. Scheutz F, Teel LD, Beutin L, Pierard D, Buvens G, Karch H, et al. Multicenter evaluation of a sequence-based protocol for subtyping Shiga toxins and standardizing Stx nomenclature. *J Clin Microbiol* (2012) 50:2951–63. doi: 10.1128/JCM.00860-12

34. Needham BD, Trent MS. Fortifying the barrier: the impact of lipid A remodelling on bacterial pathogenesis. *Nat Rev Microbiol* (2013) 11:467–81. doi: 10.1038/nrmicro3047

35. Needham BD, Carroll SM, Giles DK, Georgiou G, Whiteley M, Trent MS. Modulating the innate immune response by combinatorial engineering of endotoxin. *Proc Natl Acad Sci U.S.A.* (2013) 110:1464–9. doi: 10.1073/pnas.1218080110

36. Hankins JV, Madsen JA, Needham BD, Brodbelt JS, Trent MS. The outer membrane of Gram-negative bacteria: lipid A isolation and characterization. *Methods Mol Biol* (2013) 966:239–58. doi: 10.1007/978-1-62703-245-2_15

37. O'Brien JP, Needham BD, Brown DB, Trent MS, Brodbelt JS. Top-down strategies for the structural elucidation of intact gram-negative bacterial endotoxins. *Chem Sci* (2014) 5:4291–301. doi: 10.1039/C4SC01034E

38. Lee J-J, Kang JA, Ryu Y, Han S-S, Nam YR, Rho JK, et al. Genetically engineered and self-assembled oncolytic protein nanoparticles for targeted cancer therapy. *Biomaterials* (2017) 120:22–31. doi: 10.1016/j.biomaterials.2016.12.014

39. Mozhei O, Kasparov S. Viral vectors as gene therapy agents for treatment of glioblastoma. *Cancers (Basel)* (2020) 12:3724. doi: 10.3390/cancers12123724

40. Umlauf BJ, Ovsyannikova IG, Haralambieva IH, Kennedy RB, Vierkant RA, Pankratz VS, et al. Correlations between vaccinia-specific immune responses within a cohort of armed forces members. *Viral Immunol* (2011) 24:415–20. doi: 10.1089/vim.2011.0029

41. Kennedy R, Poland GA. T-Cell epitope discovery for variola and vaccinia viruses. *Rev Med Virol* (2007) 17:93–113. doi: 10.1002/rmv.527

42. Haddad N, Carr M, Balian S, Lannin J, Kim Y, Toth C, et al. The blood-brain barrier and pharmacokinetic/pharmacodynamic optimization of antibiotics for the treatment of central nervous system infections in adults. *Antibiotics (Basel)* (2022) 11:1843. doi: 10.3390/antibiotics11121843

43. Din MO, Danino T, Prindle A, Skalak M, Selimkhanov J, Allen K, et al. Synchronized cycles of bacterial lysis for *in vivo* delivery. *Nature* (2016) 536:81–5. doi: 10.1038/nature18930

44. Akbari B, Farajnia S, Ahdi Khosroshahi S, Safari F, Yousefi M, Dariushnejad H, et al. Immunotoxins in cancer therapy: Review and update. *Int Rev Immunol* (2017) 36:207–19. doi: 10.1080/08830185.2017.1284211

45. Carnemolla B, Borsi L, Balza E, Castellani P, Meazza R, Berndt A, et al. Enhancement of the antitumor properties of interleukin-2 by its targeted delivery to the tumor blood vessel extracellular matrix. *Blood* (2002) 99:1659–65. doi: 10.1182/blood.v99.5.1659

46. Weiss T, Puca E, Silginer M, Hemmerle T, Pazahr S, Bink A, et al. Immunocytokines are a promising immunotherapeutic approach against glioblastoma. *Sci Transl Med* (2020) 12:eabb2311. doi: 10.1126/scitranslmed.abb2311

47. Goldman SR, Tu Y, Goldberg MB. Differential regulation by magnesium of the two MsbB paralogs of *Shigella flexneri*. *J Bacteriol* (2008) 190:3526–37. doi: 10.1128/JB.00151-08

48. D'Hauteville H, Khan S, Maskell DJ, Kussak A, Weintraub A, Mathison J, et al. Two msbB genes encoding maximal acylation of lipid A are required for invasive *Shigella flexneri* to mediate inflammatory rupture and destruction of the intestinal epithelium. *J Immunol* (2002) 168:5240–51. doi: 10.4049/jimmunol.168.10.5240

49. Coutermarsh-Ott SL, Broadway KM, Scharf BE, Allen IC. Effect of Salmonella enterica serovar Typhimurium VNP20009 and VNP20009 with restored chemotaxis on 4T1 mouse mammary carcinoma progression. *Oncotarget* (2017) 8:33601–13. doi: 10.18632/oncotarget.16830

50. Ranallo RT, Kaminski RW, George T, Kordis AA, Chen Q, Szabo K, et al. Virulence, inflammatory potential, and adaptive immunity induced by *Shigella flexneri* msbB mutants. *Infect Immun* (2010) 78:400–12. doi: 10.1128/IAI.00533-09

51. Hoffman O, Weber RJ. Pathophysiology and treatment of bacterial meningitis. *Ther Adv Neurol Disord* (2009) 2:1–7. doi: 10.1177/1756285609337975

52. Swanson L, Katkar GD, Tam J, Pranadinata RF, Chareddy Y, Coates J, et al. TLR4 signaling and macrophage inflammatory responses are dampened by GIV/Girdin. *Proc Natl Acad Sci USA* (2020) 117:26895–906. doi: 10.1073/pnas.2011667117

53. Verheul AF, Snippe H, Poolman JT. Meningococcal lipopolysaccharides: virulence factor and potential vaccine component. *Microbiol Rev* (1993) 57:34–49. doi: 10.1128/mr.57.1.34-49.1993

54. Mamat U, Wilke K, Bramhill D, Schromm AB, Lindner B, Kohl TA, et al. Detoxifying Escherichia coli for endotoxin-free production of recombinant proteins. *Microb Cell Fact* (2015) 14:57. doi: 10.1186/s12934-015-0241-5

55. Wang B, Dai T, Sun W, Wei Y, Ren J, Zhang L, et al. Protein N-myristoylation: functions and mechanisms in control of innate immunity. *Cell Mol Immunol* (2021) 18:878–88. doi: 10.1038/s41423-021-00663-2

56. Savage TM, Vincent RL, Rae SS, Huang LH, Ahn A, Pu K, et al. Chemokines expressed by engineered bacteria recruit and orchestrate antitumor immunity. *Sci Adv* (2023) 9:eadc9436. doi: 10.1126/sciadv.adc9436

57. Toso JF, Gill VJ, Hwu P, Marincola FM, Restifo NP, Schwartzentruber DJ, et al. Phase I study of the intravenous administration of attenuated Salmonella typhimurium to patients with metastatic melanoma. *J Clin Oncol* (2002) 20:142–52. doi: 10.1200/JCO.2002.20.1.142

58. Pinho SS, Reis CA. Glycosylation in cancer: mechanisms and clinical implications. *Nat Rev Cancer* (2015) 15:540–55. doi: 10.1038/nrc3982

59. He H, Conrad CA, Nilsson CL, Ji Y, Schaub TM, Marshall AG, et al. Method for lipidomic analysis: p53 expression modulation of sulfatide, ganglioside, and phospholipid composition of U87 MG glioblastoma cells. *Anal Chem* (2007) 79:8423–30. doi: 10.1021/ac071413m

60. Ghosh D, Funk CC, Caballero J, Shah N, Rouleau K, Earls JC, et al. A cell-surface membrane protein signature for glioblastoma. *Cell Syst* (2017) 4:516–29:e517. doi: 10.1016/j.cels.2017.03.004

frontiers | Frontiers in Oncology

TYPE Review
PUBLISHED 24 November 2023
DOI 10.3389/fonc.2023.1291177

OPEN ACCESS

EDITED BY
Theophilos Tzaridis,
Sanford Burnham Prebys Medical Discovery Institute, United States

REVIEWED BY
Aman Sharma,
ExoCan Healthcare Technologies Pvt Ltd, India
Benjamin Umlauf,
The University of Texas at Austin, United States
Stoyan Tankov,
University of Geneva, Switzerland
Jeroen De Vrij,
Erasmus Medical Center, Netherlands

*CORRESPONDENCE
Lisa Nieland
lnieland@mgh.harvard.edu
Xandra O. Breakefield
breakefield@hms.harvard.edu

†These authors have contributed equally to this work

RECEIVED 08 September 2023
ACCEPTED 10 November 2023
PUBLISHED 24 November 2023

CITATION
Lunavat TR, Nieland L, Vrijmoet AB, Zargani-Piccardi A, Samaha Y, Breyne K and Breakefield XO (2023) Roles of extracellular vesicles in glioblastoma: foes, friends and informers. *Front. Oncol.* 13:1291177. doi: 10.3389/fonc.2023.1291177

Roles of extracellular vesicles in glioblastoma: foes, friends and informers

Taral R. Lunavat[1,2†], Lisa Nieland[1,3*†], Anne B. Vrijmoet[1], Ayrton Zargani-Piccardi[1], Youssef Samaha[1], Koen Breyne[1] and Xandra O. Breakefield[1*]

[1]Molecular Neurogenetics Unit, Massachusetts General Hospital and Harvard Medical School, Charlestown, MA, United States, [2]Department of Biomedicine, University of Bergen, Bergen, Norway, [3]Department of Neurosurgery, Leiden University Medical Center, Leiden, RC, Netherlands

Glioblastoma (GB) tumors are one of the most insidious cancers which take over the brain and defy therapy. Over time and in response to treatment the tumor and the brain cells in the tumor microenvironment (TME) undergo many genetic/epigenetic driven changes in their phenotypes and this is reflected in the cellular contents within the extracellular vesicles (EVs) they produce. With the result that some EVs try to subdue the tumor (friends of the brain), while others participate in the glioblastoma takeover (foes of the brain) in a dynamic and ever changing process. Monitoring the contents of these EVs in biofluids can inform decisions based on GB status to guide therapeutic intervention. This review covers primarily recent research describing the different cell types in the brain, as well as the tumor cells, which participate in this EV deluge. This includes EVs produced by the tumor which manipulate the transcriptome of normal cells in their environment in support of tumor growth (foes), as well as responses of normal cells which try to restrict tumor growth and invasion, including traveling to cervical lymph nodes to present tumor neo-antigens to dendritic cells (DCs). In addition EVs released by tumors into biofluids can report on the status of living tumor cells via their cargo and thus serving as biomarkers. However, EVs released by tumor cells and their influence on normal cells in the tumor microenvironment is a major factor in immune suppression and coercion of normal brain cells to join the GB "band wagon". Efforts are being made to deploy EVs as therapeutic vehicles for drugs and small inhibitory RNAs. Increasing knowledge about EVs in the TME is being utilized to track tumor progression and response to therapy and even to weaponize EVs to fight the tumor.

KEYWORDS

glioblastoma, tumor microenvironement, extracellular vesicles, pro-tumorigenic, immunosuppressive biomarkers

Introduction

From the human perspective, any factors that support progression of glioblastomas (GBs) are considered foes and any that hinder their growth or support therapeutic intervention are friends. GB is an extremely fast growing and almost always a lethal malignancy arising presumably from neural precursor or glial cells in the brain (1). The lethality of the GB can be attributed in part to the usually advanced stage at the time of diagnosis and the many modes of resistance to treatment. Extracellular vesicles (EVs) are a stealthy means of communication within the brain that can transfer components of one cell to other cells, thereby altering their physiologic state. EVs are secreted by all cell-types in the tumor microenvironment (TME), including the tumor cells themselves, and have unique and conflicting roles in this fight for survival. These vesicles are membrane enclosed, retaining the orientation of the membrane of the cells from which they are derived. Typically, 50-200 nm in diameter they contain cargo from the source cell including protein, RNA, DNA, lipids and sugars (2, 3). Tumor-derived EVs can be considered as packets of directives to instruct other cells on how to respond to the tumor, inform on the status of the tumor, and potentially be manipulated to contribute to therapeutic intervention. They have an important role, working in conjunction with secreted factors and cell-to-cell contact in changing the phenotype of normal cells in the TME, controlling immune responses to the tumor and regulating the rate of tumor cell proliferation and invasion into the brain.

This review will focus on advances in understanding these dynamic interactions in research articles over the past five-or-so years. We also recommend a few other reviews which have provided insight into this ongoing dialogue, although there is still much to be discovered (4–6). Other relevant reviews include protumorigenic mechanisms in GB (7); interactions of tumor EVs in radiotherapy (8), therapeutic vesicles for GB (9) and EVs as biomarkers for GB (10). A timeline (Figure 1) of important publications related to EVs in GB is provided.

Foe activity – EVs promote tumor progression

GB-derived EVs change the phenotype of surrounding brain cells in support of tumor growth

GBs are known for their heterogeneity between patients and even at the genome/phenotype level within a single tumor (30–32), as well as the complexity of the TME, which comprises various cell-types, including tumor cells, neurons, microglia, astrocytes, macrophages, endothelial cells and immune cells (4). Glioma cells affect almost all cell types in the TME, and recruit non-tumor cells to support glioma expansion, such as monocytes from the bloodstream (33) and microglia from other areas of the brain (34). Multiple studies have shown that GB cells are capable of hijacking healthy brain cells to promote tumor growth through "instructions" mediated in part by EV cargo (35, 36) (Figure 2). EVs regulate gene expression by surface signaling and depositing their cargo into cells in their proximity and at even more distant sites, and are also released into the cerebral spinal fluid (CSF) and blood (37). For example, EVs mediate crosstalk between GB cells and astrocytes, the latter being the most abundant glial cells in the brain (38). GB cells secrete EVs that alter normal astrocytes, which are intended to protect healthy brain tissue, and turn them into highly reactive GB-associated astrocytes via activation of MYC and inhibition of p53 pathways (39). These GB-associated

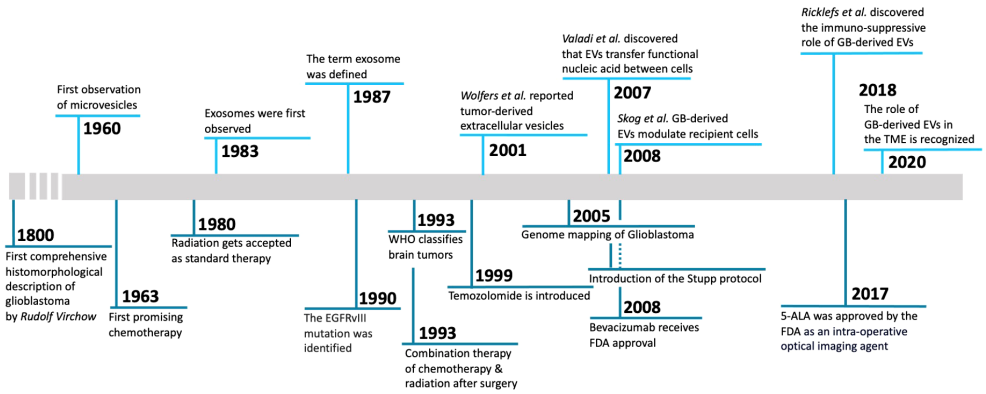

FIGURE 1
Timeline of milestone discoveries regarding GB-derived EVs. 1800, First comprehensive histomorphological description of glioblastoma by Rudolf Virchow (11). 1960, First observation of microvesicles (12). 1963, First promising chemotherapy (13). 1980, Radiation is accepted as standard therapy (14). 1983, Exosomes were first observed (15). 1987, The term exosome was defined (16). 1990, The EGFRvIII mutation was identified (17). 1993, WHO classifies brain tumors (18). 1993, Combination therapy of chemotherapy & radiation after surgery (19). 1999, Temozolomide is introduced (20). 2001, Report of tumor-derived extracellular vesicles (21). 2005, Genome mapping of glioblastoma (22). 2005, Introduction of the Stupp protocol (23). 2007, Discovery that extracellular vesicles transfer functional nucleic acid between cells (24). 2008, EV RNA as blood biomarker for GB and GB-derived extracellular-vesicles modulate recipient cells (25). 2008, Bevacizumab receives FDA approval (26). 2017, 5-ALA approved by the FDA as an intra-operative optical imaging agent (27). 2018, Discover of the immuno-suppressive role of glioblastoma-derived extracellular vesicles (28). 2020, The role of glioblastoma-derived extracellular vesicles in the tumor microenvironment is recognized (29).

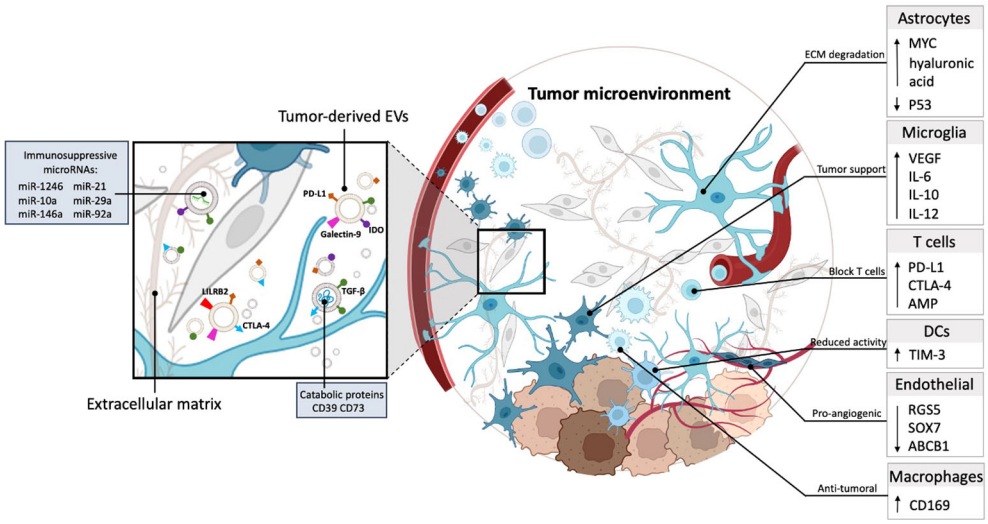

FIGURE 2
GB-derived EVs are capable of hijacking healthy brain cells to promote tumor growth. Tumor-derived EVs carry catabolic proteins and express immunosuppressive molecules, including PD-L1, TGF-β, IDO, and galectin 9. Moreover, they contain immunosuppressive miRNAs (miR-1246, miR-10a, miR-21, miR-29a, miR-92a). These EVs operate within the ECM and are taken up by cells in the TME, contributing to immune evasion and other tumor-promoting processes (left). The TME consists of many cell types, including astrocytes, microglia, T cells, DCs, endothelial cells, and macrophages. Astrocytes contribute to the degradation of the ECM within the TME. Microglia cells within the TME promote tumor growth by increasing the production of pro-inflammatory and endothelial factors, including VEGF, IL-6, IL-12, and IL-10. T cells are hindered within the TME due to the increased expression of immune checkpoint proteins, including PD-L1, CTLA-4, and AMP. This blockade restricts the functionality of T cells within the TME. DCs in the TME potentially reduce tumor cell functionality by increasing the expression of TIM-3, which may contribute to impairing tumor cell function. Endothelial cells in the TME promote angiogenesis, by downregulating RGS5, SOX7, and ABCB1, thereby creating a pro-angiogenic environment. A unique group of macrophages identifiable by the CD169 marker contributes to the establishment of an anti-tumor surrounding within GB.

astrocytes transition into a tumor-promoting phenotype characterized by secretion of pro-inflammatory molecules, such as interleukin (IL)-6 (39), increase in their migrational capacity with enhanced cytokine production through signaling pathways, such as nuclear factor kappa B (NF-κB) and transforming growth factor-β (TGF-β) (40). In addition, through JNK signaling, high levels of CD147 secreted by GB lead to matrix metalloproteinase-mediated degradation of the extracellular matrix (ECM) supporting tumor growth and invasiveness (41).

In addition, GB-derived EVs promote vascularization via reprogramming of endothelial cells, a main component of the perivascular niche – the microenvironment around a blood vessel (42). RNA-sequencing (RNA-seq) analysis has identified candidate microRNAs (mi-RNAs), including miR-9 which mediates post-transcriptional downregulation of angiostatic genes, including *RGS5*, *SOX7*, and *ABCB1* and could explain the failure of anti-angiogenic therapy using anti-vascular endothelial growth factor (VEGF) strategies (43). RNAseq analysis further revealed that microglia, the innate immune cells of the brain which have taken up tumor-derived EVs downregulate genes that are involved in sensing tumor cells and generating an immune reponse to tumor neo-antigens, and actually end up supporting tumor growth (34).

GB-derived EVs also promote proliferation and migration of neuronal progenitor cells through the PI3K-Akt-mTOR pathway (44) and can potentially participate in transformation of these stem-like cells, such that they become tumor-like and may participate in support of tumor recurrence (45). Moreover, EVs play a role in resistance to therapy through their function as decoys of antibody-based therapy, or as drug efflux transporters, as elaborated in a recent review (5). Additionally, GB-derived EVs are involved in radiation-resistance through specific mi-RNA cargosuch as mir320e, miR520f-3p, miR363-3p, miR144-4p, miR16-5p, miR495-3p, miR23a-3p, and miR155-5p which target the PTEN pathway (46).

In conclusion, current evidence points towards a pro-tumorigenic role for GB-derived EVs in modulating the TME, reprogramming healthy brain cells towards a more tumor supportive state and protecting tumor cells from therapy. Although studies have shown that glioma-derived EVs affect neighboring cells in the brain, the many mechanisms by which GB-EVs regulate the TME and affect current therapeutic strategies needs to be further elucidated. One major player - miR-21 is high in GB cells and knocking out miR-21 results in reduced tumor growth (47). GB EVs also have high miR-21 and when transferred to microglia results in changes in their transcriptome which support tumor growth (48). Further studies are crucial to understand glioma-derived EV communication and its interplay with healthy cells of the brain, which could potentially open new therapeutic avenues.

GB-derived EVs suppress the immune response to tumor antigens

Overall, GBs effectively counter anti-tumor immunity essential for a positive immunotherapy outcome (49). As well-recognized intercellular mediators, GB EVs incorporate immune attenuating

molecules, such as checkpoint inhibitor proteins - programmed death ligand-1 (PD-L1;(28), cytotoxic T-lymphocyte associated protein 4 (CTLA-4;(50), and immunosuppressive cytokines, such as TGF-β (29). GB EVs also contain small immunosuppressive miRNA species such as miR-1246, miR-10a, miR-21, miR-29a, and miR-92a, which serve to generate an "immunosuppressive halo" around tumor cells (51). The goal of these regulatory signals transported by GB-derived EVs is to manipulate oncogenic cells associated with the tumor for example microglia, myeloid-derived suppressor cells, and dendritic cells (DCs), while blocking potential anti-tumor activity in the TME by interfering with the recruitment from the periphery and activity of immune cells, including CD4+ effector T cells and CD8+ effector T cells (52).

EVs mimic immunosuppressive signals that act through direct contact with immune target cells. GB-derived EVs are enriched with membrane-associated PD-L1 interacting with PD-1+ tumor-reactive T cells to impair their proliferation and stimulation (28). In addition to PD-L1, other immune checkpoint proteins, such as CTLA-4, can be exposed to GB-derived EVs and act to suppress natural killer (NK) cell and CD4+ T cell activation (50). The same study showed that CD39 and CD73 are also transported by these EVs. These catabolic proteins convert ADP/ATP into AMP or adenosine, leading to blockage of clonal expansion and homing of T cells by interacting with the adenosine receptor, A2AR (53–55). Another inhibitory molecule transferred by GB-EVs known to modulate T cells is leukocyte immunoglobulin-like receptor subfamily 2 (LILRB2) (56).

Unlike EVs of non-GB origin, GB-EVs uniquely modulate the transcriptome of monocytes, macrophages, and microglia into tumor-supportive phenotypes. Oncogenic EV-uptake by tumor associated cells leads to changes in cytokine secretion (e.g., VEGF and IL-6), changes in antigen display to deviate T cells from their target, and increased expression of matrix metalloproteinases (57) or lowering of miR-146a-5p (58) rendering the extracellular space more permissive for tumor cell migration. Immunosuppression by GB-EVs results in altered release of cytokines from monocytes, such as arginase, TGF-β, and IL-10, which lead to T cell dysfunction in glioma, while blocking pro-inflammatory cytokines such as IL-12, and TNF-α (59). Other functions of GB-EVs include the transfer of information to myeloid cells to obtain pro-tumor immunogenic properties in a process called superinduction (60). Superinduction occurs when exposure of GB cells to IFN-γ during a T-cell response leads to the release of PD-L1 and indoleamine 2,3-dioxygenase (IDO) via GB-derived EVs. These molecules are then internalized by monocytes, promoting the differentiation of myeloid-derived suppressor cells. These myeloid derived suppressor cell, in turn, have the ability to reduce T cell proliferation. Tumor-recruited astrocytes can also contribute to the GB-myeloid immunosuppression circuit. It is known that astrocytes that have taken up GB-derived EVs increase levels of hyaluronic acid (61). This is an important ligand for CD44-positive macrophage differentiation at the GB site attenuating tumor immunogenicity and, consequently, promoting GB growth (62). Other indirect blockage systems involve reducing the functionality of DCs to suppress T-cell maturation, proliferation, and activation (63). Galectin-9 on GB-EVs isolated from the CSF of GB patients binds the TIM-3 receptor on DCs and inhibits antigen recognition, processing, and presentation by DCs and thus a subsequent cytotoxic T cell response (63).

In conclusion, EVs derived from a number of cell types in the TME help mediate the immunosuppressive milieu dictated by GB cells (Figure 3). These EVs work to ensure that immune cells are not able to respond appropriately to GB neoantigens and thereby aid in tumor establishment and growth, as well as resistance to immunotherapy.

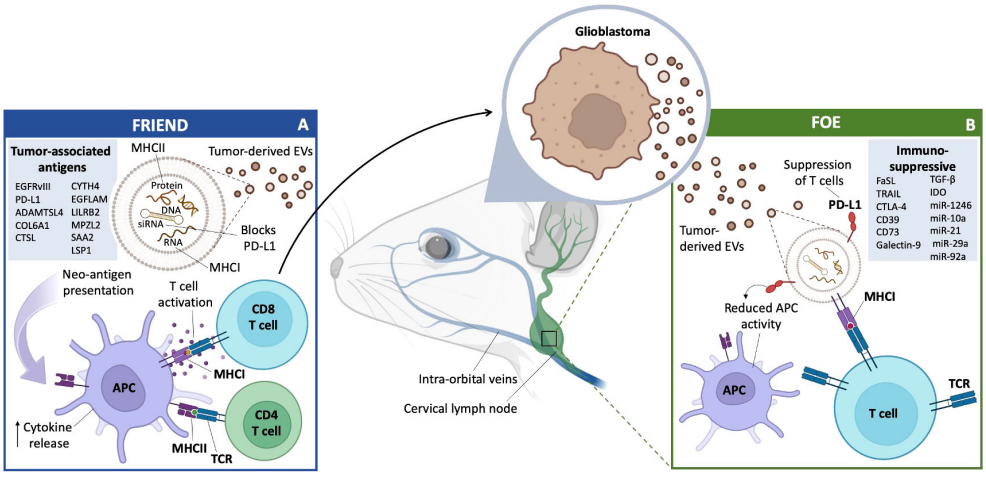

FIGURE 3
GB EVs and Immunity: Friend or Foe. **(A)** Friend GB-derived EVs travel through the lymphatic system and carry macromolecules from the tumor to various immune system accessory cells, primarily in the cervical lymph nodes. This includes antigen presentation directly to T cells for activation, or T cell activation mediated by APCs and increase in cytokine release. GB-derived EVs can also act as a blockade of PD-L1 secretion, allowing for a more effective immune response. A list of confirmed and potential TAA (left box). **(B)** Foe GB-derived EVs carry immune blocking proteins, such as PD-L1, which can lead to the suppression of T cells and a reduction in APC activity through a number of cytokines, proteins and miRNAs (right box).

Friend activity - EVs block tumor progression

EVs released by TME cells can act to restrict tumor growth/invasion

EVs have emerged as significant regulators of the immune response throughout tumor progression, as they carry a diverse array of molecular cargo that has a critical role in modulating the immune response (64). In recent years, researchers have discovered that brain cell-derived EVs have the potential to suppress tumor growth, offering new insights into the complex interactions between the brain and cancer.

Communication between microglia and GB cells through EVs plays a role in maintaining or restoring the balance of glutamate levels, important in maintaining homeostasis in the central nervous system (CNS) (65). These microglia-derived EVs serve as carriers of specific molecular messages targeted at cancer cells, prompting alterations in the metabolism of GB cells. Notably, these effects are orchestrated by miR-124, encapsulated within small EVs (sEVs) released by microglia which are internalized by GB cells. Once internalized, miR-124 exerts an influence on the behavior and metabolism of GB cells, resulting in a diminished release of lactate, nitric oxide, and glutamate into the extracellular environment. This interplay between microglia and GB cells contributes to the rebalancing of CNS homeostasis and have an effect on how GB cell responses to their surroundings (65). However, it is important to note that the role of microglia secreted EVs in tumor growth can vary depending on the context and specific factors involved.

Another example of EVs acting as a tumor friendly influencer is in regard to oligodendroglioma. These tumor cells release EVs carrying TRAIL and molecular chaperones, which wield their impact by triggering cell demise in astrocytes, potentially hindering tumor growth (66). Moreover, these EVs have the capability to initiate neuronal apoptosis as well (67), which potentially reduces the tumor's ability to interact with neurons for its benefit an activity against the tumor.

The limited infiltration of NK cells into GB and the effective evasion strategies employed by such tumors have made targeting GB cells challenging (68). However, NK-EVs have been implicated in multiple mechanisms of cancer cell destruction (68, 69) employing both caspase-independent and caspase-dependent pathways to induce cytotoxicity (70). The actions of NK-EVs contribute, at least partially, to the cytotoxic effects observed in NK cell-induced tumor cell death (68, 70). Furthermore, increased levels of specific proteins, such as perforin, granzyme A, granzyme B, and granulysin are associated with the cytotoxic potential of NK-EVs (70).

Endothelial cells in the neovasculature of tumors also put up a good fight. The involvement of endothelial cell-derived EVs carrying esophageal cancer-related gene-4 (ECRG4) protein can result in the inhibition of glioma cell proliferation (71). Furthermore, the expression of inflammatory cytokines and angiogenesis-related factors, including NF-κB, IL-1β, IL-6, IL-8, monocyte chemoattractant protein-1 (MCP-1), hypoxia-inducible factor 1-alpha (HIF-1α), VEGF and vascular endothelial growth factor receptor 2 (VEGFR2) in the TME are suppressed by ECRG4-EVs (71). GBs also release EVs containing podoplanin (PDPN), resulting in platelet activation and a clotting cascade, which can lead to thrombosis in the tumor and peripheral vasculature, although definitely a health risk to patients it is not clear whether this helps or hurts the tumor itself.

In conclusion, the release of EVs by different brain cells represents a fascinating avenue in cancer research. The ability of some of these EVs to suppress tumor growth through various mechanisms highlights their potential therapeutic significance. Further exploration of these interactions between brain cells and tumors may help to develop targeted anti-cancer therapies that exploit the natural tumor-suppressive properties of some brain cell-derived EVs.

EVs released by GBs can travel to cervical lymph nodes to present neo-antigens

An effective T cell response is an important step in mounting an immune response against a tumor. The cervical lymph nodes serve as one of the primary sites of tumor antigen presentation to T cells. DCs, a type of professional antigen presenting cell (APC), expose their loaded antigens to naive T cells, which can prime the T cells into effector T cells, with cytotoxic, regulatory or helper capabilities (72) (Figure 3).

To launch an antigen specific response, cytotoxic T-lymphocytes (CTLs) must form a close relationship, called the immune synapse (IS), between themselves and target cells to begin an antigen specific response (73). EVs have been shown to be effective in activating CTLs, by activating naïve T cells, even in the absence of APCs (74). GB is considered to be a "cold" tumor, i.e. low in tumor neoantigens. Neoantigens arise from somatic mutations that occur in coding regions of genes during tumorigenesis and are not found in healthy cells (75).

GB is known for its low mutation burden and a low frequency of mutations in the tumor cells. One of the most recognized neoantigens is EGFRvIII, a mutant form of EGFR found in ~ 30% of GBs (76). Using RNA-seq data from 142 GB patients, 6,585 mutated genes were identified as potential sources of tumor specific antigens (TSAs) and 5,221 genes were overexpressed and identified as potential tumor-associated antigens (TAAs) (77). Of the 1,322 GB-associated genes that fell under both categories, nine genes (ADAMTSL4, COL6A1, CTSL, CYTH4, EGFLAM, LILRB2, MPZL2, SAA2, and LSP1) were identified as being associated with both overall survival and relapse free survival. These nine genes had positive correlations with DC infiltration, implying recognition of potential neoantigens which could be presented to APCs and be involved in an immune response. These potential neoantigens were identified as possible targets for an mRNA vaccine, and may even be transported by GB-derived EVs to elicit an immune response. Tumor cell-derived proteins have been detected in and on EVs isolated from plasma using a cross-species xenograft model, providing additional proof that tumor-

derived EVs circulate in the blood (78). As tumor-derived EVs are carriers of neoantigens, it is possible that they could be mediators of an anti-tumor immune response. In two murine glioma models, major histocompatibility complex I (MHC-I) (H-2Db)–restricted Imp3D81N (GL261 cells) and Odc1Q129L (SMA-560 cells) were confirmed to be endogenous neoantigens with immunogenic properties, with neoantigen-specific T cell populations being detected both intratumorally and within cervical lymph nodes (79). Thus, MHCI molecules exposed to tumor antigens on the surface of EVs can directly prime naive T cells into CD8+ T cells with cytotoxic capabilities.

Alternatively, EVs can be taken up by professional APCs, such as DCs, and GB neoantigens presented to T cells as another form of antigen presentation, known as cross-presentation (49). Migratory DCs presenting tumor antigens can travel to regional lymph nodes and present their antigens, or release EVs that will present these antigens to resident-lymphoid DCs through vesicle transfer to facilitate antigen presentation to T cells (49). This process aids circulating naive T cells in becoming active against a corresponding tumor-antigen (49). The process of EVs presenting tumor-antigens to immune cells reveals the potential of EVs to be beneficial in mounting an immune response against GB and other malignancies.

EVs can serve as therapeutic vehicles

EVs hold promise a means of delivering drugs and other therapeutics to GB in various applications. When administered systemically to rodents, GB EVs have demonstrated the ability to transport functional cargo while evading immune clearance more effectively than conventional delivery methods, such as surgery, chemotherapy and targeted immunotherapy (80), and intravenous administered EVs can pass through the blood-brain barrier (BBB) (81). The latter can be facilitated with focused ultrasound (82).

The therapeutic potential of EVs is further supported by clinical data emerging from cancer research. For comparison nanoparticles (NPs) containing doxorubicin (DOX) were employed for the treatment of intracranial GB (83–85). After uptake by U87 glioma cells, NPs facilitated the release of DOX from lysosomes with cytotoxic effects (84). Red blood cells (RBC) EVs loaded with drugs exhibited no systemic toxicity, while direct doses of DOX demonstrated systemic toxicity at levels which were therapeutically effective. RBC-derived EVs loaded with combination of cytoplasmic phospholipase A2 (cPLA2) siRNA/metformin served to downregulate GB energy metabolism (86). Impaired GB metabolism resulted in reduced tumor growth and increased mouse survival in a patient-derived xenograft GB model (86). miR-1208 loaded EVs led to suppression of the TGB-β pathway and reduction of glioma growth in mice (82). EVs have also been loaded with CRISPR-Cas9 to sensitize glioma cells to radiotherapy by enhancing induction of ferroptosis (87) and with the cytokine IL-12 in EVs from mature DCs to enhance immune response to the tumor (88). These recent examples from the literature illustrate loading of EVs with drugs, RNA and proteins for therapeutic effect on GB.

The specific use of EVs as drug carriers also presents opportunities for immunotherapy. A recent study demonstrated that the CpG-STAT3 antisense oligonucleotides loaded into neural stem cells derived EVs potently stimulated immune activity of human DCs or mouse macrophages, inducing NF-κB signaling and IL-12 production in the glioma microenvironment in mice (89). Furthermore, an anesthetic Propofol suppressed the communication between pro-tumorigenic GB stem cells (GSCs) and microglia by interfering with the transmission of EVs (90). This study substantiated the anticancer attributes of Propofol, delineating its capacity to modulate GSCs, rendering them more receptive to ionizing radiation and temozolomide (TMZ) therapy. Furthermore, Propofol can perturb the pro-tumorigenic interactions between GSCs and microglia when combined with EV-mediated transport of antisense RNA to brain-derived neurotrophic factor (BDNF) (90).

In a rat GB model, EVs carrying yeast cytosine deaminase:: uracilphosphoribosyl transferase (yCD::UPRT-MSC) conjugated with 5-fluoroytocysine (5-FC) cured a significant number of rats when injected intraperitoneally or intranasally, with 5-FC being converted to the cytotoxic 5-fluorouracil (91). Recently, it has been shown that adipose stem cell-derived EVs may prove intrinsically therapeutic by regulating, proliferation, invasiveness and angiogenesis of GB cells, as shown in *in vitro* and *in vivo* chorioallantoic membrane model assays (92).

The inherent potential of EVs to selectively interact with target cells upon introduction into an organism is a fundamental characteristic crucial for precise targeting of particular cell populations, such as tumor cells. It has been established that EVs derived from zebrafish brain endothelial cells, carrying paclitaxel and DOX payloads, exhibit the remarkable capability not only to traverse the BBB, but also to exhibit a high degree of specificity in targeting GB cells (93). Other targeting mechanisms for GB have included docking of antibodies to PD-L1 on CD64 on the EV surface for delivery of mRNA for IFN-γ (94) and conjugation of cyclic-RGDyC to the EV surface to target integrin alpha v beta 3 on GB cells to deliver DOX (95). EVs derived from engineered MSCs expressing anti-EGFRvIII antibody on their surface selectively induced apoptosis in U87-EGFRvIII GB cells, as compared to U87 cells *in vitro* (96).

Neoantigens have also proven to be promising candidates for immunotherapy, targeting various malignancies, including GB. In a Phase Ib GB clinical trial, MHCI-based neoantigen vaccines were used to induce an immune response after surgery and chemotherapy (97). The results suggested that levels of infiltrating T cells increased only in patients who developed an immune response specific to the neoepitopes of the vaccine. In a Phase IIa clinical study against newly diagnosed GB, SurVaxM, a peptide vaccine targeting a member of the inhibitor of apoptosis protein family, was shown to be safe with no serious side effects attributed to SurVaxM. A randomized, large-scale clinical trial of SurVaxM is currently ongoing (NCT02455557; source ClinicalTrail.gov) (98). In a Phase I clinical trial, an ITI-1001 multi-antigen DNA vaccine was given to patients with newly diagnosed GB. The ITI-1001 vaccine utilized the UNITE platform, which combines the

lysosomal targeting protein LAMP1 with target antigens (pp65, gB, and IE-1) (NCT05698199; source ClinicalTrail.gov). Treatment of a syngeneic GB mouse model (CT-2A) with ITI-1001 resulted in increased antigen presentation, multi-antigen-specific CD4 and CD8 T cell responses, and around 56% long-term survival in tumor-bearing mice (99). These promising findings led to a follow-up phase I clinical trial with GBM patients (NCT05698199; source ClinicalTrail.gov). Further studies could elucidate more potential neoantigens that provide an anti-tumor immune response and apply them to existing EV-nano vaccine approaches targeting GB.

Despite the encouraging prospects of EVs as a prospective diagnostic and therapeutic avenue for GB, there remains a scarcity of clinical-level investigations evaluating their potential therapeutic applications in GB. Although the involvement of EVs in the progression of GB is well-established, substantial challenges persist in harnessing EVs for therapeutic purposes in GB. These challenges encompass the isolation, subtyping, enrichment, cargo loading, and conferring of target specificity to EVs, among other aspects. Overcoming these impediments holds the potential to establish EV-based therapies as a routine treatment modality for glioma patients in the future.

Informer activity - EVs serve as biomarkers

EVs released by GBs can serve as biomarkers (informers) for cancer drivers and response to therapy

Currently, magnetic resonance imaging (MRI) is the most commonly used method for detecting GB and monitoring tumor progression. This process is, however, time-consuming, inconvenient for patients, and not always reliable in patients who previously received tumor resection followed by radiotherapy or immunotherapy, referred to as pseudo-progression (100–102). Additionally, invasive tumor biopsies are performed to confirm tumor subtypes and genetic drivers, as well as to tailor treatments precisely to patients (100). Therefore, there is a great need for minimally invasive techniques to detect and monitor GB progression and response to therapy at all stages.

Biomarkers found in blood, CSF, urine or saliva can provide detailed information about tumors using a minimally invasive approach and have a prominent role in tumor diagnosis, and assessment of disease progression and treatment response (102, 103). In GB, however, the search for biomarkers has been challenging mainly due to the restricted permeability of the BBB, which limits the passage of tumor-derived biomarkers into the circulation (102, 104). EVs released by tumor cells and other cells in the TME contain various proteins and RNA species and can pass through the BBB, carrying detailed information about the tumor and the TME, including tumor-specific biomarkers (105). Moreover, EVs have relatively short half-lives in circulation, thereby reporting on the current status of the tumor (106).

EV isolation methods pose many challenges, resulting in either loss of EV quantity or purity of EV samples (107, 108). Nevertheless, new methods are continuously being created to identify EV content, such as Surface-enhanced Raman spectroscopy with nanocavity microchips (MoSERS microchip) (109) and tunable micropattern arrays (110). GB-EVs found in the blood are present in small quantities, especially in early GB stages, and mixed into a complex composition of EVs derived from other cell types, circulating cells, proteins, nucleic acids and lipids (107, 108). Protein biomarkers are found to be valuable biomarkers in a variety of cancers (111, 112), but have shown limitations as biomarkers in GB as serum contains a limited amount of GB-derived protein (107, 111). This makes it challenging to isolate enough tumor-derived protein for early GB diagnostic purposes. As tumor-derive proteins will be present in higher quantities at later stages of tumor progression, proteins could be useful for analyzing treatment response and prognosis. RNA, on the other hand, has great potential as a diagnostic biomarker for GB, as RNA is protected from degradation in EVs and can be amplified after EV isolation (111).

Early studies identified the EGFRvIII mutant RNA in serum of patients harboring EGFRvIII-positive tumors (25). This now includes a host of other tumor markers including amplified EGFR (113); miR-21 (114), miR-486-3p (115); O6-methylguanine DNA methyltransferase, and isocitrate dehydrogenase (116). In patients with GB, the levels of PD-L1 RNA in EVs derived from serum and plasma have exhibited correlation with tumor volume up to 60 cm^3 (110).

Even though proteins pose challenges as potential biomarkers in early GB diagnosis, several studies have revealed their potential. Cilibrasi et al. (106) compared sEVs (< 200 nm) derived from the plasma of healthy controls with those from GB patients, explicitly looking at protein content within EVs. They found ninety-four proteins derived from EVs to be significantly different between GB patients and healthy controls, including Von Willebrand-Factor (VWF), complement signature C3, Fc Gamma Binding Protein (FCGBP), Protein S 1 (PROS1) and Serpin Family A Member 1 (SERPINA1). These proteins were previously identified as linked to GB and have been associated with immune evasion and poor prognosis (106). In addition, CD29, CD44, CD146, CD81, C1Qa, and histone H3 were also recently identified as potential protein markers for the tumor progression of GB. These markers were upregulated in sEVs of recurrent GB patients and are associated with angiogenesis, invasiveness, and proliferation (102). Another protein that promotes angiogenesis, LGALS3BP is overexpressed in plasma EVs of several cancers, including GB, making it a good marker for GB diagnosis (117). The EV levels of LGALS3BP are thought to correlate with tumor grade and increased tumor burden (117, 118).

Saliva also contains EVs with protein biomarkers (105). Some potential biomarkers found in sEVs of saliva are aldolase A (ALDOA), 14-3-3 protein ϵ (1433E), transmembrane protease serine 11B (TM11B), and enoyl CoA hydratase 1 (ECH1). These proteins are increasingly present in pre-operative GB patients with unfavorable outcomes compared to pre-operative patients with favorable outcomes. These proteins have a role in cell

proliferation, apoptosis, migration, and invasion, potentially increasing the likelihood of poor outcomes in patients (105).

Research studies vary with regard to EV size and concentration in GB patients compared to healthy controls. The majority of studies indicate higher EV levels in patients compared to healthy subjects (3, 102, 103). Whereas others, found no significant differences (106). The variation in findings among research groups might be attributed to differences in EV isolation techniques or patient cohorts (106, 119).

In addition to sEVs derived from plasma or saliva, sEVs isolated from the CSF may also provide in-depth information about the internal interactions between the tumor and the TME. As these sEVs will not have passed through the BBB, they may provide a more accurate representation of the current situation within the TME. EVs isolated from CSF have shown higher sensitivity in detecting GB than EVs isolated from other bodily fluids (104, 120). This method of EV isolation, however, is more invasive for patients, making it a more challenging method for tumor monitoring and treatment response (5, 120). An example of CSF biomarkers released in EVs of GB cells and glioma stem cells are miR-21 and miR-9 (120). These potential biomarkers play a role in tumor migration and proliferation.

Recently, urine samples of GB patients have been studied and urine-derived EVs contain useful diagnostic and prognostic biomarkers for GB (119, 121). It is challenging to extract EVs and biomarkers from urine, but several research groups have shown that nanowire assays can be a useful tool for extracting these biomarkers. Urine is easily accessible and would provide a minimally invasive way to diagnose or analyze treatment response in GB. Fifty-seven miRNAs are differentially expressed in patients with CNS tumors compared to healthy subjects, of which 23 most strongly associated with GB were selected using logistic LASSO regression analysis - miR-6070, miR-22-3p, miR-4538, miR-1285-3p, miR-372-5p, miR-4525, miR-5698 were increasingly expressed in CNS tumor patients, including GB patients, and miR-204-3p, miR-6763-5p, miR-101-5p, miR-208a-5p, miR-371a-3p, miR-378a-5p, miR-216a-5p, miR-6864-3p, miR-450b-3p, miR-640, miR-4426, miR-17-3p, miR-450a-2-3p, miR-1248, miR-100-5p, and miR-16-5p were under expressed in these patients as compared to controls (121). In addition, the EV membrane protein CD31/CD63 was overexpressed in urine of GB patients compared to healthy patients (119). CD31 is correlated with tumor progression and prognosis as it plays a role in vasculogenesis (119). All in all, urine has potential as a source for EV biomarkers, but further research needs to explore the extent and application of EV biomarkers present in urine, as well as how small the EVs need to be to pass through the kidney filtration. Besides using EVs in GB diagnosis, EVs can serve as predictive markers for treatment response and can, thus, have a role in personalized medicine. Several studies observed increased expression of heat shock proteins (HSPs), mainly HSP70, in both sEVs (< 200 nm) and the TME of TMZ resistant human glioma lines tested *in vitro*, most prominently U87 (122–124). TMZ-sensitive U87 cells showed a decrease in HSPs compared to untreated U87 cells (123). HSPs are proteins broadly involved in proteome homeostasis, with HSP70 specifically playing a role in treatment resistance and increasing survival in cultured U87 cells (123). Similar decreases of isocitrate dehydrogenase type 1 (IDH1), PDPN, and Hsp90 were observed in both sEVs (< 200 nm) and large (l) EVs (> 200 nm) of TMZ treatment-sensitive GB cells in culture compared to untreated samples. HSPs, IDH1 and PDPN have great potential as predictive markers for GB and should be further explored *in vivo*.

RNA content of EVs is known to be a highly sensitive and predictive biomarker of GB. Upregulation in the long-non-coding RNA - SBF2-AS1 was associated with TMZ resistance *in vitro* and *in vivo* (122). Moreover, Dacomitinib, a tyrosine kinase inhibitor, showed differences in gene expression in recurrent GB with amplified EGFR as measured in EV mRNA comparing GB patients with responsive and non-responsive tumors. EGFRvIII or EGFR-extracellular domain (ECD) mutation status was, however, not correlated with the clinical response (122, 125). In addition, expression of the *RAD51* gene and the *MDM2* gene increase significantly in the TME of the U87 MG and LN229 glioma cell lines in association with HSP proteins *in vitro*. MDM2 plays a role in the degradation of p53, resulting in evasion of apoptosis. An increase of MDM2 is observed in both the TME and EVs, whereas RAD51 is only increased in the TME (124). RAD51 is involved in DNA repair mechanisms, so increasing expression of this gene could fortify resistance in treatment that induces DNA damage, such as chemotherapy. In clinical tissue samples and serum derived-EVs from GB patients, the lncRNA HOX transcript antisense RNA (HOTAIR) was overexpressed, which has great potential as a prognostic and diagnostic biomarker and may also provide further information about TMZ treatment resistance (126).

Ding et al. (127) compared GB patients' immunological states and treatment responses and categorized patients based on EV gene expression and survival (high risk vs. low risk). Three EV transcripts for nerve growth factor (NGF), insulin-like growth factor binding protein 6 (IGFBP6), and T cell receptor constant β chain-1 (TRBC1) were identified as the most relevant features in predicting patients' risk. The high-risk group showed significantly shorter survival compared to low-risk group. In addition, they demonstrated differences in immune cell invasion, with the high-risk groups expressing more immune checkpoint markers, including programmed cell death protein (PD1), and having a worse prognosis. Due to the expression of PD1/PD-L1, these patients were found to have improved responses when treated with anti-PD-L1 compared to those in the low-risk group. On the other hand, the low-risk patients displayed more somatic mutations, such as in EGFR and TP53. Targeted therapies may, thus, benefit patients in the low-risk groups. Therefore, exploring gene expression in EVs from patients may be valuable for anticipating treatment response and might aid in the development of personalized therapies for patients (122, 125, 127).

Finally, positive treatment response to photon- and proton-based radiotherapy showed an increase in patients with EVs expressing the cell surface proteins - CD9 and CD81 (128). A substantial increase in CD9- and CD81-positive EVs post-treatment was found to be a valuable indicator of treatment effect. This

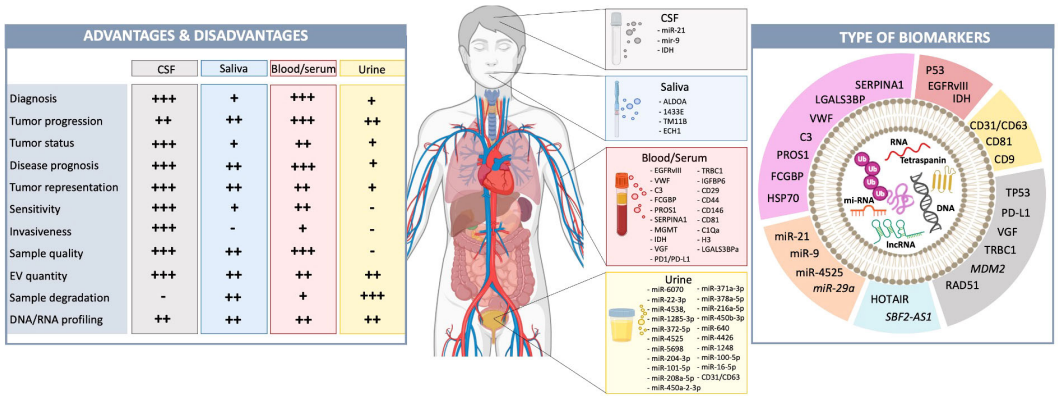

FIGURE 4
GB-derived EVs function as biomarkers in liquid biopsies. Liquid biopsies from blood, CSF, urine, or saliva are becoming valuable, minimally invasive tools for tumor diagnosis and prognosis (102, 103). Each type has advantages and disadvantages (left). CSF is closest to the tumor and in contact with the TME, accurately representing the current tumor status (102, 103). However, obtaining CSF is highly invasive, making it more challenging to analyze tumor progression and treatment response. Biomarkers in saliva, blood and urine have crossed the BBB and have, thus, been filtered. This is even more extreme in urine as they travel through the kidneys (129, 130). This makes these liquid biopsies less reliable for analyzing tumor status and representation, however, obtaining these biopsies is less invasive for patients. Previously identified potential biomarkers have been listed. The source (CSF, saliva, blood/serum, urine) and type (i.e., RNA, DNA, protein, mi-RNAs). of these EV biomarkers are illustrated (pink, protein; red, RNA; yellow, tetraspanin; grey, DNA; blue, lon-noncoding RNA; orange, mi-RNA) (right). Biomarkers written in italics are identified in pre-clinical models, but not in patient samples yet.

increase was also observed when GB cells (A172, LN229, U373, and T98G) in culture underwent apoptosis. An increased presence of CD9- and CD81-positive EVs are not, however, indicative of radiosensitivity, as these markers are highly expressed in the majority of GB patient EVs regardless of how effective the treatment is (128).

In conclusion, EVs can be valuable biomarkers for GB diagnosis, tumor progression and treatment response (Figure 4). EV size and concentration are currently unreliable for GB diagnosis or progression, but protein and RNA markers can be informative. Further research is needed to expand distinguishing EV characteristics in GB patients of various types, at different stages of the disease and in response to therapy.

Conclusion

EVs function as cargo vehicles transporting a variety of cellular contents throughout the TME and are therefore promising as biomarkers and even targets for therapeutic approaches in treatment of cancer, including GB. However, EVs – especially those released from tumor cells are very adept at promoting tumor progression, including changing the phenotype of normal cells in the TME so that they come to support tumor growth. In addition these EV enemies of the brain have multiple roles in suppressing the immune response to the tumor. All in all it is sometimes difficult to categorize EVs as friends or foes as they have so many cross acting communicative functions. In general, early in tumor growth EVs from normal cells, such as microglia and astrocytes, are focused on eliminating this "foreign object", but later as the tumor progresses and bombards them with its own EVs they switch camps and are more supportive of the tumor. In this review we have summarized the roles of EVs in protection of brain from GB and tumor progression and discussed recent and current research regarding the use of EVs as a diagnostic and therapeutic tool.

Author contributions

TRL: Writing – original draft, Writing – review & editing. LN: Visualization, Writing – original draft, Writing – review & editing. ABV: Writing – original draft. AZ: Writing – original draft. YS: Writing – original draft. KB: Writing – original draft, Writing – review & editing. XOB: Funding acquisition, Supervision, Writing – original draft, Writing – review & editing.

Funding

The author(s) declare financial support was received for the research, authorship, and/or publication of this article. XOB acknowledges the National Institutes of Health (NIH) CA179563, CA069246, NS122163 and CA232103 grants for supporting this work. CA179563 is supported by the NIH Common Fund through the Office of Strategic Coordination/Office of the NIH Director. TRL acknowledges research grant from Norwegian Research Council (NFR), 315566.

Conflict of interest

The authors declare that the research was conducted in the absence of any commercial or financial relationships that could be construed as a potential conflict of interest.

Publisher's note

All claims expressed in this article are solely those of the authors and do not necessarily represent those of their affiliated organizations, or those of the publisher, the editors and the reviewers. Any product that may be evaluated in this article, or claim that may be made by its manufacturer, is not guaranteed or endorsed by the publisher.

Supplementary material

The Supplementary Material for this article can be found online at: https://www.frontiersin.org/articles/10.3389/fonc.2023.1291177/full#supplementary-material

References

1. Le Rhun E, Devos P, Houillier C, Cartalat S, Chinot O, Di Stefano AL, et al. 'Romiplostim for temozolomide-induced thrombocytopenia in glioblastoma: The PLATUM trial'. *Neurology* (2019) 93:e1799–e806. doi: 10.1212/WNL.0000000000008440

2. Mathieu M, Martin-Jaular L, Lavieu G, Thery C. 'Specificities of secretion and uptake of exosomes and other extracellular vesicles for cell-to-cell communication'. *Nat Cell Biol* (2019) 21:9–17. doi: 10.1038/s41556-018-0250-9

3. Maire CL, Fuh MM, Kaulich K, Fita KD, Stevic I, Heiland DH, et al. 'Genome-wide methylation profiling of glioblastoma cell-derived extracellular vesicle DNA allows tumor classification'. *Neuro Oncol* (2021) 23:1087–99. doi: 10.1093/neuonc/noab012

4. Broekman ML, Maas SLN, Abels ER, Mempel TR, Krichevsky AM, Breakefield XO. 'Multidimensional communication in the microenvirons of glioblastoma'. *Nat Rev Neurol* (2018) 14:482–95. doi: 10.1038/s41582-018-0025-8

5. Yekula A, Taylor A, Beecroft A, Kang KM, Small JL, Muralidharan K, et al. 'The role of extracellular vesicles in acquisition of resistance to therapy in glioblastomas'. *Cancer Drug Resist* (2021) 4:1–16. doi: 10.20517/cdr.2020.61

6. Khayamzadeh M, Niazi V, Hussen BM, Taheri M, Ghafouri-Fard S, Samadian M. 'Emerging role of extracellular vesicles in the pathogenesis of glioblastoma'. *Metab Brain Dis* (2023) 38:177–84. doi: 10.1007/s11011-022-01074-6

7. Teran Pumar OY, Lathia JD, Watson DC, Bayik D. "Slicing' glioblastoma drivers with the Swiss cheese model'. *Trends Cancer.* (2023). doi: 10.1016/j.trecan.2023.08.002

8. Robinson SD, Samuels M, Jones W, Gilbert D, Critchley G, Giamas G. 'Shooting the messenger: a systematic review investigating extracellular vesicle isolation and characterisation methods and their influence on understanding extracellular vesicles-radiotherapy interactions in glioblastoma'. *BMC Cancer* (2023) 23:939. doi: 10.1186/s12885-023-11437-6

9. Dong YJ, Hu JJ, Song YT, Gao YY, Zheng MJ, Zou CY, et al. 'Extracellular vesicles from urine-derived stem cell for tissue engineering and regenerative medicine'. *Tissue Eng Part B Rev* (2023). doi: 10.1089/ten.teb.2023.0100

10. Zanganeh S, Abbasgholinejad E, Doroudian M, Esmaelizad N, Farjadian F, Benhabbour SR. 'The current landscape of glioblastoma biomarkers in body fluids'. *Cancers (Basel)* (2023) 15(15):3804. doi: 10.3390/cancers15153804

11. Stoyanov GS, Dzhenkov DL. 'On the concepts and history of glioblastoma multiforme - morphology, genetics and epigenetics'. *Folia Med (Plovdiv)* (2018) 60:48–66. doi: 10.1515/folmed-2017-0069

12. Dalton AJ. 'Microvesicles and vesicles of multivesicular bodies versus "virus-like" particles. *J Natl Cancer Inst* (1975) 54:1137–48. doi: 10.1093/jnci/54.5.1137

13. Gilman A. 'The initial clinical trial of nitrogen mustard'. *Am J Surg* (1963) 105:574–8. doi: 10.1016/0002-9610(63)90232-0

14. Gianfaldoni S, Gianfaldoni R, Wollina U, Lotti J, Tchernev G, Lotti T. 'An overview on radiotherapy: from its history to its current applications in dermatology. *Open Access Maced J Med Sci* (2017) 5:521–25. doi: 10.3889/oamjms.2017.122

15. Pan BT, Teng K, Wu C, Adam M, Johnstone RM. 'Electron microscopic evidence for externalization of the transferrin receptor in vesicular form in sheep reticulocytes'. *J Cell Biol* (1985) 101:942–8. doi: 10.1083/jcb.101.3.942

16. Johnstone RM, Bianchini A, Teng K. 'Reticulocyte maturation and exosome release: transferrin receptor containing exosomes shows multiple plasma membrane functions'. *Blood* (1989) 74:1844–51. doi: 10.1182/blood.V74.5.1844.1844

17. Humphrey PA, Wong AJ, Vogelstein B, Zalutsky MR, Fuller GN, Archer GE, et al. 'Anti-synthetic peptide antibody reacting at the fusion junction of deletion-mutant epidermal growth factor receptors in human glioblastoma'. *Proc Natl Acad Sci U.S.A.* (1990) 87:4207–11. doi: 10.1073/pnas.87.11.4207

18. Kleihues P, Burger PC, Scheithauer BW. 'The new WHO classification of brain tumours'. *Brain Pathol* (1993) 3:255–68. doi: 10.1111/j.1750-3639.1993.tb00752.x

19. Recht A, Come SE, Henderson IC, Gelman RS, Silver B, Hayes DF, et al. 'The sequencing of chemotherapy and radiation therapy after conservative surgery for early-stage breast cancer'. *N Engl J Med* (1996) 334:1356–61. doi: 10.1056/NEJM199605233342102

20. Fine HA, Dear KB, Loeffler JS, Black PM, Canellos GP. 'Meta-analysis of radiation therapy with and without adjuvant chemotherapy for Malignant gliomas in adults'. *Cancer* (1993) 71:2585–97. doi: 10.1002/1097-0142(19930415)71:8<2585::aid-cncr2820710825>3.0.co;2-s

21. Wolfers J, Lozier A, Raposo G, Regnault A, Thery C, Masurier C, et al. 'Tumor-derived exosomes are a source of shared tumor rejection antigens for CTL cross-priming'. *Nat Med* (2001) 7:297–303. doi: 10.1038/85438

22. Parsons DW, Jones S, Zhang X, Lin JC, Leary RJ, Angenendt P, et al. 'An integrated genomic analysis of human glioblastoma multiforme'. *Science* (2008) 321:1807–12. doi: 10.1126/science.1164382

23. Stupp R, Mason WP, van den Bent MJ, Weller M, Fisher B, Taphoorn MJ, et al. Research European Organisation for, Tumor Treatment of Cancer Brain, Groups Radiotherapy, and Group National Cancer Institute of Canada Clinical Trials. 2005. 'Radiotherapy plus concomitant and adjuvant temozolomide for glioblastoma'. *N Engl J Med* (2005) 352:987–96. doi: 10.1056/NEJMoa043330

24. Valadi H, Ekstrom K, Bossios A, Sjostrand M, Lee JJ, Lotvall JO. 'Exosome-mediated transfer of mRNAs and microRNAs is a novel mechanism of genetic exchange between cells'. *Nat Cell Biol* (2007) 9:654–9. doi: 10.1038/ncb1596

25. Skog J, Wurdinger T, van Rijn S, Meijer DH, Gainche L, Sena-Esteves M, et al. 'Glioblastoma microvesicles transport RNA and proteins that promote tumour growth and provide diagnostic biomarkers'. *Nat Cell Biol* (2008) 10:1470–6. doi: 10.1038/ncb1800

26. Miller K, Wang M, Gralow J, Dickler M, Cobleigh M, Perez EA, et al. 'Paclitaxel plus bevacizumab versus paclitaxel alone for metastatic breast cancer'. *N Engl J Med* (2007) 357:2666–76. doi: 10.1056/NEJMoa072113

27. Hadjipanayis CG, Stummer W. '5-ALA and FDA approval for glioma surgery'. *J Neurooncol* (2019) 141:479–86. doi: 10.1007/s11060-019-03098-y

28. Ricklefs FL, Alayo Q, Krenzlin H, Mahmoud AB, Speranza MC, Nakashima H, et al. 'Immune evasion mediated by PD-L1 on glioblastoma-derived extracellular vesicles'. *Sci Adv* (2018) 4:eaar2766. doi: 10.1126/sciadv.aar2766

29. Yekula A, Yekula A, Muralidharan K, Kang K, Carter BS, Balaj L. 'Extracellular vesicles in glioblastoma tumor microenvironment'. *Front Immunol* (2019) 10:3137. doi: 10.3389/fimmu.2019.03137

30. Patel AP, Tirosh I, Trombetta JJ, Shalek AK, Gillespie SM, Wakimoto H, et al. 'Single-cell RNA-seq highlights intratumoral heterogeneity in primary glioblastoma'. *Science* (2014) 344:1396–401. doi: 10.1126/science.1254257

31. Tirosh I, Suva ML. 'Tackling the many facets of glioblastoma heterogeneity'. *Cell Stem Cell* (2020) 26:303–04. doi: 10.1016/j.stem.2020.02.005

32. Eisenbarth D, Wang YA. 'Glioblastoma heterogeneity at single cell resolution'. *Oncogene* (2023) 42:2155–65. doi: 10.1038/s41388-023-02738-y

33. Friedmann-Morvinski D, Hambardzumyan D. 'Monocyte-neutrophil entanglement in glioblastoma'. *J Clin Invest* (2023) 133(1):e163451. doi: 10.1172/JCI163451

34. Maas SLN, Abels ER, Van De Haar LL, Zhang X, Morsett L, Sil S, et al. 'Glioblastoma hijacks microglial gene expression to support tumor growth'. *J Neuroinflamm* (2020) 17:120. doi: 10.1186/s12974-020-01797-2

35. Matarredona ER, Pastor AM. 'Extracellular vesicle-mediated communication between the glioblastoma and its microenvironment'. *Cells* (2019) 9(1):96. doi: 10.3390/cells9010096

36. Ciccocioppo F, Lanuti P, Marchisio M, Miscia S. 'Extracellular vesicles involvement in the modulation of the glioblastoma environment'. *J Oncol* (2020) 2020:3961735. doi: 10.1155/2020/3961735

37. Del Bene M, Osti D, Faletti S, Beznoussenko GV, DiMeco F, Pelicci G. 'Extracellular vesicles: The key for precision medicine in glioblastoma'. *Neuro Oncol* (2022) 24:184–96. doi: 10.1093/neuonc/noab229

38. Nieland L, Morsett LM, Broekman MLD, Breakefield XO, Abels ER. 'Extracellular vesicle-mediated bilateral communication between glioblastoma and astrocytes'. *Trends Neurosci* (2021) 44:215–26. doi: 10.1016/j.tins.2020.10.014

39. Hallal S, Mallawaaratchy DM, Wei H, Ebrahimkhani S, Stringer BW, Day BW, et al. 'Extracellular vesicles released by glioblastoma cells stimulate normal astrocytes to acquire a tumor-supportive phenotype via p53 and MYC signaling pathways'. *Mol Neurobiol* (2019) 56:4566–81. doi: 10.1007/s12035-018-1385-1

40. Oushy S, Hellwinkel JE, Wang M, Nguyen GJ, Gunaydin D, Harland TA, et al. 'Glioblastoma multiforme-derived extracellular vesicles drive normal astrocytes towards a tumour-enhancing phenotype'. *Philos Trans R Soc Lond B Biol Sci* (2018) 373(1737):20160477. doi: 10.1098/rstb.2016.0477

41. Colangelo NW, Azzam EI. 'Extracellular vesicles originating from glioblastoma cells increase metalloproteinase release by astrocytes: the role of CD147 (EMMPRIN) and ionizing radiation'. *Cell Commun Signal* (2020) 18:21. doi: 10.1186/s12964-019-0494-4

42. Nowosad A, Marine JC, Karras P. 'Perivascular niches: critical hubs in cancer evolution'. *Trends Cancer* (2023) 9:897–910. doi: 10.1016/j.trecan.2023.06.010

43. Lucero R, Zappulli V, Sammarco A, Murillo OD, Cheah PS, Srinivasan S, et al. 'Glioma-derived miRNA-containing extracellular vesicles induce angiogenesis by reprogramming brain endothelial cells'. *Cell Rep* (2020) 30:2065–74.e4. doi: 10.1016/j.celrep.2020.01.073

44. Pan J, Sheng S, Ye L, Xu X, Ma Y, Feng X, et al. 'Extracellular vesicles derived from glioblastoma promote proliferation and migration of neural progenitor cells via PI3K-Akt pathway'. *Cell Commun Signal* (2022) 20:7. doi: 10.1186/s12964-021-00760-9

45. Wang J, Liu J, Sun G, Meng H, Wang J, Guan Y, et al. 'Corrigendum to "Glioblastoma extracellular vesicles induce the tumour-promoting transformation of neural stem cells"'. *Cancer Lett* (2021) 498:245–46. doi: 10.1016/j.canlet.2020.10.025

46. Ma C, Nguyen HPT, Jones JJ, Stylli SS, Whitehead CA, Paradiso L, et al. 'Extracellular vesicles secreted by glioma stem cells are involved in radiation resistance and glioma progression'. *Int J Mol Sci* (2022) 23(5):2770. doi: 10.3390/ijms23052770

47. Nieland L, van Solinge TS, Cheah PS, Morsett LM, El Khoury J, Rissman JI, et al. 'CRISPR-Cas knockout of miR21 reduces glioma growth'. *Mol Ther Oncolytics* (2022) 25:121–36. doi: 10.1016/j.omto.2022.04.001

48. Abels ER, Maas SLN, Nieland L, Wei Z, Cheah PS, Tai E, et al. Glioblastoma-associated microglia reprogramming is mediated by functional transfer of extracellular miR-21. *Cell Rep* (2019) 28:3105–19.e7. doi: 10.1016/j.celrep.2019.08.036

49. Buzas EI. 'The roles of extracellular vesicles in the immune system'. *Nat Rev Immunol* (2023) 23:236–50. doi: 10.1038/s41577-022-00763-8

50. Azambuja JH, Ludwig N, Yerneni S, Rao A, Braganhol E, Whiteside TL. 'Molecular profiles and immunomodulatory activities of glioblastoma-derived exosomes'. *Neurooncol Adv* (2020) 2:vdaa056. doi: 10.1093/noajnl/vdaa056

51. Peng J, Liang Q, Xu Z, Cai Y, Peng B, Li J, et al. 'Current understanding of exosomal microRNAs in glioma immune regulation and therapeutic responses'. *Front Immunol* (2021) 12:813747. doi: 10.3389/fimmu.2021.813747

52. Musatova OE, Rubtsov YP. 'Effects of glioblastoma-derived extracellular vesicles on the functions of immune cells'. *Front Cell Dev Biol* (2023) 11:1060000. doi: 10.3389/fcell.2023.1060000

53. Antonioli L, Pacher P, Vizi ES, Hasko G. 'CD39 and CD73 in immunity and inflammation'. *Trends Mol Med* (2013) 19:355–67. doi: 10.1016/j.molmed.2013.03.005

54. Ma SR, Deng WW, Liu JF, Mao L, Yu GT, Bu LL, et al. 'Blockade of adenosine A2A receptor enhances CD8(+) T cells response and decreases regulatory T cells in head and neck squamous cell carcinoma'. *Mol Cancer* (2017) 16:99. doi: 10.1186/s12943-017-0665-0

55. Moesta AK, Li XY, Smyth MJ. 'Targeting CD39 in cancer'. *Nat Rev Immunol* (2020) 20:739–55. doi: 10.1038/s41577-020-0376-4

56. Wu P, Guo Y, Xiao L, Yuan J, Tang C, Dong J, et al. 'LILRB2-containing small extracellular vesicles from glioblastoma promote tumor progression by promoting the formation and expansion of myeloid-derived suppressor cells'. *Cancer Immunol Immunother* (2023) 72:2179–93. doi: 10.1007/s00262-023-03395-6

57. de Vrij J, Maas SL, Kwappenberg KM, Schnoor R, Kleijn A, Dekker L, et al. 'Glioblastoma-derived extracellular vesicles modify the phenotype of monocytic cells'. *Int J Cancer* (2015) 137:1630–42. doi: 10.1002/ijc.29521

58. Xu C, Wang P, Guo H, Shao C, Liao B, Gong S, et al. 'MiR-146a-5p deficiency in extracellular vesicles of glioma-associated macrophages promotes epithelial-mesenchymal transition through the NF-kappaB signaling pathway'. *Cell Death Discovery* (2023) 9:206. doi: 10.1038/s41420-023-01492-0

59. Luong N, Lenz JA, Modiano JF, Olson JK. 'Extracellular vesicles secreted by tumor cells promote the generation of suppressive monocytes'. *Immunohorizons* (2021) 5:647–58. doi: 10.4049/immunohorizons.2000017

60. Jung MY, Aibaidula A, Brown DA, Himes BT, Cumba Garcia LM, Parney IF. 'Superinduction of immunosuppressive glioblastoma extracellular vesicles by IFN-gamma through PD-L1 and IDO1'. *Neurooncol Adv* (2022) 4:vdac017. doi: 10.1093/noajnl/vdac017

61. Koessinger D, Novo D, Koessinger A, Campos A, Peters J, Dutton L, et al. Glioblastoma extracellular vesicles influence glial cell hyaluronic acid deposition to promote invasiveness. *Neuro-Oncology Adv* (2023) 5(1):1–13. doi: 10.1093/noajnl/vdad067

62. Yan T, Wang K, Li J, Hu H, Yang H, Cai M, et al. 'Suppression of the hyaluronic acid pathway induces M1 macrophages polarization via STAT1 in glioblastoma'. *Cell Death Discovery* (2022) 8:193. doi: 10.1038/s41420-022-00973-y

63. Wang M, Cai Y, Peng Y, Xu B, Hui W, Jiang Y. 'Exosomal LGALS9 in the cerebrospinal fluid of glioblastoma patients suppressed dendritic cell antigen presentation and cytotoxic T-cell immunity'. *Cell Death Dis* (2020) 11:896. doi: 10.1038/s41419-020-03042-3

64. Vergani E, Daveri E, Vallacchi V, Bergamaschi L, Lalli L, Castelli C, et al. Extracellular vesicles in anti-tumor immunity'. *Semin Cancer Biol* (2022) 86:64–79. doi: 10.1016/j.semcancer.2021.09.004

65. Serpe C, Monaco L, Relucenti M, Iovino L, Familiari P, Scavizzi F, et al. 'Microglia-Derived Small Extracellular Vesicles Reduce Glioma Growth by Modifying Tumor Cell Metabolism and Enhancing Glutamate Clearance through miR-124'. *Cells* (2021) 10(8):2066. doi: 10.3390/cells10082066

66. Lo Cicero A, Schiera G, Proia P, Saladino P, Savettieri G, Di Liegro CM, et al. 'Oligodendroglioma cells shed microvesicles which contain TRAIL as well as molecular chaperones and induce cell death in astrocytes'. *Int J Oncol* (2011) 39:1353–7. doi: 10.3892/ijo.2011.1160

67. D'Agostino S, Salamone M, Di Liegro I, Vittorelli ML. 'Membrane vesicles shed by oligodendroglioma cells induce neuronal apoptosis'. *Int J Oncol* (2006) 29:1075–85. doi: 10.3892/ijo.29.5.1075

68. Farcas M, Inngjerdingen M. 'Natural killer cell-derived extracellular vesicles in cancer therapy'. *Scand J Immunol* (2020) 92:e12938. doi: 10.1111/sji.12938

69. Zhu L, Kalimuthu S, Oh JM, Gangadaran P, Baek SH, Jeong SY, et al. 'Enhancement of antitumor potency of extracellular vesicles derived from natural killer cells by IL-15 priming'. *Biomaterials* (2019) 190-191:38–50. doi: 10.1016/j.biomaterials.2018.10.034

70. Wu CH, Li J, Li L, Sun J, Fabbri M, Wayne AS, et al. 'Extracellular vesicles derived from natural killer cells use multiple cytotoxic proteins and killing mechanisms to target cancer cells'. *J Extracell Vesicles* (2019) 8:1588538. doi: 10.1080/20013078.2019.1588538

71. Huo H, Yang S, Wu H, Sun Y, Zhao R, Ye R, et al. 'Brain endothelial cells-derived extracellular vesicles overexpressing ECRG4 inhibit glioma proliferation through suppressing inflammation and angiogenesis'. *J Tissue Eng Regener Med* (2021) 15:1162–71. doi: 10.1002/term.3244

72. Munoz MA, Biro M, Weninger W. 'T cell migration in intact lymph nodes in *vivo*'. *Curr Opin Cell Biol* (2014) 30:17–24. doi: 10.1016/j.ceb.2014.05.002

73. Ortega-Carrion A, Vicente-Manzanares M. 'Concerning immune synapses: a spatiotemporal timeline'. *F1000Res* (2016) 5. doi: 10.12688/f1000research.7796.1

74. Kovar M, Boyman O, Shen X, Hwang I, Kohler R, Sprent J. 'Direct stimulation of T cells by membrane vesicles from antigen-presenting cells'. *Proc Natl Acad Sci U.S.A.* (2006) 103:11671–6. doi: 10.1073/pnas.0603466103

75. Zhang Z, Lu M, Qin Y, Gao W, Tao L, Su W, et al. 'Neoantigen: A new breakthrough in tumor immunotherapy'. *Front Immunol* (2021) 12:672356. doi: 10.3389/fimmu.2021.672356

76. Vengoji R, Macha MA, Nimmakayala RK, Rachagani S, Siddiqui JA, Mallya K, et al. 'Afatinib and Temozolomide combination inhibits tumorigenesis by targeting EGFRvIII-cMet signaling in glioblastoma cells'. *J Exp Clin Cancer Res* (2019) 38:266. doi: 10.1186/s13046-019-1264-2

77. Wu C, Qin C, Long W, Wang X, Xiao K, Liu Q. 'Tumor antigens and immune subtypes of glioblastoma: the fundamentals of mRNA vaccine and individualized immunotherapy development'. *J Big Data* (2022) 9:92. doi: 10.1186/s40537-022-00643-x

78. Barlin M, Erdmann-Gilmore P, Mudd JL, Zhang Q, Seymour RW, Guo Z, et al. 'Proteins in tumor-derived plasma extracellular vesicles indicate tumor origin'. *Mol Cell Proteomics* (2023) 22:100476. doi: 10.1016/j.mcpro.2022.100476

79. Johanns TM, Ward JP, Miller CA, Wilson C, Kobayashi DK, Bender D, et al. 'Endogenous neoantigen-specific CD8 T cells identified in two glioblastoma models using a cancer immunogenomics approach'. *Cancer Immunol Res* (2016) 4:1007–15. doi: 10.1158/2326-6066.CIR-16-0156

80. Herrmann IK, Wood MJA, Fuhrmann G. 'Extracellular vesicles as a next-generation drug delivery platform'. *Nat Nanotechnol* (2021) 16:748–59. doi: 10.1038/s41565-021-00931-2

81. Alvarez-Erviti L, Seow Y, Yin H, Betts C, Lakhal S, Wood MJ. Delivery of siRNA to the mouse brain by systemic injection of targeted exosomes'. *Nat Biotechnol* (2011) 29:341–5. doi: 10.1038/nbt.1807

82. Zhan Y, Song Y, Qiao W, Sun L, Wang X, Yi B, et al. 'Focused ultrasound combined with miR-1208-equipped exosomes inhibits Malignant progression of glioma'. *Br J Cancer* (2023) 129:1083–94. doi: 10.1038/s41416-023-02393-w

83. Jose S, Juna BC, Cinu TA, Jyoti H, Aleykutty NA. 'Carboplatin loaded Surface modified PLGA nanoparticles: Optimization, characterization, and in *vivo* brain targeting studies'. *Colloids Surf B Biointerfaces* (2016) 142:307–14. doi: 10.1016/j.colsurfb.2016.02.026

84. Malinovskaya Y, Melnikov P, Baklaushev V, Gabashvili A, Osipova N, Mantrov S, et al. 'Delivery of doxorubicin-loaded PLGA nanoparticles into U87 human glioblastoma cells'. *Int J Pharm* (2017) 524:77–90. doi: 10.1016/j.ijpharm.2017.03.049

85. Khan AR, Yang X, Fu M, Zhai G. 'Recent progress of drug nanoformulations targeting to brain'. *J Control Release* (2018) 291:37–64. doi: 10.1016/j.jconrel.2018.10.004

86. Zhan Q, Yi K, Cui X, Li X, Yang S, Wang Q, et al. 'Blood exosomes-based targeted delivery of cPLA2 siRNA and metformin to modulate glioblastoma energy metabolism for tailoring personalized therapy'. *Neuro Oncol* (2022) 24:1871–83. doi: 10.1093/neuonc/noac071

87. Liu X, Cao Z, Wang W, Zou C, Wang Y, Pan L, et al. 'Engineered extracellular vesicle-delivered CRISPR/cas9 for radiotherapy sensitization of glioblastoma'. *ACS Nano* (2023) 17:16432–47. doi: 10.1021/acsnano.2c12857

88. Barnwal A, Ganguly S, Bhattacharyya J. 'Multifaceted nano-DEV-IL for sustained release of IL-12 to avert the immunosuppressive tumor microenvironment and IL-12-associated toxicities'. *ACS Appl Mater Interfaces* (2023) 15:20012–26. doi: 10.1021/acsami.3c02934

89. Adamus T, Hung CY, Yu C, Kang E, Hammad M, Flores L, et al. Glioma-targeted delivery of exosome-encapsulated antisense oligonucleotides using neural stem cells. *Mol Ther Nucleic Acids* (2022) 27:611–20. doi: 10.1016/j.omtn.2021.12.029

90. Nizar R, Cazacu S, Xiang C, Krasner M, Barbiro-Michaely E, Gerber D, et al. 'Propofol inhibits glioma stem cell growth and migration and their interaction with microglia via BDNF-AS and extracellular vesicles'. *Cells* (2023) 12(15). doi: 10.3390/cells12151921

91. Tibensky M, Jakubechova J, Altanerova U, Pastorakova A, Rychly B, Baciak L, et al. 'Gene-directed enzyme/prodrug therapy of rat brain tumor mediated by human mesenchymal stem cell suicide gene extracellular vesicles *in vitro* and *in vivo*'. *Cancers (Basel)* (2022) 14(3):735. doi: 10.3390/cancers14030735

92. Gecys D, Skredeniene R, Gecyte E, Kazlauskas A, Balnyte I, Jekabsone A. 'Adipose tissue-derived stem cell extracellular vesicles suppress glioblastoma proliferation, invasiveness and angiogenesis'. *Cells* (2023) 12(9):1247. doi: 10.3390/cells12091247

93. Yang T, Martin P, Fogarty B, Brown A, Schurman K, Phipps R, et al. 'Exosome delivered anticancer drugs across the blood-brain barrier for brain cancer therapy in Danio rerio'. *Pharm Res* (2015) 32:2003–14. doi: 10.1007/s11095-014-1593-y

94. Dong S, Liu X, Bi Y, Wang Y, Antony A, Lee D, et al. 'Adaptive design of mRNA-loaded extracellular vesicles for targeted immunotherapy of cancer'. *Nat Commun* (2023) 14:6610. doi: 10.1038/s41467-023-42365-5

95. Geng T, Leung E, Chamley LW, Wu Z. 'Functionalisation of extracellular vesicles with cyclic-RGDyC potentially for glioblastoma targeted intracellular drug delivery'. *Biomater Adv* (2023) 149:213388. doi: 10.1016/j.bioadv.2023.213388

96. Rahmani R, Kiani J, Tong WY, Soleimani M, Voelcker NH, Arefian E. 'Engineered anti-EGFRvIII targeted exosomes induce apoptosis in glioblastoma multiforme'. *J Drug Target* (2023) 31:310–19. doi: 10.1080/1061186X.2022.2152819

97. Keskin DB, Anandappa AJ, Sun J, Tirosh I, Mathewson ND, Li S, et al. 'Neoantigen vaccine generates intratumoral T cell responses in phase Ib glioblastoma trial'. *Nature* (2019) 565:234–39. doi: 10.1038/s41586-018-0792-9

98. Ahluwalia MS, Reardon DA, Abad AP, Curry WT, Wong ET, Figel SA, et al. Phase IIa study of surVaxM plus adjuvant temozolomide for newly diagnosed glioblastoma. *J Clin Oncol* (2023) 41:1453–65. doi: 10.1200/JCO.22.00996

99. Adhikari AS, Macauley J, Johnson Y, Connolly M, Coleman T, Heiland T. Development and characterization of an HCMV multi-antigen therapeutic vaccine for glioblastoma using the UNITE platform'. *Front Oncol* (2022) 12:850546. doi: 10.3389/fonc.2022.850546

100. Davis ME. 'Glioblastoma: overview of disease and treatment'. *Clin J Oncol Nurs* (2016) 20:S2–8. doi: 10.1188/16.CJON.S1.2-8

101. Thust SC, van den Bent MJ, Smits M. 'Pseudoprogression of brain tumors'. *J Magn Reson Imaging* (2018) 48:571–89. doi: 10.1002/jmri.26171

102. Tzaridis T, Weller J, Bachurski D, Shakeri F, Schaub C, Hau P, et al. 'A novel serum extracellular vesicle protein signature to monitor glioblastoma tumor progression'. *Int J Cancer* (2023) 152:308–19. doi: 10.1002/ijc.34261

103. Osti D, Del Bene M, Rappa G, Santos M, Matafora V, Richichi C, et al. 'Clinical significance of extracellular vesicles in plasma from glioblastoma patients'. *Clin Cancer Res* (2019) 25:266–76. doi: 10.1158/1078-0432.CCR-18-1941

104. Gelb S, Lehtinen MK. 'Snapshot: Choroid plexus brain barrier'. *Cell* (2023) 186:3522–22.e1. doi: 10.1016/j.cell.2023.07.015

105. Muller Bark J, Trevisan Franca de Lima L, Zhang X, Broszczak D, Leo PJ, Jeffree RL, et al. 'Proteome profiling of salivary small extracellular vesicles in glioblastoma patients'. *Cancer* (2023) 2836–47. doi: 10.1002/cncr.34888

106. Cilibrasi C, Simon T, Vintu M, Tolias C, Samuels M, Mazarakis NK, et al. 'Definition of an inflammatory biomarker signature in plasma-derived extracellular vesicles of glioblastoma patients'. *Biomedicines* (2022) 10(1):125. doi: 10.3390/biomedicines10010125

107. Brennan K, Martin K, FitzGerald SP, O'Sullivan J, Wu Y, Blanco A, et al. 'A comparison of methods for the isolation and separation of extracellular vesicles from protein and lipid particles in human serum'. *Sci Rep* (2020) 10:1039. doi: 10.1038/s41598-020-57497-7

108. Westphal M, Pantel K, Ricklefs FL, Maire C, Riethdorf S, Mohme M, et al. 'Circulating tumor cells and extracellular vesicles as liquid biopsy markers in neuro-oncology: prospects and limitations'. *Neurooncol Adv* (2022) 4:ii45–52. doi: 10.1093/noajnl/vdac015

109. Jalali M, Del Real Mata C, Montermini L, Jeanne O, Hosseini I I, Gu Z, et al. 'MoS (2)-plasmonic nanocavities for raman spectra of single extracellular vesicles reveal molecular progression in glioblastoma'. *ACS Nano* (2023) 17:12052–71. doi: 10.1021/acsnano.2c09222

110. Zhang J, Rima XY, Wang X, Nguyen LTH, Huntoon K, Ma Y, et al. 'Engineering a tunable micropattern-array assay to sort single extracellular vesicles and particles to detect RNA and protein in situ'. *J Extracell Vesicles* (2023) 12:e12369. doi: 10.1002/jev2.12369

111. Xu R, Rai A, Chen M, Suwakulsiri W, Greening DW, Simpson RJ. 'Extracellular vesicles in cancer - implications for future improvements in cancer care'. *Nat Rev Clin Oncol* (2018) 15:617–38. doi: 10.1038/s41571-018-0036-9

112. Tian F, Zhang S, Liu C, Han Z, Liu Y, Deng J, et al. 'Protein analysis of extracellular vesicles to monitor and predict therapeutic response in metastatic breast cancer'. *Nat Commun* (2021) 12:2536. doi: 10.1038/s41467-021-22913-7

113. Figueroa JM, Skog J, Akers J, Li H, Komotar R, Jensen R, et al. 'Detection of wild-type EGFR amplification and EGFRvIII mutation in CSF-derived extracellular vesicles of glioblastoma patients'. *Neuro Oncol* (2017) 19:1494–502. doi: 10.1093/neuonc/nox085

114. Masoudi MS, Mehrabian E, Mirzaei H. 'MiR-21: A key player in glioblastoma pathogenesis'. *J Cell Biochem* (2018) 119:1285–90. doi: 10.1002/jcb.26300

115. Hallal S, Ebrahim Khani S, Wei H, Lee MYT, Sim HW, Sy J, et al. 'Deep sequencing of small RNAs from neurosurgical extracellular vesicles substantiates miR-486-3p as a circulating biomarker that distinguishes glioblastoma from lower-grade astrocytoma patients'. *Int J Mol Sci* (2020) 21(14):4954. doi: 10.3390/ijms21144954

116. Jelski W, Mroczko B. 'Molecular and circulating biomarkers of brain tumors'. *Int J Mol Sci* (2021) 22(13):7039. doi: 10.3390/ijms22137039

117. Dufrusine B, Capone E, Ponziani S, Lattanzio R, Lanuti P, Giansanti F, et al. 'Extracellular LGALS3BP: a potential disease marker and actionable target for antibody-drug conjugate therapy in glioblastoma'. *Mol Oncol* (2023) 1460–73. doi: 10.1002/1878-0261.13453

118. Rana R, Chauhan K, Gautam P, Kulkarni M, Banarjee R, Chugh P, et al. 'Plasma-derived extracellular vesicles reveal galectin-3 binding protein as potential biomarker for early detection of glioma'. *Front Oncol* (2021) 11:778754. doi: 10.3389/fonc.2021.778754

119. Chattrairat K, Yasui T, Suzuki S, Natsume A, Nagashima K, Iida M, et al. 'All-in-one nanowire assay system for capture and analysis of extracellular vesicles from an ex vivo brain tumor model'. *ACS Nano* (2023) 17:2235–44. doi: 10.1021/acsnano.2c08526

120. Geng L, Xu J, Zhu Y, Hu X, Liu Y, Yang K, et al. 'Targeting miR-9 in glioma stem cell-derived extracellular vesicles: A novel diagnostic and therapeutic biomarker'. *Transl Oncol* (2022) 22:101451. doi: 10.1016/j.tranon.2022.101451

121. Kitano Y, Aoki K, Ohka F, Yamazaki S, Motomura K, Tanahashi K, et al. 'Urinary microRNA-based diagnostic model for central nervous system tumors using nanowire scaffolds'. *ACS Appl Mater Interfaces* (2021) 13:17316–29. doi: 10.1021/acsami.1c01754

122. Zhang Z, Yin J, Lu C, Wei Y, Zeng A, You Y. 'Exosomal transfer of long non-coding RNA SBF2-AS1 enhances chemoresistance to temozolomide in glioblastoma'. *J Exp Clin Cancer Res* (2019) 38:166. doi: 10.1186/s13046-019-1139-6

123. Panzarini E, Tacconi S, Carata E, Mariano S, Tata AM, Dini L. 'Molecular characterization of temozolomide-treated and non temozolomide-treated glioblastoma cells released extracellular vesicles and their role in the macrophage response'. *Int J Mol Sci* (2020) 21(21):8353. doi: 10.3390/ijms21218353

124. Kiyga E, Adiguzel Z, Onay Ucar E. 'Temozolomide increases heat shock proteins in extracellular vesicles released from glioblastoma cells'. *Mol Biol Rep* (2022) 49:8701–13. doi: 10.1007/s11033-022-07714-5

125. Chi AS, Cahill DP, Reardon DA, Wen PY, Mikkelsen T, Peereboom DM, et al. 'Exploring predictors of response to dacomitinib in EGFR-amplified recurrent glioblastoma'. *JCO Precis Oncol* (2020) 593–613. doi: 10.1200/PO.19.00295

126. Wang X, Yu X, Xu H, Wei K, Wang S, Wang Y, et al. 'Serum-derived extracellular vesicles facilitate temozolomide resistance in glioblastoma through a HOTAIR-dependent mechanism'. *Cell Death Dis* (2022) 13:344. doi: 10.1038/s41419-022-04699-8

127. Ding M, Xu Q, Jin X, Han Z, Jiang H, Sun H, et al. 'Novel exosome-related risk signature as prognostic biomarkers in glioblastoma'. *Front Immunol* (2023) 14:1071023. doi: 10.3389/fimmu.2023.1071023

128. Jennrich S, Pelzer M, Tertel T, Koska B, Vullings M, Thakur BK, et al. 'CD9- and CD81-positive extracellular vesicles provide a marker to monitor glioblastoma cell response to photon-based and proton-based radiotherapy'. *Front Oncol* (2022) 12:947439. doi: 10.3389/fonc.2022.947439

129. Lourenco C, Constancio V, Henrique R, Carvalho A, Jeronimo C. 'Urinary extracellular vesicles as potential biomarkers for urologic cancers: an overview of current methods and advances'. *Cancers (Basel)* (2021) 13(7):1529. doi: 10.3390/cancers13071529

130. Oshi M, Murthy V, Takahashi H, Huyser M, Okano M, Tokumaru Y, et al. 'Urine as a source of liquid biopsy for cancer'. *Cancers (Basel)* (2021) 13(11):2652. doi: 10.3390/cancers13112652

frontiers | Frontiers in Neurology

TYPE Original Research
PUBLISHED 08 January 2024
DOI 10.3389/fneur.2023.1322815

OPEN ACCESS

EDITED BY
Konstantinos Gousias,
University of Münster, Germany

REVIEWED BY
Francesco Marchi,
Ente Ospedaliero Cantonale (EOC), Switzerland
Fan Zhang,
University of Electronic Science and Technology of China, China

*CORRESPONDENCE
Vatche G. Baboyan
✉ vatchebaboyan@gmail.com

RECEIVED 16 October 2023
ACCEPTED 19 December 2023
PUBLISHED 08 January 2024

CITATION
Koga SF, Hodges WB, Adamyan H, Hayes T, Fecci PE, Tsvankin V, Pradilla G, Hoang KB, Lee IY, Sankey EW, Codd PJ, Huie D, Zacharia BE, Verma R and Baboyan VG (2024) Preoperative validation of edema-corrected tractography in neurosurgical practice: translating surgeon insights into novel software implementation. *Front. Neurol.* 14:1322815. doi: 10.3389/fneur.2023.1322815

Preoperative validation of edema-corrected tractography in neurosurgical practice: translating surgeon insights into novel software implementation

Sebastian F. Koga[1], Wesley B. Hodges[2], Hayk Adamyan[2], Tim Hayes[2], Peter E. Fecci[3], Vadim Tsvankin[4], Gustavo Pradilla[5], Kimberly B. Hoang[5], Ian Y. Lee[6], Eric W. Sankey[3], Patrick J. Codd[3], David Huie[3], Brad E. Zacharia[7], Ragini Verma[8,9] and Vatche G. Baboyan[2]*

[1]Franciscan Missionaries of Our Lady Health System, Baton Rouge, LA, United States, [2]Synaptive Medical Inc., Toronto, ON, Canada, [3]Department of Neurosurgery, Duke University Medical Center, Durham, NC, United States, [4]Colorado Brain and Spine Institute, Englewood, CO, United States, [5]Department of Neurosurgery, Emory University School of Medicine, Atlanta, GA, United States, [6]Department of Neurosurgery, Henry Ford Health System, Detroit, MI, United States, [7]Department of Neurosurgery, Penn State Hershey Medical Center, Hershey, PA, United States, [8]Department of Radiology, University of Pennsylvania, Philadelphia, PA, United States, [9]Cohen Veterans Bioscience, New York, NY, United States

Background: Peritumoral edema alters diffusion anisotropy, resulting in false negatives in tractography reconstructions negatively impacting surgical decision-making. With supratotal resections tied to survival benefit in glioma patients, advanced diffusion modeling is critical to visualize fibers within the peritumoral zone to prevent eloquent fiber transection thereafter. A preoperative assessment paradigm is therefore warranted to systematically evaluate multi-subject tractograms along clinically meaningful parameters. We propose a novel noninvasive surgically-focused survey to evaluate the benefits of a tractography algorithm for preoperative planning, subsequently applied to Synaptive Medical's free-water correction algorithm developed for clinically feasible single-shell DTI data.

Methods: Ten neurosurgeons participated in the study and were presented with patient datasets containing histological lesions of varying degrees of edema. They were asked to compare standard (uncorrected) tractography reconstructions overlaid onto anatomical images with enhanced (corrected) reconstructions. The raters assessed the datasets in terms of overall data quality, tract alteration patterns, and the impact of the correction on lesion definition, brain-tumor interface, and optimal surgical pathway. Inter-rater reliability coefficients were calculated, and statistical comparisons were made.

Results: Standard tractography was perceived as problematic in areas proximal to the lesion, presenting with significant tract reduction that challenged assessment of the brain-tumor interface and of tract infiltration. With correction applied, significant reduction in false negatives were reported along with additional insight into tract infiltration. Significant positive correlations were shown between favorable responses to the correction algorithm and the lesion-to-edema ratio, such that the correction offered further clarification in increasingly edematous and malignant lesions. Lastly, the correction was perceived to introduce false tracts in CSF spaces and - to a lesser degree - the grey-white

matter interface, highlighting the need for noise mitigation. As a result, the algorithm was modified by free-water-parameterizing the tractography dataset and introducing a novel adaptive thresholding tool for customizable correction guided by the surgeon's discretion.

Conclusion: Here we translate surgeon insights into a clinically deployable software implementation capable of recovering peritumoral tracts in edematous zones while mitigating artifacts through the introduction of a novel and adaptive case-specific correction tool. Together, these advances maximize tractography's clinical potential to personalize surgical decisions when faced with complex pathologies.

KEYWORDS

tractography, peritumoral zone, edema correction, fiber tracking, diffusion tensor imaging, free-water correction

Introduction

For several decades, *in vivo* white matter dissections made possible by diffusion-weighted MRI (dMRI) and fiber tractography algorithms have been used routinely as technological adjuncts when treating brain tumors (1). In the presence of aggressive brain malignancies, however, the utility of tractography in surgical planning is significantly challenged by the dMRI signal dilution caused by pathology-induced tract invasion and vasogenic edema (2, 3) which compromise accurate tract reconstructions in clinically significant areas of interest; namely, at the brain-tumor interface and the broader edematous zone (4). The clinical implementation of advanced diffusion modeling to more accurately characterize the subcortical anatomy in the presence of complex oncological lesions is motivated by the finding that maximizing extent of resection improves survival insofar as neurological deficits are mitigated during surgery (5). With histopathological studies demonstrating the presence of tumor cells outside of contrast-enhancing margins located within the fluid-attenuated inversion recovery (FLAIR) signal abnormality (2, 6, 7), and with the understanding that gliomas (but not metastases) migrate along white matter tracts (8–11), improved neuroimaging of subcortical structures is essential. Interestingly, direct electrical stimulation (DES) mapping studies have also reported the presence of positive sensorimotor and language sites located *within* intratumoral margins of gliomas to further underscore the need to preoperatively assess the white matter integration patterns of the glioma-network interface (12). Although efforts have focused on resolving heterogeneous fiber populations using crossing fiber models with advanced dMRI acquisition protocols (13–17), resolving the issue of tractography-susceptible edematous voxels is needed both in clinically realistic acquisitions and with commercially available implementations for maximum broader impact (15, 18, 19).

If diffusion weighted tractography is to evolve as a standard of care in neurosurgical oncology, diffusion signal modeling proximal to pathological brain tissue must improve to better account for the true signal characteristics of the underlying white matter therein. Recent efforts have attempted to address this problem - specifically in clinically feasible (single-shell) DTI acquisitions (18) - by fitting bi-compartmental models that estimate the free-water present at every voxel while also modeling tissue anisotropy (15, 18–20). Such free-water correction (FWC) efforts intend to improve the tractography process by correcting the diffusion signal in voxels impacted by edema. Indeed, recent intraoperative motor mapping studies have reported better anatomical correspondence between positive DES sites and white matter tract reconstructions generated by a free-water corrected tractography algorithm called FERNET (18, 21).

In spite of these research breakthroughs, the field lacks (1) a systematic preoperative evaluation paradigm to derive clinically meaningful insights of advanced tractography algorithms beyond what is reported by DES analyses of individual tracts and (2) a commercially available implementation of free-water corrected tractography that flexibly accommodates pathologies with varying edematous zones (18, 21). The primary surgical indication for the use of this adjunct is to aid in the selection of an optimal parafascicular trajectory when facing lesions that engage eloquent white matter structures and minimize the likelihood of iatrogenic injury thereafter. Although DES remains the gold standard for intraoperative functional mapping and guidance of resection strategy, its preoperative unavailability precludes its utility in neurological risk assessment, patient counseling, and trajectory planning. Moreover, a qualitative radiographic assessment tool to validate multi-subject tractograms along clinically meaningful parameters is warranted particularly aiming to detect subcortical effects such as white matter tract displacement (2, 22), tract infiltration (2, 12, 23, 24), and tract reduction (2, 19). In this study, we present a novel and noninvasive subcortical tractogram assessment survey to evaluate the "edema-invariant" FERNET tractography algorithm for neurosurgical planning. Ten surgeons specialized in neuro-oncology were prompted to assess various properties of the peritumoral environment when selecting the optimal surgical approach in patient datasets featuring heterogenous histological lesions with varying edematous zones. In deriving clinician insights from this survey, a commercially available software implementation is introduced to facilitate a practical integration of FWC into the neurosurgical workflow.

Materials and methods

Patients and study design

The imaging data from ten patients previously treated for oncological neurosurgery at Ochsner Medical Center (Table 1) were

TABLE 1 Demographics and histology.

Subject ID	Age	Sex	Histopathological diagnosis
01	29	Male	Pilocytic astrocytoma (Anaplastic) IDH wild type (WHO III)
02	41	Female	Hemangiopericytoma (WHO II)
03	75	Female	Amyloid angiopathy
04	74	Male	Glioblastoma IDH wild type (WHO IV)
05	76	Male	Metastatic melanoma (skin)
06	53	Male	Metastatic adenocarcinoma (lung)
07	57	Female	Metastatic neuroendocrine carcinoma (lung)
08	70	Female	Glioblastoma IDH wild type (WHO IV)
09	73	Female	Meningioma (WHO I)
10	71	Male	Glioblastoma IDH wild type (WHO IV)

IDH, isocitrate dehydrogenase.

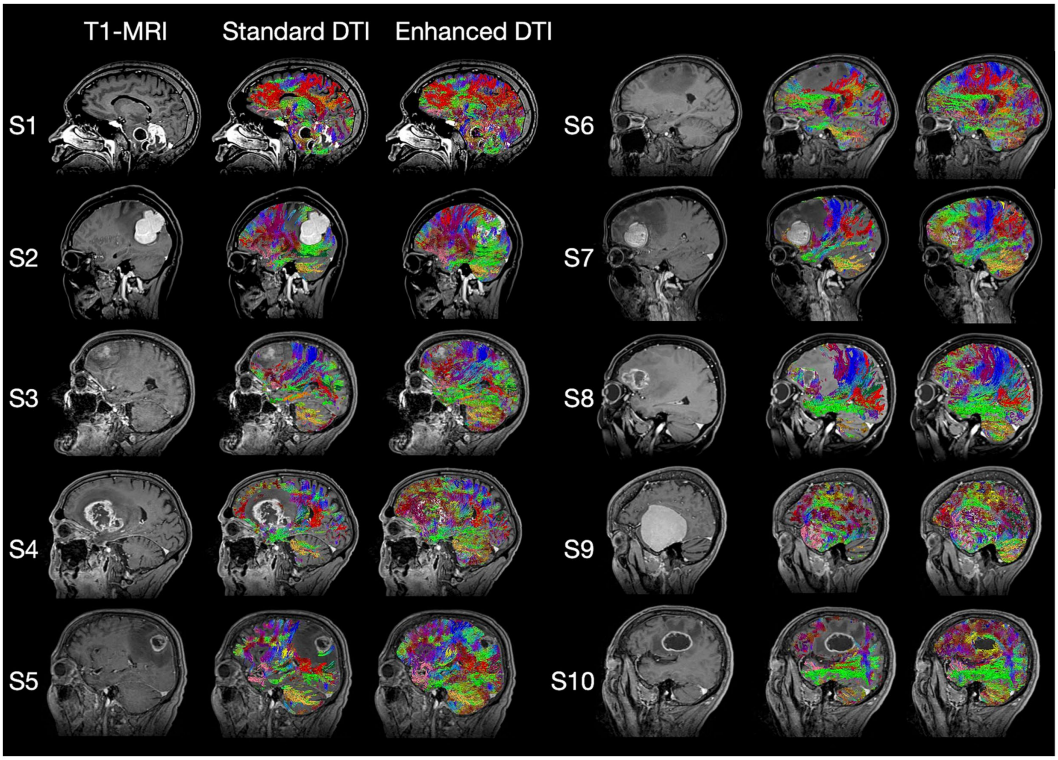

FIGURE 1
Standard T1-weighted MRI, Standard DTI Tractography, and Enhanced DTI Tractography neuroimages for each of the 10 subjects (i.e., patients) evaluated. Tract recovery profiles with enhanced DTI (Columns 3 and 6) will vary depending on the associated intra- and peritumoral dynamics of the underlying pathology, with each tumor type featuring distinctly varying degrees of tract invasion, mass effect, necrosis, and peritumoral edema impacting the recovery process.

selected by their surgeon (S. Koga) on the basis of clinical and imaging findings demonstrating varying degrees of pathology-associated intracranial edema evident on structural MRI (Figure 1). MRI data were anonymized in accordance with Health Insurance Portability and Accountability Act (HIPAA) guidelines.

MRI imaging analysis

The preoperative MRI protocol was acquired on a 1.5 T Siemens MAGNETOM Aera scanner (Siemens Healthcare) to include high-resolution, 3D magnetization-prepared rapid acquisitions with gradient echo (MPRAGE) with and without contrast-enhancement (TE = 3.32 ms, TR = 2,370 ms, TI = 1,430 ms, pixel resolution = 1 mm x 1 mm, slice thickness = 2 mm, flip angle = 8 degrees, FOV = 22.4 cm × 25.6 cm). DTI was acquired with 20 directions (b = 1,000 s/mm^2, pixel size = 2 mm, slice thickness = 3 mm).

Neuroimages were processed using commercially available surgical planning software (Modus Plan, Synaptive Medical, Toronto). Modus Plan was modified to toggle the visualization of uncorrected and corrected whole-brain deterministic tractography. The latter was achieved by integrating a modified, licensed version of the Freewater

estimatoR using the iNtErpolated iniTialization (FERNET) algorithm (developed by Verma and colleagues (19) through a Sponsored Research Agreement between Synaptive and the University of Pennsylvania) into Modus Plan's processing pipeline to enable direct intra-subject comparisons between the datasets and qualitative assessment by each rater.

To assess the correlations between survey responses and histopathology, lesions and perilesional (i.e., non-enhancing) free-water maps were manually delineated on contrast-enhanced T1s and apparent diffusion coefficient (ADC) maps, respectively. To quantify the extent of free-water, the following ratio was calculated: Volume of abnormal *perilesional* voxels (evident on ADC) divided by the volume of total abnormal voxels (lesion + edema).

Surgical tractography examination and aims

Fly-through video recordings were presented in three hierarchical stages: (Section 1) visualization of pathology on T1 scans (without overlaid tracts), (Section 2) visualization of pathology with standard (uncorrected) tractography, and (Section 3) visualization of the pathology with enhanced (corrected) tractography. At each stage of the recording, the survey items (Table 2) are narrated by a surgeon and audibly presented to the raters, with them being prompted to respond with their level of agreement (True/Partially True/False).

Items from Section 2 (of Table 2) were designed to assess the quality of standard tractography data as a baseline (aim 1) before progressing to the added benefits of enhanced tractography in Section 3 (aim 2):

- Tracts appear to begin at the grey-white matter junction
- Tracts are missing in significant areas of the normal brain (False Negatives)
- Tracts are missing in the vicinity of the lesion (False Negatives)

Next, we assessed the added clinical benefits of enhancing tractography with FWC when planning the optimal surgical approach (aim 2). To this aim, the five following prompts from Section 2 (*standard tractography assessment*) were repeated (i.e., paired) in Section 3 (*enhanced tractography assessment*):

- Tracts appear to begin at the grey-white matter interface
- False tracts are seen in sulci or ventricles (i.e., False Positives in CSF spaces)
- This scan demonstrates the following anatomical effects: Tract Reduction
- This scan demonstrates the following anatomical effects: Tract Displacement
- This scan demonstrates the following anatomical effects: Tract Infiltration

To assess false positives, raters were explicitly instructed to evaluate the presence of streamlines extending into the sylvian fissure, ventricular systems, or perimesencephalic cisterns. Lastly, raters directly assessed the added clarity provided by enhanced tractography when evaluating perilesional microarchitecture:

- The definition of the lesion is further clarified
- The interface between brain and pathological tissue is further clarified
- The optimal surgical pathway to the region of interest is further clarified

The video recordings and survey items for each of the ten patients were shared with the surgeon raters for scoring.

Data analysis

The responses to each of the three survey sections were scored *(False = 1, Partially True = 2, True = 3)* and imported into RStudio for subsequent analysis (version 3.6.1, RStudio, Inc.). To assess rater confidence for each item, inter-rater reliability (IRR) was calculated using Gwet's "second-order agreement coefficient" (Gwet AC2) with ordinal weighting applied (25). This IRR metric is robust in the presence of missing data and when high agreement is observed among multiple raters (>2), and therefore offers more stable IRR coefficients when compared to conventional metrics. We report the agreement percentages along with respective Gwet AC2 coefficients and value of *p*s associated with each questionnaire item. The Gwet AC2 coefficients reflect the extent of agreement among the raters and here they are interpreted with respect to the benchmark criteria developed and set forth by Richard and Koch (26): ≤0.20: poor, 0.21 to 0.40: fair, 0.41 to 0.60: moderate, 0.61 to 0.80: substantial, and 0.81 to 1.0: excellent reliability.

To compare the four matched paired survey items from Sections 2 and 3 (of Table 2), the Stuart-Maxwell Marginal Homogeneity Test (or generalized McNemar's χ^2 test for $k \times k$ contingency tables) was performed to evaluate the difference in response probabilities between the conditions – testing the null hypothesis that the response probabilities for the respective survey items were indistinguishable between sections. This test was performed using the *DescTools* package library in R (DescTools Version: 0.99.29) and resulting value of ps were corrected for multiple comparisons. Nonparametric spearman's correlations were computed between the response rates in the survey items evaluating the added clarity provided with corrected tractography and the free-water ratios using the *stats* package library in R (stats version 3.6.1).

Results

Of the 10 total surgeon raters enrolled, 7 completed the survey for all 10 datasets and 3 completed 5 out of 10. The response rates and responses to each of the survey items are listed in Table 2, along with their respective interrater reliability (IRR) statistics.

Standard tractography assessment

When assessing the quality of conventional tractography data (Section 2, Table 2), substantial agreement was observed to the item, "tracts are missing in the vicinity of the lesion," with the raters responding "True" in 58/84 (69%) of instances (AC2: 0.74, $p < 0.001$).

TABLE 2 Survey items, responses, and inter-rater reliability statistics for standard and enhanced DTI tractography datasets.

Section 2: Standard DTI survey items	UN-corrected tractography				Inter-rater reliability (IRR)				
	True (%)	Partially true (%)	False (%)	Ratings (N)	Agreement %	Chance agreement %	AC2 coefficient (SE)	Value of *p*	IRR rating
Brain-tumor interface: the scan demonstrates a clear interface between brain and pathological tissue	36 (42.35%)	24 (28.24%)	25 (29.41%)	85	63.64%	61.89%	0.05 (0.08)	0.566	Poor
False signal: false tracts are seen in sulci or ventricles (CSF spaces)	13 (15.29%)	21 (24.71%)	51 (60%)	85	70.84%	52.23%	0.39 (0.13)	0.015	Fair
False negative: tracts are missing in significant areas of the normal brain	11 (13.1%)	24 (28.57%)	49 (58.33%)	84	69.24%	53.70%	0.34 (0.1)	0.009	Fair
False negative: tracts are missing in the vicinity of the lesion	58 (69.05%)	12 (14.29%)	14 (16.67%)	84	85.33%	43.29%	0.74 (0.14)	<0.001	Substantial
Grey-white matter interface: the tracts appear to begin at the grey-white matter interface	51 (60.71%)	31 (36.9%)	2 (2.38%)	84	80.35%	46.16%	0.64 (0.04)	<0.001	Substantial
The scan aids spatial orientation compared to single axis images	65 (76.47%)	10 (11.76%)	10 (11.76%)	85	73.95%	35.41%	0.6 (0.09)	<0.001	Moderate
This scan demonstrates the following anatomical effects: tract reduction	52 (61.9%)	18 (21.43%)	14 (16.67%)	84	76.03%	49.78%	0.52 (0.17)	0.013	Moderate
This scan demonstrates the following anatomical effects: tract displacement	64 (75.29%)	17 (20%)	4 (4.71%)	85	81.60%	37.56%	0.71 (0.09)	<0.001	Substantial
This scan demonstrates the following anatomical effects: tract infiltration	26 (30.59%)	26 (30.59%)	33 (38.82%)	85	66.79%	62.69%	0.11 (0.12)	0.375	Poor
Surgical pathway: the optimal surgical pathway to the ROI is clear to me	57 (67.06%)	25 (29.41%)	3 (3.53%)	85	84.48%	45.91%	0.71 (0.11)	<0.001	Substantial

Section 3: Enhanced DTI survey items	Free-water corrected tractography				Inter-rater reliability (IRR)				
	True (%)	Partially true (%)	False (%)	Ratings (N)	Agreement %	Chance agreement %	AC2 coefficient (SE)	Value of *p*	IRR rating
Grey-white matter interface: the tracts appear to begin at the grey-white matter interface	53 (62.35%)	17 (20%)	15 (17.65%)	85	64.26%	51.97%	0.26 (0.09)	0.017	Fair
Lesion: definition of the lesion is further clarified	36 (42.35%)	23 (27.06%)	26 (30.59%)	85	60.14%	61.51%	−0.04 (0.08)	0.67	Poor
Brain-tumor interface: the interface between brain and pathological tissue is further clarified	34 (40%)	30 (35.29%)	21 (24.71%)	85	68.24%	61.87%	0.17 (0.12)	0.198	Poor
False signal: false tracts are seen in sulci or ventricles (CSF spaces)	39 (46.99%)	34 (40.96%)	10 (12.05%)	83	70.95%	56.40%	0.33 (0.09)	0.006	Fair
This scan demonstrates the following anatomical effects: tract reduction	27 (32.53%)	23 (27.71%)	33 (39.76%)	83	61.26%	61.80%	−0.01 (0.08)	0.866	Poor
This scan demonstrates the following anatomical effects: tract displacement	67 (78.82%)	15 (17.65%)	3 (3.53%)	85	83.72%	33.19%	0.76 (0.08)	<0.001	Substantial
This scan demonstrates the following anatomical effects: tract infiltration	44 (52.38%)	15 (17.86%)	25 (29.76%)	84	67.10%	56.23%	0.25 (0.17)	0.172	Fair
Surgical pathway: the optimal surgical pathway to the ROI is further clarified	31 (36.9%)	25 (29.76%)	28 (33.33%)	84	62.29%	62.56%	−0.01 (0.1)	0.941	Poor
Surgical pathway: the optimal surgical pathway is less clear	6 (7.14%)	17 (20.24%)	61 (72.62%)	84	83.82%	38.17%	0.74 (0.11)	<0.001	Substantial

DTI, Diffusion Tensor Imaging; AC2, Gwet's 2nd Order Agreement Coefficient.

10.3389/fneur.2023.1322815

This indicates that the conventional DTI data presents with considerable false negatives in areas surrounding the pathology (Figure 2; Table 2). Opinions otherwise relating to general data accuracy were favorable, with substantial agreement to the statement pertaining to tracts beginning at the grey-white matter interface (False: 2%, Partially True: 37%, True: 2%; AC2: 0.64, $p < 0.001$), and moderate agreement that the 3D rendering aided spatial orientation compared to single-axis images (True: 76%, AC2: 0.6, $p < 0.001$). Similarly, raters showed moderate and substantial agreement when prompted that the images demonstrated tract reduction and displacement, respectively (Tract Reduction: 62% True, AC2: 0.52, $p < 0.05$; Tract Displacement: 75% True, AC2: 0.71, $p < 0.001$).

When assessing tract infiltration, raters showed poor agreement with mixed responses weighted nearly equally (AC2: 0.11, $p = 0.375$). Lastly, raters substantially agreed that the optimal surgical pathway was clear (False: 3%, Partially True: 29%, True: 67%; AC2: 0.71, $p < 0.001$).

Enhanced tractography assessment

When assessing the quality of enhanced tractography data (Section 3, Table 2), the majority of raters fairly agreed that the tracts appear to begin at the grey-white matter interface (62.35% True, AC2: 0.26, $p < 0.05$), but also that false tracts were seen in CSF spaces (12% False, AC2: 0.33, $p < 0.01$).

When comparing the matched items, significant differences in response probabilities were observed when assessing tract reduction and infiltration, as standard tractography data showed tract reduction (62% True) and responses declined to 32% with the enhanced data [χ^2

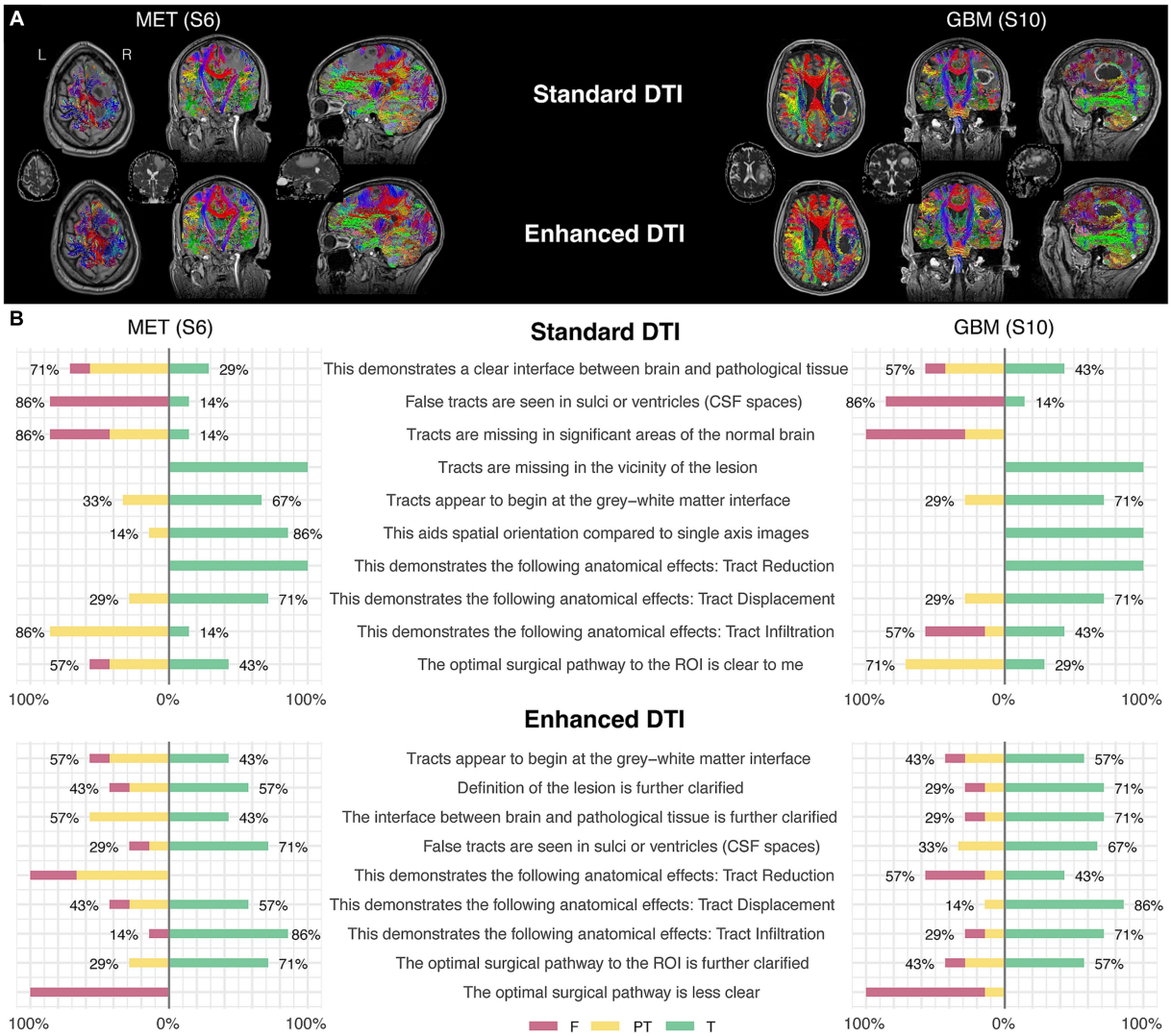

FIGURE 2
Two illustrative case examples and their respective survey scoring evaluations. **(A)** Two case examples of pathology-induced edema resulting in false negatives in the standard DTI tractograms (top row) impacting commissural (red), projection (blue), and association fascicles (green/yellow) in the peritumoral zone and the subsequent tract recovery with enhanced DTI (bottom row). Tractography-susceptible edematous zones are also shown on the respective ADC maps for each case (middle row). **(B)** Survey scoring from the two case examples corresponding to the images shown in the upper panel **(A)**, rated by the surgeon participants enrolled in the study.

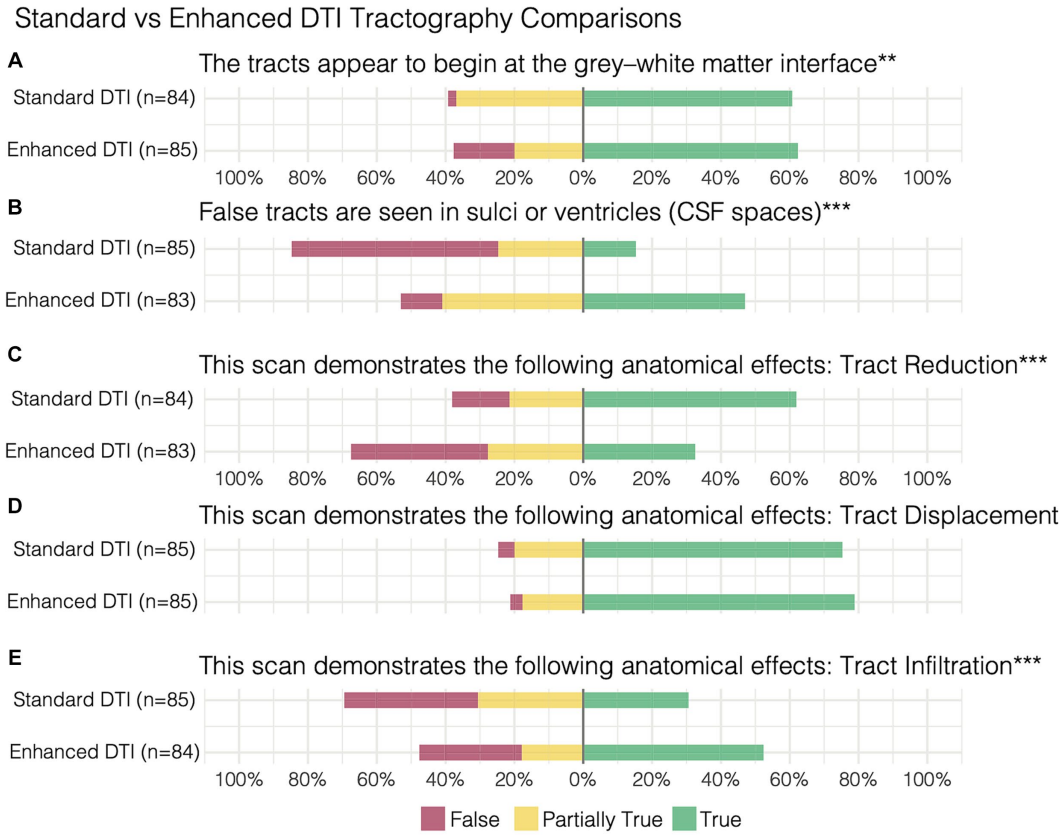

FIGURE 3
Paired survey items and results comparing standard vs. enhanced tractography assessment of **(A)** the tracts appearing at the grey-white matter interface, **(B)** false tracts appearing in CSF spaces in addition to demonstration of **(C)** tract reduction, **(D)** displacement, and **(E)** infiltration. $^{**}p < 0.01$, $^{***}p < 0.001$.

(dof) = 21.38(2), $p < 0.001$, corrected] (Figures 3C,E). Moreover, significant differences were observed regarding the assessment of tract infiltration between the datasets, with 31% rating this as true with the standard tractography which increased to 52% with enhanced tractography [χ^2 (dof) = 18.01(2), $p < 0.001$, corrected] (Figure 3E). Interestingly, significant differences in responses were also observed when assessing tract terminations at the grey-white matter interface, such that the false responses in the standard tractography condition (2%) increased in the enhanced condition (18%) [χ^2 (dof) = 13.62(2), $p < 0.01$, corrected]. When evaluating whether false tracts were seen in sulci or ventricles (i.e., CSF spaces), true responses increased from 15% in the standard tractography condition to 47% in the enhanced condition [χ^2 (dof) = 38.93(2), $p < 0.001$, corrected].

In contrast, the assessments on the presence of tract displacement were not significantly different between the datasets [χ^2 (dof) = 0.81(2), $p = 1$, corrected], indicating that tractography data - irrespective of free-water correction – is effective at demonstrating pathology-induced tract displacement (Figure 3D). When prompted with "the optimal surgical pathway was less clear," respondes favored enhanced tractography with substantial agreement that this statement was false (False 73%, AC2: 0.74, $p < 0.001$).

When surveying the further clarification provided by enhanced tractography, rater responses were highly variable – resulting in poor agreement across the three items surveyed. This was driven by the variation in responses being associated with variations in perilesional free-water severity, such that the rates of "True" (i.e., favorable) responses to the enhanced data were positively correlated with the free-water ratio present across the datasets (Figure 4). For instance, patient 9 presented with a non-edematous meningioma and the majority of raters answered "False" on these survey items (i.e., further clarification was not added with FWC). Conversely, patient 6 presented with a highly edematous lesion (metastatic adenocarcinoma) and the majority of raters answered with "True." When evaluating the lesion definition and brain-tumor interface, significant positive correlations were observed between the True response rate and free-water ratio ($r_s = 0.9$, $p = 0.0004$; $r_s = 0.68$, $p = 0.0315$, respectively). This positive correlation was also observed when evaluating the optimal surgical pathway ($r_s = 0.6278$, $p = 0.052$).

Spurious tracts and adaptive correction

Although FWC-enhanced data offered positive insight into the optimal surgical approach, showed less tract reduction, and improved assessment of tract infiltration (Figures 3C,E), these benefits came at the cost of increasing artifacts in CSF spaces and around the grey-white matter interface (Figure 3B). This finding resulted in a modification of Synaptive's software implementation to minimize spurious tract reconstructions via free-water-parameterizing the tractography dataset, whereby each segment of the tractogram was

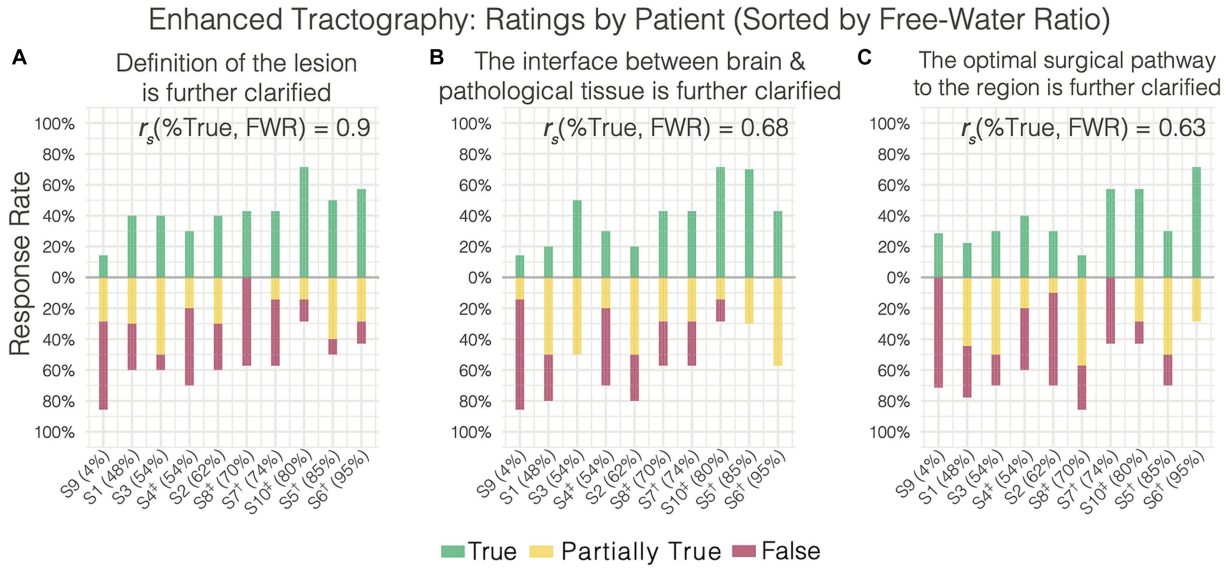

FIGURE 4
Enhanced tractography survey responses on individual patients (sorted increasingly by free water ratio) relating to further clarification of the **(A)** lesion definition, **(B)** brain-tumor interface, and **(C)** the optimal surgical pathway. Free water ratio was expressed as a percentage of abnormal perilesional voxels (evident on ADC) divided by the total abnormal voxels (lesion + edema). Nonparametric spearman's correlations between the free water ratio and rate of true responses are shown for each item. †Cerebral Metastases. ‡Glioblastoma.

encoded by the free-water map which assigns a normalized value representing the 'degree of free water' present along the segment. With the observation and understanding that spurious tract segments within CSF spaces are maximally occluded by free-water, the software's graphical user interface was redesigned to enable dynamic thresholding of the tractogram to constrain tract recovery to non-CSF areas with higher concentrations of free-water (Figure 5). The adaptive thresholding method is demonstrated in the varying edematous zones of 3 illustrative cases: at its minimum value, FWC is un-applied and false negatives are observed (column 2), and at its maximum FWC is fully applied and tracts are completely recovered (column 4). With progressive increases to the correction slider, sub-threshold tract segments are dynamically recovered and visualized in real-time to facilitate inspection of subcortical effects regarding the lesion definition, tract infiltration, and mass effect (displacement). This individualized approach adapts to the surgeon's intuition regarding the pathological and patient-specific effects impacting tracts within the peritumoral edematous zone (US patent No. 11,355,230) (27).

Discussion

Given the implications of non-enhancing tumor (NET) cells on recurrence, surgical resection strategies have evolved to extend into the NET areas of the so-called "peritumoral zone" (PTZ) with substantial survival benefits being reported in patients with primary malignancies (16, 28). The ability to image this tractography-susceptible PTZ is therefore crucial not only to the assessment and mitigation of neurological risk preoperatively, but also to facilitate onco-functional decisions intraoperatively through visualization and preservation of eloquent white matter tracts when resections extend into these areas (i.e., for supratotal resections) (29, 30). In the case of secondary tumors such as brain metastases, they present with distinct extracellular free-water patterns which have been leveraged as features in their differentiation from glioblastomas (31–34). Although meningiomas are benign tumors whose growth is often contained in a tumor capsule (35), the perilesional brain is similarly affected by gliosis and sometimes by tumor invasion. Taken together, diffusion tractography has the unique potential to provide a noninvasive radiographic assessment of white matter tract alteration profiles caused by various neoplasms (2, 17, 22–24). In the present study, we demonstrate the perceived clinical potential of enhancing tractography within edematous voxels by showing that tract recovery improves assessment of both the brain-tumor interface and lesion definition while further clarifying the optimal surgical approach primarily in cases with brain malignancies (metastases and glioblastoma).

Lesion definition and brain-tumor interface

The PTZ plays a crucial role in advancing our understanding of brain neoplasms, their behavior, and the development of targeted treatment strategies. With meningiomas typically encapsulated, the PTZ has been characterized by a well-defined border with inflammatory and compressive effects on surrounding brain tissue which frequently impacts the presence of vasogenic edema especially with larger tumor volumes (35). Gliomas, including both low- and high-grade, have been characterized as diffuse infiltrative diseases proliferating primarily along white matter tracts (2, 28, 36). Consequently, the glioma PTZ consists of infiltrative tumor cells nested within the edematous zone (23), a disruption to white matter architecture (28), and equivocal tumor margins beyond what is observed on conventional imaging. For cerebral metastases, the PTZ has been shown to be highly irregular depending on the primary tumor origin (32, 33), with more recent reports casting doubt on whether a sharp delineation from surrounding parenchymal tissue

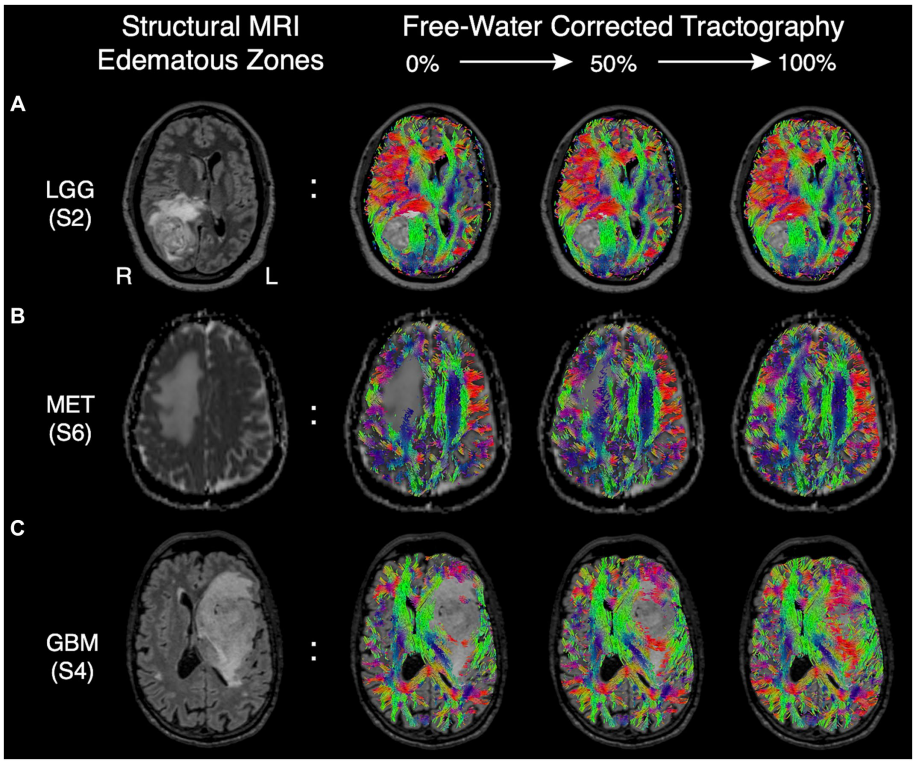

FIGURE 5
Edematous zones of 3 illustrative cases on structural MRI (Column 1) with subsequent recovery of false negative tracts using the dynamic free-water correction slider (Columns 2–4). The adaptive slider allows the user to control the desired level of tract recovery along a continuum of thresholds ranging from 0% (uncorrected, column 2) to 100% (fully corrected. Column 4). **(A)** Edematous zone of a low-grade (WHO grade II) glioma shown on T2 FLAIR, with progressive tract recovery delineating lesion-definition and mass effect on fibers in sagittal stratum of sachs. **(B)** Edematous zone of a metastatic adenocarcinoma shown on ADC, with progressive tract recovery within areas of vasogenic edema and subsequent midline shift (tract displacement) of frontal projection fibers but without tract invasion. **(C)** Edematous zone of a glioblastoma IDH-wild type shown on T2 FLAIR, with progressive tract recovery demonstrating tract infiltration (disruption) of fronto-temporal association fascicles, improved lesion definition, and mass effect (tract displacement).

exists given the tumor invasion patterns commonly observed in histological samples further complicating its differentiation from glioblastomas (23) while potentially explaining the higher rates of recurrence. Moreover, vascular disruption to the blood–brain-barrier is strongly associated with significant increases in vasogenic edema within the metastatic PTZ (23), in contrast to infiltrative edema observed in the PTZ in gliomas (33).

Here, we have shown that enhancing tractography with FWC improved the visualization of subcortical anatomy in peritumoral areas with edema by recovering and delineating tracts at the brain-tumor interface (Figures 1, 4B). We've also shown that standard tractography is effective at evaluating tract displacement, but is problematic due to the presence of pathology-induced tract reduction (Figures 3C,D; Table 2). In contrast, enhancement unveils neuroanatomical data at the lesional interface and broader edematous zone evidenced by the poor agreement regarding responses in tract reduction apparent in corrected tractography (Table 2). This allowed surgeons to then qualify subcortical mass effect (tract displacement) which resulted in significantly increased capacity for assessment of white matter tract infiltration (Figure 3E; Table 3). These previously unavailable subcortical insights may subsequently be used in a variety of applications ranging from the quantification of disease progression or recovery after surgery, functional correlations, or serve as radiographic biomarkers especially when differentiating glioblastoma from cerebral metastases (31, 33, 34). Although responses were variable in assessment of the lesion definition and brain tumor-interface (Table 2), these items were affected by the amount of edema, such that benefits were more pronounced in highly edematous datasets consisting primarily of cerebral metastases and glioblastoma (Figures 4A,B), as expected and consistent with other studies (15). Significant positive correlations between the True (favorable) response rate and free-water ratio on the items assessing whether the enhancement provided further clarification into the lesion definition ($r_s = 0.9$) and brain-tumor interface ($r_s = 0.68$). The majority of surgeons, for example, showed favorable responses to these survey items for corrected tractography in patients 10 and 5 with histopathologies of glioblastoma (S10) and cerebral metastases (S5 and S6) (Figures 4A,B).

Optimal surgical pathway

We sought to establish the primary limitation of standard tractography when evaluating the optimal surgical approach; namely, the presence of tract reduction in areas essential to the intervention strategy (Figures 2, 3C). Such false negatives will

TABLE 3 Comparison of differences in response probabilities between standard (uncorrected) and enhanced (corrected) tractography datasets.

Survey item	Un-corrected tractography			Free-water corrected tractography			Stuart-Maxwell test	
	True (%)	Partially true (%)	False (%)	True (%)	Partially true (%)	False (%)	$\chi 2$ (dof)	Value of p
False signal: false tracts are seen in sulci or ventricles (CSF spaces)	13 (15.29%)	21 (24.71%)	51 (60%)	39 (46.99%)	34 (40.96%)	10 (12.05%)	38.93 (2)	<0.001
Grey-white matter interface: the tracts appear to begin at the grey white matter interface	51 (60.71%)	31 (36.9%)	2 (2.38%)	53 (62.35%)	17 (20%)	15 (17.65%)	13.62 (2)	$p < 0.01$
3D-rendering: this scan demonstrates the following anatomical effects: tract reduction	52 (61.9%)	18 (21.43%)	14 (16.67%)	27 (32.53%)	23 (27.71%)	33 (39.76%)	21.38 (2)	<0.001
3D-rendering: this scan demonstrates the following anatomical effects: tract displacement	64 (75.29%)	17 (20%)	4 (4.71%)	67 (78.82%)	15 (17.65%)	3 (3.53%)	0.81 (2)	1
3D-rendering: this scan demonstrates the following anatomical effects: tract infiltration	26 (30.59%)	26 (30.59%)	33 (38.82%)	44 (52.38%)	15 (17.86%)	25 (29.76%)	18.01 (2)	<0.001

CSF, Cerebrospinal Fluid.

preclude the valuable clinical differentiation of vasogenic edema from infiltrative tumor preoperatively (36), which may impact the resection margins during surgery. Indeed, this undesirable feature of tractography was confirmed with rater agreement that (1) tracts were missing in the vicinity of the lesion and (2) that standard tractography demonstrated tract reduction (Table 2; Figure 3C). Despite false negatives, however, raters strongly agreed that the optimal surgical approach was clear – ascertaining its value as a clinical adjunct. Importantly, a presurgical plan is optimal insofar as its intraoperative execution minimizes postoperative deficits within the desired onco-functional tradeoff. The perilesional sparsity of tract-reconstructions would undoubtedly contradict this objective. When asked whether the enhanced data further clarified the optimal surgical approach, a positive correlation ($r_s = 0.63$) was observed between the True response rate and the free-water ratio in the dataset (Figure 4C). This pattern is unsurprising when considering enhanced datasets with less edema will resemble their standard counterparts and when they diverge in their edema extent, the benefits of the enhancement are emphasized – providing evidence that a correction is best applied on select pathologies (i.e., not a one-size-fits all approach).

Mitigation of false positives

Although advanced diffusion modeling offers insights absent with conventional processing pipelines, these benefits are often counterbalanced by the introduction of false positives (i.e., spurious tracts) (15, 37–39). In the present survey, this trend was noticed by raters particularly along the grey-white matter interface and CSF spaces (Figures 3A,B) - underscoring the need to mitigate such artifacts for surgical planning. Together with the understanding that peritumoral diffusion properties vary across unique brain tumors and patients (15), we introduce a novel free-water-parameterized tractogram and thresholding technique which allows for individualized corrections to be applied by the surgeon's discretion (based on US patent no. 11,355,230) (27). This novel methodology is demonstrated within the edematous zones of a metastatic lesion and in gliomas (Figure 5), where the varying subcortical effects of infiltration, mass effect, and brain-tumor interface can be inspected with progressive changes to the correction strength. Our preliminary observations while using this technique have demonstrated that false positive segments often occur in CSF spaces with consistently high scoring free-water parameters, making the FWC slider an effective filtering tool. Moreover, when the slider is combined with automated methods for clustering tracts of interest, the negative impact of artifactual tracts are further diminished by the anatomical constraints imposed at the clustering step. Nevertheless, the thresholding and tract visualization process for edematous pathologies should be guided solely at the surgeon's discretion to evaluate the sensitivity of the algorithm within the context of the surgical intervention being planned and the patient's functional status prior to surgery (40, 41).

Limitations

The histopathological heterogeneity in cases selected for this analysis were chosen to highlight the variation in edematous zones

across a spectrum of neuro-oncologic pathologies and the perceived clinical value of the correction algorithm therein. Given the limited sample of brain malignancies evaluated here, future studies are needed to systematically assess the differential patterns of peritumoral tractography both within (e.g., low- vs. high-grade glioma) and between distinct tumor types (e.g., glioma vs. cerebral metastasis) to ascertain the diagnostic value of this novel tract-based imaging data. Moreover, the benefits of the enhancement for selecting the optimal parafascicular surgical approach must also be further validated against postoperative patient neurological outcomes. With the software implementation of the adaptive thresholding technique presented in this work, such hypotheses can be readily tested with clinically feasible diffusion imaging acquisitions.

Conclusion

In this work, we implement a novel and noninvasive tractography assessment survey to qualitatively validate multi-subject free-water corrected tractograms along clinically relevant parameters across a variety of edematous pathologies by neurosurgical oncologists. We report that the perceived clinical benefits of free-water corrected tractography are pathology-specific, with favorable assessments of lesion margins, the brain-tumor interface, and optimal surgical pathway being positively correlated with the increasingly edematous datasets consisting of brain malignancies. Surgeon feedback from this novel survey was incorporated into a commercially available software implementation to introduce a first-of-its-kind adaptive FWC tractography thresholding method which may accommodate variability in peritumoral edema effects across patients and pathologies, thereby maximizing its potential as a clinically informative adjunct in otherwise challenging datasets.

Data availability statement

The MRI datasets presented in this article cannot be made available, however survey response data supporting the conclusions of this article can be made available by the authors. Requests to access the datasets should be directed to WH, Wes.Hodges@SynaptiveMedical.com.

Ethics statement

Ethical approval was not required for the studies involving humans because this study surveys surgeon perspectives in previously treated neurosurgical patients with anonymized radiographic images. The research did not include interaction or intervention in human subjects. The studies were conducted in accordance with the local legislation and institutional requirements. The human samples used in this study were acquired from a by- product of routine care or industry. Written informed consent to participate in this study was not required from the participants or the participants' legal guardians/next of kin in accordance with the national legislation and the institutional requirements.

Author contributions

SK: Formal analysis, Methodology, Writing – original draft, Writing – review & editing, Conceptualization, Data curation, Investigation, Project administration, Resources, Supervision. WH: Conceptualization, Investigation, Methodology, Project administration, Resources, Supervision, Writing – original draft, Writing – review & editing, Software, Validation, Visualization. HA: Formal analysis, Resources, Software, Visualization, Methodology, Writing – review & editing. TH: Resources, Software, Visualization, Methodology, Writing – review & editing. PF: Formal analysis, Investigation, Writing – review & editing. VT: Formal analysis, Writing – review & editing, Investigation. GP: Formal analysis, Investigation, Writing – review & editing. KH: Formal analysis, Investigation, Writing – review & editing. IL: Formal analysis, Writing – review & editing, Investigation. ES: Formal analysis, Investigation, Writing – review & editing. PC: Formal analysis, Investigation, Writing – review & editing. DH: Formal analysis, Investigation, Writing – review & editing. BZ: Formal analysis, Investigation, Writing – review & editing. RV: Investigation, Methodology, Software, Supervision, Validation, Writing – review & editing, Formal analysis. VB: Formal analysis, Writing – review & editing, Methodology, Visualization, Writing – original draft.

Funding

The author(s) declare that no financial support was received for the research, authorship, and/or publication of this article.

Acknowledgments

The authors acknowledge the great help of Alicia McNeely and Natalie Dandurand of Synaptive Medical in the organization of the survey and the preparation of this manuscript.

Conflict of interest

SK is a consultant to Synaptive Medical. VB, HA, and TH are employees of Synaptive Medical and WH is a founder. SK, HA, TH, and WH are listed as inventors on the patent regarding the method presented in this paper.

The remaining authors declare that the research was conducted in the absence of any commercial or financial relationships that could be construed as a potential conflict of interest.

The author(s) declared that they were an editorial board member of Frontiers, at the time of submission. This had no impact on the peer review process and the final decision.

Publisher's note

References

1. Panesar SS, Abhinav K, Yeh F-C, Jacquesson T, Collins M, Fernandez-Miranda J. Tractography for surgical neuro-oncology planning: towards a gold standard. *Neurotherapeutics*. (2018) 16:36–51. doi: 10.1007/s13311-018-00697-x

2. Mahmoodi AL, Landers MJF, Rutten G-JM, Brouwers HB. Characterization and classification of spatial white matter tract alteration patterns in glioma patients using magnetic resonance tractography: a systematic review and meta-analysis. *Cancers*. (2023) 15:3631. doi: 10.3390/cancers15143631

3. Yeh F-C, Irimia A, de Bastos DC, A, Golby AJ. Tractography methods and findings in brain tumors and traumatic brain injury. *NeuroImage*. (2021) 245:118651. doi: 10.1016/j.neuroimage.2021.118651

4. Freyschlag CF, Kerschbaumer J, Pinggera D, Bodner T, Grams AE, Thomé C. Preoperative prediction of language function by diffusion tensor imaging. *Brain Informat*. (2017) 4:201–5. doi: 10.1007/s40708-017-0064-8

5. Rahman M, Abbatematteo J, De Leo EK, Kubilis PS, Vaziri S, Bova F, et al. The effects of new or worsened postoperative neurological deficits on survival of patients with glioblastoma. *J Neurosurg*. (2017) 127:123–31. doi: 10.3171/2016.7.jns16396

6. Haddad AF, Young JS, Morshed RA, Berger MS. FLAIRectomy: resecting beyond the contrast margin for glioblastoma. *Brain Sci*. (2022) 12:544. doi: 10.3390/brainsci12050544

7. Lemée J-M, Clavreul A, Aubry M, Com E, de TM, Eliat P-A, et al. Characterizing the peritumoral brain zone in glioblastoma: a multidisciplinary analysis. *J Neuro-Oncol*. (2015) 122:53–61. doi: 10.1007/s11060-014-1695-8

8. Cuddapah VA, Robel S, Watkins S, Sontheimer H. A neurocentric perspective on glioma invasion. *Nat Rev Neurosci*. (2014) 15:455–65. doi: 10.1038/nrn3765

9. Duffau H. Is supratotal resection of glioblastoma in noneloquent areas possible? *World Neurosurg*. (2014) 82:e101–3. doi: 10.1016/j.wneu.2014.02.015

10. Scherer H-J. Structural development in gliomas. *Am J Cancer*. (1938) 34:333–51. doi: 10.1158/ajc.1938.333

11. Zetterling M, Roodakker KR, Berntsson SG, Edqvist P-H, Latini F, Landtblom A-M, et al. Extension of diffuse low-grade gliomas beyond radiological borders as shown by the coregistration of histopathological and magnetic resonance imaging data. *J Neurosurg*. (2016) 125:1155–66. doi: 10.3171/2015.10.JNS15583

12. Young JS, Morshed RA, Gogos AJ, Amara D, Villanueva-Meyer JE, Berger MS, et al. The glioma-network Interface: A review of the relationship between glioma molecular subtype and Intratumoral function. *Neurosurgery*. (2020) 87:1078–84. doi: 10.1093/neuros/nyaa362

13. Ashmore J, Pemberton H, Crum WD, Jarosz J, Barker GJ. Implementation of clinical tractography for pre-surgical planning of space occupying lesions: an investigation of common acquisition and post-processing methods compared to dissection studies. *PLoS One*. (2020) 15:e0231440–0. doi: 10.1371/journal.pone.0231440

14. Becker D, Neher P, Jungk C, Jesser J, Pflüger I, Brinster R, et al. Comparison of diffusion signal models for fiber tractography in eloquent glioma surgery–determination of accuracy under awake craniotomy conditions. *World Neurosurg*. (2022) 158:e429–40. doi: 10.1016/j.wneu.2021.11.006

15. Gong S, Zhang F, Norton I, Ibn Essayed W, Unadkat P, Rigolo L, et al. Free water modeling of peritumoral edema using multi-fiber tractography: application to tracking the arcuate fasciculus for neurosurgical planning. *PLoS One*. (2018) 13:e0197056–6. doi: 10.1371/journal.pone.0197056

16. Li YM, Suki D, Hess K, Sawaya R. The influence of maximum safe resection of glioblastoma on survival in 1229 patients: can we do better than gross-total resection? *J Neurosurg*. (2016) 124:977–88. doi: 10.3171/2015.5.jns142087

17. Sheng Z, Yu J, Chen Z, Sun Y, Bu X, Wang M, et al. Constrained-spherical deconvolution Tractography in the evaluation of the corticospinal tract in glioma surgery. *Front Surg*. (2021) 8:646465. doi: 10.3389/fsurg.2021.646465

18. Henderson F Jr, Parker D, Vijayakumari AA, Elliott M, Lucas T, McGarvey ML, et al. Enhanced fiber tractography using edema correction: application and evaluation in high-grade gliomas. *Neurosurgery*. (2021) 89:246–56. doi: 10.1093/neuros/nyab129

19. Parker D, Ould Ismail AA, Wolf R, Brem S, Alexander S, Hodges W, et al. Freewater estimatoR using iNtErpolated iniTialization (FERNET): characterizing peritumoral edema using clinically feasible diffusion MRI data. *PLoS One*. (2020) 15:e0233645. doi: 10.1371/journal.pone.0233645

20. Henderson F, Abdullah KG, Verma R, Brem S. Tractography and the connectome in neurosurgical treatment of gliomas: the premise, the progress, and the potential. *Neurosurg Focus*. (2020) 48:E6. doi: 10.3171/2019.11.focus19785

21. Almairac F, Parker D, Mondot L, Isan P, Onno M, Papadopoulo T, et al. Free-water correction DTI-based tractography in brain tumor surgery: assessment with functional and electrophysiological mapping of the white matter. *Acta Neurochir*. (2023) 165:1675–81. doi: 10.1007/s00701-023-05608-4

22. Castellano A, Bello L, Michelozzi C, Gallucci M, Fava E, Iadanza A, et al. Role of diffusion tensor magnetic resonance tractography in predicting the extent of resection in glioma surgery. *Neuro-Oncology*. (2011) 14:192–202. doi: 10.1093/neuonc/nor188

23. Sternberg EJ, Lipton ML, Burns J. Utility of diffusion tensor imaging in evaluation of the peritumoral region in patients with primary and metastatic brain tumors. *Am J Neuroradiol*. (2013) 35:439–44. doi: 10.3174/ajnr.a3702

24. Wei Y, Li C, Cui Z, Mayrand RC, Zou J, Wong ALKC, et al. Structural connectome quantifies tumour invasion and predicts survival in glioblastoma patients. *Brain*. (2022) 146:1714–27. doi: 10.1093/brain/awac360

25. Gwet KL. Computing inter-rater reliability and its variance in the presence of high agreement. *Br J Math Stat Psychol*. (2008) 61:29–48. doi: 10.1348/000711006x126600

26. Richard LJ, Koch GG. The measurement of observer agreement for categorical data. *Biometrics*. (1977) 33:159–74. doi: 10.2307/2529310

27. Hodges WB, McNeely A, Koga S, Hayes T, Adamyan H, Inventors; Synaptive medical Inc, assignee: system and method of selectively showing tractography in areas containing free water. US patent 11355230 (2022)

28. Silva M, Vivancos C, Duffau H. The concept of "peritumoral zone" in diffuse low-grade gliomas: oncological and functional implications for a connectome-guided therapeutic attitude. *Brain Sci*. (2022) 12:504. doi: 10.3390/brainsci12040504

29. Rossi M, Ambrogi F, Gay L, Gallucci M, Conti Nibali M, Leonetti A, et al. Is supratotal resection achievable in low-grade gliomas? Feasibility, putative factors, safety, and functional outcome. *J Neurosurg*. (2020) 132:1692–705. doi: 10.3171/2019.2.jns183408

30. Tabor JK, Bonda DJ, LeMonda BC, D'Amico RS. Neuropsychological outcomes following supratotal resection for high-grade glioma: a review. *J Neuro-Oncol*. (2021) 152:429–37. doi: 10.1007/s11060-021-03731-9

31. Byrnes TJD, Barrick TR, Bell BA, Clark CA. Diffusion tensor imaging discriminates between glioblastoma and cerebral metastases in vivo. *NMR Biomed*. (2011) 24:54–60. doi: 10.1002/nbm.1555

32. Cacho-Díaz B, García-Botello DR, Wegman-Ostrosky T, Reyes-Soto G, Ortiz-Sánchez E, Herrera-Montalvo LA. Tumor microenvironment differences between primary tumor and brain metastases. *J Transl Med*. (2020) 18:1. doi: 10.1186/s12967-019-02189-8

33. Lee EJ, Ahn KJ, Lee EK, Lee YS, Kim DB. Potential role of advanced MRI techniques for the peritumoural region in differentiating glioblastoma multiforme and solitary metastatic lesions. *Clin Radiol*. (2013) 68:e689–97. doi: 10.1016/j.crad.2013.06.021

34. Samani ZR, Parker D, Wolf R, Hodges W, Brem S, Verma R. Distinct tumor signatures using deep learning-based characterization of the peritumoral microenvironment in glioblastomas and brain metastases. *Sci Rep*. (2021) 11:14469. doi: 10.1038/s41598-021-93804-6

35. Nakasu S, Fukami T, Jito J, Matsuda M. Microscopic anatomy of the brain–meningioma interface. *Brain Tumor Pathol*. (2005) 22:53–7. doi: 10.1007/s10014-005-0187-0

36. Giambra M, Di Cristofori A, Valtorta S, Manfrellotti R, Bigiogera V, Basso G, et al. The peritumoral brain zone in glioblastoma: where we are and where we are going. *J Neurosci Res*. (2022) 101:199–216. doi: 10.1002/jnr.25134

37. Maier-Hein KH, Neher PF, Houde J-C, Côté M-A, Garyfallidis E, Zhong J, et al. The challenge of mapping the human connectome based on diffusion tractography. *Nat Commun*. (2017) 8:1349. doi: 10.1038/s41467-017-01285-x

38. Starck L, Zaccagna F, Pasternak O, Gallagher FA, Grüner R, Riemer F. Effects of multi-Shell free water correction on glioma characterization. *Diagnostics*. (2021) 11:2385. doi: 10.3390/diagnostics11122385

39. Thomas C, Ye FQ, Irfanoglu MO, Modi P, Saleem KS, Leopold DA, et al. Anatomical accuracy of brain connections derived from diffusion MRI tractography is inherently limited. *Proc Natl Acad Sci U S A*. (2014) 111:16574–9. doi: 10.1073/pnas.1405672111

40. Lau R, Malhotra AK, McAndrews MP, Kongkham P. Subcortical language localization using sign language and awake craniotomy for dominant posterior temporal glioma resection in a hearing-impaired patient. *Acta Neurochir*. (2023) 165:1665–9. doi: 10.1007/s00701-023-05586-7

41. Voets NL, Pretorius P, Birch MD, Apostolopoulos V, Stacey R, Plaha P. Diffusion tractography for awake craniotomy: accuracy and factors affecting specificity. *J Neurooncol*. (2021) 153:547–57. doi: 10.1007/s11060-021-03795-7

frontiers | Frontiers in Oncology

TYPE Original Research
PUBLISHED 22 May 2024
DOI 10.3389/fonc.2024.1288820

OPEN ACCESS

EDITED BY
Konstantinos Gousias,
University of Münster, Germany

REVIEWED BY
Peidong Liu,
First Affiliated Hospital of Zhengzhou University, China
Mariana Magalhães,
University of Coimbra, Portugal

*CORRESPONDENCE
Hang Zhao
zhaohang@jlu.edu.cn

RECEIVED 04 September 2023
ACCEPTED 25 April 2024
PUBLISHED 22 May 2024

CITATION
Jin X, Chen Z and Zhao H (2024) Deciphering glycosylation-driven prognostic insights and therapeutic prospects in glioblastoma through a comprehensive regulatory model. *Front. Oncol.* 14:1288820. doi: 10.3389/fonc.2024.1288820

Deciphering glycosylation-driven prognostic insights and therapeutic prospects in glioblastoma through a comprehensive regulatory model

Xingyi Jin, Zhuo Chen and Hang Zhao*

Neurosurgery Department, China-Japan Union Hospital of Jilin University, Changchun, Jilin, China

The oncogenesis and development of glioblastoma multiforme have been linked to glycosylation modifications, which are common post-translational protein modifications. Abnormal glycosyltransferase development leads to irregular glycosylation patterns, which hold clinical significance for GB prognosis. By utilizing both single-cell and bulk data, we developed a scoring system to assess glycosylation levels in GB. Moreover, a glycosylation-based signature was created to predict GB outcomes and therapy responsiveness. The study led to the development of an glyco-model incorporating nine key genes. This risk assessment tool effectively stratified GB patients into two distinct groups. Extensive validation through ROC analysis, RMST, and Kaplan-Meier (KM) survival analysis emphasized the model's robust predictive capabilities. Additionally, a nomogram was constructed to predict survival rates at specific time intervals. The research revealed substantial disparities in immune cell infiltration between low-risk and high-risk groups, characterized by differences in immune cell abundance and elevated immune scores. Notably, the glyco-model predicted diverse responses to immune checkpoint inhibitors and drug therapies, with high-risk groups exhibiting a preference for immune checkpoint inhibitors and demonstrated superior responses to drug treatments. Furthermore, the study identified two potential drug targets and utilized Connectivity Map analysis to pinpoint promising therapeutic agents. Clofarabine and YM155 were identified as potent candidates for the treatment of high-risk GB. Our well-crafted glyco-model effectively discriminates patients by calculating the risk score, accurately predicting GB outcomes, and significantly enhancing prognostic assessment while identifying novel immunotherapeutic and chemotherapeutic strategies for GB treatment.

KEYWORDS

glycosyltransferases, glyco-model, GB, immune checkpoint inhibitors, clofarabine

1 Introduction

Glioblastoma (GB) has evolved into a highly threatening and deathly brain tumor, with an overall survival time of 15-17 months as the median (1). GB is characterized by its rapid proliferation and extensive vascularization, which is supported by the tumor's aggressive growth dynamics promoting angiogenesis (2). Immunotherapy is a potential novel medication that increases anticancer immune responses by controlling T cells' stimulation and function activities (3). Monoclonal antibodies targeting PD-1/PD-L1 or CTLA-4 have been used in many clinical trials to induce long-lasting therapeutic responses in some cancer patients (4). Therefore, it is of the utmost importance to investigate new markers predicting immunotherapy response and to build solid prognostic signatures for GB patients, enabling the classification of patients and targeted therapy.

Glycosylation is a protein modification progress regulated by glycosyltransferases (5). Several glycosylation modifications, such as O-glycosylation, N-glycosylation, sialylation and fucosylation, are significantly correlated to cancer; these alterations drive multiple cancerous behavior patterns of tumors, including tumor depersonalization, metastasis, and immune regulation (6). A poor prognosis is predicted for glioma patients with the ST3GAL1-associated O-linked sialylation, which also enriches increasing cancer stages in the heterogeneous molecular classification (7). The deregulation of FUT8 contributes to GB tumorigenesis and provides unique insights into the role of fucosylation in receptor tyrosine kinase activity and TMZ resistance (8). Therefore, glycosylation is implicated in numerous aspects of GB oncogenesis, progression, and immune regulation. Emerging data have established those dynamic glycosylation alterations are intimately connected with the course of tumors due to the development of glycomics. Some literature suggests that protein glycosylation is a viable event for diagnosing and tracking a variety of malignancies (9). For example, low MGAT1 expression was associated with liver cancer cell dedifferentiation, metastases, and poor outcomes (10). In addition, Liu et al. found that high levels of GALNT6 expression were correlated with decreased survival rates and that GALNT6 promotes breast cancer metastasis through α2M O-glycosylation (11). Identifying underlying glycosylation biomarkers and expression abnormalities is essential to predict diagnostics, outcomes, and treatment responses for malignancies. For this reason, exploring the role of glycosylation regulators in creating a GB risk prediction model is fascinating.

In the current investigation, we constructed the glyco-score and assessed the GB samples on bulk and single-cell levels. Then we established a glyco-model that predicts GB prognosis, immunotherapy and chemotherapy responses. Survival time, glycosyltransferase expression, tumor microenvironment, immunotherapy response, and chemosensitivity significantly correlate with risk score. Meanwhile, clinical experiments demonstrated that the chosen glycosylation regulators are related to the immunological status and malignant characteristics of GB. Our comprehensive analysis of glycosylation patterns offers promising avenues for GB diagnosis and therapy choice, facilitating a more tailored treatment strategy. By identifying specific glycosylation signatures, we aim to predict patient outcomes and therapy responses more accurately, which is critical in the context of personalized medicine for GB.

2 Materials and methods

2.1 Data acquisition

We meticulously collected gene profiles, mutational landscapes, and clinical data from the TCGA database, which served as our training set. To ensure a robust dataset, we excluded any samples lacking complete survival information. For validation purposes, additional datasets were retrieved from the CGGA and GlioVis databases, rigorously adhering to similar criteria for data completeness and reliability (12, 13).

2.2 Single-cell data processing and analysis

Single-cell data of GB was downloaded from the GEO database under the accession number GSE162631. We removed the genes that were not expressed in every case (counts = 0), then normalized the gene expression matrix using the "SCTransform" function in the Seurat R package. Moreover, we performed the PCA and UMAP analysis and classified the cells using the FindNeighbors and FindClusters functions. Doublets were filtered using the DoubletFinder R package. Cells with > 15% mitochondrial genes or gene number< 500 were also removed. After quality control, about 100 thousand cells were subjected to cell-type annotation using the Celltypist package in Python.

2.3 Functional enrichments

The GO and KEGG databases were employed to conduct fully functioning activity and pathway analysis involving the differential expression glycosylation regulators between glioma tumors and normal tissues using the Enrichplot package in R (14, 15). Moreover, using the clusterProfiler algorithm (16), GSEA was used to evaluate the functions between the two risk subgroups. Statistical significance was considered to exist when the FDR< 0.05 after 1,000 permutations.

2.4 Establishment of glyco-score

A total of 223 glycosylation regulators were retrieved from the GlycoGene DataBase (GGDB). To explore the glycosylation affections on GB, we performed the differential analysis between the GB and normal tissues in the GTEx-TCGA dataset. The differentially expressed genes were shown in the heatmap, and the gene correlation was analyzed using the igraph package. The glyco-score was assessed based on the differentially expressed glycosylation regulators using the ssGSEA and Ucell algorithms in bulk and single-cell data, respectively (17, 18).

2.5 Development and validation of glyco-signature

To determine predictive glycosylation regulators, a univariate Cox regression analysis was conducted on differentially expressed glycosylation regulators in a training set to choose nine glycosylation regulators associated with the GB outcomes. For Cox regression analysis for GB prognosis, the OS of GB patients was examined and computed. Additionally, the lasso regression was leveraged to extract glycosylation regulators and construct a glyco-model for gauging the outcome of GB patients. The mathematical methodology was utilized to ascertain the risk rating:

$$riskscore = \sum_{i=1}^{n}(\beta_i \times Exp_i)$$

Where n is the glycosylation regulator counts; Exp is the glycosylation gene profile; β indicates the multi-Cox coefficient. Patients were then classified into different risk subgroups according to their risk scores. Moreover, the external sets were used to examine the generality of the risk characteristic. Using R v4.2 and Kaplan–Meier (KM) survival analysis, the variation in outcome between the two risk subgroups was determined to be statistically significant (P< 0.05).

2.6 Assessing risk model reliability and generating nomogram

Prognosis analysis assessed the difference between glyco-model and common characteristics, including age, gender, and grades. In the forest plots, P-values and HR were displayed. A nomogram was established using a glyco-model and selected characters in the rms R package to assess three-time points' OS in GB patients. To assess the reliability of our glyco-model, we integrated it with demographic and clinical factors using multivariable Cox regression analyses to develop a comprehensive nomogram. This tool projects 1-, 3-, and 5-year survival probabilities for GB patients, employing calibration plots and AUC curves to evaluate predictive accuracy.

2.7 Analysis of immune infiltration

The ssGSEA algorithm was employed to calculate 20 critical pathways using the gsva R package (19), and CIBERSORT was leveraged to specify the cells in the tumor microenvironment (TME) (20). We further quantified the stromal score, immunological score, and tumor purity using the ESTIMATE algorithm (21).

2.8 Estimation of drug target

We acquired comprehensive target data for 6,125 compounds from the Drug Repurposing Hub (https://clue.io/repurposing) and got 2,249 unique drug targets following the elimination of duplicates (22). To isolate genes amenable to targeting, holding potential for therapeutic implications in high-risk GB patients, we initially conducted Spearman correlation analysis. This assessment involved correlating gene expression of targetable genes with risk scores. Any gene exhibiting a correlation coefficient exceeding 0.25 (with a significance level of P< 0.05) was identified as a candidate drug target associated with an unfavorable prognosis. Subsequently, we determined the risk score for brain cell lines from the CCLE project. We then undertook a correlation analysis between the CERES score and risk score, utilizing these specific cell lines. CERES represents a method used to estimate gene dependency while compensating for the impact of copy-number variations. The Avana dataset applies this methodology to calculate CERES scores for every gene and cell line (23). A lower CERES score for a particular gene suggests an increased likelihood of its dependency on a given cancer cell line. Hence, genes displaying a correlation coefficient below -0.2 (with P< 0.05) were categorized as drug targets linked to poor prognosis dependence. Consequently, therapeutic drug targets suitable for high-risk score GBs encompassed those identified through both aforementioned analyses.

2.9 Chemotherapeutic response prediction

Two extensive pharmacogenomic datasets, namely CTRP and PRISM, offer expansive drug screening and molecular data spanning numerous cancer cell lines. This extensive dataset facilitates precise prognostication of drug response in clinical samples. Distinct differential expression analyses were conducted both between bulk samples and cell lines and between the samples and cell lines, respectively.

For the task of predicting drug responses, a plethora of machine learning (ML) methods have been documented, encompassing multivariate linear regression, support vector machine (SVM), random forests (RF), and k-nearest neighbors (KNN). Among the array of ML methods, linear regression techniques, such as ridge regression and elastic net, have demonstrated consistent and robust performance across diverse contexts (24). Therefore, the present study employed the ridge regression model encapsulated within the pRRophetic package. This model, which has demonstrated reliability across multiple studies, was employed to forecast drug responses for clinical samples (25, 26). Training of the predictive model relied on expression profiles and drug response data derived from solid Cancer Cell Lines (CCLs), with the exclusion of hematopoietic and lymphoid tissue-derived CCLs. The predictive model exhibited satisfactory performance assessed through default 10-fold cross-validation, facilitating the estimation of drug responses for clinical samples based on refined expression profiles.

2.10 Connectivity map analysis

As a supplementary approach, the analysis of the Connectivity Map (CMap) was conducted to explore the potential therapeutic utility of candidate agents in GB (27). Initially, a comparative analysis of gene expression was executed between samples from tumor and normal tissue. Subsequently, the top 300 genes exhibiting the most pronounced fold changes (including 150 up-regulated genes and 150 down-regulated genes) were submitted to the dedicated CMap website, accessible at https://clue.io/query. The gene expression signatures

utilized by this platform are sourced from a combination of CMap v1 and the Library of Integrated Network-Based Cellular Signatures (LINCS) database. Remarkably, the CMap analysis incorporates a comprehensive selection of 2,429 compounds. The outcome of this analysis generated a distinct connectivity score for each perturbation, calibrated on a standardized scale that ranges from -100 to 100. Significantly, a negative score indicates a gene expression pattern linked to a specific perturbation that runs contrary to the disease-specific expression pattern. This implies the potential therapeutic efficacy of the respective perturbation within the context of the disease.

2.11 Clinical sample collection and patient stratification

This study employed human specimens obtained from a cohort of 20 patients diagnosed with GB. These specimens were procured from patients undergoing surgical procedures at China-Japan Union Hospital. All collected materials were subjected to HE staining, following established protocols. Notably, two distinct pathologists independently conducted the diagnostic assessments.

Total RNA was extracted using the Trizol method (Invitrogen), which is widely recognized for its efficiency. The quantitative real-time PCR (qRT-PCR) was conducted using the One-Step qPCR Kit (Invitrogen) and the CFX Connect^{TM} Real-Time System (BIO-RAD), strictly following the protocols provided by the manufacturers. For data analysis, we used the $2^{-\Delta\Delta Cq}$ method, normalizing gene expression levels to GAPDH as a reference. This normalization is critical for ensuring consistency across samples. Based on these gene expression levels, patients were stratified into low-risk and high-risk groups using a threshold calculated from the glyco-model's equation, which helps in predicting patient outcomes more accurately.

2.12 Histological evaluation

To prepare glioma tissue sections for immunohistochemistry (IHC), we deparaffinized and rehydrated the sections in a series of gradient ethanol and recovered them by heating the slides at 100° C citrate buffer for 1 hour. Then, the slices were incubated with the primary antibodies and HRP-conjugated secondary antibodies in sequence. DAB Peroxidase Substrate Kit was used to visualize the antigen-antibody combination. The IHC images were acquired utilizing a microscope. Immunohistochemistry was performed using antibodies against CD3 (ab16669, Abcam), CD57 (ab82749, Abcam), CD163 (ab79056, Abcam) and FOXP3 (ab20034, Abcam).

3 Results

3.1 Potential role of glycosylation regulators in GB

Of 223 glycosylation regulators, 100 genes were abnormally expressed in GB patients compared with the normal tissues, indicating a significant variation in biological processes between the GB patients and healthy individuals. Heatmap demonstrated the landscape of 100 differential genes between the two groups. Therein, we observed that 8 genes were downregulated in GMB patients, while 92 genes were dramatically increased in GB relative to the normal cases (Figure 1A). To systemically explore the relationship among the 100 differential genes, we classified them into four clusters and constructed the correlation network. We detected a strong association of 100 genes, for instance, in cluster A, EXT2 and POFUT1 are highly synergistic (r = 0.798), whereas GAL3ST4 and ST8SIA3 from cluster B are antagonistic (r = -0.562). Moreover, we observed the highest association between ALG11 and POMK (r = 0.802) and the remarkably converse correlation between GALNT13 and HS3ST3B1 (r = -0.581) (Figure 1B).

To delineate the communication of glycosylation with GB, we estimated the glyco-score for every GB patient using the ssGSEA algorithm established from the differential glycosylation regulators. We found that the glyco-score was dramatically higher in GB than in normal cases, validated in the other three datasets (Rembrandt, Gil, and CGGA.mRNAseq_325) (Figures 1C-F). Furthermore, functional investigations were employed to determine the physiological activities of glycosylation regulator-associated differentially expressed genes. In Figure 1G, a distribution chart illustrates the top 10 enriched GO terms of the molecular mechanism for glycosylation regulators. These concepts were linked with glycosylation, glycoprotein biosynthesis, and glycoprotein metabolism. As shown in Figure 1H, KEGG analysis revealed that glycosylation regulators were abundant in O-glycan biosynthesis, glycosaminoglycan biosynthesis, and N-Glycan biosynthesis. These results implied that the mutual effect of the differential glycosylation regulators might be the significant reason for triggering GB.

Since TME is involved in tumor formation, we evaluated the relationship between the glyco-score and immune infiltration (Figure 1I). We found a strong positive correlation of glyco-score with M2 macrophages but a negative association with CD 8^+ T cells (Figures 1J, K), indicating the antagonistic effects of glyco-score in shaping the hot TME of GB.

3.2 Evaluation of glyco-score at the single-cell level

To deeply explore the TME variation between GB and normal individuals, we analyzed single-cell data from GB patients in-depth. After quality control, we got 99132 cells from the GB and adjacent tissue (Figure 2A). We then classified them into 20 clusters and annotated 10 types of cells using the Celltypist algorithm (Figures 2B, C), such as endothelial cells, fibroblasts, macrophages, plasma cells, T cells, B cells, monocytes, DC, ILC, and mono-mac. Cell infiltration analysis demonstrated a variety of variations between the two groups (Figure 2D). The representative markers of each cell type are shown in Figure 2E. We next assessed the glyco-score in the single-cell level leveraging the Ucell algorithm and observed a higher level of glyco-score in GB relative to the adjacent tissue, especially in macrophages and DC cells, which followed the bulk-seq results (Figures 2F, G).

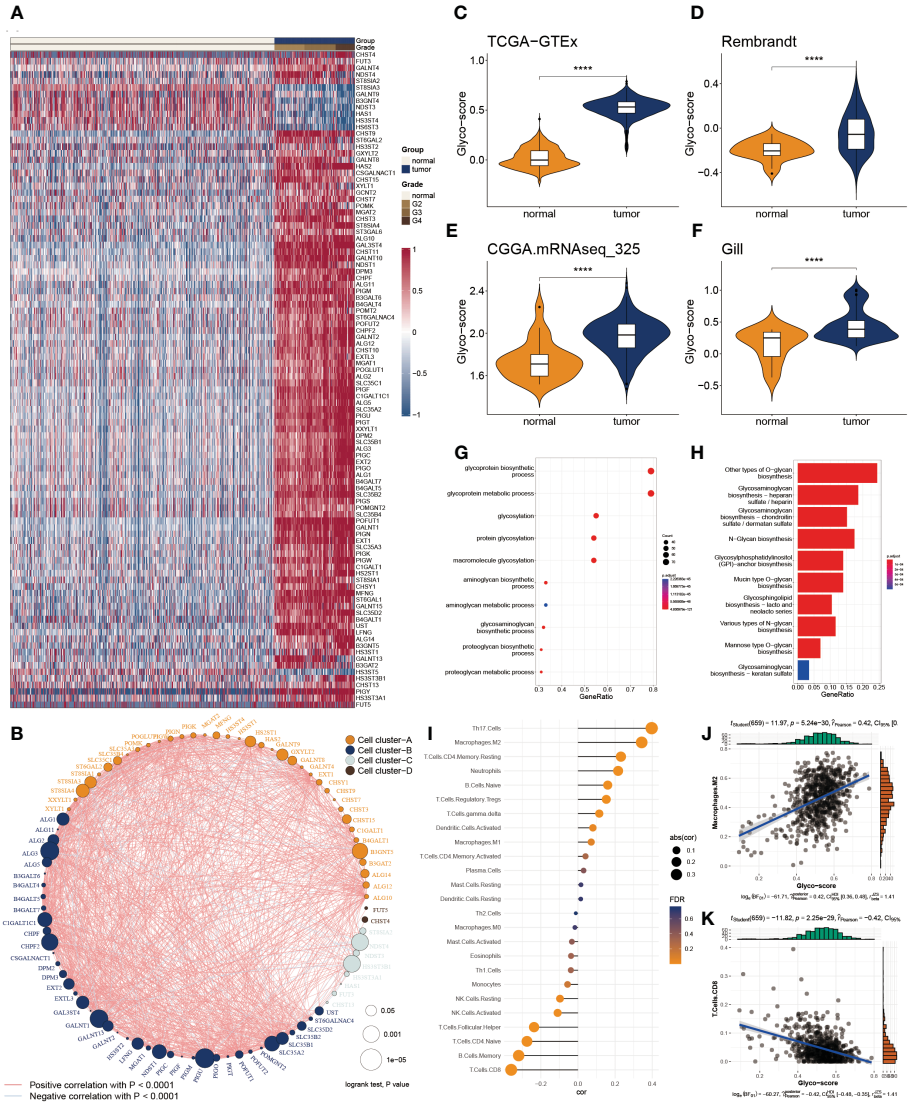

FIGURE 1
Functional enrichment and prognostic characters of glycosylation regulators. **(A)** Heatmap showing the 100 differential glycosylation genes in glioma. **(B)** Interactive correlation of top 50 glycosylation genes. **(C-F)** Distribution of glyco-score in four datasets, GTEx-TCGA **(C)**, Rembrandt **(D)**, CGGA.mRNAseq_325 **(D)** and Gill **(F)**. **(G)** GO enrichment of differential glycosylation regulators. **(H)** KEGG analysis of differential glycosylation regulators. **(I)** Correlation of glyco-score with immune cell inflictions. **(J)** Representative positive correlation: M2 macrophage. **(K)** Representative negative correlation: $CD8^+$ T cells. ****P < 0.0001.

Due to the largest proportion of macrophages in the TME of GB, we estimated the glyco-score in distinct macrophage subsets. We then filled out the macrophages and worked over again. Five subtypes of macrophages were identified, including alveolars, intermediate, erythrophagocytic, intestinal, and macrophages (Figure 2H). We observed that glyco-score significantly diversity among each macrophage subset (Figure 2I).

3.3 Construction and assessment of glyco-model

We applied Cox regression analysis to determine that 82 glycosylation regulators with differential expression were linked with GB prognosis ($p< 0.05$). Lasso regression was used to screen out significant genes. Based on the glioma cases in the TCGA dataset, 25 chosen glycosylation regulators were further analyzed to predict the risk model (Figures 3A, B). To strengthen the rigor of the prediction signature, we randomly divided the TCGA training set into an internal training set and an internal testing set. Then we validated the model using three independent external testing sets. After training our model, we screened nine glycosylation regulators to generate the predictive model as shown in the following formula:

$$\begin{aligned}\text{riskscore} = {} & \text{ALG3} \times 0.042 + \text{B3GNT5} \times 0.261 + \\ & \text{C1GALT1C1} \times 0.205 - \text{CHST15} \times 0.411 - \\ & \text{GALNT9} \times 0.025 + \text{HS3ST3B1} \times 0.349 + \\ & \text{MFNG} \times 0.421 - \text{NDST4} \times 0.117 + \text{SLC35A2} \times 0.248\end{aligned}$$

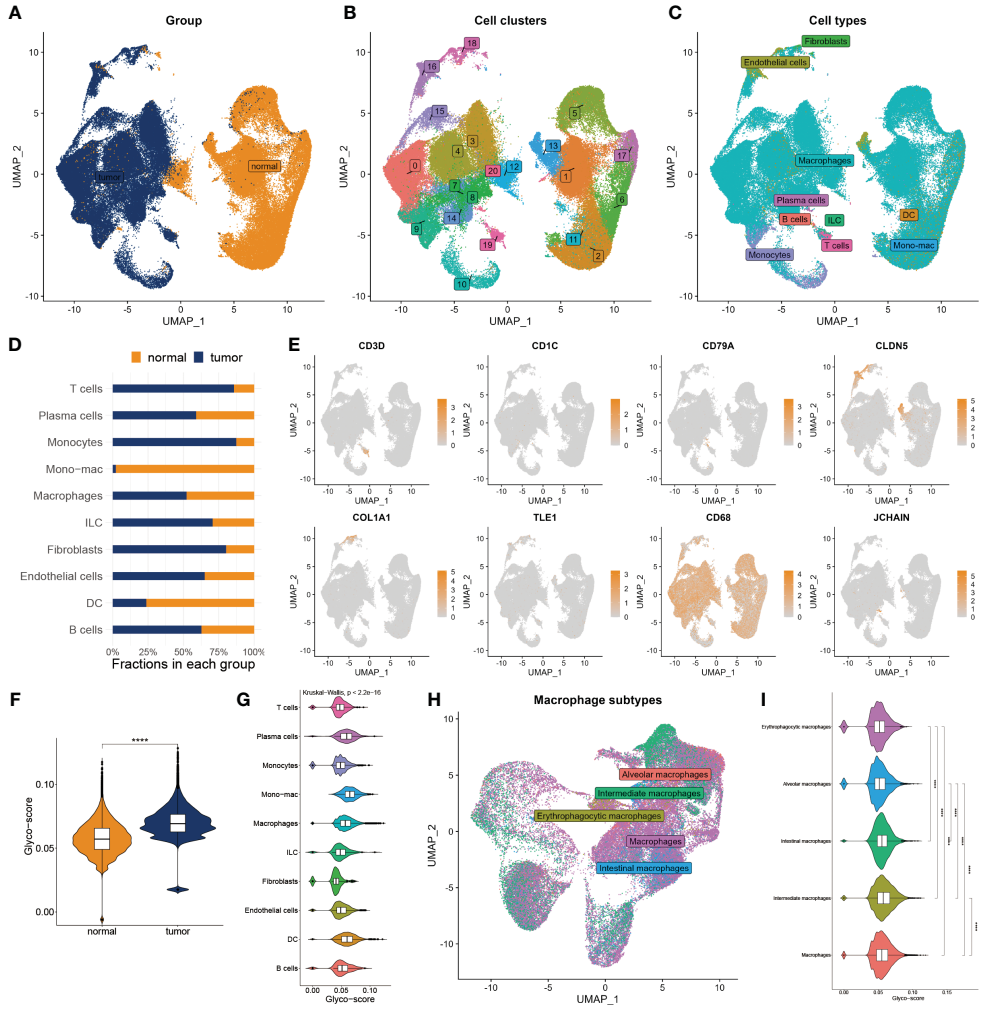

FIGURE 2
Landscape of glyco-score in single-cell sequence. **(A)** Cell distribution in tumor vs normal tissues. **(B)** Distribution of cell cluster. **(C)** Distribution of cell annotation. **(D)** Cell proportions in tumor vs. normal tissue. **(E)** Representative immune marker in each cell type. **(F)** Distribution of glyco-score. **(G)** Glyco-score correlates immune cell types. **(H)** Distribution of cell annotation in macrophage subtypes. **(I)** Glyco-score correlates with macrophage subtypes. ****P < 0.0001.

We categorized glioma cases into risk subtypes for survival status and time. We proved that patients from the high risk presented a considerably more proportion of deceased individuals than the low-risk subgroup. The external cohorts were categorized using the same risk signature as the training cohort. Additionally, the higher-score patients had worse outcomes and distinct gene expression profiles. KM plots demonstrated that the lower-score patients lived longer than the higher ones (Figure 3C). The heatmap depicts the expression characteristics of the nine chosen glycosylation regulators (Figure 3D).

3.4 Assessment of glyco-model

To adapt the glyco-model for clinical application, we estimated the risk score with outcome in both univariate and multivariate analyses performed using TCGA data (p< 0.05) (Figures 4A, B), indicating that the risk model was reliable for GB prognosis. A nomogram was developed to estimate survival probability precisely and accurately at 1-, 3-, and 5-year, considering both the glyco-model and some standard features (Figure 4C). Calibration analysis verified the authenticity of nomograms in the indicated time, proving it was highly congruent with real survival time (Figure 4D). We further evaluated the glyco-model using the time-dependent ROC method. Survival AUCs were 0.86 (1-year), 0.91 (3-year), and 0.88 (5-year), respectively (Figure 4E). More so than age (AUC = 0.83), sex (AUC = 0.51), and clinical grade (AUC = 0.82), risk score (AUC = 091) AUC was a strong predictor (Figure 4F).

Next, we reviewed the literature and chose five current GB risk models for comparison with our novel model (28–32). Our model shows remarkable advantages over other models in C-index (Figure 4G) and restricted mean survival time (RMST) analysis (Figure 4H).

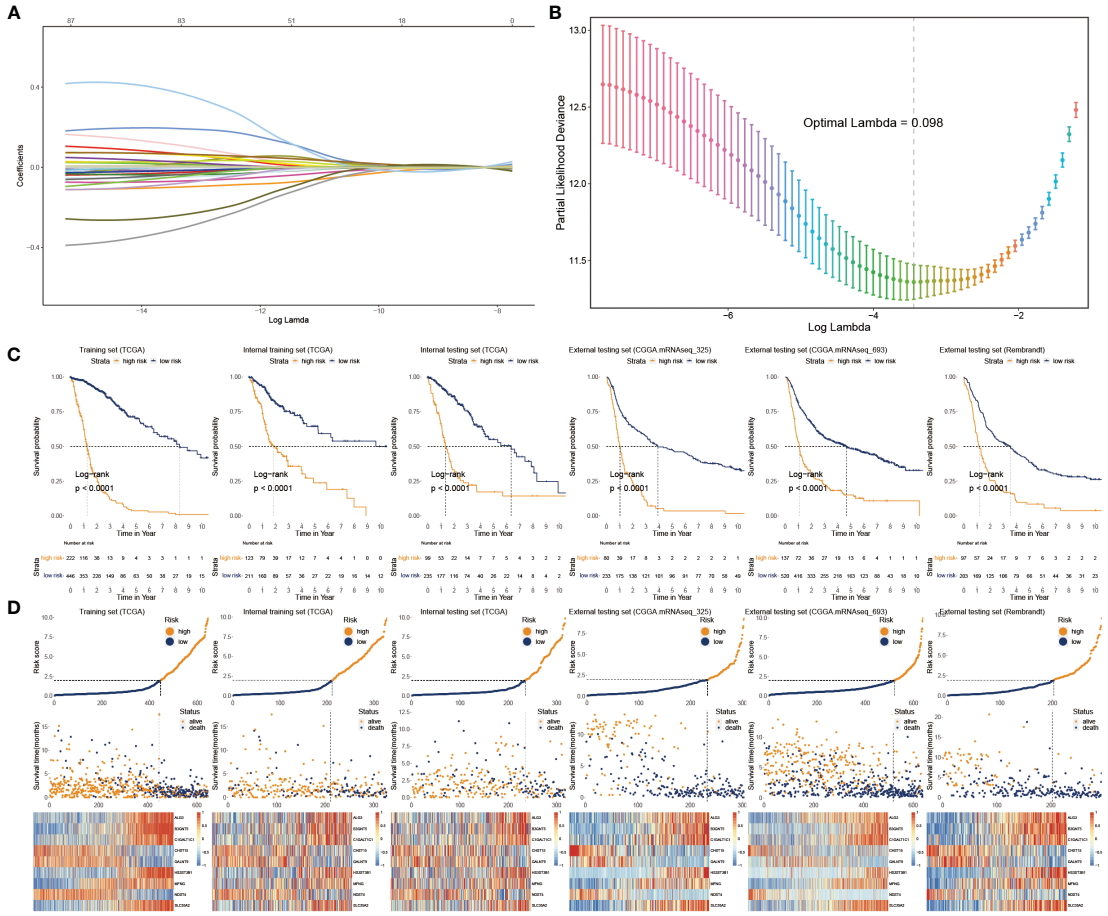

FIGURE 3
Construction and validation of glyco-model. **(A, B)** Lasso regression was used to screen out significant genes. **(C)** KM survival curve in the training sets and the testing sets. **(D)** Risk plot distribution, survival status, and relative expression of risk factors in the training and testing sets.

3.5 Significance of glyco-model to clinical features and functional deviations

The heatmap plot illustrates the pattern of the nine glycosylation regulators and the clinicopathological variables (Figure 5A). Further analyses showed that the glyco-model positively predicts the age, OS status, and clinicopathological grade (Figure 5B), as indicated. We also observed positive correlations between six genes and the risk score, whereas negative correlations existed between three genes and the score (Figure 5C).

To investigate the dysfunctions between the two subgroups, GSEA was applied. We observed that adaptive immune response, B cell-mediated immunity, immunoglobulin-mediated immune response, lymphocyte-mediated immunity, and autoimmune thyroid disease were enriched in the higher subgroup. Moreover, positive regulation of T cell activation, regulation of leukocyte cell-cell adhesion, regulation of lymphocyte activation, and AMPK signaling pathway had inhibited activity in the lower subgroup (Figures 5D, E). We then conducted PCA using the entire genes (Figure 5F), glycosylation regulators (Figure 5G), and nine chosen glycosylation regulators from the model (Figure 5H). The outcome suggested that the expression patterns of the nine chosen glycosylation regulators effectively distinguished between the two subgroups.

3.6 Glyco-model correlates the tumor environment and responses to immunotherapy for GBs

The CIBERSORT was used to calculate the 22 immune cell fractions, and ssGSEA was used to validate the score of 20 associated pathways in the two subgroups (Figures 6A, B). The lower-risk subtypes showed a greater abundance of the TEM cells, including activated DC cells, Eosinophils, and some types of B and T cells, but lower infiltration of M2 macrophages and Tregs. Meanwhile, 17 pathways were considerably variated between the two risk subtypes. Moreover, a significant correlation between the risk score and the proportion of immune cells was also observed (Figure 6C). We also confirmed the immune infiltration in glioma samples using immune cell markers (Figure 6D). We observed that high-risk patients had greater Tregs, tumor-associated macrophages, and NK cells but fewer T cells.

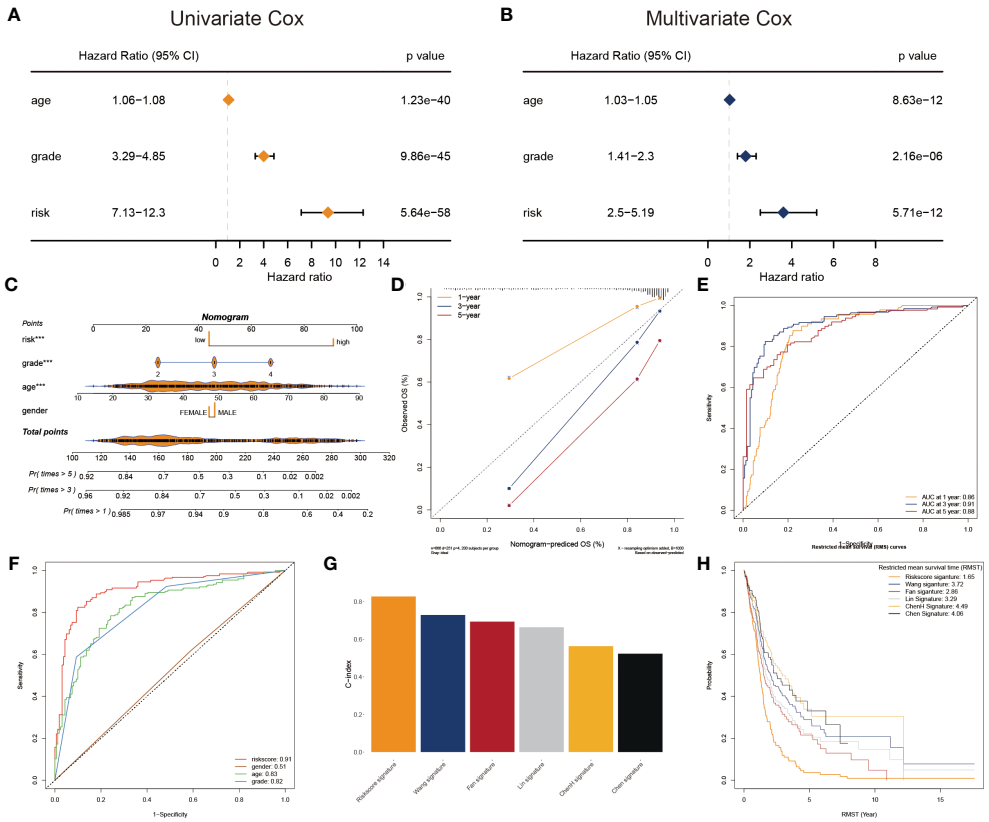

FIGURE 4
Prognostic characters of glyco-model. **(A)** The univariate Cox regression analyses the risk score and other clinical factors. **(B)** The multivariate Cox regression analyses of the risk score and other clinical factors. **(C)** Nomogram was used to predict 1-, 3-, and 5-year OS of GB. **(D)** Calibration curves were used to demonstrate the nomogram–predicted and observed OS of GB patients. **(E)** ROC curve indicating the AUC at 1-, 3-, and 5-year for the risk score. **(F)** ROC curve demonstrating the AUC of risk score and other clinical factors. **(G)** Barplot demonstrating the C-index of six risk signatures. **(H)** RMST for each of the six models.

The ESTIMATE algorithm was leveraged to evaluate three scores and tumor purity. Three scores were dramatically higher in the higher risk score subtype, whereas tumor purity was lower in the lower ones, indicating immunotherapy may be less practical (Figure 6E). Moreover, tumor TIDE and dysfunction, but not exclusion, were significantly more prevalent in the lower risk score subtype (Figure 6F). On the side, individuals with higher TIDE and low-risk scores had the most favorable outcomes (Figure 6G).

Based on IMvigor210 cohorts (33), we discovered that anti-PD-L1 therapeutic response was adversely correlated with risk score (Figure 7A). KM plot showed that the lower risk score subtype from the IMvigor210 cohort demonstrated a better outcome for anti-PD-L1 treatment (Figure 7B). Moreover, the combination of TMB and risk score showed better than one of them (Figure 7C). The risk score was also lower in the CR/PR group relative to the SD/PD group. (Figure 7D). These results showed that a positive reaction to anti-PD-L1 treatment might result in a favorable outcome for the low-risk subgroup. We then employed the SubMAP algorithm to predict the anti-PD1/CTLA4 response probability of immunotherapeutic strategy between the two risk subgroups. The findings suggested that PD-1 treatment could be more effective in the lower-risk population (Figure 7E). However, there was no significant alteration between the two risk subgroups in anti-CTLA4 responsiveness. We further evaluated the seven steps of the immune cycle and observed substantial variations between the two types (34) (Figure 7F). The risk score was adversely linked with the degree of expression of immune inhibitors PD1, PD-L1, HAVCR2, LAG3, and CTLA-4 (Figure 7G). In addition, the low-risk subgroup was more likely to respond to monoclonal antibody therapy, such as PD-1, PD-L1, and CTLA-4 (Figure 7H).

3.7 Discovery of potential drugs for high glyco-model GBs

Genes exhibiting a robust positive correlation with the risk score could potentially hold therapeutic implications for individuals with elevated risk scores (35). Nevertheless, the majority of human proteins remain challenging to target due to their lack of distinct active sites amenable to binding with small molecule compounds, or due to their cellular localization that restricts accessibility for biological agents. As a result, the pursuit of potentially druggable therapeutic targets for GB patients grappling with dismal prognoses was initiated. In this endeavor, a compilation of target information encompassing 6,125 compounds was amassed. This was followed by a two-tiered analytical process aimed at unveiling prospective targets.

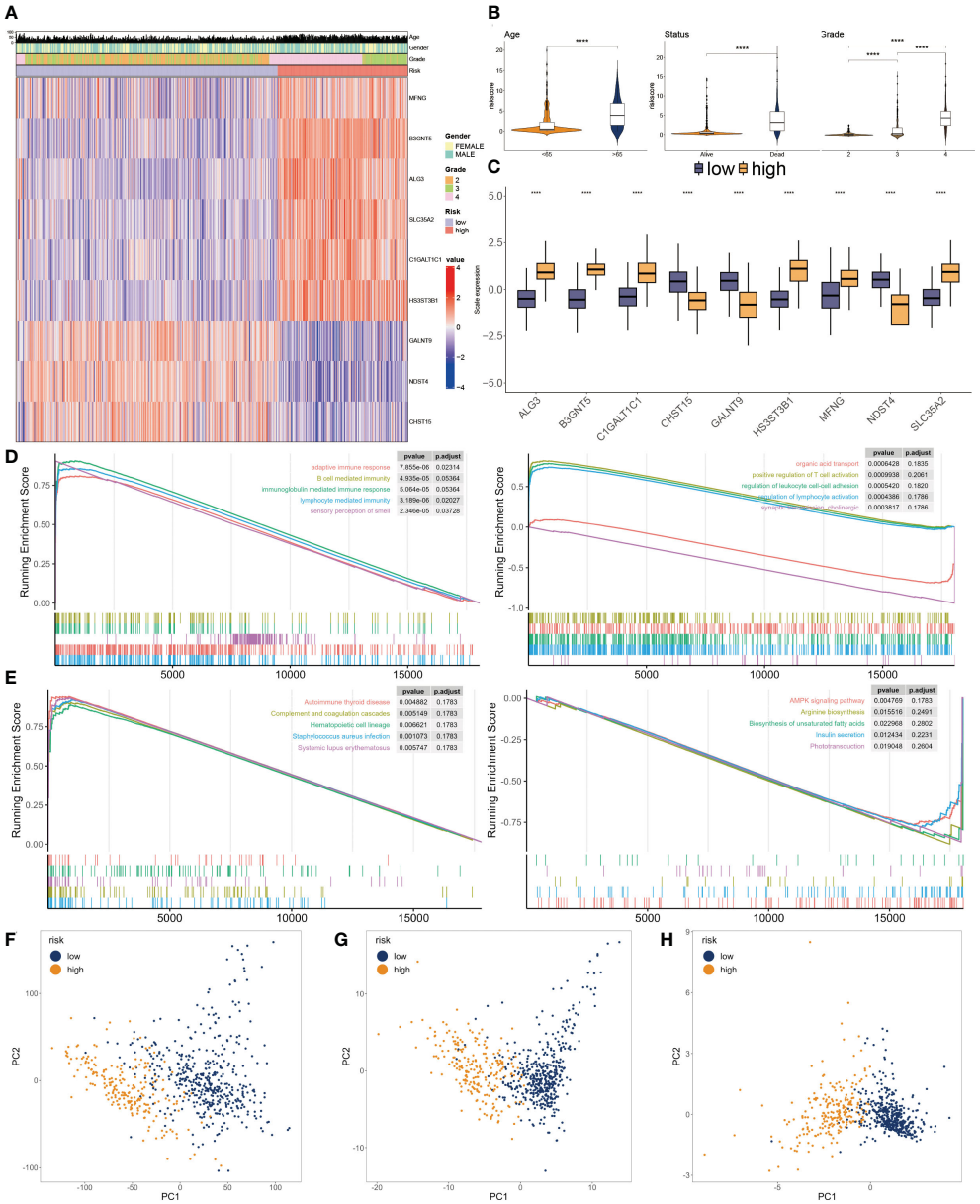

FIGURE 5
Clinicopathological characteristics of glyco-model. **(A)** Heatmap demonstrating the distribution of clinical factors (age, gender, and stage) and relative expression of nine glycosylation regulators in the two risk subgroups. **(B)** The scatter diagram of risk score and age, survival status and grade. **(C)** Relative expression of nine glycosylation regulators between the two risk subgroups. **(D)** Representative GO enrichment between the two risk subgroups. **(E)** Representative KEGG enrichment between the two risk subgroups. **(F)** PCA for all gene expression profiles. **(G)** PCA for all glycosylation regulators expression profiles. **(H)** PCA for nine glycosylation regulators expression profile. ****P < 0.001.

Initially, we computed the correlation coefficient between the expression levels of druggable genes and risk score. This preliminary step yielded 607 gene targets, each marked by a correlation coefficient exceeding 0.25 (with a significance threshold of P< 0.05). Subsequently, we embarked on a parallel analysis by conducting a correlation study between the CERES score and risk score. This was predicated on glioma cancer cell lines. This supplementary analysis unveiled an additional 85 targets, distinctly associated with unfavorable prognosis (characterized by Spearman's r< -0.2 and P< 0.05). Intriguingly, six genes—ARPC4, CPA2, MAP3K6, MET, MMP25, and WEE1—consistently emerged through both analytical approaches (Figure 8A).

The CTRP and PRISM datasets encompass comprehensive gene expression profiles and drug sensitivity data across a multitude of CCLs, forming an ideal foundation for constructing a predictive model for drug response. Two distinct methodologies were employed to identify candidate agents displaying elevated drug sensitivity in patients with high-risk scores. These analyses were executed employing drug response data derived from both the CTRP and PRISM datasets.

In the initial step, a comparative analysis of differential drug response was undertaken between the high-risk score (top decile) and low-risk score (bottom decile) groups. The objective was to

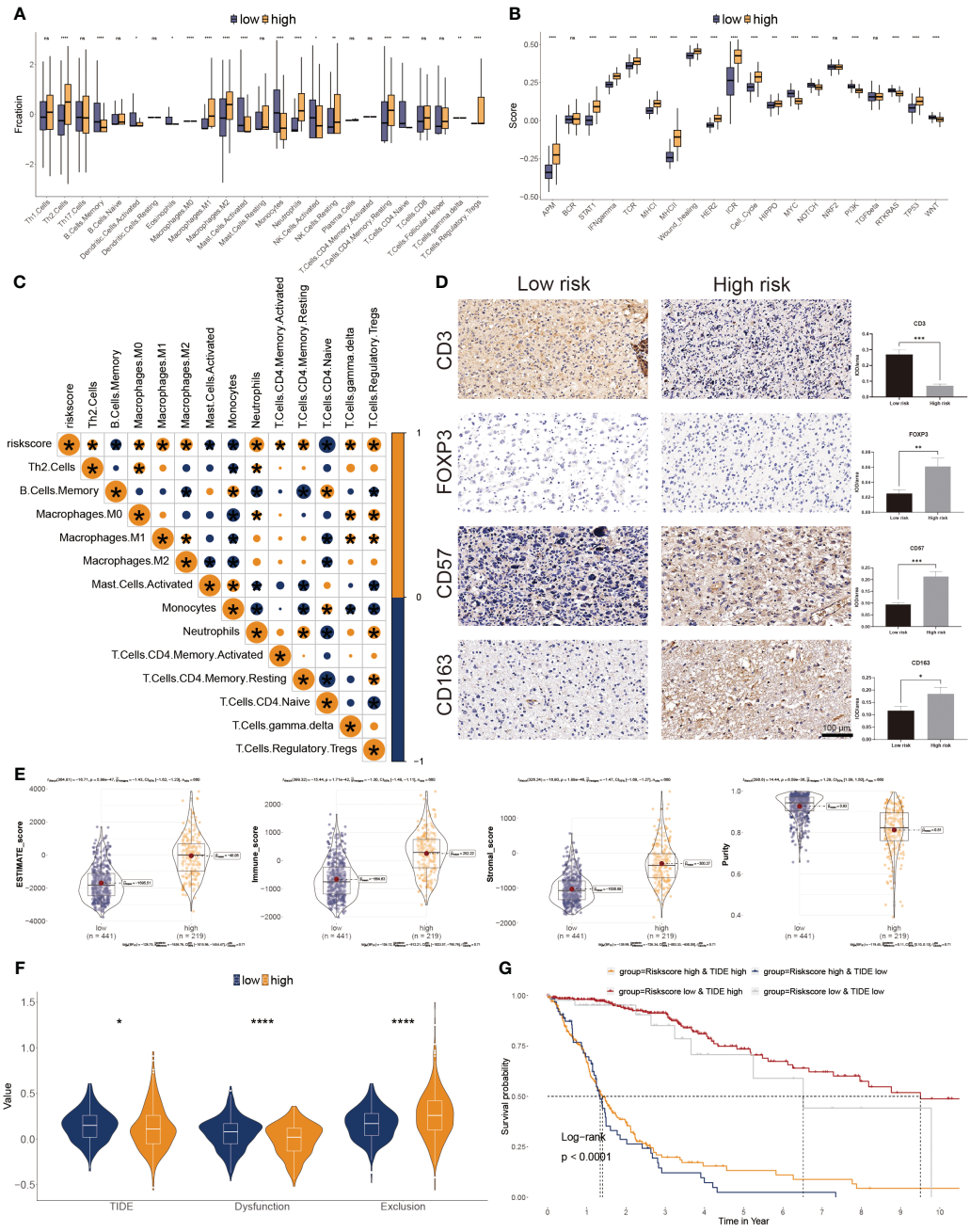

FIGURE 6
Correlation between immune infiltration and glyco-model. **(A)** Differential immune infiltration of 22 immune cell fractions between the two risk subgroups. **(B)** Pathway activities between the two risk subgroups. **(C)** The association of 22 immune cell types with the risk score. **(D)** Representative IHC images of immune cell markers between the two risk subgroups. *P< 0.05, **P< 0.01, ***P< 0.001, n.s, not significant. **(E)** Correlation of risk score with tumor microenvironment. **(F)** TIDE, T cell dysfunction, and exclusion between the two risk subgroups. **(G)** Survival analysis of patients with different combinations of risk scores and TIDE in TCGA cohort. ****P < 0.0001.

identify compounds demonstrating lower estimated AUC values within the high-risk score group (with a log2 fold change > 0.2). Subsequently, a Spearman correlation analysis was conducted between AUC values and risk scores. This facilitated the selection of compounds showcasing a negative correlation coefficient (Spearman's r< -0.30 for CTRP or -0.35 for PRISM). Through this approach, a total of six compounds derived from CTRP (including clofarabine, SB743921, tanespimycin, methotrexate, and paclitaxel) and four compounds derived from PRISM (including dolastatin10, YM155, LY2606368, and vincristine) emerged. Importantly, all these compounds exhibited reduced estimated AUC values within the high-risk score group and a negative correlation with risk score as demonstrated in Figure 8B.

Despite the observation that the identified 10 candidate compounds displayed heightened drug sensitivity in high-risk score patients, it is crucial to acknowledge that these analyses in

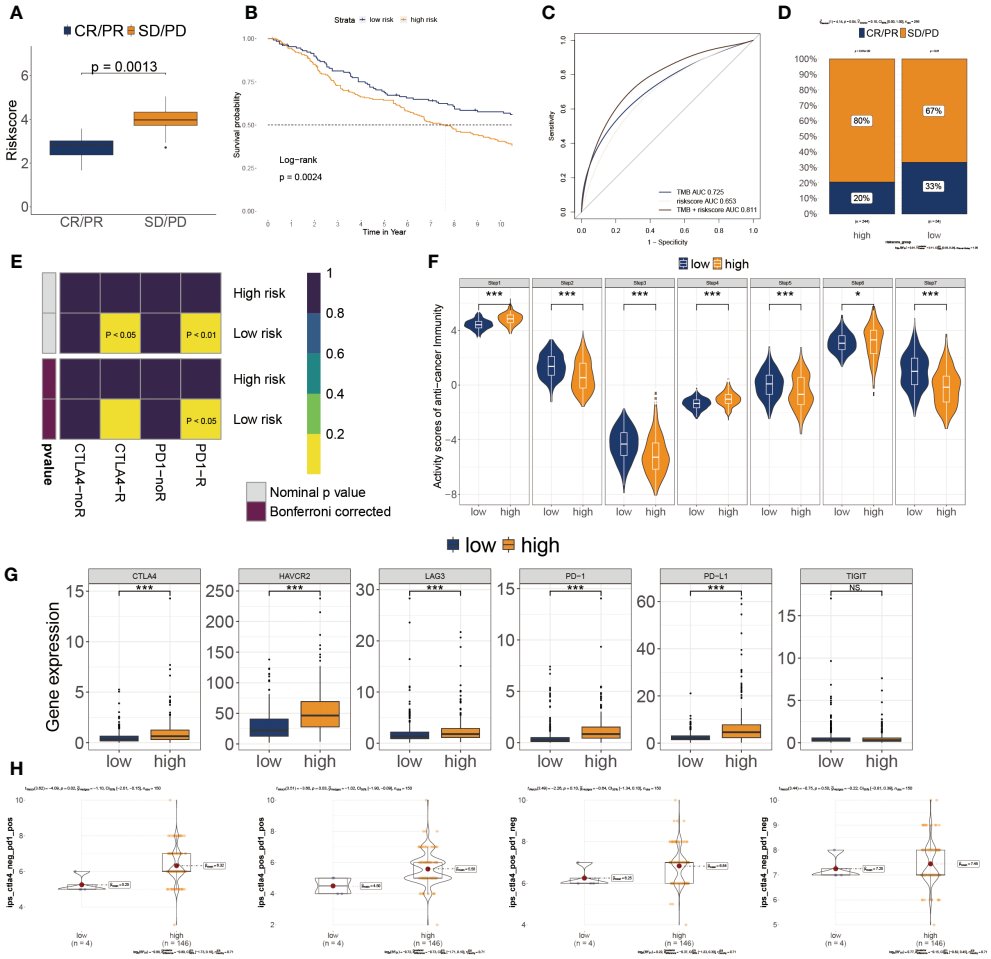

FIGURE 7
Association of risk score to the tumor microenvironment and response to immune checkpoint inhibitors. **(A)** Risk score distribution for different anti-PD-L1 clinical responses in the IMvigor210 cohort. **(B)** Survival analysis of risk score in the IMvigor210 cohort. **(C)** ROC curve of the risk score in the IMvigor210 cohort. **(D)** The relative proportion to anti-PD-L1 immunotherapy in the IMvigor210 cohort. *P< 0.05, ***P< 0.001. **(E)** Putative immunotherapy response between the two risk subgroups. **(F)** Differential immune cycle processes between the two risk subgroups. **(G)** Differential expression of six immunosuppressive molecules between the two risk subgroups. **(H)** Four subtypes of IPS values between the two risk subgroups.

isolation do not substantiate the therapeutic efficacy of these compounds in the context of GB. Consequently, an array of multifaceted analyses was subsequently undertaken to delve into the therapeutic potential of these compounds within GB. Firstly, the CMap analysis was employed to identify compounds whose gene expression patterns ran counter to those specific to GB (characterized by increased gene expression in tumor tissues yet attenuated by treatment with particular compounds). Notably, two compounds—clofarabine, and YM-155—secured CMap scores below -80. This inference suggests the potential therapeutic impact of these compounds in GB. Secondly, a thorough literature review was undertaken on PubMed to ascertain experimental and clinical evidence about the efficacy of candidate compounds in GB treatment. The cumulative outcomes of these analyses were depicted in Figure 8C.

Overall, on a broad scale, clofarabine and YM-155 exhibited robust *in vitro* and silico evidence, positioning them as the most promising therapeutic contenders for GB patients with elevated risk scores.

4 Discussion

GB is hard to combat, and its prognosis varies based on the molecular subtypes. To evaluate the prognosis of GB, there is a critical need for unique and effective techniques. This work effectively constructed a risk signature based on nine glycosylation regulators screened: ALG3, B3GNT5, C1GALT1C1, CHST15, GALNT9, HS3ST3B1, MFNG, NDST4, and SLC35A2. We also showed that patients from high-risk subgroups based on target glycosyltransferases are strongly related to a shorter OS, a poorer immunological impact, and greater chemosensitivity than the lower subgroup. Glycosyltransferases are a vast group of enzymes that regulate glycosylation and promote tumor development and metastasis. In this work, each of the nine glycosyltransferases in our model has unique properties and roles.

Glycosylation-related regulators are highly effective diagnostic tools for early cancer diagnosis, grade identification, and therapy methods. Mohamed et al., for instance, developed a glyco-model by evaluating glycosylation regulators' expression patterns that may be

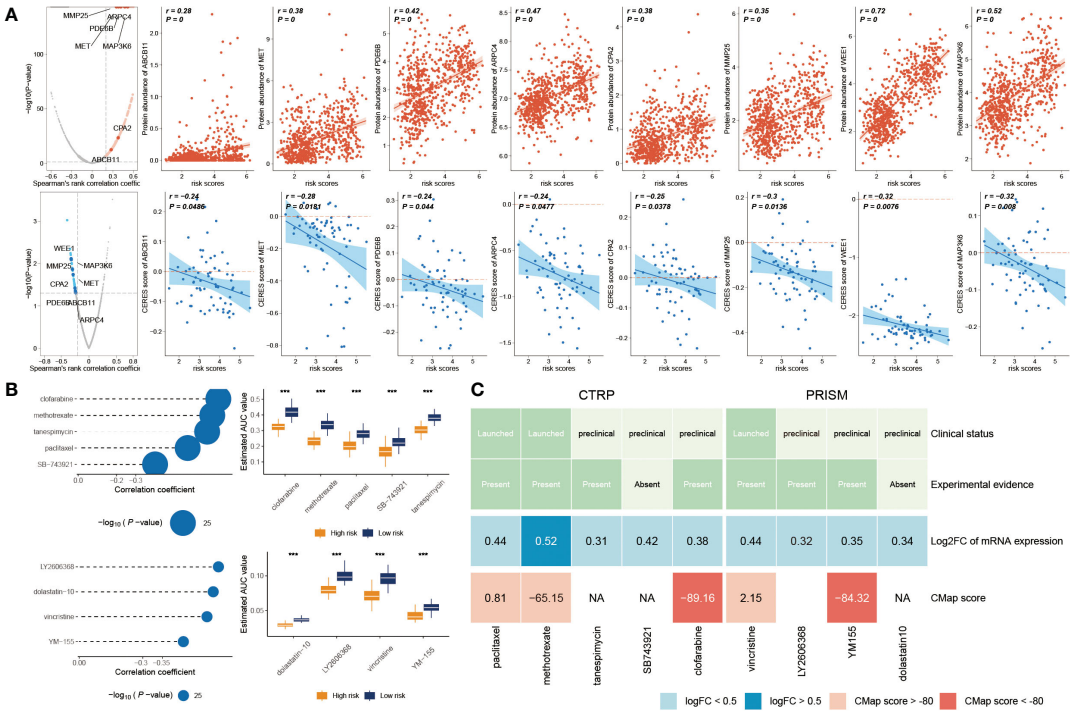

FIGURE 8
Prediction of potential drugs for high risk GB patients. **(A)** The volcano plot visually portrays the outcomes of Spearman's correlation analysis, wherein r > 0.25 and P< 0.05 are depicted as vivid red dots. Subsequent scatter plots illustrate the correlations between the risk score and the gene abundance of identified drug targets. Analogously, Spearman's correlation outcomes, illustrated by blue dots, signify negative associations (P< 0.05 and r< -0.2). These scatter plots depict the relationships between the risk score and the CERES score of the designated drug targets. **(B)** Compound correlation analysis and boxplot: On the left, Spearman's correlation analysis showcases the interrelation of five compounds extracted from the CTRP dataset (top left), and the four compounds procured from the PRISM dataset (bottom left). The corresponding boxplot on the right succinctly illustrates the contrast in estimated Area Under the Curve (AUC) values across the distinct compounds within the two groups. **(C)** The diagram encapsulates a comprehensive overview, encompassing the clinical status, empirical evidence, mRNA expression levels, and CMap scores for the nine agents sourced from CTRP and the four agents derived from PRISM, respectively. ***P < 0.001.

used to distinguish pancreatic cancer subtypes (36). Additionally, the expression of glycosylation regulators may aid the detection of CTCs in cancer patients' blood samples utilizing PCR (11). Although various glycosylation regulators demonstrated adequate and satisfactory consequences in the risk model, no notable features may suggest the presence of CTCs in the blood (37). Therefore, their clinical applicability requires further development. However, the predictive utility of glycosylation regulators has been studied before (38, 39), usually just by looking at a single gene rather than a set of genes together, as we did in the GB.

Moreover, there has been little bioinformatics-based research on the prognostics of GB connected with the glycosyltransferase gene. The glycosylation-based model was able to differentiate between the risk subgroups in our elaborate work. The lower risk subgroup was significantly correlated with longer OS compared to the higher ones, indicating that our model may accurately predict the outcomes of GB patients.

We then identified the clinical characteristics and prediction of GB. The importance of glycosylation in modulating immune-related function and anticancer immunity is growing. The essential glycosyltransferase, such as selectins, singles, and galectins, are crucial regulators of the immune response in tumor spread (40). Numerous immune response-related signals were abundant in the higher-risk score patients. The immunological and stromal scores were significantly higher in the high-risk patients, although tumor purity was considerably elevated in the lower-score patients. Wang et al. found that the glycosyltransferase gene ADRB1 is a significant immunotherapy biomarker among gene mutations (41).

Additionally, we found that tumor glycosylation was significantly correlated with the expression of immunological checkpoints. Current research indicated the higher expression of PD1/PD-L1, the more sensitive to immunosuppressive therapy. Similar to our results, the group with a low score was more responsive to anti-PD-1/PDL1 treatment in the IMvigor210 cohort. We found that the low-risk subset of GB patients may respond better to PD-1 therapy. Nonetheless, the two risk subtypes failed to respond to CTLA4 immunotherapy. The high-score group also showed greater drug sensitivity than the lower ones. Hence, we found significant differences in the prediction of chemotherapy response. We expect the risk score to differentiate between the two risk groupings and provide more accurate predictions about the efficacy of anti-PD1 or anti-PD-L1 immunotherapy treatments. One hypothesis about the effectiveness of ICI for GB is that therapy is more likely to assist those with a low-risk score.

However, specific issues still need to be resolved in the present research. Firstly, this is retrospective research primarily created using bioinformatics analysis of TCGA information and IMvigor210. Validation of the clinical predictive validity of this well-established glyco-signature is still absent. In the future, adequate external verifications should be conducted. Second, we solely validated the immune cell infiltration of the GB samples using the IHC test. These validated results were insufficient to account for all anticipated consequences. These glycosylation regulators' multiple functions and essential mechanisms in GB oncogenesis, development, and prognosis remain deciphered. To corroborate the risk score model's originality, future prospective studies evaluating a large and multicenter population may be advantageous.

5 Conclusion

To sum up, we mined the TCGA database for nine glycosylation regulators and used them to build a functional glyco-model. The immunosuppression and prognosis of the high-risk category were shown to be worse. Immune cell invasion, the tumor-immune cycle, the ICI response, and chemosensitivity in GB are all interconnected with this glyco-model. Investigating glycosylation regulators levels in GB patients might improve our understanding of TME and aim for the design of more efficient therapy protocols. The prognosis for treating GB can be significantly enhanced by integrating our glyco-model with the standard gold techniques.

Data availability statement

The original contributions presented in the study are included in the article/supplementary material. Further inquiries can be directed to the corresponding author.

Ethics statement

The studies involving humans were approved by Ethics Committee of China-Japan Union Hospital of Jilin University. The studies were conducted in accordance with the local legislation and institutional requirements. The participants provided their written informed consent to participate in this study.

Author contributions

XJ: Writing – review & editing, Writing – original draft, Visualization, Validation, Resources, Methodology, Investigation, Funding acquisition, Formal analysis, Data curation, Conceptualization. ZC: Writing – original draft, Visualization, Resources, Project administration, Methodology, Investigation, Formal analysis. HZ: Writing – review & editing, Writing – original draft, Validation, Resources, Formal analysis, Data curation, Conceptualization.

Funding

The author(s) declare financial support was received for the research, authorship, and/or publication of this article. This work was supported by the Natural Science Foundation of Jilin Province (20200201604JC).

Conflict of interest

The authors declare that the research was conducted in the absence of any commercial or financial relationships that could be construed as a potential conflict of interest.

Publisher's note

References

1. Monteiro AR, Hill R, Pilkington GJ, Madureira PA. The role of hypoxia in glioblastoma invasion. *Cells*. (2017) 6:45. doi: 10.3390/cells6040045

2. Musah-Eroje A, Watson S. Adaptive changes of glioblastoma cells following exposure to hypoxic (1% Oxygen) tumour microenvironment. *Int J Mol Sci*. (2019) 20:2091. doi: 10.3390/ijms20092091

3. Syn NL, Teng MWL, Mok TSK, Soo RA. *De-novo* and acquired resistance to immune checkpoint targeting. *Lancet Oncol*. (2017) 18:e731–41. doi: 10.1016/s1470-2045(17)30607-1

4. Lee EQ. Immune checkpoint inhibitors in GBM. *J Neurooncol*. (2021) 155:1–11. doi: 10.1007/s11060-021-03859-8

5. Silsirivanit A. Glycosylation markers in cancer. *Adv Clin Chem*. (2019) 89:189–213. doi: 10.1016/bs.acc.2018.12.005

6. Pinho SS, Reis CA. Glycosylation in cancer: mechanisms and clinical implications. Nature reviews. *Cancer*. (2015) 15:540–55. doi: 10.1038/nrc3982

7. Chong YK, Sandanaraj E, Koh LW, Thangaveloo M, Tan MS, Koh GR, et al. ST3GAL1-associated transcriptomic program in glioblastoma tumor growth, invasion, and prognosis. *J Natl Cancer Institute*. (2016) 108:djv326. doi: 10.1093/jnci/djv326

8. Wei KC, Lin YC, Chen CH, Chu YH, Huang CY, Liao WC, et al. Fucosyltransferase 8 modulates receptor tyrosine kinase activation and temozolomide resistance in glioblastoma cells. *Am J Cancer Res*. (2021) 11:5472–84.

9. Kirwan A, Utratna M, O'Dwyer ME, Joshi L, Kilcoyne M. Glycosylation-based serum biomarkers for cancer diagnostics and prognostics. *BioMed Res Int*. (2015) 2015:490531. doi: 10.1155/2015/490531

10. Takayama H, Ohta M, Iwashita Y, Uchida H, Shitomi Y, Yada K, et al. Altered glycosylation associated with dedifferentiation of hepatocellular carcinoma: a lectin microarray-based study. *BMC Cancer*. (2020) 20:192. doi: 10.1186/s12885-020-6699-5

11. Liu C, Li Z, Xu L, Shi Y, Zhang X, Shi S, et al. GALNT6 promotes breast cancer metastasis by increasing mucin-type O-glycosylation of α2M. *Aging*. (2020) 12:11794–811. doi: 10.18632/aging.103349

12. Bowman RL, Wang Q, Carro A, Verhaak RG, Squatrito M. GlioVis data portal for visualization and analysis of brain tumor expression datasets. *Neuro Oncol*. (2017) 19:139–41. doi: 10.1093/neuonc/now247

13. Zhao Z, Zhang KN, Wang Q, Li G, Zeng F, Zhang Y, et al. Chinese glioma genome atlas (CGGA): A comprehensive resource with functional genomic data from Chinese glioma patients. *Genomics Proteomics Bioinf*. (2021) 19(1):1–12. doi: 10.1016/j.gpb.2020.10.005

14. Ashburner M, Ball CA, Blake JA, Botstein D, Butler H, Cherry JM, et al. Gene ontology: tool for the unification of biology. The Gene Ontology Consortium. *Nat Genet*. (2000) 25:25–9. doi: 10.1038/75556

15. Kanehisa M, Sato Y, Kawashima M, Furumichi M, Tanabe M. KEGG as a reference resource for gene and protein annotation. *Nucleic Acids Res*. (2016) 44:D457–62. doi: 10.1093/nar/gkv1070

16. Yu G, Wang LG, Han Y, He QY. clusterProfiler: an R package for comparing biological themes among gene clusters. *OMICS*. (2012) 16:284–7. doi: 10.1089/omi.2011.0118

17. Andreatta M, Carmona SJ. UCell: Robust and scalable single-cell gene signature scoring. *Comput Struct Biotechnol J*. (2021) 19:3796–8. doi: 10.1016/j.csbj.2021.06.043

18. Hänzelmann S, Castelo R, Guinney J. GSVA: gene set variation analysis for microarray and RNA-seq data. *BMC Bioinf*. (2013) 14:7. doi: 10.1186/1471-2105-14-7

19. Wang T, Li T, Li B, Zhao J, Li Z, Sun M, et al. Immunogenomic landscape in breast cancer reveals immunotherapeutically relevant gene signatures. *Front Immunol*. (2022) 13:805184. doi: 10.3389/fimmu.2022.805184

20. Newman AM, Liu CL, Green MR, Gentles AJ, Feng W, Xu Y, et al. Robust enumeration of cell subsets from tissue expression profiles. *Nat Methods*. (2015) 12:453–7. doi: 10.1038/nmeth.3337

21. Yoshihara K, Shahmoradgoli M, Martínez E, Vegesna R, Kim H, Torres-Garcia W, et al. Inferring tumour purity and stromal and immune cell admixture from expression data. *Nat Commun*. (2013) 4:2612. doi: 10.1038/ncomms3612

22. Corsello SM, Bittker JA, Liu Z, Gould J, McCarren P, Hirschman JE, et al. The Drug Repurposing Hub: a next-generation drug library and information resource. *Nat Med*. (2017) 23:405–8. doi: 10.1038/nm.4306

23. Meyers RM, Bryan JG, McFarland JM, Weir BA, Sizemore AE, Xu H, et al. Computational correction of copy number effect improves specificity of CRISPR-Cas9 essentiality screens in cancer cells. *Nat Genet*. (2017) 49:1779–84. doi: 10.1038/ng.3984

24. The Cancer Cell Line Encyclopedia, C, Stransky N, Ghandi M, Kryukov GV, Garraway LA, Lehár J, et al. Pharmacogenomic agreement between two cancer cell line data sets. *Nature*. (2015) 528:84. doi: 10.1038/nature15736

25. Geeleher P, Zhang Z, Wang F, Gruener RF, Nath A, Morrison G, et al. Discovering novel pharmacogenomic biomarkers by imputing drug response in cancer patients from large genomics studies. *Genome Res*. (2017) 27:1743–51. doi: 10.1101/gr.221077.117

26. Shen R, Li P, Li B, Zhang B, Feng L, Cheng S. Identification of distinct immune subtypes in colorectal cancer based on the stromal compartment. *Front Oncol*. (2019) 9:1497. doi: 10.3389/fonc.2019.01497

27. Lamb J, Crawford ED, Peck D, Modell JW, Blat IC, Wrobel MJ, et al. The Connectivity Map: using gene-expression signatures to connect small molecules, genes, and disease. *Science*. (2006) 313:1929–35. doi: 10.1126/science.1132939

28. Wang Z, Gao L, Guo X, Feng C, Lian W, Deng K, et al. Development and validation of a nomogram with an autophagy-related gene signature for predicting survival in patients with glioblastoma. *Aging*. (2019) 11:12246–69. doi: 10.18632/aging.102566

29. Fan W, Wang D, Li G, Xu J, Ren C, Sun Z, et al. A novel chemokine-based signature for prediction of prognosis and therapeutic response in glioma. *CNS Neurosci Ther*. (2022) 28:2090–103. doi: 10.1111/cns.13944

30. Lin CQ, Chen LK. Effect of differential hypoxia-related gene expression on glioblastoma. *J Int Med Res*. (2021) 49:3000605211013774. doi: 10.1177/03000605211013774

31. Chen H, Xu C, Yu Q, Zhong C, Peng Y, Chen J, et al. Comprehensive landscape of STEAP family functions and prognostic prediction value in glioblastoma. *J Cell Physiol*. (2021) 236:2988–3000. doi: 10.1002/jcp.30060

32. Chen X, Fan X, Zhao C, Zhao Z, Hu L, Wang D, et al. Molecular subtyping of glioblastoma based on immune-related genes for prognosis. *Sci Rep*. (2020) 10:15495. doi: 10.1038/s41598-020-72488-4

33. Mariathasan S, Turley SJ, Nickles D, Castiglioni A, Yuen K, Wang Y, et al. TGFβ attenuates tumour response to PD-L1 blockade by contributing to exclusion of T cells. *Nature*. (2018) 554:544–8. doi: 10.1038/nature25501

34. Chen DS, Mellman I. Oncology meets immunology: the cancer-immunity cycle. *Immunity*. (2013) 39:1–10. doi: 10.1016/j.immuni.2013.07.012

35. Yang C, Huang X, Li Y, Chen J, Lv Y, Dai S. Prognosis and personalized treatment prediction in TP53-mutant hepatocellular carcinoma: an in silico strategy towards precision oncology. *Brief Bioinform*. (2021) 22(3):bbaa164. doi: 10.1093/bib/bbaa164

36. Mohamed Abd-El-Halim Y, El Kaoutari A, Silvy F, Rubis M, Bigonnet M, Roques J, et al. A glycosyltransferase gene signature to detect pancreatic ductal adenocarcinoma patients with poor prognosis. *EBioMedicine*. (2021) 71:103541. doi: 10.1016/j.ebiom.2021.103541

37. Saldova R, Reuben JM, Abd Hamid UM, Rudd PM, Cristofanilli M. Levels of specific serum N-glycans identify breast cancer patients with higher circulating tumor cell counts. *Ann Oncol*. (2011) 22:1113–9. doi: 10.1093/annonc/mdq570

38. Watson ME, Diepeveen LA, Stubbs KA, Yeoh GC. Glycosylation-related diagnostic and therapeutic drug target markers in hepatocellular carcinoma. *J Gastrointestin Liver Dis*. (2015) 24:349–57. doi: 10.15403/jgld.2014.1121.243.mew

39. Kifer D, Louca P, Cvetko A, Deriš H, Cindrić A, Grallert H, et al. N-glycosylation of immunoglobulin G predicts incident hypertension. *J Hypertens*. (2021) 39:2527–33. doi: 10.1097/hjh.0000000000002963

40. Rodrigues JG, Balmaña M, Macedo JA, Poças J, Fernandes Â, de-Freitas-Junior JCM, et al. Glycosylation in cancer: Selected roles in tumour progression, immune modulation and metastasis. *Cell Immunol*. (2018) 333:46–57. doi: 10.1016/j.cellimm.2018.03.007

41. Wang J, Zhang X, Li J, Ma X, Feng F, Liu L, et al. ADRB1 was identified as a potential biomarker for breast cancer by the co-analysis of tumor mutational burden and immune infiltration. *Aging*. (2020) 13:351–63. doi: 10.18632/aging.104204

Frontiers in Oncology

Advances knowledge of carcinogenesis and tumor progression for better treatment and management

The third most-cited oncology journal, which highlights research in carcinogenesis and tumor progression, bridging the gap between basic research and applications to imrpove diagnosis, therapeutics and management strategies.

Discover the latest Research Topics

See more →

Frontiers

Avenue du Tribunal-Fédéral 34
1005 Lausanne, Switzerland
frontiersin.org

Contact us

+41 (0)21 510 17 00
frontiersin.org/about/contact